QUANTIFYING SECONDARY ORGANIC AEROSOL (SOA) FORMED THROUGH CLOUD CHEMISTRY AND CLOUD DROPLET EVAPORATION

by

DIANA L. ORTIZ-MONTALVO

A dissertation submitted to the

Graduate School-New Brunswick

Rutgers, The State University of New Jersey

In partial fulfillment of the requirements

for the degree of

Doctor of Philosophy

Graduate Program in Environmental Sciences

written under the direction of

Barbara J. Turpin

and approved by

_____

_____

_____

_____

New Brunswick, New Jersey

MAY, 2013

ABSTRACT OF THE DISSERTATION

Quantifying Secondary Organic Aerosol (SOA) Formed through Cloud Chemistry and Cloud Droplet Evaporation

By DIANA L. ORTIZ-MONTALVO

Dissertation Director:

Barbara J. Turpin

Secondary organic aerosol (SOA) is a substantial contributor to atmospheric organic particulate matter; however, its formation via aqueous oxidation reactions is only beginning to be understood. Although the aqueous organic chemistry that drives SOA formation in clouds (SOA_{Cld}) has now been incorporated into a few photochemical transport models, it is yet unknown to what extent the newly formed organic material remains in the particle-phase after droplet evaporation. ***This work investigates SOA formation through cloud water chemistry and droplet evaporation.*** Aqueous hydroxyl radical oxidation and droplet evaporation experiments were conducted using precursors commonly found in cloud water: glycolaldehyde, methylglyoxal, and glyoxal. A new method was used to measure the volatility of the product mixture. The effective vapor pressure, enthalpy of vaporization, and mass yields of SOA_{Cld} were determined.

Aqueous oxidation produced carboxylic acids and oligomers (i.e., small polymers), which are major constituents of atmospheric aerosols. Enhanced yields (e.g., ~50-80% yields from glycolaldehyde) provide evidence for additional chemistry during droplet evaporation. The overall vapor pressure and enthalpy of vaporization of SOA_{Cld} were ~10^{-7} atm and ~70 kJ/mol, respectively, similar to the mix of organic acids identified. Lastly, a substantial decrease in volatility (~ 10^{-8} - 10^{-16} atm) was observed when glyoxal SOA_{Cld} products were exposed to sufficient ammonia to form organic salts. These results provide an important insight on the effects that cloud droplet evaporation and neutralization have on SOA formation through cloud processing.

This work furthers our understanding of SOA_{Cld} formation, and provides measurements that are needed for accurate prediction of SOA in global and regional air quality models.

ACKNOWLEDGMENTS

This dissertation is a great accomplishment for me, and I want to thank those who have helped to make this dream come true. First, I want to express my deepest appreciation and gratitude to my adviser, Dr. Barbara Turpin, for all the time she has invested in mentoring and guiding me. She is an excellent role model of a passionate scientist and well-balanced mentor. Barb, I will always look back with fond memories of you and with much admiration. I am also very grateful to my committee members (Dr. Ann Marie Carlton, Dr. Gediminas Mainelis, and Dr. V.Faye McNeill) for their valuable expertise, support and help in completing this dissertation. Ann Marie, it has been my pleasure having you as a "sister" in our academic genealogy, I look up to you and I hope to continue learning from you as I progress in our field. Also, I want to give special thanks to my hard-working collaborators, Dr. Allison Schwier and Dr. Yong Lim, who have made valuable contributions to this dissertation; your commitment to research has truly inspired me! A warm thank you to my fellow lab mates, past and present: Jeff (aka singing grad student), Ron (the best lab tech!), Natasha, Neha, Nancy, Tan, Anjuli, Mark, Craig, and Katie. I have enjoyed being "cultured" by all of you (sometimes in a teasing way, you know who you are!). More importantly, I truly appreciate your willingness to help me (with experiments, scientific discussions, long practice presentations, etc.) even when your own workloads were weighing on you, and I hope I was able to return the favor. In addition, I want to thank Dr. Evelyn Erenrich for recruiting me to the Dept. of Environmental Sciences, where I've had wonderful experiences as a graduate student.

To my undergraduate research adviser, Dr. Olga L. Mayol-Bracero, thank you so much for opening your doors to me and helping me obtain my first research experience in

atmospheric chemistry, but mostly for motivating me to pursue a Ph.D. degree. You were my first role model of a Latina scientist and I will always be grateful for that.

A big thank you to all my friends and family, you make my life so enjoyable! To my faithful friends who have supported me for the past 10+ years: Natalia, Niviann, Maricela, Aracelis, Omar Torres, Catherine, Adriana, Frances, Omayra, Milton, Gabriel, Flavia, Lydia, Luis Ortiz, Melani, Ruby, Tatiana, Grisely, Carlos I., Felix, Hector, Armando, Omar Arce, Alex Roldan, and Nilsa. ¡Gracias por el apoyo y la amistad tan bonita que me han brindado durante todos estos años! To the new friends I have gained along the way: Francis, Sarat, Sophia, Kelly, my lab mates, Allie, Khoi, Caroline, Andy, Michael, Jillian, Imtiaz, Natz, La Reina, Nicole, Ivan G and Blanche, George Parra, and the lovely family of Robert Torres, Anabelle, and Amanda! I am so grateful for your friendship and love, and thank you for being part of this special moment in my life. A la familia de Manny, gracias por todo el amor y respaldo que me dan día a día, los quiero mucho. A mi hermosa familia, los quiero incondicionalmente por todo lo que hacen por mi y me siento muy dichosa de tenerlos en mi vida. Mami, Papi, and Danny, thank you so much for always believing and supporting my dreams even when that meant I had to be far from you. It has been the toughest thing I've ever done and I know it has been hard on you too, but it finally paid off, now we have the first Ph.D. in the family!

Finally, to my sweet love, Manny. You have been the perfect companion throughout this process and the best support system a partner could ever ask for. Thank you for all the things you have done and continue to do for me. Your selfless acts and devotion towards me are just some of your best traits, and are the main reasons I dedicate this dissertation to you, my love. ¡Te amo hoy y siempre!

TABLE OF CONTENTS

LIST OF TABLES

LIST OF ILLUSTRATIONS

Chapter 1. Introduction

1.1 Motivation

Secondary organic aerosol (SOA), which is formed in the atmosphere rather than being directly emitted, is a substantial contributor to atmospheric particulate matter (PM)[1-5]. Atmospheric PM can have adverse effects on climate, visibility, and health[6-9]. Despite its importance, the formation processes of SOA are poorly understood[10]. Recent evidence suggests that organic PM is enhanced through cloud processing and that including this SOA formation pathway in air quality models could double the predicted SOA, although uncertainties are large (e.g., Carlton et al.[11]; Fu et al.[12]). Briefly, during cloud processing, gaseous organic compounds dissolve into cloud water droplets and undergo further reactions with oxidants present in the cloud water (e.g., hydroxyl radicals) leaving behind organic material in the particle-phase when the droplets evaporate, thus forming SOA[13]. Although the aqueous chemistry involved in organic cloud processing has now been incorporated into a few photochemical transport models, *it is yet unknown to what degree the produced organic material remains in the particle-phase after droplet evaporation.* This dissertation provides an important perspective on the effects that cloud droplet evaporation has on SOA formation and offers new insights into condensed-phase photochemically initiated reactions that form secondary organic particulate matter in our atmosphere. It also provides enthalpies of vaporization and vapor pressure estimates that are needed to add SOA formation via aqueous chemistry into climate and regional air quality models. These models link emissions sources to air pollution concentrations and effects (e.g., on climate, visibility, ecosystems, and health) and are vital to the development of effective air quality management plans.

1.2 Background: Atmospheric Aerosols

Aerosols are solid or liquid particles suspended in a gas[14]. Atmospheric aerosols contain materials that are directly emitted (primary) from a variety of sources, both natural and anthropogenic (man-made). In addition, chemical reactions in the atmosphere convert gaseous emissions to (secondary) particulate matter, altering the mass composition and behavior of atmospheric aerosols[15]. A brief introduction to the sources, effects, and chemical composition of atmospheric aerosols follows below. (In this dissertation the terms *aerosol* and *particles* are used interchangeably even though the official definition of an aerosol is "particles suspended in a gas").

1.2.1 Sources and Effects

Natural sources of atmospheric particles include volcanic emissions, sea-spray from bursting bubbles at the ocean surface, smoke from wild fires, wind abrasion of the Earth's surface, biogenic emissions of seeds, pollen, spores, and fragments of plants and animals, as well as, microorganisms[16]. These aerosols are called "primary" because they are emitted directly as particles into the atmosphere. Primary anthropogenic sources include industrial processes, fuel combustion, biomass burning, together with dust from roads, and wind erosion of labored land[16]. Secondary aerosol is formed in the atmosphere through chemical reactions resulting in gas-to-particle conversion of anthropogenic and biogenic gases[15]. The major precursors of secondary aerosol are sulfur dioxide, nitrogen oxides, and volatile to semi-volatile organic compounds (i.e., VOCs to SVOCs, including intermediate volatility compounds [IVOC's])[15,17-20]. Also, there is growing recognition that (gaseous) ammonia and amines may be important contributors to new particle formation in the atmosphere[21-24]. Secondary products include sulfates, nitrates and

organics. This dissertation focuses on organic particulate matter (PM) formed via secondary processes, described in more detail in section 1.3.

Atmospheric aerosols consist of particles with diameters between a few nanometers to hundreds of micrometers[20]. Particles in the coarse mode (PM with diameters > 2.5 μm) are generally a result of primary sources, while most of the fine particle (PM with aerodynamic diameter < 2.5 μm, $PM_{2.5}$) mass is secondary[15].

Fine particles have several adverse effects. They impact the radiative balance in the Earth's atmosphere directly and indirectly. Specifically, they directly scatter and absorb solar and terrestrial radiation, producing a cooling or warming effect, respectively, in our atmosphere. Particles also act as cloud condensation nuclei. Thus changes in particle number or properties alter cloud properties (e.g., lifetime, cloud cover, precipitation) and perturb the Earth's albedo[6,20,25]; this is an indirect effect on climate. Fine particles ($PM_{2.5}$) scatter light very efficiently and reduce visibility, which might be the most noticeable trait of air pollution[20,26]. Importantly, $PM_{2.5}$ is respirable and can reach deep into the human respiratory system where gas exchange occurs, causing adverse health effects. For example, deaths due to chronic obstructive pulmonary disease and ischemic heart disease have been linked to $PM_{2.5}$ exposure[27-30]. Moreover, fossil fuel combustion and secondary formation generally produce fine (2.5 μm) PM, a size range that is of concern to both health and visibility reduction.

Size is an important property of atmospheric particles because it is commonly associated with formation mechanisms and it has a large impact on fate and effects. Particle number, chemical composition, hygroscopic, aerodynamic and optical properties are also important. The complexity of particle composition, along with the current lack of

knowledge concerning particle sources and mechanisms of formation, creates a challenge to health, ecological, and climate change studies[6,31,32], as well as to the development of effective air quality management plans[8].

1.2.2 Chemical Composition

The chemical composition of atmospheric aerosols varies seasonally and spatially. In general, atmospheric aerosols contain inorganic compounds like ammonium sulfate, ammonium nitrate, sodium chloride, and trace metals, as well as crustal elements, water and chemically complex organic material[15]. Organic aerosol (OA) mass contributes roughly 20-80% of submicron particulate mass, and up to 90% in tropical forested areas[3,5,33]. Much remains unknown about the detailed chemical composition, sources, and formation processes of OA. The OA formed through secondary processes (i.e., secondary organic aerosol, SOA) accounts for a substantial fraction of the OA mass, ranging from 20% to ~95% of the mass[5,33-37]. Although SOA has been traditionally believed to be formed by gas-phase photochemistry followed by absorption of semi-volatile products into pre-existing OA mass, this dissertation focuses on SOA formed through a rather newly-recognized formation pathway that is discussed in detail below (section 1.3). Furthermore, the "black and white" distinction between primary and secondary organic aerosol has been complicated by recent studies which revealed that most of primary organic aerosol is semi-volatile[38], and evaporates at high dilution ratios found in ambient conditions. Thus evaporated "primary" OA can form "secondary" OA[19] through gas-phase photochemistry and partitioning into organic matter or into liquid water and subsequent reaction (as described below). Overall, the chemical composition of OA is very complex and depends on various formation processes (e.g., primary, secondary).

These processes need to be better understood in order to have more effective control strategies and improved air quality management.

1.3 Secondary Organic Aerosol (SOA) Formation

This section describes two atmospheric processes that form SOA. Both processes begin with gas-phase photochemical oxidation of organic gases. In the first process (traditional SOA formation) gas-phase oxidation produces semi-volatile condensable compounds that partition into particulate organic matter—SOA_{OM} (Odum et al.[39]; Seinfeld and Pankow[18] and references therein). In the other more recently elucidated process (aqueous SOA, SOA_{aq}) gas-phase chemistry is followed by aqueous chemistry in clouds, fogs and wet aerosols[13,40,41]. The precursors of SOA_{OM} are different from the SOA_{aq} precursors, and so instead of competing these processes both contribute to the total SOA burden. The relative magnitude of their contributions is a topic of current research and is discussed in section 1.4.

1.3.1 SOA_{OM} – Gas/Particle Partitioning

The traditional view of SOA formation is that organic gases are oxidized photochemically in the gas-phase by hydroxyl (OH) radical, ozone (O_3), or nitrate radical (NO_3), and form products that are more oxidized and polar. If oxidation does not fragment the compound, the volatility of the products is lowered by the addition of polar functional groups. Thus, if the precursor is sufficiently large, one or two oxidation steps produces compounds with low enough vapor pressure to partition into the organic matter of pre-existing particles (SOA_{OM}). According to the gas/particle partitioning described by Pankow et al.[42,43] and applied to SOA by Odum et al.[39], the formation of SOA_{OM} depends on the volatility of the products, temperature, and the organic mass in pre-existing

particles. SOA_{OM} precursors can be from biogenic (e.g. vegetation) or anthropogenic (e.g. gasoline and diesel combustion, meat cooking) sources, but must have more than seven carbons in their structure to have high SOA yields[18,44]. According to this theory and early laboratory experiments (e.g., Pandis et al.[45]) the SOA yield from a five-carbon compound like isoprene (C_5H_8) is expected to be small. However, because global isoprene emissions are high (~600 Tg yr^{-1})[46], even with low SOA yields the contribution of isoprene to organic PM in our atmosphere is substantial (14-19 Tg yr^{-1} of SOA; Henze and Seinfeld[47]; Carlton et al.[48] and references therein).

SOA_{OM} yields derived from dry smog chamber experiments have been gathered throughout the years and used in air quality and climate models; however, these models frequently underpredict the measured atmospheric OA mass (e.g., Tsigaridis and Kanakidou[49]; Heald et al.[50]). These models also fail to capture the variance in observations[51] as well as the vertical profile of OA (Heald et al.[52] and references therein). Also, the oxidation state (e.g. oxygen-to-carbon ratio [O/C ratio] or organic mass/organic carbon OM/OC] ratio) of SOA_{OM} is much lower than O/C and OM/OC ratios found in atmospheric OA[53,54]. Additionally, in SOA_{OM} modeling studies, the enthalpy of vaporization is used as a parameter that characterizes the temperature sensitivity of SOA yields. These values are highly uncertain (due to the complexities of measuring properties for a composite of products), and become a significant source of uncertainty in predicting SOA budgets, especially the vertical distributions of SOA, which are directly affected by temperature changes[49].

Discrepancies in properties, magnitude, and variability between atmospheric OA and SOA_{OM} suggest that there are missing pathways to SOA formation. SOA_{aq} helps to resolve these discrepancies, as discussed in the following sections.

1.3.2 SOA_{aq} – Aqueous-Phase SOA Formation

About a decade ago Blando and Turpin[13] hypothesized that secondary organic aerosol forms through aqueous chemistry in clouds and fogs. Following the well-studied formation of particulate sulfate from aqueous-phase oxidation of SO_2 in clouds (Lamb et al.[17]; Burkhard et al.[55]; Finlayson-Pitts and Pitts[20] and references therein), Blando and Turpin[13] proposed a similar atmospheric process for secondary organic particulate matter (see Figure 1-1). The argument that SOA can be formed through aqueous photooxidation reactions in cloud and fog water was supported by the following observations: (1) organic compounds can be sorbed into suspended cloud/fog droplets and have been measured in those media, (2) dissolved organics can participate in aqueous-phase oxidation reactions, and (3) organic PM has been detected in droplet mode particles – a size mode formed through volume phase reactions (i.e., associated with cloud processing)[56-58]. More specifically, reactive organic gases (e.g., VOCs like alkenes and aromatics) are oxidized (e.g., by hydroxyl radicals) in the interstitial spaces of clouds and form highly water-soluble compounds (e.g., aldehydes)[20]. These compounds dissolve into atmospheric liquid water and undergo photooxidation reactions (e.g., with dissolved hydroxyl (OH) radicals)[59], forming less volatile organics (e.g., carboxylic acids and oligomers)[60-63]. The fact that these same compounds are found in atmospheric particles suggests that they remain in the particle-phase when cloud droplets evaporate. [This process is also

commonly referred to as *cloud processing* or *in-cloud SOA formation*, used interchangeably in this dissertation.]

In contrast to SOA_{OM} precursors, the precursors involved in SOA_{aq} are small, highly polar, water-soluble compounds that readily dissolve in atmospheric waters and participate in oxidation reactions. SOA_{aq} studies have been focused on water-soluble products formed from the gas-phase oxidation of isoprene, toluene, and xylene by hydroxyl radicals ($^{\bullet}OH$). The most commonly studied SOA_{aq} precursors are glyoxal, methylglyoxal, glycolaldehyde, pyruvic acid, acetic acid, methacrolein, methyl vinyl ketone, and phenols, which upon aqueous $^{\bullet}OH$ oxidation form low volatility products including organic acids and oligomers that are expected to remain at least in part in the particle-phase after water evaporation, forming SOA_{aq}[41,60,61,63-69]. Laboratory and modeling studies have examined the underlying aqueous chemistry in both the dilute aqueous-phase (e.g., in cloud droplets) and at higher organic concentrations (e.g., in aerosol water). A compilation of SOA_{aq} laboratory, field, and modeling studies conducted over the past decade are summarized by Ervens et al.[41] and Gong et al.[70] review papers. Section 1.4 discusses the major advancements in our understanding of SOA_{aq} formation.

1.4 Current Knowledge of SOA_{aq} Formation

Major advancements in our understanding of SOA_{aq} include: (1) more evidence that SOA_{aq} is important in the atmosphere, and (2) better chemical understanding about the properties of SOA_{aq}, for example that oxidation of aldehydes forms organic acids/salts in clouds but oligomers in aerosol water[149]. Accumulating evidence on the degree of oxidation and loading of SOA_{aq} suggests that this recently accepted formation pathway helps to resolve discrepancies between observed SOA and SOA formed from

traditional gas-phase oxidation mechanisms (SOA_{OM}). Also, recent incorporation of SOA_{aq} formation into several global and regional air quality models has helped to bring better agreement between measured OA and atmospheric model predictions[11,70,103-106,109]. However, there are still large limitations in the modeling of SOA_{aq}. This work will improve SOA modeling by providing information on SOA_{aq} mass yields and physicochemical properties (i.e., vapor pressure and enthalpy of vaporization), which are currently very limited.

1.4.1 Evidence of SOA_{aq} Formation from Field Observations

SOA_{aq} could help explain the high oxidation states observed in atmospheric OA. O/C and OM/OC ratios of ambient total OA typically range between 0.2 – 1 and 1.6 – 2.51, respectively[34,53,71-73]. Aiken et al.[74] showed that elemental ratios (e.g., O/C and OM/OC) could be estimated for ambient aerosols (measured during the MILAGRO campaign in Mexico City), by using relative intensities of chemically identified ion fragments analyzed by a high-resolution time-of-flight aerosol mass spectrometer (HR-ToF-AMS). Aiken et al.[53] then furthered this HR-ToF-AMS analysis by incorporating positive matrix factorization (PMF) to the aerosol dataset collected during MILAGRO. They found four major OA components for which they were able to measure the O/C and OM/OC ratios: hydrocarbon-like organic aerosol (HOA; surrogate of primary combustion OA), two types of oxygenated organic aerosol (OOA-I and OOA-II; surrogates of "aged" and "fresher" SOA, respectively), and biomass burning organic aerosol (BBOA). They interpreted OOA-I (aka low-volatility OOA; LV-OOA) as aged regional OA because it had the highest O/C and OM/OC ratios compared to the other components (O/C = 0.83 – 1.02; OM/OC ≈ 2.3 – 2.5). The high OM/OC ratios found for LV-OOA by Aiken et al.[53]

correspond with values previously reported by Turpin and Lim[71] and Polidori et al.[72] for the water-soluble fraction of aged ambient OA (OM/OC = 2.1 – 2.54), in Pittsburgh, PA in the summertime PAQS. In contrast, O/C ratios of laboratory-generated SOA_{OM} (produced in smog chamber experiments with anthropogenic and biogenic precursors) are lower (between 0.27 – 0.7) than those observed for low-volatility OA (LV-OOA) [53,75-77]. Interestingly, typical O/C and OM/OC ratios measured for laboratory-generated SOA_{aq} are about 0.69 – 2 and 1.0 – 3.8, respectively (as discussed in section 1.4.3), coinciding with typical oxidation states of the LV-OOA and the water-soluble fraction of aged ambient OA. Overall, the oxidation state of SOA_{aq} is higher than SOA_{OM} and more like aged atmospheric aerosols (LV-OOA). These observations suggest that LV-OOA could be a good surrogate for SOA formed through aqueous chemistry.

In addition to the similarities in properties between laboratory-generated SOA_{aq} and atmospheric aerosol LV-OOA, SOA_{aq} products measured in laboratory experiments are also important components measured in atmospheric aerosols, consistent with the hypothesis that SOA_{aq} is important in our atmosphere. For example, humic-like substances (e.g., oligomers and HWMC) are the largest component of water-soluble organic carbon in ambient aerosols (up to 72% on a carbon basis; Graber and Rudich[78], Lin et al.[79] and references therein); they are measured in clouds[80], fogs[81,82], and rainwater[83], and can also form through aqueous-phase reactions of SOA_{aq} precursors, as discussed in more detail in section 1.4.3. The same can be said about one of the main SOA_{aq} products, oxalate, which is the most abundant water-soluble dicarboxylic acid found in ambient aerosols and atmospheric waters (e.g., Sorooshian et al.[84]; Collett et al.[85] and references therein). Additionally, oxalate measured in clouds (e.g., continental

clouds[86] and marine clouds[87]) and aerosols[88] has been strongly correlated with sulfate, which is primarily formed through cloud processing. Furthermore, oxalate concentrations[84,87], as well as the ratio of oxalate to sulfate mass[89], and the ratio of oxalate to organic mass[90] are higher above-clouds than below-clouds (e.g., increase with altitude), suggesting an in-cloud production. Also, particles containing oxalate have been measured in the droplet mode (0.5 – 1 μm in diameter)[87,91,92], a mode formed through volume-phase reactions (e.g., in-clouds)[56-58]. Finally, enrichment of oxalic acid when aerosol liquid water content is high provides additional atmospheric evidence for SOA_{aq} formation[89,93]. These studies suggest that, although oxalate may represent only a small fraction of the overall OA, it is potentially an important tracer for SOA_{aq} by cloud processing.

Aerosol liquid water content (LWC) has recently been suggested as a parameter to look for evidence of SOA_{aq}. Field observations during the summer time in Atlanta, Georgia, indicate that the fraction of water-soluble organic carbon measured in the particle-phase ($WSOC_p$) (used as a surrogate of SOA in this region)[94] had a strong dependence on RH suggesting a dependence on aerosol LWC (i.e., $WSOC_p$ and estimated LWC increased dramatically with RH > 70%)[95,96]. Additionally, Hennigan et al.[97] and Zhang et al.[96] observed that at RH > 70%, the $WSOC_p$ was not correlated with particulate organic mass (OM), contrary to what would have been expected for SOA_{OM} based on partitioning theory[39,42]. On the other hand, at RH < 70% the relationship between the fraction of $WSOC_p$ and particulate OM was nearly linear. This suggests that secondary organic aerosol formed because water-soluble compounds partitioned into and reacted in particle water (absorbing phase) when sufficient LWC was present (i.e., high RH), and

because semi-volatile compounds partitioned into the OM-absorbing-phase at drier conditions. These findings are important for two reasons. First, the sudden increase of particle-phase WSOC at RH > 70%, which was greater than expected based solely on Henry's law partitioning, is consistent with expectations for SOA_{aq} formation. Second, the observation that $WSOC_p$ (SOA surrogate in Atlanta) had no clear dependence on particle OM suggests the importance of an additional SOA (other than SOA_{OM}) formation process, like SOA_{aq}. Moreover, recent comparisons of case field studies by Ervens et al.[41] and Zhang et al.[96] indicate that $WSOC_p$ measured in Los Angeles is independent of RH and correlates well with OM, contrary to Atlanta and indicative of partitioning theory of SOA_{OM} as the dominant formation process of SOA in that region. In contrast, the measurements of Hersey et al.[98] show that summertime marine-influenced periods in the Los Angeles basin experience high OM concentrations and droplet mode OM and sulfate in contrast to hot dry periods where the OM is found in the condensation mode. This suggests there are times when SOA_{aq} formation occurs even in Los Angeles.

Additional examples of locations that provide evidence of SOA_{aq} include Whistler, Canada, and Mexico City, Mexico. Whistler, like Atlanta, is influenced by biogenic emissions. A recent study conducted at this site provides further evidence that aqueous chemistry is important in SOA formation and aging in our atmosphere[99]. It is the first study to conduct aqueous hydroxyl radical ($^{\bullet}OH$) oxidation of the water-soluble fraction of fresh/aged biogenic SOA, plus of ambient cloud water samples, and evaluate their relation to laboratory-generated SOA_{aq} (i.e., from $^{\bullet}OH$ oxidation of glyoxal and mixtures of glyoxal with *cis*-pinonic acid and α-pinene SOA components). They used aerosol mass spectrometry (AMS) data to evaluate the evolution pathways of aqueous

•OH oxidation of ambient SOA and cloud water, by using the AMS-based observational framework created by Ng et al.[54] for the characterization of ambient OOA. The evolution of laboratory-generated SOA_{aq} was also evaluated using the latter framework. They found that the aging and characteristics of the ambient OA and cloud water organics was better portrayed by the aqueous •OH oxidation of biogenic SOA in the presence of glyoxal, and could not be accurately represented by the individual aqueous oxidation of glyoxal, *cis*-pinonic acid or α-pinene SOA. Furthermore, observations by Ng et al.[100] indicate that ambient OA converges towards highly aged LV-OOA with atmospheric oxidation, and the study by Lee et al.[99] suggests this happens through aqueous oxidation of ambient organics. The latter study is the first of its kind to directly compare field and laboratory observations of SOA_{aq}. In a related development, Mexico City has been a site used by earlier researchers to make comparisons between field observations and model predictions, and has provided perhaps the first evidence of aqueous chemistry contribution to the total SOA (as discussed in more detail below, section 1.4.2).

1.4.2 Modeling Studies

There are several modeling studies that have emerged in the past decade trying to elucidate the magnitude and relevance of SOA_{aq}, but maybe one of the first modeling studies to provide observational evidence suggesting a missing SOA formation process was by Volkamer et al.[101]. Their study compared measured SOA formation from the Mexico City Metropolitan Area (MCMA) 2003 field campaign with modeled SOA calculated using a multicomponent (traditional) gas-particle partitioning model. They found that their model substantially underpredicted observed SOA amounts and those differences in measured-to-predicted SOA increase with photochemical age (i.e., longer

$^{\bullet}$OH oxidation). They also evaluated results from other state-of-the-art SOA models available at that time (that only accounted for traditional SOA; SOA_{OM}) and showed that the modeled SOA from these models were one to two orders of magnitude lower than measured SOA (Volkamer et al.[101] and references therein). Those modeling studies led to believe that the precursors and chemical pathways of SOA formation were far from being fully represented in models. The awareness of a missing source of SOA motivated studies to consider other unthought-of SOA precursors as potential contributors to SOA. For example, Volkamer et al.[102] evaluated glyoxal ($C_2H_2O_2$), which is highly volatile and does not qualify as a good SOA_{OM} precursor, as discussed in section 1.3.1. The latter study found a missing sink of glyoxal in the models as evidenced by significantly lower observed concentrations of glyoxal. In light of these findings, it was suggested that the reactive uptake of glyoxal by aerosol (e.g., by aqueous-phase processing) could contribute at least 15% of the total SOA in Mexico City. Overall, the constant underprediction[44,49,50,101] of atmospheric SOA mass from models that only consider SOA_{OM} formation has led current modeling studies to include SOA_{aq} formation.

The relative magnitude of SOA_{OM} and SOA_{aq} contribution to the total SOA burden is a topic of current research, and studies generally agree that SOA_{aq} contributes to the total SOA mass observed in the atmosphere. Recent modeling studies have found comparable amounts of SOA_{OM} and SOA_{aq} globally and in certain regions, although uncertainties are large[11,12,70,103-106]. One of the earliest regional modeling studies to incorporate cloud chemistry was conducted by Chen et al.[103], which coupled new aqueous-phase chemistry mechanisms (AqChem) with gas-phase chemistry mechanisms from Caltech Atmospheric Chemistry Mechanism (CACM) and the Model to Predict the

Multiphase Partitioning of Organics (MPMPO). The AqChem was incorporated into a zero-dimensional model as well as into a three-dimensional Community Multiscale Air Quality Model (CMAQ) to simulate SOA formation. After adding the aqueous in-cloud SOA mechanism of isoprene, they observed a 27% increase in predicted SOA formation for rural northeastern U.S. (with strong biogenic emissions) during August 2004, and 7% for an urban scenario with strong anthropogenic emissions. Similarly, Carlton et al.[11] added in-cloud SOA_{aq} formation using fixed yields into a regional-scale atmospheric model (CMAQ) to simulate SOA formation with altitude over the northeastern U.S. and to validate its predictions by simulating and comparing with aircraft measurements taken during the International Consortium for Atmospheric Research on Transport and Transformation (ICARTT) campaign in summer 2004. Even though this study did not use an explicit representation of aqueous chemistry, they found reduced bias and improved correlation (better captured variance) between measurements and model predictions of OC for every flight. Subsequently, Carlton et al.[109] made substantial improvements to the previous CMAQ model[11] by adding newly recognized SOA precursors (i.e., benzene, isoprene, and sesquiterpenes). In-cloud oxidation of glyoxal and methylglyoxal were included as described above. They compared temporal and seasonal predictions of secondary organic carbon to semi-empirical estimates from routinely monitored sites across the continental U.S. This study showed that the new robust model had a better temporal and seasonal prediction of SOA, but that a negative bias still remained mainly for the summer season. Furthermore, recently the AURAMS model (A Unified Regional Air-quality Modeling System, from Environment Canada) was used to get a broad idea of how cloud processing of organic gases might impact predictions of OA on a regional

scale over North America[70]. Their 2-month (from 1 July to 31 August 2004) simulation showed that the addition of cloud uptake and processing of organic gases results in a reduced negative bias and an improved correlation between modeled $PM_{2.5}$ OA and observations from the IMPROVE network data. They concluded that in-cloud processing of water-soluble organics is an important contributor to OA, in addition to the traditional SOA_{OM} pathway. Another recent study contrasting SOA_{aq} and SOA_{OM} yields and mass contributions supports the conclusion that SOA_{aq} (~60 ng m^{-3}) and SOA_{OM} (~ 80 – 100 ng m^{-3}) both contribute in areas like the Amazon that are dominated by biogenic emissions[41]. They expect SOA_{aq} to be most important in regions with high relative humidity (RH > ~60%) and during photochemical activity of biogenic emissions with some anthropogenic influences (e.g., highest aldehyde-precursor yields at high NO_x), like for example in the Southeast U.S. or the Brazilian Amazon.

Global modeling studies have also recently incorporated SOA_{aq} formation and found better agreements between model predictions and atmospheric observations. Fu et al.[106] used estimates of OA from a global three-dimensional atmospheric chemistry model (GEOS-Chem)[12] to simulate surface and aircraft measurements of OC from the ICARTT campaign with the objective of evaluating SOA formation via reactive wet aerosol uptake of dicarbonyl gases like glyoxal and methylglyoxal. They treated SOA_{aq} formation as a reactive uptake of glyoxal and methylglyoxal by clouds and aqueous particles (surface area controlled) and used reported reactive uptake coefficients from laboratory (dark) chamber studies with sulfate aerosols[107,108]. Fu et al. found that the inclusion of this SOA formation pathway (e.g., reactive uptake) doubled the contribution of SOA to WSOC aerosol at all altitudes, and that 90% of this process occurred in clouds[12]. Moreover, a

recent modeling study has found that in-cloud processing could explain the observed oxalate concentrations globally, and suggested that SOA_{aq} contributes significantly to the global SOA burden[110]. The latter study used a three-dimensional chemistry-transport global model (TM4-ECPL) with comprehensive gas-phase chemistry mechanisms, organic aerosol parameterizations, and aqueous-phase chemical mechanisms from recently published box modeling studies (references therein), to evaluate the spatial and temporal global distribution of oxalate (i.e., a potential tracer of SOA_{aq}, as discussed in section 1.4.1). The latest studies incorporating SOA_{aq} formation into global models include Liu et al.[104], Lin et al.[105], and He et al.[111]. Liu et al.[104] also found comparable global contributions from in-cloud SOA_{aq} production (23 Tg yr^{-1}; during the years around 2000) and gas-phase SOA_{OM} production (20–30 Tg yr^{-1}). They included detailed cloud chemistry from glycolaldehyde, glyoxal, methylglyoxal and acetic acid into the GFDL (Geophysical Fluid Dynamics Laboratory) global coupled chemistry-climate model (AM3) and found that the largest sources of SOA_{aq} were gas-phase glycolaldehyde (9 Tg yr^{-1}) and acetic acid (7 Tg yr^{-1}). Based on the framework by Liu et al.[104], He et al.[111] examined potential determinants of the global spatial and temporal distribution of in-cloud SOA_{aq} formation: liquid water content (LWC), the chemical loss rate of total carbon mass (TC_{loss}), temperature, the concentration of OH and O_3, and the VOC to NO_x ratio. They found that (1) LWC and TC_{loss} are most strongly correlated with in-cloud SOA production, (2) LWC alone determines the spatial distribution of in-cloud SOA_{aq} production, mostly over the tropical, subtropical, and temperate forest regions, (3) TC_{loss} mainly represents the seasonal variability of vegetation growth and the rate of gas-phase chemical reactions, and that (4) the production of in-cloud SOA_{aq} responded linearly to

the spatiotemporal distribution of LWC, but non-linearly (concavely) to TC_{loss}, indicating the contribution from liquid-phase processes and gas-phase processes, respectively. Note that liquid water (in aerosol, clouds, and fog) is atmospherically abundant. The mass of aerosol water is predicted to be 2 to 3 times the mass of dry particles globally[112], and depends not only of RH but also on aerosol hygroscopicity. Globally, liquid water is more abundant than particulate organic matter.

Overall, these modeling studies demonstrate that the inclusion of aqueous-phase chemistry in models can improve the predicted magnitude, spatial, vertical, and temporal distribution, and better capture the variability and properties of SOA. Additionally, they predict comparable amounts of SOA_{OM} and SOA_{aq} globally and locally. Although progress continues in the field of atmospheric modeling, there remains a limited understanding of the precursors and chemistry of SOA_{aq} and of the gas-particle partitioning of cloud OM upon droplet evaporation. These limitations could lead to significant biases in the magnitude, spatial, vertical, and temporal OA distributions, as well as properties of OA mass, and hamper efforts to develop effective control strategies.

While refined treatment of SOA_{OM} (emissions, reactions and gas-particle partitioning of semi-volatile and intermediate volatility organic compounds, S/IVOCs, have also improved agreement between predicted and measured OA mass[113-115], only SOA_{aq} has been able to explain observed atmospheric SOA properties (e.g., degree of oxidation). A discussion of laboratory-measured SOA_{aq} properties and similarities with atmospheric SOA properties follows (section 1.4.3).

1.4.3 Laboratory Studies

A growing number of laboratory groups now recognize the potential importance of SOA formation through aqueous chemistry in clouds, fogs and wet aerosols, and have put a great effort into documenting the aqueous chemistry of potential precursors[41,60-69,83,99,116-148]. For the most part laboratory experiments have been conducted with individual SOA_{aq} precursors that form lower volatility products through reactions with $^{\bullet}OH$, O_3, NO_3 radicals, UV light, H_2SO_4, amines and ammonium sulfate in the aqueous-phase. These aqueous-phase reactions include radical reactions (e.g., photochemically-initiated) and non-radical reactions (e.g., acid catalyzed)[149].

Radical reactions can involve a variety of atmospheric oxidants like $^{\bullet}OH$, O_3, NO_3 radicals and can also be initiated by photolysis. For example, aqueous-phase $^{\bullet}OH$-initiated reactions of methylglyoxal[63,129,146], glyoxal[61,128,139,146], glycolaldehyde[64,65,144], pyruvic acid[60,62], acetic acid[69], methacrolein[66,123,124], methyl vinyl ketone[67,123,148], and some phenols[68,136] can yield products like mono- and dicarboxylic acids, oligomers, higher molecular weight compounds (HMWC), and phenolic dimers. Organosulfate products have also been identified from $^{\bullet}OH$ oxidation of glycolaldehyde (1 mM) in the presence of sulfuric acid (1 mM)[65], from UV irradiated solutions of glyoxal (~ 0.1 – 1 M) and ammonium sulfate (~6 M)[127], and from sulfate radical formation of UV irradiated solutions of methacrolein (0.1 – 0.5 M), or methyl vinyl ketone (0.1 – 0.5 M) with ammonium- or sodium- sulfate (3.7 M and 1 M, respectively)[121]. Carbon-nitrogen (C-N) containing products were also found under UV irradiated solutions of glyoxal (~ 0.1 – 1 M) and ammonium sulfate (~6 M)[127]. The latter study also detected the formation of C-N

containing products (e.g., imidazole) under non-irradiated conditions, as observed by other studies discussed below.

In the absence of photochemically generated radicals, SOA_{aq} can also form through non-radical reactions such as acid catalysis including imine formation, aldol condensation, hemiacetal formation, anhydrate formation, and esterification. For example, C-N containing compounds (e.g. imidazoles, and light-absorbing C-N containing oligomers) can be formed by reactions between glyoxal and amino acids, ammonium ions, and imines in highly concentrated aqueous solutions[119,126,150,151], wet aerosols[127], and evaporating droplets[130,132]. An extensive discussion of the acid catalysis of glyoxal in the aqueous-phase is provided by Lim et al.[149]. Glyoxal and methylglyoxal can also form oligomers by self-reactions and cross-reactions via both hemiacetal formation and aldol condensation, depending on pH[134,135,152]. The formation of light-absorbing (e.g., C-N) compounds through these non-radical mechanisms could potentially affect the optical properties of atmospheric aerosols and radiative forcing.

New understanding derived from chemical modeling of laboratory studies have distinguished between SOA_{aq} formed through dilute aqueous chemistry (cloud-relevant SOA_{aq}) and at higher organic concentrations (i.e., in wet aerosols). At low cloud-relevant concentrations (< mM) the products of photochemically-initiated reactions are typically small mono- and dicarboxylic acids (e.g., pyruvic, acetic, formic, glycolic, succinic, malonic, and, mainly, oxalic acid), whereas at the higher concentrations of reactive organics found in wet aerosols (~ mM), humic-like substances with many functional groups (e.g., HMWC and oligomers) are formed[69,123,129,149]. Lim et al.[149] argues that although both radical and non-radical reactions (e.g. acid catalysis discussed above) both

occur, organic radical reactions are dominant during daytime because they are fast. In contrast, Nozière et al.[119,120] argues that because ammonium ion (NH_4^+) concentrations are so high in aerosols, NH_4^+ catalysis (non-radical) is able to compete with radical reactions in wet aerosols despite the fact that such reactions are slower. Therefore, the formation of organosulfates, C-N containing products, and oligomers through acid (or ammonium ion) catalysis and through organic radical-radical reactions seems to be important at the high concentration found in wet aerosols and not in cloud water. Nevertheless, as cloud droplets evaporate the concentrations of all the components in the droplet increase, making oligomer formation possible in the outflow of clouds.

The oxidation properties of cloud SOA_{aq} and wet aerosol SOA_{aq} differ somewhat because of differences in their composition. Nevertheless, their O/C and OM/OC ratios are still higher than those of SOA_{OM}, mainly because the precursors for SOA_{aq} formation need to be highly oxidized (polar) in order to be water-soluble. For example, the main products of the aqueous OH radical oxidation of glyoxal and methylglyoxal are oxalate and pyruvate, respectively. Oxalate has an O/C = 2 (OM/OC = 3.8) and pyruvate has an O/C = 1 (OM/OC = 2.4). The O/C and OM/OC ratios of oligomers formed by the photooxidation (and/or photolysis) of methylglyoxal, glycolaldehyde and phenols ranged from 0.69 – 1.06 and 1.0 – 2.55, respectively[63,64,68]. Overall, the O/C and OM/OC ratios of laboratory-generated SOA_{aq} range between 0.69 – 2 and 1.0 – 3.8, respectively. As discussed in section 1.4.1, the oxidation properties of SOA_{aq} are similar to those of ambient low-volatility oxygenated OA (O/C = 0.83 – 1.02; OM/OC = 2.3 – 2.5) and of the water-soluble fraction of aged ambient OA (OM/OC = 2.1 – 2.54), whereas the

typical O/C ratios (0.27 – 0.7) of laboratory-generated SOA_{OM} are not. Again, this suggests that SOA_{aq} is an atmospherically important contributor.

SOA_{aq} formation through cloud processing involves the evaporation of cloud droplets, yet the effect of droplet evaporation on aerosol composition and properties has received little attention to date. Acid catalyzed reactions like hemiacetal formation, aldol condensation, anhydrate formation, and possibly esterification, could occur during cloud droplet evaporation. For example, studies by Loeffler et al.[117] and De Haan et al.[131] have shown that glyoxal molecules can undergo self-reactions to form oligomers via acid catalyzed hemiacetal formation during water evaporation of dilute ($\geq$ 4 μM) aqueous glyoxal droplets. It was shown that glyoxal acetal oligomers can form within minutes of evaporating 1 μm droplets[117] and wet aerosols[107], and that droplet evaporation traps glyoxal in the aerosol-phase (33 ± 11)%[131]. Briefly, during droplet evaporation some hydrated glyoxal becomes dehydrated (forming singly hydrated or dehydrated glyoxal) and reacts with remaining hydrated glyoxal to form a hemiacetal, which then participates in intermolecular reactions to form dimers and trimers. Similarly, methylglyoxal (4 – 1000 μM) can also undergo self-reactions and remain in the aerosol-phase (19 ± 13)% after droplet evaporation via acid catalyzed aldol condensation reactions[131]. Based on these laboratory observations we expect other aldehyde SOA_{aq} precursors (e.g., glycolaldehyde) to undergo similar hemiacetal formation (or aldol condensation) reactions during cloud water evaporation and be retained in aerosol-phase to some extent. This dissertation (outlined in sections 1.6 and 1.7) evaluates the effects that droplet evaporation has on SOA_{aq} mass loadings; with the objective of improving the understanding of SOA formation through cloud processing.

1.5 Critical Knowledge Gaps

Considerable progress has been made (1) elucidating and documenting the aqueous chemistry involved in SOA_{aq}, (2) examining observations for evidence of SOA_{aq} in the atmosphere, and (3) assessing the magnitude of SOA_{aq} through regional and global modeling. However, SOA formation through aqueous chemistry is still a new and rapidly emerging field of study[41,44,70]. Considerable work is needed to reduce model uncertainties and improve linkages between emissions and ambient OA concentrations. In particular, while there are good reasons to believe that glyoxal, methylglyoxal, and glycolaldehyde are important SOA_{aq} precursors and that their daytime (OH radical) cloud chemistry is now understood, there is limited information on how the chemical processes during cloud droplet evaporation impact the formation of SOA through cloud processing. As cloud droplets evaporate, the loss of water increases the concentration of the organics and potentially initiates complex chemistry (e.g., radical-radical and non-radical reactions). Furthermore, the physicochemical properties (e.g., vapor pressure and enthalpies of evaporation) of this OM are needed to understand its gas-particle partitioning after droplet evaporation and therefore predict SOA_{aq} formation in global and regional air quality models.

Droplet evaporation of organic products of aqueous photochemistry – The first laboratory study that combined aqueous photooxidation and droplet evaporation was conducted by El Haddad et al.[124]. They reacted ($2 - 5$ mM) methacrolein with OH radicals (from photolysis of 0.4 M H_2O_2), then nebulized and dried the sample droplets in a mixing chamber and monitored the SOA mass, number, and size distribution. By doing this they proved that products of methacrolein $^{\bullet}OH$ oxidation (e.g., several mono- and

dicarboxylic acids including oxalic acid, dihydroxymethacrilic acid, and unidentified HMWCs and oligomers) remained in the particle-phase forming SOA, and provided a measure of SOA mass yields (2 – 12%; SOA mass per mass of methacrolein reacted). The major limitations of that study were: the need for substantial particle loss corrections, the use of high precursor concentrations (not cloud-relevant conditions), that SOA mass yields were measured from samples after 5 h of reaction, and that OH radical concentrations in the vessel were not known. Note, typical cloud droplet lifetimes are on the order of 10-30 minutes and an air parcel frequently undergoes several (perhaps ten) cloud cycles on a cloudy day[153]. Liu et al.[123] has recently employed the El Haddad et al.[124] method to evaluate methyl vinyl ketone (MVK) and report similar SOA mass yields (4 – 10%) under similar conditions (i.e., 4 mM MVK + ~10^{-13} M $^{\bullet}$OH; 5-20 hours reaction time). In more recent work by Lee et al.[139], the aqueous oxidation of (3 mM) glyoxal with OH radicals (10^{-13} M from photolysis of 13.3 mM H_2O_2) was studied by using a reaction vessel where aqueous solution samples were atomized, passed through a diffusion dryer, and then analyzed by an AMS. This study reported SOA_{aq} mass yields (cumulative mass of formic, glyoxylic and oxalic acid divided by the mass of glyoxal reacted) of 20% at 20 min reaction time and as high as 78% after 5 hrs. They have provided a better chemical characterization and a new mechanistic understanding of glyoxal SOA_{aq}. Nevertheless, since their SOA mass yields were calculated based on quantified products and quantified products did not fully account for the measured total carbon content, the estimated SOA mass yield might be underrepresented due to unidentified products. Overall, a major limitation in current SOA_{aq} studies that combine aqueous chemistry with droplet evaporation is the underrepresentation of products that

are not identified or quantified. More information is needed on the effect that droplet evaporation has on SOA_{aq} mass yields for a variety of precursors not covered by current studies. Also, these types of studies should better simulate cloud-relevant conditions (e.g., precursor concentration and droplet lifetime). In Chapters 2, 3 and 4, I present a novel approach that (1) accounts for aqueous photooxidation + droplet evaporation processes, (2) negates the need to correct for particle loss, and (3) includes any unidentified products. I use this method to report SOA mass yields of glycolaldehyde, glyoxal and methylglyoxal. As discussed earlier (section 1.4), glycolaldehyde, glyoxal and methylglyoxal are potentially important precursors of SOA_{aq} that (1) form low-volatility compounds in aqueous-phase photooxidation reactions, as shown by laboratory studies[61,63-65,99,128,129,139,146], (2) have been identified as a major source of SOA_{aq} by modeling studies (e.g., Liu et al.[104]), and (3) are expected to remain, at least partially, in the aerosol-phase during droplet evaporation[131].

Droplet evaporation of aldehydes (SOA_{aq} precursors) – Glyoxal and methylglyoxal partially dehydrate during droplet evaporation and undergo self-oligomerization by hemiacetal formation and/or aldol condensation, thus contributing to SOA_{aq} formation through cloud droplet evaporation[117,131]. In Chapter 2, I demonstrate that glycolaldehyde is also retained in the aerosol-phase upon droplet evaporation and propose a mechanism in which glycolaldehyde could undergo hemiacetal formation and aldol condensation to produce oligomers. I also confirm the retention of glyoxal in the aerosol-phase from evaporating droplets as observed by Loeffler et al.[117] and De Haan et al.[131].

Volatility and temperature dependence of SOA_{aq} – Before this dissertation virtually no information had been provided concerning the volatility of SOA_{aq}. Only the study by Michaud et al.[125] has come close; they used a Volatility-Hygroscopicity Tandem DMA (VHTDMA) to analyze nebulized solutions of the aqueous mixtures formed by reacting $^{\bullet}OH$ (from photolysis of 0.4 M H_2O_2) and methacrolein (2 – 5 mM). They found that 80% of the volume of methacrolein SOA_{aq} was volatile at 100°C after 5 h of reaction and that the volatility decreased with reaction time (20% after 22 h, at 100°C). This study provided the first quantitative measure of SOA_{aq} volatility. However, cloud droplet lifetimes are minutes, not hours, and the atmospherically-relevant photochemical age is not known, since the concentration of OH radical in the reaction vessel is unknown (it depends not only on H_2O_2, but also on the photon flux from the lamp). As discussed briefly in section 1.3.1, enthalpy of vaporization (ΔH_{vap}) values are used by modeling studies to characterize the temperature dependence of SOA yields; however, they remain highly uncertain and are a significant source of uncertainty in predicting SOA budgets and vertical distributions[49]. Preferably, modeling studies use experimental ΔH_{vap} values that best characterize the properties of all the SOA species being studied (e.g., Carlton et al.[109]); however, when ΔH_{vap} values are unknown, modeling studies rely on various ΔH_{vap} assumptions to best fit the observational data (reaching from physically unrealistic ΔH_{vap} values (<40 kJ/mol) to 150 kJ/mol)[44,52,154]. Currently there are no ΔH_{vap} values reported for SOA_{aq} other than the values conveyed in this dissertation. Chapters 2, 3, and 4 report estimated values of effective enthalpies of vaporization and vapor pressures for the product + precursor mixtures formed by reacting OH radicals with glycolaldehyde, methylglyoxal, or glyoxal. I demonstrate a method to study the gas-particle partitioning

behavior of these mixtures and provide key physicochemical properties that can be used by models to describe the temperature sensitivity of SOA yields.

1.6 Hypothesis and Specific Aims

Hypothesis: A substantial fraction of aqueous (in-cloud) photooxidation products of glycolaldehyde, glyoxal, and methylglyoxal remain in the particle-phase after cloud droplet evaporation, forming secondary organic aerosol (SOA).

To test this hypothesis, the following *specific aims* were addressed:

1. Develop a droplet evaporation experimental method to quantify SOA_{aq} formation from cloud processing.
2. Investigate the aqueous-phase photooxidation of glycolaldehyde by OH radicals and droplet evaporation of the resulting mixtures.
3. Calculate SOA_{aq} mass yields from glycolaldehyde, glyoxal, or methylglyoxal and OH radicals.
4. Estimate the effective vapor pressures and enthalpies of vaporization of aqueous OH radical - glycolaldehyde, glyoxal, and methylglyoxal precursor/product mixtures for two atmospheric scenarios.
5. Examine the effect of ammonium addition on the volatility of SOA_{aq} product mixtures.

1.7 Dissertation Overview

The research presented in this dissertation focuses on SOA formation through cloud water chemistry and droplet evaporation (SOA_{Cld}) and verifies that droplet evaporation enhances SOA production. This work incorporates batch aqueous-phase experiments, chemical analyses, kinetic model outputs, and droplet evaporation

experiments for glycolaldehyde, glyoxal, and methylglyoxal. These precursors were chosen because they are considered potentially important SOA_{Cld} precursors and their aqueous $^{\bullet}OH$ oxidation has been reasonably well studied, as discussed in the previous sections. This dissertation demonstrates for the first time that products of glycolaldehyde and methylglyoxal $^{\bullet}OH$ oxidation remain in the particle-phase after simulated cloud droplet evaporation, thus forming SOA_{Cld}. It also confirms SOA_{Cld} formation through glyoxal $^{\bullet}OH$ oxidation and droplet evaporation. I report mass yields (defined as SOA mass divided by the mass of precursor reacted) of 60–120%, 100–207%, and 5–20% for glycolaldehyde, glyoxal, and methylglyoxal SOA_{Cld}, respectively, for 10-40 min reaction times (i.e., cloud droplet lifetime). This dissertation also provides, for the first time, estimates of effective liquid vapor pressure ($\sim 10^{-7}$ atm) and enthalpy of vaporization (~67–70 kJ/mol) of OM precursor/product mixtures formed from the aqueous OH radical oxidation of glycolaldehyde, glyoxal and methylglyoxal. Neutralization (pH 7) of the glyoxal mixture with ammonium hydroxide increases the mass yield substantially (to 438 ± 84%), and the organic material becomes less volatile (i.e., effective liquid vapor pressure of $\sim(10^{-9} - 10^{-12})$ atm and enthalpy of vaporization ~80–120 kJ/mol). The experimental properties provided in this dissertation can be incorporated into models to predict SOA_{Cld} mass yields and account for the dependence of gas-particle partitioning on temperature. Thus, this work contributes to a refined treatment of in-cloud SOA_{aq} formation in regional and global chemical transport models. SOA_{Cld} is most likely to be important in areas that have high liquid water concentrations, relative humidity, biogenic emissions with anthropogenic influences (e.g., high NO_x conditions), and frequent cloud cover.

Chapter 2 describes the aqueous photooxidation of (1 mM) glycolaldehyde by (~10^{-12} M) OH radicals followed by droplet evaporation. It provides new insights on the chemical characterization of glycolaldehyde SOA_{Cld} and the effect of droplet evaporation on SOA_{Cld} mass yields. It also introduces a novel approach to estimate the effective liquid vapor pressure and enthalpy of vaporization of glycolaldehyde SOA_{Cld}. Reaction samples were identified and quantified by ion chromatography (IC), electrospray ionization mass spectrometry (ESI-MS), and for total organic carbon (TOC), following the methodology of Perri et al.[64]. Organic acid and TOC concentration dynamics agreed reasonably well with those reported previously by Perri et al.[64]. Product samples were analyzed for the first time by coupled IC-ESI-MS to offer new insights into glycolaldehyde cloud chemistry, and by a vibrating orifice aerosol generator (VOAG) to generate droplets of solution and simulate the cloud droplet evaporation. New IC-ESI-MS results verify the formation of glycolic and oxalic acid in the mechanism published in Lim et al.[155] While Perri et al.[64] reported the formation of succinic and malonic acid based on IC alone, IC-ESI-MS analysis reported herein revealed that the main contributing species in these IC peaks were malic and malonic acids. Note "malonic and tartaric acids" coelute, as do "succinic and malic acids." VOAG analyses allowed, for the first time, the evaluation of SOA_{Cld} mass yields that include any unidentified compounds (e.g., HMWCs) and any chemistry that occurs during droplet evaporation. SOA_{Cld} yields were highest (~80–120%) at reaction times (~10–20 min) that are typical of cloud droplet lifetimes (one cloud processing cycle). Results were consistent with the existence of additional chemistry during droplet evaporation enhancing SOA_{Cld} production (e.g., oligomerization of aldehydes). The volatility assessment indicates that aqueous glycolaldehyde + $^{\bullet}OH$

precursor/product mixtures behaves like a dicarboxylic acid, with a liquid vapor pressure of $\sim 10^{-7}$ atm and the enthalpy of vaporization of $\sim$70 kJ/mol. The results obtained from these experiments suggest that the aqueous-phase processing of glycolaldehyde followed by droplet evaporation could be an important source of SOA_{aq}.

Chapter 3 describes the volatility of the precursor/product mix formed after 10 min of glyoxal cloud processing (5 μM glyoxal + $\sim 10^{-12}$ M $^{\bullet}OH$) with the use of kinetic modeling and droplet evaporation experiments. For the first time, estimates of fundamental physicochemical properties (vapor pressure and enthalpy of vaporization) are provided for this mixture, which includes glyoxal, its oxidation products (i.e., glyoxylic and oxalic acids), and any additional chemistry that occurs in the evaporating droplets. Thanks to the collaboration of Dr. Yong B. Lim, laboratory-validated kinetic models were used to predict the precursor/product mix present after 10 min of cloud processing (about 1 cloud processing cycle). Two atmospheric scenarios were considered that assumed: (1) depletion of glyoxal in the cloud droplet (Batch Reactor) or (2) continuous replacement of glyoxal in the droplet (Continuously Stirred-Tank Reactor; CSTR). Mimic solutions were prepared based on model results and analyzed by the droplet evaporation methodology (VOAG) developed in Chapter 2. The volatility was insensitive to the assumptions made to model the droplet composition: estimated vapor pressure and enthalpy of vaporization were $\sim 10^{-7}$ atm and ~70 kJ/mol, respectively, for Batch and CSTR scenarios. These estimates are in line with the properties of the main product, oxalic acid ($\sim 10^{-7}$ atm and 67 kJ/mol). This work also provides the first evaluation of the influence of ammonium hydroxide (i.e., neutralization, pH 7) on the volatility of the glyoxal + $^{\bullet}OH$ mixture. Neutralization to pH 7 (salt formation) reduced

the effective liquid vapor pressure to about 10^{-9} – 10^{-12} atm and increased the enthalpy of vaporization to about 80 – 120 kJ/mol, consistent with the vapor pressure of ammonium oxalate (~10^{-11} atm). Salt formation appears to have a large effect on the gas-particle partitioning of the product mixture and therefore on the yield of glyoxal SOA_{Cld}. These findings suggest that the gas-particle partitioning of the SOA_{Cld} mixture is highly dependent on the chemical form of the organic products (acid vs. salt), and that glyoxal SOA_{Cld} could be an important source of SOA_{aq}, especially at high ammonia levels.

Chapter 4 provides the first reported estimates of the volatility of the precursor/product mix formed after 10-30 min of methylglyoxal (MGly) cloud processing (5 µM MGly + ~10^{-12} M $^{\bullet}$OH). Kinetic modeling and droplet evaporation experiments were conducted, as in Chapter 3. Model runs were done thanks to the help of Dr. Yong B. Lim. I provide liquid vapor pressure and enthalpy of vaporization estimates for the MGly + $^{\bullet}$OH precursor/product mix through droplet evaporation experiments (VOAG method) of mimic solutions (from model results). The influence of ammonium hydroxide (i.e., neutralization, pH 7) on the volatility of the MGly + $^{\bullet}$OH mixture was also evaluated for the first time. Results from VOAG suggest that 10-30 minutes of in-cloud MGly oxidation produces an organic mixture with an effective vapor pressure of (4±7) x 10^{-7} atm at pH 3, which is essentially unaffected by the addition of ammonium hydroxide (neutralization to pH 7). The latter observation contrasts the strong neutralization effect observed in Chapter 3 for the volatility of glyoxal + $^{\bullet}$OH mixture. Thanks to a collaboration with Dr. V. Faye McNeill and Dr. Allison Schwier (Columbia University, NY), an Aerosol Chemical Ionization Mass Spectrometer (Aerosol-CIMS) was used to estimate the enthalpies of vaporization of individual products in the MGly SOA_{Cld} mix

(pyruvic acid and oxalic acid + MGly). The individual enthalpies of vaporization of pyruvic acid and oxalic acid + MGly (from Aerosol-CIMS) were smaller than the theoretical enthalpies of the pure compounds and smaller than that estimated for the entire precursor/product mix (from VOAG method). These results show that for one cloud cycle the MGly + $^{\bullet}$OH precursor/product mix (even neutralized) has an intermediate vapor pressure, meaning that a majority of this organic mixture will not remain in a dry particle after droplet evaporation. Lower temperatures, higher RH to retain liquid water and water-soluble compounds, longer contact times (i.e., multiple cloud cycles) to form oxalate, continued chemistry in resulting wet aerosols (i.e., to form oligomers), and/or formation of lower volatility salts or complexes (e.g., with pyruvate) will decrease the vapor pressure and increase the yield of MGly SOA_{Cld}. These findings indicate that, under the conditions studied here and in Chapter 3 (one cloud cycle and neutralization by ammonium hydroxide), MGly is a lower yield precursor compared to glyoxal. A remaining uncertainty is why pyruvate in the atmosphere appears to be more than 50% in the particle-phase, whereas in these experiments pyruvate was more volatile.

Conclusions, future directions and atmospheric implications for research concerning SOA_{aq} formation through cloud chemistry and cloud droplet evaporation are provided in Chapter 5. This research demonstrates that OA does in fact form as a result of aqueous-phase processing of water-soluble compounds and characterizes some key physicochemical properties of SOA_{aq} that can be used in models to describe its evolution in the atmosphere. This work helps to explain the existence of layers of particulate pollution above clouds[89], which have an enhanced impact on the Earth's energy balance[156]. Finally, this work provides insights into condensed-phase photochemical

reactions that form secondary organic particulate matter in our atmosphere.

1.8 References

(1) Turpin, B. J.; Huntzicker, J. J. Identification of secondary organic aerosol episodes and quantitation of primary and secondary organic aerosol concentrations during SCAQS. *Atmospheric Environment* **1995**, *29*, 3527–3544.

(2) Turpin, B. J.; Saxena, P.; Andrews, E. Measuring and simulating particulate organics in the atmosphere: problems and prospects. *Atmospheric Environment* **2000**, *34*, 2983–3013.

(3) Kanakidou, M.; Seinfeld, J. H.; Pandis, S. N.; Barnes, I.; Dentener, F. J.; Facchini, M. C.; Van Dingenen, R.; Ervens, B.; Nenes, A.; Nielsen, C. J.; Swietlicki, E.; Putaud, J. P.; Balkanski, Y.; Fuzzi, S.; Horth, J.; Moortgat, G. K.; Winterhalter, R.; Myhre, C. E. L.; Tsigaridis, K.; Vignati, E.; Stephanou, E. G.; Wilson, J. Organic aerosol and global climate modelling: a review. *Atmos. Chem. Phys.* **2005**, *5*, 1053–1123.

(4) Polidori, A.; Turpin, B. J.; Lim, H.-J.; Cabada, J. C.; Subramanian, R.; Pandis, S. N.; Robinson, A. L. Local and Regional Secondary Organic Aerosol: Insights from a Year of Semi-Continuous Carbon Measurements at Pittsburgh. *Aerosol Science and Technology* **2006**, *40*, 861–872.

(5) Zhang, Q.; Jimenez, J. L.; Canagaratna, M. R.; Allan, J. D.; Coe, H.; Ulbrich, I.; Alfarra, M. R.; Takami, A.; Middlebrook, A. M.; Sun, Y. L.; Dzepina, K.; Dunlea, E.; Docherty, K.; DeCarlo, P. F.; Salcedo, D.; Onasch, T.; Jayne, J. T.; Miyoshi, T.; Shimono, A.; Hatakeyama, S.; Takegawa, N.; Kondo, Y.; Schneider, J.; Drewnick, F.; Borrmann, S.; Weimer, S.; Demerjian, K.; Williams, P.; Bower, K.; Bahreini, R.; Cottrell, L.; Griffin, R. J.; Rautiainen, J.; Sun, J. Y.; Zhang, Y. M.; Worsnop, D. R. Ubiquity and dominance of oxygenated species in organic aerosols in anthropogenically-influenced Northern Hemisphere midlatitudes. *Geophys. Res. Lett.* **2007**, *34*, L13801.

(6) IPCC *Climate Change 2007: The Physical Science Basis*, Contribution of Working Group I to the Fourth Assessment Report of the Intergovernmental Panel on Climate Change (IPCC), edited by S. Solomon et al., Cambridge University Press, Cambridge, U.K., **2007**.

(7) U.S. EPA. Integrated Science Assessment for Particulate Matter (Final Report); U.S. Environmental Protection Agency (U.S. EPA), Washington, DC, EPA/600/R-08/139F, **2009**, 1–2228.

(8) NARSTO. McMurry, P., Shepherd, M., Vickery, J. *Particulate Matter Assessment for Policy Makers: A NARSTO Assessment*; Cambridge University Press, Cambridge, U.K., **2004**.

(9) McMurry, P. H.; Zhang, X.; Lee, C.-T. Issues in aerosol measurement for optics assessments. *J. Geophys. Res.* **1996**, *101*, 19189–19197.

(10) U.S. EPA. *Air Quality Criteria for Particulate Matter*; United States Environmental Protection Agency (U.S. EPA), Research Triangle Park, NC, **2004**.

(11) Carlton, A. G.; Turpin, B. J.; Altieri, K. E.; Seitzinger, S. P.; Mathur, R.; Roselle, S. J.; Weber, R. J. CMAQ Model Performance Enhanced When In-Cloud Secondary Organic Aerosol is Included: Comparisons of Organic Carbon Predictions with Measurements. *Environmental Science & Technology* **2008**, *42*, 8798–8802.

(12) Fu, T.-M.; Jacob, D. J.; Wittrock, F.; Burrows, J. P.; Vrekoussis, M.; Henze, D. K. Global budgets of atmospheric glyoxal and methylglyoxal, and implications for formation of secondary organic aerosols. *J. Geophys. Res.* **2008**, *113*, D15303.

(13) Blando, J. D.; Turpin, B. J. Secondary organic aerosol formation in cloud and fog droplets: a literature evaluation of plausibility. *Atmospheric Environment* **2000**, *34*, 1623–1632.

(14) Friedlander, S. K. Smoke, Dust, and Haze: Fundamentals of Aerosol Dynamics. *Oxford University Press*, New York, **2000**.

(15) Seinfeld, J. H.; Pandis, S. N. Atmospheric Chemistry and Physics: From Air Pollution to Climate Change. *John Wiley & Sons*, New York, **1998**.

(16) Warneck, P. Chemistry of the natural atmosphere. International Geophysical Series. *Academic Press*, San Diego, California, USA, **2000**, *71*, 346–450.

(17) Lamb, D.; Miller, D. F.; Robinson, N. F.; Gertler, A. W. The importance of liquid water concentration in the atmospheric oxidation of SO2. *Atmospheric Environment* **1987**, *21*, 2333–2344.

(18) Seinfeld, J. H.; Pankow, J. F. Organic Atmospheric Particulate Material. *Annu. Rev. Phys. Chem.* **2003**, *54*, 121–140.

(19) Robinson, A. L.; Donahue, N. M.; Shrivastava, M. K.; Weitkamp, E. A.; Sage, A. M.; Grieshop, A. P.; Lane, T. E.; Pierce, J. R.; Pandis, S. N. Rethinking Organic Aerosols: Semivolatile Emissions and Photochemical Aging. *Science* **2007**, *315*, 1259–1262.

(20) Finlayson, B. J.; Pitts, J. N., Jr Chemistry of the Upper and Lower Atmosphere: Theory, Experiments, and Applications. *Academic Press*, San Diego, California, USA, **2000**.

(21) Kulmala, M.; Vehkamäki, H.; Petäjä, T.; Dal Maso, M.; Lauri, A.; Kerminen,

V. M.; Birmili, W.; McMurry, P. H. Formation and growth rates of ultrafine atmospheric particles: a review of observations. *Journal of Aerosol Science* **2004**, *35*, 143–176.

(22) Kurtén, T.; Loukonen, V.; Vehkamäki, H.; Kulmala, M. Amines are likely to enhance neutral and ion-induced sulfuric acid-water nucleation in the atmosphere more effectively than ammonia. *Atmos. Chem. Phys.* **2008**, *8*, 4095–4103.

(23) Smith, J. N.; Barsanti, K. C.; Friedli, H. R.; Ehn, M.; Kulmala, M.; Collins, D. R.; Scheckman, J. H.; Williams, B. J.; McMurry, P. H. Atmospheric Chemistry Special Feature: Observations of aminium salts in atmospheric nanoparticles and possible climatic implications. *Proceedings of the National Academy of Sciences* **2010**, *107*, 6634–6639.

(24) Dawson, M. L.; Varner, M. E.; Perraud, V.; Ezell, M. J.; Gerber, R. B.; Finlayson-Pitts, B. J. Simplified mechanism for new particle formation from methanesulfonic acid, amines, and water via experiments and ab initio calculations. In; 2012; Vol. 109, pp. 18719–18724.

(25) Charlson, R. J.; Schwartz, S. E.; Hales, J. M.; Cess, R. D.; Coakley, J. A.; Hansen, J. E.; Hoffman, D. J. Climate Forcing by Anthropogenic Aerosols. *Science* **1992**, *255*, 423–430.

(26) Sisler, J. F.; Malm, W. C. The relative importance of soluble aerosols to spatial and seasonal trends of impaired visibility in the United States. *Atmospheric Environment* **1994**, *28*, 851–862.

(27) Schwartz, J.; Dockery, D. W.; Neas, L. M. Is Daily Mortality Associated Specifically with Fine Particles? *Journal of the Air & Waste Management Association* **1996**, *46*, 927–939.

(28) Englert, N. Fine particles and human health—a review of epidemiological studies. *Toxicology Letters* **2004**, *149*, 235–242.

(29) Pope, C. A., III; Ezzati, M.; Dockery, D. W. Fine-particulate air pollution and life expectancy in the United States. *New England Journal of Medicine* **2009**, *360*, 376–386.

(30) Pope, C. A., III; Dockery, D. W. Health effects of fine particulate air pollution: lines that connect. *Journal of Air & Waste Management* **2006**, *56*, 709–742.

(31) NRC Research Priorities for Airborne Particulate Matter: Continuing Research Progress. National Research Council (US). Committee on Research Priorities for Airborne Particulate Matter. **2004**.

(32) Monks, P. S.; Granier, C.; Fuzzi, S.; Stohl, A.; Williams, M. L.; Akimoto, H.;

Amann, M.; Baklanov, A.; Baltensperger, U.; Bey, I.; Blake, N.; Blake, R. S.; Carslaw, K.; Cooper, O. R.; Dentener, F.; Fowler, D.; Fragkou, E.; Frost, G. J.; Generoso, S.; Ginoux, P.; Grewe, V.; Guenther, A.; Hansson, H. C.; Henne, S.; Hjorth, J.; Hofzumahaus, A.; Huntrieser, H.; Isaksen, I. S. A.; Jenkin, M. E.; Kaiser, J.; Kanakidou, M.; Klimont, Z.; Kulmala, M.; Laj, P.; Lawrence, M. G.; Lee, J. D.; Liousse, C.; Maione, M.; McFiggans, G.; Metzger, A.; Mieville, A.; Moussiopoulos, N.; Orlando, J. J.; Dowd, C. D. O.; Palmer, P. I.; Parrish, D. D.; Petzold, A.; Platt, U.; Pöschl, U.; Prévôt, A. S. H.; Reeves, C. E.; Reimann, S.; Rudich, Y.; Sellegri, K.; Steinbrecher, R.; Simpson, D.; Brink, ten, H.; Theloke, J.; van der Werf, G. R.; Vautard, R.; Vestreng, V.; Vlachokostas, C.; Glasow, von, R. Atmospheric composition change - global and regional air quality. *Atmospheric Environment* **2009**, *43*, 5268–5350.

(33) Lanz, V. A.; Prévôt, A. S. H.; Alfarra, M. R.; Weimer, S.; Mohr, C.; DeCarlo, P. F.; Gianini, M. F. D.; Hueglin, C.; Schneider, J.; favez, O.; D'Anna, B.; George, C.; Baltensperger, U. Characterization of aerosol chemical composition with aerosol mass spectrometry in Central Europe: an overview. *Atmos. Chem. Phys.* **2010**, *10*, 10453–10471.

(34) Zhang, Q.; Worsnop, D. R.; Canagaratna, M. R.; Jimenez, J. L. Hydrocarbon-like and oxygenated organic aerosols in Pittsburgh: insights into sources and processes of organic aerosols. *Atmos. Chem. Phys.* **2005**, *5*, 3289–3311.

(35) Yu, S.; Bhave, P. V.; Dennis, R. L.; Mathur, R. Seasonal and Regional Variations of Primary and Secondary Organic Aerosols over the Continental United States: Semi-Empirical Estimates and Model Evaluation. *Environmental Science & Technology* **2007**, *41*, 4690–4697.

(36) Lanz, V. A.; Alfarra, M. R.; Baltensperger, U.; Buchmann, B.; Hueglin, C.; Prévôt, A. S. H. Source apportionment of submicron organic aerosols at an urban site by factor analytical modelling of aerosol mass spectra. *Atmos. Chem. Phys.* **2007**, *7*, 1503–1522.

(37) Lanz, V. A.; Alfarra, M. R.; Baltensperger, U.; Buchmann, B.; Hueglin, C.; Szidat, S.; Wehrli, M. N.; Wacker, L.; Weimer, S.; Caseiro, A.; Puxbaum, H.; Prevot, A. S. H. Source Attribution of Submicron Organic Aerosols during Wintertime Inversions by Advanced Factor Analysis of Aerosol Mass Spectra. *Environmental Science & Technology* **2008**, *42*, 214–220.

(38) Shrivastava, M. K.; Lipsky, E. M.; Stanier, C. O.; Robinson, A. L. Modeling Semivolatile Organic Aerosol Mass Emissions from Combustion Systems. *Environmental Science & Technology* **2006**, *40*, 2671–2677.

(39) Odum, J. R.; Hoffmann, T.; Bowman, F.; Collins, D.; Flagan, R. C.; Seinfeld, J. H. Gas/particle partitioning and secondary organic aerosol yields. *Environmental Science & Technology* **1996**, *30*, 2580–2585.

(40) Gelencsér, A.; Varga, Z. Evaluation of the atmospheric significance of multiphase reactions in atmospheric secondary organic aerosol formation. *Atmos. Chem. Phys.* **2005**, *5*, 2823–2831.

(41) Ervens, B.; Turpin, B. J.; Weber, R. J. Secondary organic aerosol formation in cloud droplets and aqueous particles (aqSOA): a review of laboratory, field and model studies. *Atmos. Chem. Phys.* **2011**, *11*, 11069–11102.

(42) Pankow, J. F. An absorption model of gas/particle partitioning of organic compounds in the atmosphere. *Atmospheric Environment* **1994**, *28*, 185–188.

(43) Pankow, J. An absorption model of the gas/aerosol partitioning involved in the formation of secondary organic aerosol. *Atmospheric Environment* **1994**, *28*, 189–193.

(44) Hallquist, M.; Wenger, J.; Baltensperger, U.; Rudich, Y.; Simpson, D.; Claeys, M.; Dommen, J.; Donahue, N.; George, C.; Goldstein, A. The formation, properties and impact of secondary organic aerosol: current and emerging issues. *Atmos. Chem. Phys.* **2009**, *9*, 5155–5236.

(45) Pandis, S. N.; Paulson, S. E.; Seinfeld, J. H.; Flagan, R. C. Aerosol formation in the photooxidation of isoprene and β-pinene. *Atmospheric Environment. Part A. General Topics* **1991**, *25*, 997–1008.

(46) Guenther, A.; Karl, T.; Harley, P.; Wiedinmyer, C.; Palmer, P. I.; Geron, C. Estimates of global terrestrial isoprene emissions using MEGAN (Model of Emissions of Gases and Aerosols from Nature). *Atmos. Chem. Phys.* **2006**, *6*, 3181–3210.

(47) Henze, D. K.; Seinfeld, J. H. Global secondary organic aerosol from isoprene oxidation. *Geophys. Res. Lett.* **2006**, *33*, L09812.

(48) Carlton, A.; Wiedinmyer, C.; Kroll, J. A review of Secondary Organic Aerosol (SOA) formation from isoprene. *Atmos. Chem. Phys.* **2009**, *9*, 4987–5005.

(49) Tsigaridis, K.; Kanakidou, M. Global modelling of secondary organic aerosol in the troposphere: A sensitivity analysis. *Atmos. Chem. Phys.* **2003**, *3*, 1849–1869.

(50) Heald, C. L.; Jacob, D. J.; Park, R. J.; Russell, L. M.; Huebert, B. J.; Seinfeld, J. H.; Liao, H.; Weber, R. J. A large organic aerosol source in the free troposphere missing from current models. *Geophys. Res. Lett.* **2005**, *32*, L18809.

(51) Heald, C. L.; Jacob, D. J.; Turquety, S.; Hudman, R. C.; Weber, R. J.; Sullivan, A. P.; Peltier, R. E.; Atlas, E. L.; de Gouw, J. A.; Warneke, C.; Holloway, J. S.; Neuman, J. A.; Flocke, F. M.; Seinfeld, J. H. Concentrations and sources of organic carbon aerosols in the free troposphere over North America. *J. Geophys. Res.* **2006**, *111*.

(52) Heald, C. L.; Coe, H.; Jimenez, J. L.; Weber, R. J.; Bahreini, R.; Middlebrook, A. M.; Russell, L. M.; Jolleys, M.; Fu, T. M.; Allan, J. D.; Bower, K. N.; Capes, G.; Crosier, J.; Morgan, W. T.; Robinson, N. H.; Williams, P. I.; Cubison, M. J.; DeCarlo, P. F.; Dunlea, E. J. Exploring the vertical profile of atmospheric organic aerosol: comparing 17 aircraft field campaigns with a global model. *Atmos. Chem. Phys.* **2011**, *11*, 12673–12696.

(53) Aiken, A. C.; DeCarlo, P. F.; Kroll, J. H.; Worsnop, D. R.; Huffman, J. A.; Docherty, K. S.; Ulbrich, I. M.; Mohr, C.; Kimmel, J. R.; Sueper, D.; Sun, Y.; Zhang, Q.; Trimborn, A.; Northway, M.; Ziemann, P. J.; Canagaratna, M. R.; Onasch, T. B.; Alfarra, M. R.; Prevot, A. S. H.; Dommen, J.; Duplissy, J.; Metzger, A.; Baltensperger, U.; Jimenez, J. L. O/C and OM/OC Ratios of Primary, Secondary, and Ambient Organic Aerosols with High-Resolution Time-of-Flight Aerosol Mass Spectrometry. *Environmental Science & Technology* **2008**, *42*, 4478–4485.

(54) Ng, N. L.; Canagaratna, M. R.; Zhang, Q.; Jimenez, J. L.; Tian, J.; Ulbrich, I. M.; Kroll, J. H.; Docherty, K. S.; Chhabra, P. S.; Bahreini, R.; Murphy, S. M.; Seinfeld, J. H.; Hildebrandt, L.; Donahue, N. M.; DeCarlo, P. F.; Lanz, V. A.; Prévôt, A. S. H.; Dinar, E.; Rudich, Y.; Worsnop, D. R. Organic aerosol components observed in Northern Hemispheric datasets from Aerosol Mass Spectrometry. *Atmos. Chem. Phys.* **2010**, *10*, 4625–4641.

(55) Burkhard, E. G.; Ghauri, B. M.; Dutkiewicz, V. A.; Husain, L. A multielement tracer technique for the determination of SO2 oxidation in clouds. *J. Geophys. Res.* **1995**, *100*, 26051–26059.

(56) Hering, S. V.; Friedlander, S. K. Origins of aerosol sulfur size distributions in the Los Angeles basin. *Atmospheric Environment* **1982**, *16*, 2647–2656.

(57) John, W.; Wall, S. M.; Ondo, J. L.; Winklmayr, W. Modes in the size distributions of atmospheric inorganic aerosol. *Atmospheric Environment* **1990**, *24A*, 2349–2359.

(58) Meng, Z.; Seinfeld, J. H. On the Source of the Submicrometer Droplet Mode of Urban and Regional Aerosols. *Aerosol Science and Technology* **1994**, *20*, 253–265.

(59) Ervens, B.; Gligorovski, S.; Herrmann, H. Temperature-dependent rate constants for hydroxyl radical reactions with organic compounds in aqueous solutions. *Phys. Chem. Chem. Phys.* **2003**, *5*, 1811–1824.

(60) Carlton, A. G.; Turpin, B. J.; Lim, H.-J.; Altieri, K. E.; Seitzinger, S. Link between isoprene and secondary organic aerosol (SOA): Pyruvic acid oxidation yields low volatility organic acids in clouds. *Geophys. Res. Lett.* **2006**, *33*.

(61) Carlton, A. G.; Turpin, B. J.; Altieri, K. E.; Seitzinger, S.; Reff, A.; Lim, H.-J.;

Ervens, B. Atmospheric oxalic acid and SOA production from glyoxal: Results of aqueous photooxidation experiments. *Atmospheric Environment* **2007**, *41*, 7588–7602.

(62) Altieri, K. E.; Carlton, A. G.; Lim, H.-J.; Turpin, B. J.; Seitzinger, S. P. Evidence for Oligomer Formation in Clouds: Reactions of Isoprene Oxidation Products. *Environmental Science & Technology* **2006**, *40*, 4956–4960.

(63) Altieri, K. E.; Seitzinger, S. P.; Carlton, A. G.; Turpin, B. J.; Klein, G. C.; Marshall, A. G. Oligomers formed through in-cloud methylglyoxal reactions: Chemical composition, properties, and mechanisms investigated by ultra-high resolution FT-ICR mass spectrometry. *Atmospheric Environment* **2008**, *42*, 1476–1490.

(64) Perri, M. J.; Seitzinger, S.; Turpin, B. J. Secondary organic aerosol production from aqueous photooxidation of glycolaldehyde: Laboratory experiments. *Atmospheric Environment* **2009**, *43*, 1487–1497.

(65) Perri, M. J.; Lim, Y. B.; Seitzinger, S. P.; Turpin, B. J. Organosulfates from glycolaldehyde in aqueous aerosols and clouds: Laboratory studies. *Atmospheric Environment* **2010**, *44*, 2658–2664.

(66) Liu, Y.; Haddad, El, I.; Scarfogliero, M.; Nieto-Gligorovski, L.; Temime-Roussel, B.; Quivet, E.; Marchand, N.; Picquet-Varrault, B.; Monod, A. In-cloud processes of methacrolein under simulated conditions–Part 1: Aqueous phase photooxidation. *Atmos. Chem. Phys.* **2009**, *9*, 5093–5105.

(67) Zhang, X.; Chen, Z. M.; Zhao, Y. Laboratory simulation for the aqueous OH-oxidation of methyl vinyl ketone and methacrolein: significance to the in-cloud SOA production. *Atmos. Chem. Phys.* **2010**, *10*, 9551–9561.

(68) Sun, Y.; Zhang, Q.; Anastasio, C. Insights into secondary organic aerosol formed via aqueous-phase reactions of phenolic compounds based on high resolution mass spectrometry. *Atmos. Chem. Phys.* **2010**, *10*, 4809–4822.

(69) Tan, Y.; Lim, Y. B.; Altieri, K. E.; Seitzinger, S. P.; Turpin, B. J. Mechanisms leading to oligomers and SOA through aqueous photooxidation: insights from OH radical oxidation of acetic acid and methylglyoxal. *Atmos. Chem. Phys.* **2012**, *12*, 801–813.

(70) Gong, W.; Stroud, C.; Zhang, L. Cloud Processing of Gases and Aerosols in Air Quality Modeling. *Atmosphere* **2011**, *2*, 567–616.

(71) Turpin, B. J.; Lim, H.-J. Species Contributions to PM2.5 Mass Concentrations: Revisiting Common Assumptions for Estimating Organic Mass. *Aerosol Science and Technology* **2001**, *35*, 602–610.

(72) Polidori, A.; Turpin, B. J.; Davidson, C. I.; Rodenburg, L. A.; Maimone, F.

Organic PM 2.5: Fractionation by Polarity, FTIR Spectroscopy, and OM/OC Ratio for the Pittsburgh Aerosol. *Aerosol Science and Technology* **2008**, *42*, 233–246.

(73) Sun, Y.; Zhang, Q.; Macdonald, A. M.; Hayden, K.; Li, S. M.; Liggio, J.; Liu, P.; Anlauf, K. G.; Leaitch, W. R.; Steffen, A.; Cubison, M.; Worsnop, D. R.; van Donkelaar, A.; Martin, R. V. Size-resolved aerosol chemistry on Whistler Mountain, Canada with a high-resolution aerosol mass spectrometer during INTEX-B. *Atmos. Chem. Phys.* **2009**, *9*, 3095–3111.

(74) Aiken, A. C.; DeCarlo, P. F.; Jimenez, J. L. Elemental Analysis of Organic Species with Electron Ionization High-Resolution Mass Spectrometry. *Anal. Chem.* **2007**, *79*, 8350–8358.

(75) Reinhardt, A.; Emmenegger, C.; Gerrits, B.; Panse, C.; Dommen, J.; Baltensperger, U.; Zenobi, R.; Kalberer, M. Ultrahigh Mass Resolution and Accurate Mass Measurements as a Tool To Characterize Oligomers in Secondary Organic Aerosols. *Anal. Chem.* **2007**, *79*, 4074–4082.

(76) Shilling, J. E.; Chen, Q.; King, S. M.; Rosenoern, T.; Kroll, J. H.; Worsnop, D. R.; DeCarlo, P. F.; Aiken, A. C.; Sueper, D.; Jimenez, J. L.; Martin, S. T. Loading-dependent elemental composition of α-pinene SOA particles. *Atmos. Chem. Phys.* **2009**, *9*, 771–782.

(77) Chhabra, P. S.; Flagan, R. C.; Seinfeld, J. H. Elemental analysis of chamber organic aerosol using an aerodyne high-resolution aerosol mass spectrometer. *Atmos. Chem. Phys.* **2010**, *10*, 4111–4131.

(78) Graber, E.; Rudich, Y. Atmospheric HULIS: how humic-like are they? A comprehensive and critical review. *Atmos. Chem. Phys.* **2006**, *6*, 729–753.

(79) Lin, P.; Huang, X.-F.; He, L.-Y.; Yu, J. Z. Abundance and size distribution of HULIS in ambient aerosols at a rural site in South China. *Journal of Aerosol Science* **2010**, *41*, 74–87.

(80) Feng, J.; Möller, D. Characterization of water-soluble macromolecular substances in cloud water. *J Atmos Chem* **2004**, *48*, 217–233.

(81) Cappiello, A.; De Simoni, E.; Fiorucci, C.; Mangani, F.; Palma, P.; Trufelli, H.; Decesari, S.; Facchini, M. C.; Fuzzi, S. Molecular Characterization of the Water-Soluble Organic Compounds in Fogwater by ESIMS/MS. *Environmental Science & Technology* **2003**, *37*, 1229–1240.

(82) Mazzoleni, L. R.; Ehrmann, B. M.; Shen, X.; Marshall, A. G.; Collett, J. L., Jr. Water-Soluble Atmospheric Organic Matter in Fog: Exact Masses and Chemical Formula Identification by Ultrahigh-Resolution Fourier Transform Ion Cyclotron Resonance Mass

Spectrometry. *Environmental Science & Technology* **2010**, *44*, 3690–3697.

(83) Altieri, K. E.; Turpin, B. J.; Seitzinger, S. P. Oligomers, organosulfates, and nitrooxy organosulfates in rainwater identified by ultra-high resolution electrospray ionization FT-ICR mass spectrometry. *Atmos. Chem. Phys.* **2009**, *9*, 2533–2542.

(84) Sorooshian, A.; Ng, N. L.; Chan, A. W. H.; Feingold, G.; Flagan, R. C.; Seinfeld, J. H. Particulate organic acids and overall water-soluble aerosol composition measurements from the 2006 Gulf of Mexico Atmospheric Composition and Climate Study (GoMACCS). *J. Geophys. Res.* **2007**, *112*.

(85) Collett, J. L., Jr.; Herckes, P.; Youngster, S.; Lee, T. Processing of atmospheric organic matter by California radiation fogs. *Atmospheric Research* **2008**, *87*, 232–241.

(86) Sorooshian, A.; Varutbangkul, V.; Brechtel, F. J.; Ervens, B.; Feingold, G.; Bahreini, R.; Murphy, S. M.; Holloway, J. S.; Atlas, E. L.; Buzorius, G.; Jonsson, H.; Flagan, R. C.; Seinfeld, J. H. Oxalic acid in clear and cloudy atmospheres: Analysis of data from International Consortium for Atmospheric Research on Transport and Transformation 2004. *J. Geophys. Res.* **2006**, *111*.

(87) Crahan, K. K.; Hegg, D.; Covert, D. S.; Jonsson, H. An exploration of aqueous oxalic acid production in the coastal marine atmosphere. *Atmospheric Environment* **2004**, *38*, 3757–3764.

(88) Yu, J. Z.; Huang, X.-F.; Xu, J.; Hu, M. When Aerosol Sulfate Goes Up, So Does Oxalate: Implication for the Formation Mechanisms of Oxalate. *Environmental Science & Technology* **2005**, *39*, 128–133.

(89) Sorooshian, A.; Lu, M.-L.; Brechtel, F. J.; Jonsson, H.; Feingold, G.; Flagan, R. C.; Seinfeld, J. H. On the Source of Organic Acid Aerosol Layers above Clouds. *Environmental Science & Technology* **2007**, *41*, 4647–4654.

(90) Wonaschuetz, A.; Sorooshian, A.; Ervens, B.; Chuang, P. Y.; Feingold, G.; Murphy, S. M.; de Gouw, J.; Warneke, C.; Jonsson, H. H. Aerosol and gas re-distribution by shallow cumulus clouds: An investigation using airborne measurements. *J. Geophys. Res.* **2012**, *117*, D17202.

(91) Mészáros, E.; Barcza, T.; Gelencsér, A.; Hlavay, J.; Kiss, G.; Krivácsy, Z.; Molnár, A.; Polyák, K. Size distributions of inorganic and organic species in the atmospheric aerosol in Hungary. *Journal of Aerosol Science* **1997**, *28*, 1163–1175.

(92) Yao, X.; Fang, M.; Chan, C. K. Size distributions and formation of dicarboxylic acids in atmospheric particles. *Atmospheric Environment* **2002**, *36*, 2099–2107.

(93) Sorooshian, A.; Murphy, S. M.; Hersey, S.; Bahreini, R.; Jonsson, H.; Flagan,

R. C.; Seinfeld, J. H. Constraining the contribution of organic acids and AMS m/z44 to the organic aerosol budget: On the importance of meteorology, aerosol hygroscopicity, and region. *Geophys. Res. Lett.* **2010**, *37*, L21807.

(94) Weber, R. J.; Sullivan, A. P.; Peltier, R. E.; Russell, A.; Yan, B.; Zheng, M.; de Gouw, J.; Warneke, C.; Brock, C.; Holloway, J. S.; Atlas, E. L.; Edgerton, E. A study of secondary organic aerosol formation in the anthropogenic-influenced southeastern United States. *J. Geophys. Res.* **2007**, *112*, D13302.

(95) Hennigan, C. J.; Bergin, M. H.; Dibb, J. E.; Weber, R. J. Enhanced secondary organic aerosol formation due to water uptake by fine particles. *Geophys. Res. Lett.* **2008**, *35*, L18801.

(96) Zhang, X.; Liu, J.; Parker, E. T.; Hayes, P. L.; Jimenez, J. L.; de Gouw, J. A.; Flynn, J. H.; Grossberg, N.; Lefer, B. L.; Weber, R. J. On the gas-particle partitioning of soluble organic aerosol in two urban atmospheres with contrasting emissions: 1. Bulk water-soluble organic carbon. *J. Geophys. Res.* **2012**, *117*, D00V16.

(97) Hennigan, C. J.; Bergin, M. H.; Russell, A. G.; Nenes, A.; Weber, R. J. Gas/particle partitioning of water-soluble organic aerosol in Atlanta. *Atmos. Chem. Phys.* **2009**, *9*, 3613–3628.

(98) Hersey, S. P.; Craven, J. S.; Schilling, K. A.; Metcalf, A. R.; Sorooshian, A.; Chan, M. N.; Flagan, R. C.; Seinfeld, J. H. The Pasadena Aerosol Characterization Observatory (PACO): chemical and physical analysis of the Western Los Angeles basin aerosol. *Atmos. Chem. Phys.* **2011**, *11*, 7417–7443.

(99) Lee, A. K. Y.; Herckes, P.; Leaitch, W. R.; Macdonald, A. M.; Abbatt, J. P. D. Aqueous OH oxidation of ambient organic aerosol and cloud water organics: Formation of highly oxidized products. *Geophys. Res. Lett.* **2011**, *38*, L11805.

(100) Nguyen, T. B.; Bateman, A. P.; Bones, D. L.; Nizkorodov, S. A.; Laskin, J.; Laskin, A. High-resolution mass spectrometry analysis of secondary organic aerosol generated by ozonolysis of isoprene. *Atmospheric Environment* **2010**, *44*, 1032–1042.

(101) Volkamer, R.; Jimenez, J. L.; San Martini, F.; Dzepina, K.; Zhang, Q.; Salcedo, D.; Molina, L. T.; Worsnop, D. R.; Molina, M. J. Secondary organic aerosol formation from anthropogenic air pollution: Rapid and higher than expected. *Geophys. Res. Lett.* **2006**, *33*.

(102) Volkamer, R.; San Martini, F.; Molina, L. T.; Salcedo, D.; Jimenez, J. L.; Molina, M. J. A missing sink for gas-phase glyoxal in Mexico City: Formation of secondary organic aerosol. *Geophys. Res. Lett.* **2007**, *34*, L19807.

(103) Chen, J.; Griffin, R. J.; Grini, A.; Tulet, P. Modeling secondary organic aerosol

formation through cloud processing of organic compounds. *Atmos. Chem. Phys.* **2007**, *7*, 5343–5355.

(104) Liu, J.; Horowitz, L. W.; Fan, S.; Carlton, A. G.; Levy, H., II Global in-cloud production of secondary organic aerosols: Implementation of a detailed chemical mechanism in the GFDL atmospheric model AM3. *J. Geophys. Res.* **2012**, *117*, D15303.

(105) Lin, G.; Penner, J. E.; Sillman, S.; Taraborrelli, D.; Lelieveld, J. Global modeling of SOA formation from dicarbonyls, epoxides, organic nitrates and peroxides. *Atmos. Chem. Phys.* **2012**, *12*, 4743–4774.

(106) Fu, T.-M.; Jacob, D. J.; Heald, C. L. Aqueous-phase reactive uptake of dicarbonyls as a source of organic aerosol over eastern North America. *Atmospheric Environment* **2009**, *43*, 1814–1822.

(107) Liggio, J.; Li, S.-M.; McLaren, R. Reactive uptake of glyoxal by particulate matter. *J. Geophys. Res.* **2005**, *110*, D10304.

(108) Zhao, J.; Levitt, N. P.; Zhang, R.; Chen, J. Heterogeneous Reactions of Methylglyoxal in Acidic Media: Implications for Secondary Organic Aerosol Formation. *Environmental Science & Technology* **2006**, *40*, 7682–7687.

(109) Carlton, A. G.; Bhave, P. V.; Napelenok, S. L.; Edney, E. O.; Sarwar, G.; Pinder, R. W.; Pouliot, G. A.; Houyoux, M. Model Representation of Secondary Organic Aerosol in CMAQv4.7. *Environmental Science & Technology* **2010**, *44*, 8553–8560.

(110) Myriokefalitakis, S.; Tsigaridis, K.; Mihalopoulos, N.; Sciare, J.; Nenes, A.; Segers, A.; Kanakidou, M. In-cloud oxalate formation in the global troposphere: a 3-D modeling study. *Atmos. Chem. Phys. Discuss.* **2011**, *11*, 485–530.

(111) He, C.; Liu, J.; Carlton, A. G.; Fan, S.; Horowitz, L. W.; Levy, H., II; Tao, S. Evaluation of factors controlling global secondary organic aerosol production from cloud processes. *Atmos. Chem. Phys.* **2013**, *13*, 1913–1926.

(112) Liao, H.; Seinfeld, J. H. Global impacts of gas-phase chemistry-aerosol interactions on direct radiative forcing by anthropogenic aerosols and ozone. *J. Geophys. Res.* **2005**, *110*, D18208.

(113) Hodzic, A.; Jimenez, J. L.; Madronich, S.; Canagaratna, M. R.; DeCarlo, P. F.; Kleinman, L.; Fast, J. Modeling organic aerosols in a megacity: potential contribution of semi-volatile and intermediate volatility primary organic compounds to secondary organic aerosol formation. *Atmos. Chem. Phys.* **2010**, *10*, 5491–5514.

(114) Pye, H. O. T.; Seinfeld, J. H. A global perspective on aerosol from low-volatility organic compounds. *Atmos. Chem. Phys.* **2010**, *10*, 4377–4401.

(115) Jathar, S. H.; Farina, S. C.; Robinson, A. L.; Adams, P. J. The influence of semi-volatile and reactive primary emissions on the abundance and properties of global organic aerosol. *Atmos. Chem. Phys.* **2011**, *11*, 7727–7746.

(116) Guzmán, M. I.; Colussi, A. J.; Hoffmann, M. R. Photoinduced Oligomerization of Aqueous Pyruvic Acid. *J. Phys. Chem. A* **2006**, *110*, 3619–3626.

(117) Loeffler, K. W.; Koehler, C. A.; Paul, N. M.; De Haan, D. O. Oligomer Formation in Evaporating Aqueous Glyoxal and Methyl Glyoxal Solutions. *Environmental Science & Technology* **2006**, *40*, 6318–6323.

(118) Volkamer, R.; Ziemann, P.; Molina, M. Secondary Organic Aerosol Formation from Acetylene (C2H2): seed effect on SOA yields due to organic photochemistry in the aerosol aqueous phase. *Atmos. Chem. Phys.* **2009**, *9*, 1907–1928.

(119) Nozière, B.; Dziedzic, P.; Córdova, A. Products and Kinetics of the Liquid-Phase Reaction of Glyoxal Catalyzed by Ammonium Ions (NH 4+). *J. Phys. Chem. A* **2009**, *113*, 231–237.

(120) Nozière, B.; Dziedzic, P.; Córdova, A. Inorganic ammonium salts and carbonate salts are efficient catalysts for aldol condensation in atmospheric aerosols. *Phys. Chem. Chem. Phys.* **2010**, *12*, 3864–3872.

(121) Nozière, B.; Ekström, S.; Alsberg, T.; Holmström, S. Radical-initiated formation of organosulfates and surfactants in atmospheric aerosols. *Geophys. Res. Lett.* **2010**, *37*.

(122) Liu, Y.; Monod, A.; Tritscher, T.; Praplan, A. P.; DeCarlo, P. F.; Temime-Roussel, B.; Quivet, E.; Marchand, N.; Dommen, J.; Baltensperger, U. Aqueous phase processing of secondary organic aerosol from isoprene photooxidation. *Atmos. Chem. Phys.* **2012**, *12*, 5879–5895.

(123) Liu, Y.; Siekmann, F.; Renard, P.; Zein, El, A.; Salque, G.; Haddad, El, I.; Temime-Roussel, B.; Voisin, D.; Thissen, R.; Monod, A. Oligomer and SOA formation through aqueous phase photooxidation of methacrolein and methyl vinyl ketone. *Atmospheric Environment* **2012**, *49*, 123–129.

(124) Haddad, El, I.; Liu, Y.; Nieto-Gligorovski, L.; Michaud, V.; Temime-Roussel, B.; Quivet, E.; Marchand, N.; Sellegri, K.; Monod, A. In-cloud processes of methacrolein under simulated conditions – Part 2: Formation of secondary organic aerosol. *Atmos. Chem. Phys.* **2009**, *9*, 5107–5117.

(125) Michaud, V.; Haddad, El, I.; Liu, Y.; Sellegri, K.; Laj, P.; Villani, P.; Picard, D.; Marchand, N.; Monod, A. In-cloud processes of methacrolein under simulated conditions–Part 3: Hygroscopic and volatility properties of the formed secondary organic

aerosol. *Atmos. Chem. Phys.* **2009**, *9*, 5119–5130.

(126) Shapiro, E. L.; Szprengiel, J.; Sareen, N.; Jen, C. N.; Giordano, M. R.; McNeill, V. Light-absorbing secondary organic material formed by glyoxal in aqueous aerosol mimics. *Atmos. Chem. Phys.* **2009**, *9*, 2289–2300.

(127) Galloway, M.; Chhabra, P.; Chan, A.; Surratt, J.; Flagan, R.; Seinfeld, J.; Keutsch, F. Glyoxal uptake on ammonium sulphate seed aerosol: reaction products and reversibility of uptake under dark and irradiated conditions. *Atmos. Chem. Phys.* **2009**, *9*, 3331–3345.

(128) Tan, Y.; Perri, M. J.; Seitzinger, S. P.; Turpin, B. J. Effects of Precursor Concentration and Acidic Sulfate in Aqueous Glyoxal−OH Radical Oxidation and Implications for Secondary Organic Aerosol. *Environmental Science & Technology* **2009**, *43*, 8105–8112.

(129) Tan, Y.; Carlton, A. G.; Seitzinger, S. P.; Turpin, B. J. SOA from methylglyoxal in clouds and wet aerosols: Measurement and prediction of key products. *Atmospheric Environment* **2010**, *44*, 5218–5226.

(130) De Haan, D. O.; Tolbert, M. A.; Jimenez, J. L. Atmospheric condensed-phase reactions of glyoxal with methylamine. *Geophys. Res. Lett.* **2009**, *36*.

(131) De Haan, D. O.; Corrigan, A. L.; Tolbert, M. A.; Jimenez, J. L.; Wood, S. E.; Turley, J. J. Secondary Organic Aerosol Formation by Self-Reactions of Methylglyoxal and Glyoxal in Evaporating Droplets. *Environmental Science & Technology* **2009**, *43*, 8184–8190.

(132) De Haan, D. O.; Corrigan, A. L.; Smith, K. W.; Stroik, D. R.; Turley, J. J.; Lee, F. E.; Tolbert, M. A.; Jimenez, J. L.; Cordova, K. E.; Ferrell, G. R. Secondary Organic Aerosol-Forming Reactions of Glyoxal with Amino Acids. *Environmental Science & Technology* **2009**, *43*, 2818–2824.

(133) De Haan, D. O.; Hawkins, L. N.; Kononenko, J. A.; Turley, J. J.; Corrigan, A. L.; Tolbert, M. A.; Jimenez, J. L. Formation of Nitrogen-Containing Oligomers by Methylglyoxal and Amines in Simulated Evaporating Cloud Droplets. *Environmental Science & Technology* **2011**, *45*, 984–991.

(134) Sareen, N.; Schwier, A.; Shapiro, E.; Mitroo, D.; McNeill, V. Secondary organic material formed by methylglyoxal in aqueous aerosol mimics. *Atmos. Chem. Phys.* **2010**, *10*, 997–1016.

(135) Schwier, A. N.; Sareen, N.; Mitroo, D.; Shapiro, E. L.; McNeill, V. F. Glyoxal-Methylglyoxal Cross-Reactions in Secondary Organic Aerosol Formation. *Environmental Science & Technology* **2010**, *44*, 6174–6182.

(136) Chang, J. L.; Thompson, J. E. Characterization of colored products formed during irradiation of aqueous solutions containing H2O2 and phenolic compounds. *Atmospheric Environment* **2010**, *44*, 541–551.

(137) Grgić, I.; Nieto-Gligorovski, L. I.; Net, S.; Temime-Roussel, B.; Gligorovski, S.; Wortham, H. Light induced multiphase chemistry of gas-phase ozone on aqueous pyruvic and oxalic acids. *Phys. Chem. Chem. Phys.* **2010**, *12*, 698–707.

(138) Bateman, A. P.; Nizkorodov, S. A.; Laskin, J.; Laskin, A. Photolytic processing of secondary organic aerosols dissolved in cloud droplets. *Phys. Chem. Chem. Phys.* **2011**, *13*, 12199–12212.

(139) Lee, A. K. Y.; Zhao, R.; Gao, S. S.; Abbatt, J. P. D. Aqueous-Phase OH Oxidation of Glyoxal: Application of a Novel Analytical Approach Employing Aerosol Mass Spectrometry and Complementary Off-Line Techniques. *J. Phys. Chem. A* **2011**, *115*, 10517–10526.

(140) Lee, A. K. Y.; Hayden, K. L.; Herckes, P.; Leaitch, W. R.; Liggio, J.; Macdonald, A. M.; Abbatt, J. P. D. Characterization of aerosol and cloud water at a mountain site during WACS 2010: secondary organic aerosol formation through oxidative cloud processing. *Atmos. Chem. Phys.* **2012**, *12*, 7103–7116.

(141) Wong, J. P. S.; Lee, A. K. Y.; Slowik, J. G.; Cziczo, D. J.; Leaitch, W. R.; Macdonald, A.; Abbatt, J. P. D. Oxidation of ambient biogenic secondary organic aerosol by hydroxyl radicals: Effects on cloud condensation nuclei activity. *Geophys. Res. Lett.* **2011**, *38*, L22805.

(142) Li, Z.; Schwier, A. N.; Sareen, N.; McNeill, V. F. Reactive processing of formaldehyde and acetaldehyde in aqueous aerosol mimics: surface tension depression and secondary organic products. *Atmos. Chem. Phys.* **2011**, *11*, 11617–11629.

(143) Nguyen, T. B.; Lee, P. B.; Updyke, K. M.; Bones, D. L.; Laskin, J.; Laskin, A.; Nizkorodov, S. A. Formation of nitrogen- and sulfur-containing light-absorbing compounds accelerated by evaporation of water from secondary organic aerosols. *J. Geophys. Res.* **2012**, *117*, D01207.

(144) Ortiz-Montalvo, D. L.; Lim, Y. B.; Perri, M. J.; Seitzinger, S. P.; Turpin, B. J. Volatility and Yield of Glycolaldehyde SOA Formed through Aqueous Photochemistry and Droplet Evaporation. *Aerosol Science and Technology* **2012**, *46*, 1002–1014.

(145) Zarzana, K. J.; De Haan, D. O.; Freedman, M. A.; Hasenkopf, C. A.; Tolbert, M. A. Optical Properties of the Products of α-Dicarbonyl and Amine Reactions in Simulated Cloud Droplets. *Environmental Science & Technology* **2012**, *46*, 4845–4851.

(146) Zhao, R.; Lee, A. K. Y.; Abbatt, J. P. D. Investigation of Aqueous-Phase

Photooxidation of Glyoxal and Methylglyoxal by Aerosol Chemical Ionization Mass Spectrometry: Observation of Hydroxyhydroperoxide Formation. *J. Phys. Chem. A* **2012**, *116*, 6253–6263.

(147) Wang, H. L.; Huang, D.; Zhang, X.; Zhao, Y.; Chen, Z. M. Understanding the aqueous phase ozonolysis of isoprene: distinct product distribution and mechanism from the gas phase reaction. *Atmos. Chem. Phys.* **2012**, *12*, 7187–7198.

(148) Renard, P.; Siekmann, F.; Gandolfo, A.; Socorro, J.; Salque, G.; Ravier, S.; Quivet, E.; Clément, J. L.; Traikia, M.; Delort, A. M.; Voisin, D.; Thissen, R.; Monod, A. Radical mechanisms of methyl vinyl ketone oligomerization through aqueous phase OH-oxidation: on the paradoxical role of dissolved molecular oxygen. *Atmos. Chem. Phys. Discuss.* **2013**, *13*, 2913–2954.

(149) Lim, Y. B.; Tan, Y.; Perri, M. J.; Seitzinger, S. P.; Turpin, B. J. Aqueous chemistry and its role in secondary organic aerosol (SOA) formation. *Atmos. Chem. Phys.* **2010**, *10*, 10521–10539.

(150) Kampf, C. J.; Jakob, R.; Hoffmann, T. Identification and characterization of aging products in the glyoxal/ammonium sulfate system – implications for light-absorbing material in atmospheric aerosols. *Atmos. Chem. Phys.* **2012**, *12*, 6323–6333.

(151) Yu, G.; Bayer, A. R.; Galloway, M. M.; Korshavn, K. J.; Fry, C. G.; Keutsch, F. N. Glyoxal in Aqueous Ammonium Sulfate Solutions: Products, Kinetics and Hydration Effects. *Environmental Science & Technology* **2011**, *45*, 6336–6342.

(152) Yasmeen, F.; Sauret, N.; Gal, J. F.; Maria, P. C.; Massi, L.; Maenhaut, W.; Claeys, M. Characterization of oligomers from methylglyoxal under dark conditions: a pathway to produce secondary organic aerosol through cloud processing during nighttime. *Atmos. Chem. Phys.* **2010**, *10*, 3803–3812.

(153) Ervens, B.; Volkamer, R. Glyoxal processing by aerosol multiphase chemistry: towards a kinetic modeling framework of secondary organic aerosol formation in aqueous particles. *Atmos. Chem. Phys.* **2010**, *10*, 8219–8244.

(154) Cappa, C. D.; Jimenez, J. L. Quantitative estimates of the volatility of ambient organic aerosol. *Atmos. Chem. Phys.* **2010**, *10*, 5409–5424.

(155) Lim, H.-J.; Carlton, A. G.; Turpin, B. J. Isoprene Forms Secondary Organic Aerosol through Cloud Processing: Model Simulations. *Environmental Science & Technology* **2005**, *39*, 4441–4446.

(156) Seinfeld, J. Atmospheric science: Black carbon and brown clouds. *Nature Geoscience* **2008**, *1*, 15–16.

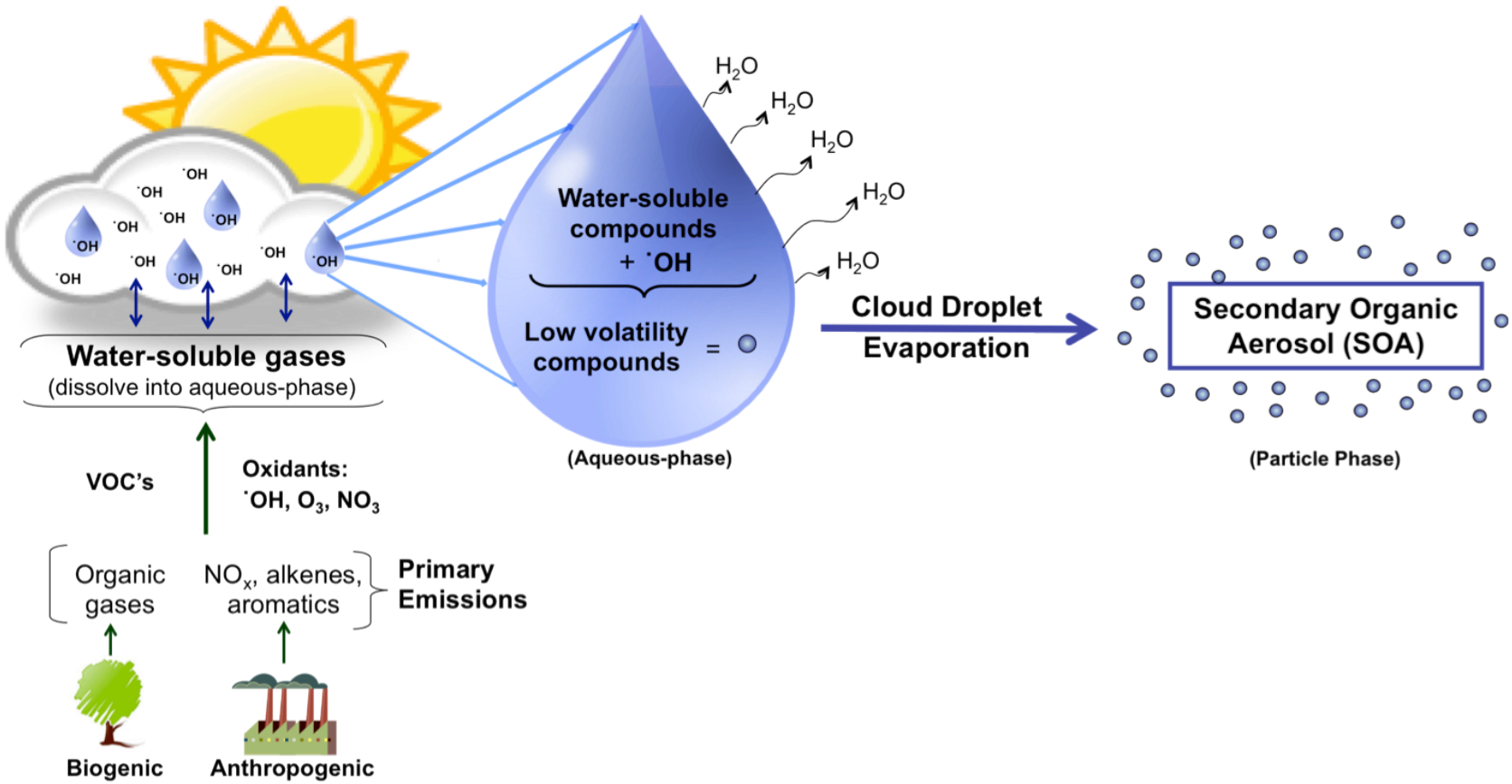

Figure 1-1. Secondary Organic Aerosol (SOA) Formation through Cloud Processing

Chapter 2. Volatility and Yield of Glycolaldehyde SOA Formed through Aqueous Photochemistry and Droplet Evaporation

Material in this chapter has been published previously as:

Ortiz-Montalvo, D. L.; Lim, Y. B.; Perri, M. J.; Seitzinger, S. P.; Turpin, B. J. Volatility and Yield of Glycolaldehyde SOA Formed through Aqueous Photochemistry and Droplet Evaporation. *Aerosol Science & Technology* **2012**, 46, (9), 1002–1014.

2.1 Abstract

Aqueous hydroxyl radical (~10^{-12} M) oxidation of glycolaldehyde (1 mM), followed by droplet evaporation, forms secondary organic aerosol (SOA) that exhibits an effective liquid vapor pressure and enthalpy of vaporization of ~10^{-7} atm and ~70 kJ/mol, respectively, similar to the mix of organic acids identified in reaction samples. Salts of these acids have vapor pressures about three orders of magnitude lower (e.g., ammonium succinate ~10^{-11} atm), suggesting that the gas–particle partitioning behavior of glycolaldehyde SOA depends strongly on whether products are present in the atmosphere as acids or salts. Several reaction samples were used to simulate cloud droplet evaporation using a vibrating orifice aerosol generator. Samples were also analyzed by ion chromatography (IC), electrospray ionization mass spectrometry (ESI-MS), IC-ESI-MS, and for total carbon. Glycolaldehyde SOA mass yields were 50–120%, somewhat higher than yields reported previously (40–60%). Possible reasons are discussed: (1) formation of oligomers from droplet evaporation, (2) inclusion of unquantified products formed by aqueous photooxidation, (3) differences in gas–particle partitioning, and (4) water retention in dried particles. These and similar results help to explain the enrichment

of organic acids in particulate organic matter above clouds compared with those found below clouds, as observed previously in aircraft campaigns.

2.2 Introduction

Secondary organic aerosol (SOA) is a substantial contributor to organic particulate matter (PM) and is poorly captured by air quality models because its formation is not well understood[1-6]. Models that accurately link emissions to air pollution concentrations and effects are important to developing effective air quality management plans and understanding to what degree SOA is controllable[7]. SOA is formed from gas-phase chemistry, followed by either vapor pressure-based partitioning into particulate organic matter—SOA_{OM} [6,8,9] or aqueous-phase chemistry in clouds and wet aerosols—SOA_{aq}[10-12]. Several papers report comparable amounts of SOA_{OM} and SOA_{aq} globally and in certain regions, although uncertainties are large[13-17]. Furthermore, model results from Myriokefalitakis et al.[18] suggest that the vast majority of oxalate globally is formed through aqueous chemistry, making oxalate a good tracer for SOA_{aq}. The enrichment of oxalate and organic acids above versus below cloud[19] and when aerosol liquid water content is high[20] provide atmospheric evidence for SOA_{aq}.

SOA_{aq} can form in clouds, fogs, and aerosol water; this work is focused on in-cloud formation. Briefly, during cloud processing, water-soluble organic gases dissolve into cloud water, undergo volume phase reactions, and form low-volatility compounds that remain in the particle-phase when the droplets evaporate, thus forming SOA_{aq}[10,12,21-29]. For example, the aqueous-phase hydroxyl (OH) radical oxidation (photooxidation) of glycolaldehyde, glyoxal, methylglyoxal, pyruvate, acetate, acetone, methacrolein, and methyl vinyl ketone directly or indirectly forms dicarboxylic acids and higher-molecular-

weight compounds (HMWCs) (e.g., oligomers)[27,30-41], with diacids forming preferentially in dilute solution (clouds) and HMWCs in concentrated solution (wet aerosols)[37,42,43]. Several aqueous-phase photooxidation products (i.e., oxalate, pyruvate, glycolate, and HMWCs) are expected to stay, at least partially, in the particle-phase once the cloud droplets evaporate and thus contribute to atmospheric organic PM.

While SOA_{aq} formation from glyoxal and methylglyoxal has received more attention, glycolaldehyde is also a potentially important SOA_{aq} precursor. Glycolaldehyde is produced in the gas-phase from isoprene (~6–22% molar yield)[44,45], ethylene (20–100% molar yield) [15,46,47], methyl vinyl ketone (51–70% molar yields)[15,48], and methylbutenol (50–78% molar yield)[48-50], and is directly emitted from biomass burning (4–20 Tg a^{-1}; Yokelson R. J., personal communication)[51-53] and biofuel use (1–2 Tg a^{-1})[15]. Like the other SOA_{aq} precursors, glycolaldehyde is a water-soluble compound ($H^*_{298} > 3 \times 10^5$ M atm^{-1})[54]. In the aqueous-phase, it hydrates and reacts with OH radical to produce glycolic, glyoxylic, and oxalic acid, as well as glyoxal and HMWCs[36,55]. The formation of malonic and succinic acid has also been reported[36]. Perri et al.[36] estimated the SOA mass yield for glycolaldehyde by measuring products of the aqueous OH radical (~10^{-13} M) oxidation of glycolaldehyde (1 mM), multiplying by the approximate fraction of each compound found in the particle-phase in the atmosphere and dividing by the mass of precursor reacted. The total SOA yield was taken to be the sum of the individual compound yields. SOA mass yields were up to 60% for reaction times less than 25 min (e.g., cloud contact times) and about 40% at later times when glycolaldehyde was depleted (>40 min). The limitations of the approach used by Perri et al.[36] are that 14–23% of organic carbon was unquantified and therefore not included in the yield calculations,

and that this approach neglects chemical transformations, if any, that occur during droplet evaporation. For example, glyoxal partially dehydrates during droplet evaporation and forms oligomers that could lead to higher SOA mass yields[25,28]. Our current understanding of the processes that occur during cloud droplet evaporation is still incomplete and contributes to the uncertainty in SOA formation from cloud processing[17].

To our knowledge, El Haddad et al.[27] were the first to combine aqueous photooxidation and droplet evaporation. They reacted methacrolein with OH radicals, then nebulized and dried the sample solution in a mixing chamber. The major limitations of that study were: the need for substantial particle loss corrections, and that SOA yields were measured from samples after 5 h of reaction, whereas the lifetime of a cloud droplet is on the order of several minutes[42,56].

The objectives of this paper are to study the formation of glycolaldehyde SOA through cloud water chemistry (e.g., aqueous photooxidation) and droplet evaporation and to further the understanding of the gas–particle partitioning behavior of aqueous glycolaldehyde oxidation products. To accomplish this, we report experimental glycolaldehyde SOA_{aq} yields at 10–13% relative humidity (RH) and compare the partitioning behavior of glycolaldehyde SOA_{aq} with that of a suite of organic acids at a range of liquid vapor pressures ($p_L°$) and enthalpies of vaporization (ΔH_{vap}). This paper builds on work conducted by Perri et al.[36] and verifies that SOA forms from cloud processing of glycolaldehyde. The experimental approach used negates the need to correct for particle losses. To our knowledge, this is the first study to provide data characterizing the volatility of glycolaldehyde SOA_{aq}.

2.3 Experimental Methods

Detailed experimental procedures are provided below. Briefly, monodisperse droplets were generated from aqueous reaction solutions formed through the OH radical oxidation of glycolaldehyde and from standard solutions (Figure 2-1). These droplets were evaporated and the diameters of the residual monodisperse aerosols were measured. The SOA yield was calculated as the mass of a residual particle divided by the mass of glycolaldehyde reacted from a single corresponding droplet. The ratio of the residual particle mass to the organic mass in the original droplet (PM mass/OM mass) is related to the fraction of the organic matter that remains in the particle-phase. By comparing the PM mass/OC mass for reaction samples and for standards, the volatility of glycolaldehyde SOA was characterized. New insights into the aqueous-phase chemistry of glycolaldehyde are also provided.

2.3.1 Aqueous-Phase Photochemistry

Aqueous photooxidation experiments were conducted with glycolaldehyde (1 mM) and OH radicals (~10^{-12} M) in a 1-L reaction vessel, as described previously[36]. Glycolaldehyde (98%; Pfaltz & Bauer) was dissolved with 18 MOhm Milli-Q water and diluted to 1 mM. OH radicals were formed in situ by photolysis of 5 mM hydrogen peroxide (diluted from 30% w/w; Sigma-Aldrich) using a 254-nm mercury lamp. Initial, final, and average OH radical concentrations were estimated to be 6×10^{-13} M, 4×10^{-12} M, and $(4\pm2)\times10^{-12}$ M, respectively, by modeling the chemistry in the reaction vessel using the mechanism published in Perri et al.[36,57]. Experiments were conducted at 22 ± 3°C (n = 3). Reaction samples were collected at several reaction times from 0 to 118 min with 50–100% duplicates. The pH of the reaction solution decreased from 4.7 to 3.6 over the

experiment, which is within typical cloud pH values (pH = 2–7)[58,59]. Samples were analyzed by ion chromatography (IC; Dionex ICS-3000) within 12 h of collection to quantify organic acids, as described previously[36,37]. Samples were analyzed for total organic carbon (TOC; Shimadzu TOC-5000A), by electrospray ionization mass spectrometry (ESI-MS; HP-Agilent 1100), and by IC-ESI-MS, as described previously[30,36,38].

While Perri et al.[36] added catalase to samples to destroy any remaining H_2O_2, we did not, so as to simplify the droplet evaporation experiments. Previous control experiments[36-38] have shown that glyoxylic acid degrades in the presence of H_2O_2, producing formic acid, while glycolic, oxalic, malonic, and succinic acid and glycolaldehyde do not. The reaction of glyoxylic acid with H_2O_2 is slow compared with its reaction with OH radicals and thus is not expected to affect the chemistry in the reaction vessel[37]. However, this reaction converts glyoxylic to formic acid in samples awaiting analysis. Glycolaldehyde photolysis generates glycolic and glyoxylic acid; however, this reaction is also slow relative to OH radical oxidation[36]. Thus, based on these past studies, we are confident that the experiments reported herein yield products generated from the reaction between glycolaldehyde and OH radicals, with the exception that the resulting samples are enriched in formic acid and depleted in glyoxylic acid.

2.3.2 Sample Solutions

In this study, droplet evaporation experiments (Section 2.3) were conducted using two types of solutions. These were used to validate previously estimated SOA yields, provide insights into the effects of cloud droplet evaporation, and characterize the volatility of the SOA_{aq} formed. Solutions were: (1) samples from glycolaldehyde

photooxidation experiments and (2) organic standards (individual and mixtures) that span a wide range of vapor pressures. Both types of solutions were used to generate monodisperse droplets that were then evaporated; the diameters of the residual particles were measured.

Reaction samples from the OH radical oxidation of glycolaldehyde were taken from the reaction vessel at specific reaction times (e.g., 0, 10, 20, 40, 50, and 70 min) using 25-mL syringes and passed through the droplet generation and evaporation system within 2–6 h (Figure 2-1). Individual solutions of ammonium oxalate (99.0%; Fluka Analytical), oxalic (0.0991 N; Fluka Analytical), acetic (99.99%; Sigma-Aldrich), succinic (99.99%; Sigma-Aldrich), glutaric (99.9%; Aldrich Chemical), and tartaric (99.4%; Aldrich Chemical) acid were diluted to 0–4000 μM C.

2.3.3 Droplet Generation and Evaporation

A vibrating orifice aerosol generator (VOAG, TSI Model 3450)[60] was used to generate and evaporate monodisperse droplets of sample solutions to form a monodisperse aerosol (Figure 2-1) (liquid flow rate 0.077 mL/min, frequency ~160 kHz, dilution air 50 L/min, dispersion air 1000 mL/min, residence time 6 s, RH = 10–13%, t = ~24°C). [The Standard Operating Procedure (SOP) of the droplet generation and evaporation system can be found in Appendix A1]. A major advantage of this approach is that one single-size droplet generates one single-size particle, facilitating the calculation of SOA mass yields by dividing the mass of one particle by the mass of precursor that reacted from one droplet. This approach is a relatively simple way of providing SOA mass yields in advance of the time when the aqueous and droplet evaporation chemistry is fully elucidated. The VOAG droplet generator was inverted and mounted on top of a

vertical column to minimize coagulation. The VOAG passed filtered solutions (0.4 μm Isopore^{TM} membrane filter) through a 10-μm diameter (nominal) vibrating orifice, which produces a 20-μm nominal droplet diameter. Due to manufacturing tolerances, the orifice and droplet diameters may differ from the nominal values by ±25%; hence, the droplet diameter was determined by calibrating the system with ammonium sulfate, $(NH_4)_2SO_4$ (3.1801 M; Fluka Analytical). The slope of D_p versus $C^{1/3}$, from the relation $D_p = D_d\, C^{1/3}$, indicated the diameter of the generated droplets (18.3 ± 0.4 μm)—where D_d is droplet diameter (μm), D_p is particle diameter (μm), and C is the volumetric concentration of the solute in the solution (cm^3_{solute} /$cm^3_{solution}$). Succinic acid standards were used as an independent accuracy check. Deflection tests were performed routinely, deflecting the droplet stream with a perpendicular airstream to verify that the generated droplets were monodisperse (i.e., droplets remained in a single stream). Droplets were merged with a larger volume of clean dry air (Filtered Air Supply, TSI Model 3074B, two coalescing filters, membrane dryer, and carbon-vapor filter), which evaporated water and other volatile components of the droplets, leaving low-volatility particles (i.e., SOA). The particle residence time at 10–13% RH (6 s) is longer than typically used to equilibrate ambient particles in tandem differential mobility analyzer measurements of aerosol hygroscopicity, and is considered to be long enough for water equilibration, assuming an accommodation coefficient of 0.02[61]; the potential for water retention is discussed below. Residual particles passed through an ionizer (NRD StaticMaster 2U500, Po-210; gives particles a Boltzmann charge distribution) and their optical diameters were measured with an optical particle counter (OPC, Grimm Aerosol Spectrometer, Model 1.109, 31 channels) for 10 min after obtaining stable liquid feed pressure. To avoid organic

contamination, the solutions, sheath/dilution air, and aerosol were transported through this system using Teflon tubing, with the exception of a short piece of flexible Tygon tubing (13 cm long, 0.3 cm wide) used to connect the OPC.

By knowing the precursor concentration, droplet diameter, resulting particle diameter, and approximate material density, we calculated the SOA mass yield, which is the mass of a residual particle (PM mass formed) divided by the mass of glycolaldehyde (GLYDE) reacted from the volume of solution contained in one droplet, in the following way:

$$\text{SOA mass yield}_{(i)} = \frac{\text{PM mass formed}}{\Delta \text{ mass of GLYDE}} = \frac{\frac{\pi}{6} \times \left(D_p\right)_i^3 \times \rho_i}{\text{Initial GLYDE mass} - \text{Final GLYDE mass}_i}$$

For reaction time *i*, PM mass formed was calculated from the measured geometric mean diameter (D_p), assuming spherical particles and using the concentration-weighted particle density (ρ)[62] estimated from measured (IC) species in reaction solutions (Table 2-1). [Example calculation of PM mass can be found in section 5 of Appendix A1]. The mass of glycolaldehyde reacted was calculated as the volume of a droplet times the difference between the initial concentration of glycolaldehyde in the reaction vessel before oxidation began (1 mM) and the modeled concentration of glycolaldehyde remaining at time *i*[36,57].

To assess the volatility of glycolaldehyde SOA_{aq}, six dilutions of five organic standards and five dilutions of 10- and 40- min reaction solutions were sampled through the VOAG system (25 mL each). The TOC content of each solution ($[TOC]_{droplet}$) and final particle diameter (D_p) were directly measured, and from these, the mass of organic matter (OM) in the droplet and the mass of residual PM were calculated, respectively.

$[TOC]_{droplet}$ was converted to OM $mass_{(droplet)}$ using OM/OC values (Appendix A2, A3). D_p was converted to PM mass by assuming spherical particles and using liquid densities (Appendix A2). Ratios of PM mass/droplet OM mass for reaction solutions and standards, and the liquid vapor pressures ($p_L°$) and enthalpies of vaporization (ΔH_{vap}) of the standards were used to characterize the volatility behavior of glycolaldehyde SOA_{aq}. Note that ratios of PM mass/droplet OM mass represent the fraction of total droplet organic matter that remains in the particle-phase (i.e., particle fraction), not to be confused with the SOA mass yields, which are defined differently. Values of $p_L°$ and ΔH_{vap} for the standards were estimated using the SIMPOL group contribution method[63] and the Joback and Reid group contribution method[64], respectively. Our experimental conditions were constant, stable, and controlled, so the differences between experiments are driven only by vapor pressure and hygroscopicity.

2.3.4 Quality Assurance and Quality Control

Measured organic acid concentrations were accurate within 6–10%, expressed as a pooled coefficient of variation based on independent standards, with the exception of formic (27%) and glyoxylic acid (60%). Calibration curves of conductivity (μS) versus concentration (M) had coefficients of determination (r^2) better than 99.76% for all measured acids (glycolic, formic, glyoxylic, succinic, malonic, and oxalic acid). Method precision was 2%, expressed as a pooled coefficient of variation of samples (n = 240) collected in duplicate during experiments. Organic acid detection limits (μM) were 0.1–4.3[36]. Method precision (3%) for TOC (four injections/sample) was calculated as the pooled coefficient of variation of duplicate samples (n = 14). Variability of TOC measurements for identical time points across experiments was 14%.

Dynamic blanks were generated before each experiment by sampling Milli-Q water directly from the reaction vessel. Dynamic blanks were analyzed for organic acids and TOC and used to generate and evaporate droplets as if they were samples. IC analysis of dynamic blanks and water blanks confirmed no contamination. TOC values of dynamic blanks (1–35 μM C) were subtracted from their corresponding TOC sample measurements. The volume of the contaminants measured from the VOAG system was also subtracted from the samples using their corresponding dynamic blanks. The volume of contaminants from blanks was ~0.01 μm^3, about 6–27% of dried residual particle volume.

The performance of the VOAG was tested daily before and after each droplet evaporation experiment with $(NH_4)_2SO_4$ standards. The performance criterion for acceptance was a ≤10% difference between the theoretical and the measured particle diameter. The method precision for diameter was 4%, calculated as the pooled standard deviation of the $(NH_4)_2SO_4$ particle diameter divided by the mean diameter of 250 μM $(NH_4)_2SO_4$ samples (n = 34) collected in duplicate during experiments. A 4% precision for particle diameter was also calculated based on 60 μM succinic acid solutions (n = 6).

2.4 Results and Discussion

2.4.1 Glycolaldehyde Aqueous Photooxidation

Time profiles of product concentrations (Figure 2-2) and TOC (Appendix A4) are in reasonable agreement with Perri et al. [36] and verify that compounds found predominantly in the particle-phase in the atmosphere (e.g., oxalate, glycolate, malonate) can form from the aqueous photooxidation of glycolaldehyde with OH radicals. The only significant differences (p = 0.05, Cochran's t-test, two-tailed) between this work and

Perri et al. [36] are that the concentrations of formic acid obtained in this work are higher, and those of glycolic and glyoxylic acid are lower, especially early in the reaction (~12 min). The lower glyoxylic acid concentrations can be explained by the fact that we did not use catalase to destroy H_2O_2 in samples and glyoxylic acid reacts with H_2O_2 in samples awaiting analysis to form formic acid. This does not explain the lower glycolic acid concentrations, as recovery of glycolic acid was 93% more than 7 h after 250 μM H_2O_2 was added to a 250 μM glycolic acid standard (this work), in agreement with previous findings[36,37]. Glycolic acid measurements reported herein are in good agreement with modeled glycolic acid (better than previous measurements; see figure 5 in Perri et al.[36]). However, the difference between glycolic acid measurements is not well understood; these differences are a source of uncertainty in SOA mass yields for reaction times <30 min.

Experiments conducted with 1 mM glycolaldehyde provide insights into the OH radical oxidation of glycolaldehyde in clouds (1–5 μM glycolaldehyde) and in wet aerosols, where the total concentration of dissolved organics is quite high (1–10 M). Previous OH radical experiments conducted with 30, 300, and 3000 μM glyoxal[37] and the subsequent detailed chemical modeling from 10 μM to 10 M[43] suggest that organic radical–radical chemistry leading to higher-carbon-number products is minor at concentrations found in cloud water and becomes dominant at the high concentrations of water-soluble organics found in wet aerosols. We expect that this is also true for glycolaldehyde. The dilute glycolaldehyde chemistry model runs for the 1–5 μM glycolaldehyde[36] and the 1 mM glycolaldehyde experiments both show that the vast majority of the mass at the beginning of the reaction (10–20 min) is in the form of

glycolic acid, glyoxylic (or formic) acid, and glyoxal (not measured here but quantified by Perri et al. [36]). Of these products, glycolic acid (and its salts) has the lowest volatility. Oxalic acid is the most abundant product after 30 min. Therefore, we expect that for typical cloud contact times (10–30 min), glycolaldehyde SOA_{aq} formed through cloud processing will be predominantly glycolate and whatever HMWCs that form during droplet evaporation (e.g., glyoxal acetal oligomers)[25,28].

Samples from experiments conducted with 1 mM glycolaldehyde also contained smaller concentrations of higher-molecular-weight products (IC-ESI-MS, Figure 2-3; ESI-MS in supplemental information, Appendix A5) and products with higher carbon number than glycolaldehyde (Figure 2-4). Since these products were formed in the presence and not in the absence of OH radicals, we expect that they formed through organic radical–radical chemistry, and that these and similar products will be the dominant products of glycolaldehyde chemistry in wet aerosols. It should be noted that while cloud contact times are typically 10–30 min, chemistry in aerosol water can proceed for hours with continuous addition of the precursor. IC-ESI-MS analyses (Figures 2-3 and 2-4) provide new insights into such chemistry.

The IC-ESI-MS negative-mode spectrum of a mixed standard solution and of experimental samples taken 17 and 52 min into the glycolaldehyde plus OH radical experiment are shown in Figure 2-3. The mixed standard (Figure 2-3a) consisted of glycolic acid (peak A, 5.8 min, m/z^- 75), formic acid (peak B, 6.8 min, not detectable by ESI-MS), succinic acid (peak C, 21.1 min, m/z^- 117), malonic acid (peak D, 22.3 min, m/z^- 103), and oxalic acid (peak F, 25.4 min, m/z^- 89). Contaminants, sulfate (m/z^- 97), can be found in peak E. Some glycolic acid can be seen in peak B. IC-ESI-MS results for

experimental samples (Figures 2-3b, 2-3c) verify the formation of glycolic and oxalic acid in the mechanism published in Lim et al.[23] and the formation of succinic and malonic acid published in Perri et al.[36] by IC alone. Interestingly, IC-ESI-MS shows that peaks with retention times of succinic and malonic acid also contain malic (peak C, m/z^- 133) and tartaric acid (peak D, m/z^- 149, 17 min sample only). HMWCs also form (peak G). Identification of HMWCs after IC separation verifies that it is not an artifact of electrospray ionization. In fact, most of the mass with retention time of succinic and malic acid is malic acid (m/z^- 133). Malic acid peaks ~20 min into the reaction, whereas succinic acid peaks after ~50 min (Figure 2-4a). IC-ESI-MS (Figure 2-4b) suggests that malonic acid (m/z^- 103) is responsible for most of the mass with the retention time of "malonic and tartaric acid"; some tartaric acid (m/z^- 149) is present early in the reaction (~20 min). Tartaric acid formation has been observed also in the aqueous OH radical oxidation of glyoxal (3 mM), a glycolaldehyde intermediate[37]. Its formation and concentration dynamics can be explained by organic radical–radical reactions[37,43]. We expect that the formation of products with higher carbon numbers than glycolaldehyde (C2) (e.g., malic acid: C4, succinic acid: C4, tartaric acid: C4, and malonic acid: C3, and HMWCs), which are formed from glycolaldehyde in the presence and not the absence of OH radicals, are also formed through organic radical–radical reactions. Time profiles of other ions measured by IC-ESI-MS are provided in Appendix A6.

2.4.2 Droplet Evaporation Experiments

2.4.2.1 Vapor Pressure and Enthalpy of Vaporization

The residual particle mass (PM mass) was well correlated with the mass of organic matter in the droplet (r^2 = 0.84–0.99, Table 2-2 and Figure 2-5) for all organic

acid standards except acetic acid, which is quite volatile. We can observe from Figure 2-5 that as we go from the most volatile compound (acetic acid) to the least volatile compound (tartaric acid), the slope (m = PM mass/droplet OM mass) increases, indicating that a larger fraction of the mass remains in the particle-phase. Shown also in Figure 2-5 are results of droplet evaporation experiments with 10- and 40-min reaction samples (black and red thick lines, respectively).

The slopes (PM mass/droplet OM mass) from Figure 2-5 are plotted versus vapor pressure ($p_L°$) in Figure 2-6 and versus enthalpy of vaporization (ΔH_{vap}) in Appendix A7 (Table 2-2). A sigmoidal curve was fit to these data in accordance with the gas–particle partitioning theory[8], since the slope (PM mass/droplet OM mass) reflects the fraction of OM found in the particle-phase. These plots suggest that glycolaldehyde SOA_{aq} behaves like a dicarboxylic acid, with a $p_L°$ of ~10^{-7} atm and ΔH_{vap} of ~70 kJ/mol, and similar to the behavior of the mix of organic acids that comprise the majority of products identified in the reaction samples (Table 2-2). To our knowledge, this is the first study to characterize the volatility behavior of glycolaldehyde SOA_{aq}.

Note that the ratio of the PM mass to droplet OM mass for tartaric acid is greater than 1 (Figure 2-6, left-most data point). This is not surprising, since tartaric acid is expected to remain almost entirely in the particle-phase, and it retains water even at low RH (5%)[65]. After accounting for the effect of water on particle density, Figure 2-6 suggests that the tartaric acid particles were <33% water. To understand to what degree water retension could alter Figure 2-6, we present PM mass/OM mass for all standards calculated using dry densities (line 1, Figure 2-6) and densities assuming 33% water (line 2, Figure 2-6). This is an upper bound for the water fraction, since the other standards are

not likely to retain as much water as tartaric acid. These corrections had a negligible effect on our characterization of the volatility behavior of glycolaldehyde SOA_{aq} (Figure 2-6).

We speculate that the vapor pressure of glycolaldehyde SOA_{aq} will be orders of magnitude lower if the products are neutralized. For example, the liquid vapor pressure of succinic acid using the SIMPOL group contribution method[63] is 7.59×10^{-8} atm and the vapor pressure of ammonium succinate is 2×10^{-11} atm (EPA-EPI Suite™ [66]). Enhancements in SOA yields in the presence of ammonia have been shown previously for α-pinene and ozone under dry (RH < 2%) and humid (RH = 50%) conditions[67]. Also, the work of Dinar et al.[68] verified that the reactive uptake of ammonia by acidic functional groups (e.g., adipic and citric acid) leads to the formation of ammonium salts and can substantially influence the chemical and physical properties of the aerosol. Interestingly, oxalate is found mostly in the particle-phase in the atmosphere[69] even though the vapor pressure of oxalic acid is not that low. We suggest that this is because oxalate is mostly present in the atmosphere as a salt (e.g, ammonium oxalate) (Figure 2-7). Certainly, the form of these acids depends on their pKa, the availability of ammonia and the abundance of stronger particle-phase acids (i.e., acidic sulfate), which impacts aerosol acidity. Oxalic acid is the strongest organic acid detected in glycolaldehyde SOA_{aq} ($pK_{a(1)}$ = 1.23 and $pK_{a(2)}$ = 4.19), followed by malonic, tartaric, glyoxylic, malic, glycolic, and succinic acid. At pH 4.5, a typical value in cloud water, most of these acids are expected to be in their dissociated form, $pH > pK_a$ (e.g., glycolic, glyoxylic, tartaric, and oxalic acid) or amphiprotic form, $pK_{a(1)} < pH < pK_{a(2)}$ (e.g., malic and succinic acid). Aerosol pH is not well characterized and depends not only on the concentrations of major

inorganic and organic ions but also on the water content, buffering capacity, and gas–particle partitioning of many semivolatile compounds[70,71]. Cation to anion ratios close to 1, suggesting a neutral aerosol, are frequently observed in the western United States and polluted rural and urban European areas[70]. In contrast, there are days in Hong Kong when aerosol pH is less than 1, suggesting that even oxalate is present as an acid[71].

2.4.2.2 Aldehyde Oligomerization

In aqueous solutions, glyoxal species (i.e., hydrated monomers and oligomers) coexist in equilibrium and the predominant form depends on the concentration. Monomers dominate when glyoxal concentrations are below 1 M; at higher concentrations, dimers and oligomers dominate[72]. Glyoxal reacts with itself to form acetal oligomers in evaporating droplets, thus contributing to SOA formation through cloud droplet evaporation[25,28]. Similarly, during droplet evaporation, we expect the dehydration of glycolaldehyde to initiate the formation of glycolaldehyde oligomers via hemiacetal formation. We propose the formation of a hemiacetal that either forms dioxane and dioxolane dimers or reacts with another glycolaldehyde molecule to form an open-chain trimer, which in the process of drying, ultimately forms a trimer ring through intermolecular nucleophilic reactions[73] (Figure 2-8a). Additionally, glycolaldehyde could oligomerize through aldol condensation (Figure 2-8b). [Unpublished evidence showing glycolaldehyde retention in the particle-phase through droplet evaporation experiments can be found in Appendix A8]. We expect that glycolaldehyde oligomers formed in this way also contribute to the formation of SOA in the atmosphere.

2.4.2.3 SOA_{aq} Mass Yields

The mass of SOA_{aq} per mass of glycolaldehyde reacted (SOA_{aq} mass yield) (Figure 2-9, Table 2-1) decreased gradually with time from about 120% to 50%. We expect that these early yields are driven by glycolic acid and oligomers formed during dehydration of glycolaldehyde and glyoxal. Later yields are driven by oxalic acid (Figure 2-2). Shown in Figure 2-9 are the yields from this work (squares), yields estimated by Perri et al. (triangles), and the yields that would have been obtained if all droplet organic matter had remained in the particle-phase (circles). These were calculated using IC quantification of organic acids and model predictions of remaining glycolaldehyde and glyoxal. Note that these values (circles) underestimate the true upper bound at later reaction times, since for later reaction times (>40 min), unquantified products accounted for about 14–23% of TOC in the reaction vessel[36]. The fact that yields for early time points are much lower than would be obtained if all droplet organic matter were retained in the particle-phase and yields for later time points are not, is consistent with the fact that the solution contained more volatile components (formic acid, glycolaldehyde, glyoxal) for early time points compared with later time points. This finding also suggests that glycolaldehyde and glyoxal are not 100% retained in the particle-phase through oligomer formation.

Our yields are higher than SOA_{aq} mass yields estimated by Perri et al. [36]. There are several possible explanations for this. First, Perri's yields were calculated based only on species quantified by IC, whereas the yields in this work also included any unquantified products from the photooxidation reaction and droplet evaporation (e.g., acetal oligomers). Second, Perri's yields were calculated assuming no water retention,

whereas our yields include any particle-bound water. Such water might exist in equilibrium with its vapor, or particles could exist in a metastable state after drying, with a kinetic barrier inhibiting the release of water, despite the theoretically adequate time for water equilibration.

Differences between yields obtained herein and those in Perri et al. [36] could also occur because of differences in gas–particle partitioning or effects of residual H_2O_2 in samples. Perri et al. [36] made use of atmospheric measurements of gas–particle partitioning to estimate the fraction of each product in the particle-phase, whereas in this work, the gas–particle partitioning was determined by experimental conditions and might not be the same as in the atmosphere. Also, this work did not use catalase and hence residual H_2O_2 could have formed complexes with glyoxal and converted glyoxylic acid to formic acid. Specifically, Lee et al.[74] found that about 15–20% of glyoxal is consumed by H_2O_2 within 2 h. Tan et al.[38] found that H_2O_2 converted 98% of glyoxylic acid to the more volatile formic acid within 2 h. Last, the OPC was calibrated by the manufacturer with polystyrene latex (PSL) particles, which have a refractive index of 1.59. Based on measured products, we expect that glycolaldehyde SOA has a refractive index of ~1.5, introducing an uncertainty of ~10% in the measured particle diameter, before accounting for the effects of retained water on refractive index.

2.5 Conclusions

Mass yields were measured for SOA_{aq} formed from the aqueous OH radical (~10^{-12} M) oxidation of glycolaldehyde (1 mM) and the volatility behavior was characterized. While SOA_{aq} mass yields are expected to vary with atmospheric conditions, vapor pressure and enthalpy of vaporization can be used to evaluate the

behavior of this material under a range of atmospheric conditions (e.g., temperature dependence). This work verifies that SOA_{aq} forms after glycolaldehyde reacts with OH radicals in droplets. Additional chemistry during droplet evaporation enhances the SOA_{aq} production (e.g., oligomerization of aldehydes). SOA_{aq} yields were highest (~80–120%) at reaction times (~10–20 min) that are most relevant to cloud droplet lifetimes. These yields include the contribution of HMWCs and account for droplet evaporation. Glycolaldehyde SOA_{aq} behaves like a dicarboxylic acid, with a liquid vapor pressure of $\sim 10^{-7}$ atm and the enthalpy of vaporization of ~70 kJ/mol. However, we expect the vapor pressure to be considerably lower if the mix of organic acids in the SOA_{aq} gets neutralized in the atmosphere to form organic salts.

2.6 References

(1) Turpin, B. J.; Saxena, P.; Andrews, E. Measuring and simulating particulate organics in the atmosphere: problems and prospects. *Atmospheric Environment* **2000**, *34*, 2983–3013.

(2) U.S. EPA. *Air Quality Criteria for Particulate Matter*; United States Environmental Protection Agency (U.S. EPA), Research Triangle Park, NC, **2004**.

(3) Heald, C. L.; Jacob, D. J.; Park, R. J.; Russell, L. M.; Huebert, B. J.; Seinfeld, J. H.; Liao, H.; Weber, R. J. A large organic aerosol source in the free troposphere missing from current models. *Geophys. Res. Lett.* **2005**, *32*, L18809.

(4) Kanakidou, M.; Seinfeld, J. H.; Pandis, S. N.; Barnes, I.; Dentener, F. J.; Facchini, M. C.; Van Dingenen, R.; Ervens, B.; Nenes, A.; Nielsen, C. J.; Swietlicki, E.; Putaud, J. P.; Balkanski, Y.; Fuzzi, S.; Horth, J.; Moortgat, G. K.; Winterhalter, R.; Myhre, C. E. L.; Tsigaridis, K.; Vignati, E.; Stephanou, E. G.; Wilson, J. Organic aerosol and global climate modelling: a review. *Atmos. Chem. Phys.* **2005**, *5*, 1053–1123.

(5) Volkamer, R.; Jimenez, J. L.; San Martini, F.; Dzepina, K.; Zhang, Q.; Salcedo, D.; Molina, L. T.; Worsnop, D. R.; Molina, M. J. Secondary organic aerosol formation from anthropogenic air pollution: Rapid and higher than expected. *Geophys. Res. Lett.* **2006**, *33*.

(6) Hallquist, M.; Wenger, J.; Baltensperger, U.; Rudich, Y.; Simpson, D.;

Claeys, M.; Dommen, J.; Donahue, N.; George, C.; Goldstein, A. The formation, properties and impact of secondary organic aerosol: current and emerging issues. *Atmos. Chem. Phys.* **2009**, *9*, 5155–5236.

(7) Carlton, A. G.; Pinder, R. W.; Bhave, P. V.; Pouliot, G. A. To What Extent Can Biogenic SOA be Controlled? *Environmental Science & Technology* **2010**, *44*, 3376–3380.

(8) Odum, J. R.; Hoffmann, T.; Bowman, F.; Collins, D.; Flagan, R. C.; Seinfeld, J. H. Gas/particle partitioning and secondary organic aerosol yields. *Environmental Science & Technology* **1996**, *30*, 2580–2585.

(9) Seinfeld, J. H.; Pankow, J. F. Organic Atmospheric Particulate Material. *Annu. Rev. Phys. Chem.* **2003**, *54*, 121–140.

(10) Blando, J. D.; Turpin, B. J. Secondary organic aerosol formation in cloud and fog droplets: a literature evaluation of plausibility. *Atmospheric Environment* **2000**, *34*, 1623–1632.

(11) Gelencsér, A.; Varga, Z. Evaluation of the atmospheric significance of multiphase reactions in atmospheric secondary organic aerosol formation. *Atmos. Chem. Phys.* **2005**, *5*, 2823–2831.

(12) Ervens, B.; Turpin, B. J.; Weber, R. J. Secondary organic aerosol formation in cloud droplets and aqueous particles (aqSOA): a review of laboratory, field and model studies. *Atmos. Chem. Phys.* **2011**, *11*, 11069–11102.

(13) Chen, J.; Griffin, R. J.; Grini, A.; Tulet, P. Modeling secondary organic aerosol formation through cloud processing of organic compounds. *Atmos. Chem. Phys.* **2007**, *7*, 5343–5355.

(14) Carlton, A. G.; Turpin, B. J.; Altieri, K. E.; Seitzinger, S. P.; Mathur, R.; Roselle, S. J.; Weber, R. J. CMAQ Model Performance Enhanced When In-Cloud Secondary Organic Aerosol is Included: Comparisons of Organic Carbon Predictions with Measurements. *Environmental Science & Technology* **2008**, *42*, 8798–8802.

(15) Fu, T.-M.; Jacob, D. J.; Wittrock, F.; Burrows, J. P.; Vrekoussis, M.; Henze, D. K. Global budgets of atmospheric glyoxal and methylglyoxal, and implications for formation of secondary organic aerosols. *J. Geophys. Res.* **2008**, *113*, D15303.

(16) Fu, T.-M.; Jacob, D. J.; Heald, C. L. Aqueous-phase reactive uptake of dicarbonyls as a source of organic aerosol over eastern North America. *Atmospheric Environment* **2009**, *43*, 1814–1822.

(17) Gong, W.; Stroud, C.; Zhang, L. Cloud Processing of Gases and Aerosols in

Air Quality Modeling. *Atmosphere* **2011**, *2*, 567–616.

(18) Myriokefalitakis, S.; Tsigaridis, K.; Mihalopoulos, N.; Sciare, J.; Nenes, A.; Kawamura, K.; Segers, A.; Kanakidou, M. In-cloud oxalate formation in the global troposphere: a 3-D modeling study. *Atmos. Chem. Phys.* **2011**, *11*, 5761–5782.

(19) Sorooshian, A.; Lu, M.-L.; Brechtel, F. J.; Jonsson, H.; Feingold, G.; Flagan, R. C.; Seinfeld, J. H. On the Source of Organic Acid Aerosol Layers above Clouds. *Environmental Science & Technology* **2007**, *41*, 4647–4654.

(20) Sorooshian, A.; Ng, N. L.; Chan, A. W. H.; Feingold, G.; Flagan, R. C.; Seinfeld, J. H. Particulate organic acids and overall water-soluble aerosol composition measurements from the 2006 Gulf of Mexico Atmospheric Composition and Climate Study (GoMACCS). *J. Geophys. Res.* **2007**, *112*.

(21) Ervens, B. A modeling study of aqueous production of dicarboxylic acids: 1. Chemical pathways and speciated organic mass production. *J. Geophys. Res.* **2004**, *109*.

(22) Ervens, B.; Carlton, A. G.; Turpin, B. J.; Altieri, K. E.; Kreidenweis, S. M.; Feingold, G. Secondary organic aerosol yields from cloud-processing of isoprene oxidation products. *Geophys. Res. Lett.* **2008**, *35*.

(23) Lim, Y. B.; Ziemann, P. J. Products and Mechanism of Secondary Organic Aerosol Formation from Reactions of n-Alkanes with OH Radicals in the Presence of NO x. *Environmental Science & Technology* **2005**, *39*, 9229–9236.

(24) Heald, C. L.; Jacob, D. J.; Turquety, S.; Hudman, R. C.; Weber, R. J.; Sullivan, A. P.; Peltier, R. E.; Atlas, E. L.; de Gouw, J. A.; Warneke, C.; Holloway, J. S.; Neuman, J. A.; Flocke, F. M.; Seinfeld, J. H. Concentrations and sources of organic carbon aerosols in the free troposphere over North America. *J. Geophys. Res.* **2006**, *111*.

(25) Loeffler, K. W.; Koehler, C. A.; Paul, N. M.; De Haan, D. O. Oligomer Formation in Evaporating Aqueous Glyoxal and Methyl Glyoxal Solutions. *Environmental Science & Technology* **2006**, *40*, 6318–6323.

(26) Sorooshian, A.; Varutbangkul, V.; Brechtel, F. J.; Ervens, B.; Feingold, G.; Bahreini, R.; Murphy, S. M.; Holloway, J. S.; Atlas, E. L.; Buzorius, G.; Jonsson, H.; Flagan, R. C.; Seinfeld, J. H. Oxalic acid in clear and cloudy atmospheres: Analysis of data from International Consortium for Atmospheric Research on Transport and Transformation 2004. *J. Geophys. Res.* **2006**, *111*.

(27) El Haddad, I.; Liu, Y.; Nieto-Gligorovski, L.; Michaud, V.; Temime-Roussel, B.; Quivet, E.; Marchand, N.; Sellegri, K.; Monod, A. In-cloud processes of methacrolein under simulated conditions – Part 2: Formation of secondary organic aerosol. *Atmos. Chem. Phys.* **2009**, *9*, 5107–5117.

(28) De Haan, D. O.; Corrigan, A. L.; Tolbert, M. A.; Jimenez, J. L.; Wood, S. E.; Turley, J. J. Secondary Organic Aerosol Formation by Self-Reactions of Methylglyoxal and Glyoxal in Evaporating Droplets. *Environmental Science & Technology* **2009**, *43*, 8184–8190.

(29) De Haan, D. O.; Corrigan, A. L.; Smith, K. W.; Stroik, D. R.; Turley, J. J.; Lee, F. E.; Tolbert, M. A.; Jimenez, J. L.; Cordova, K. E.; Ferrell, G. R. Secondary Organic Aerosol-Forming Reactions of Glyoxal with Amino Acids. *Environmental Science & Technology* **2009**, *43*, 2818–2824.

(30) Altieri, K. E.; Carlton, A. G.; Lim, H.-J.; Turpin, B. J.; Seitzinger, S. P. Evidence for Oligomer Formation in Clouds: Reactions of Isoprene Oxidation Products. *Environmental Science & Technology* **2006**, *40*, 4956–4960.

(31) Altieri, K. E.; Seitzinger, S. P.; Carlton, A. G.; Turpin, B. J.; Klein, G. C.; Marshall, A. G. Oligomers formed through in-cloud methylglyoxal reactions: Chemical composition, properties, and mechanisms investigated by ultra-high resolution FT-ICR mass spectrometry. *Atmospheric Environment* **2008**, *42*, 1476–1490.

(32) Carlton, A. G.; Turpin, B. J.; Lim, H.-J.; Altieri, K. E.; Seitzinger, S. Link between isoprene and secondary organic aerosol (SOA): Pyruvic acid oxidation yields low volatility organic acids in clouds. *Geophys. Res. Lett.* **2006**, *33*.

(33) Carlton, A. G.; Turpin, B. J.; Altieri, K. E.; Seitzinger, S.; Reff, A.; Lim, H.-J.; Ervens, B. Atmospheric oxalic acid and SOA production from glyoxal: Results of aqueous photooxidation experiments. *Atmospheric Environment* **2007**, *41*, 7588–7602.

(34) Liu, Y.; El Haddad, I.; Scarfogliero, M.; Nieto-Gligorovski, L.; Temime-Roussel, B.; Quivet, E.; Marchand, N.; Picquet-Varrault, B.; Monod, A. In-cloud processes of methacrolein under simulated conditions–Part 1: Aqueous phase photooxidation. *Atmos. Chem. Phys.* **2009**, *9*, 5093–5105.

(35) Michaud, V.; El Haddad, I.; Liu, Y.; Sellegri, K.; Laj, P.; Villani, P.; Picard, D.; Marchand, N.; Monod, A. In-cloud processes of methacrolein under simulated conditions–Part 3: Hygroscopic and volatility properties of the formed secondary organic aerosol. *Atmos. Chem. Phys.* **2009**, *9*, 5119–5130.

(36) Perri, M. J.; Seitzinger, S.; Turpin, B. J. Secondary organic aerosol production from aqueous photooxidation of glycolaldehyde: Laboratory experiments. *Atmospheric Environment* **2009**, *43*, 1487–1497.

(37) Tan, Y.; Perri, M. J.; Seitzinger, S. P.; Turpin, B. J. Effects of Precursor Concentration and Acidic Sulfate in Aqueous Glyoxal−OH Radical Oxidation and Implications for Secondary Organic Aerosol. *Environmental Science & Technology* **2009**, *43*, 8105–8112.

(38) Tan, Y.; Carlton, A. G.; Seitzinger, S. P.; Turpin, B. J. SOA from methylglyoxal in clouds and wet aerosols: Measurement and prediction of key products. *Atmospheric Environment* **2010**, *44*, 5218–5226.

(39) Tan, Y.; Lim, Y. B.; Altieri, K. E.; Seitzinger, S. P.; Turpin, B. J. Mechanisms leading to oligomers and SOA through aqueous photooxidation: insights from OH radical oxidation of acetic acid and methylglyoxal. *Atmos. Chem. Phys.* **2012**, *12*, 801–813.

(40) Poulain, L.; Katrib, Y.; Isikli, E.; Liu, Y.; Wortham, H.; Mirabel, P.; Le Calvé, S.; Monod, A. In-cloud multiphase behaviour of acetone in the troposphere: Gas uptake, Henryâ€™s law equilibrium and aqueous phase photooxidation. *Chemosphere* **2010**, *81*, 312–320.

(41) Zhang, X.; Chen, Z. M.; Zhao, Y. Laboratory simulation for the aqueous OH-oxidation of methyl vinyl ketone and methacrolein: significance to the in-cloud SOA production. *Atmos. Chem. Phys.* **2010**, *10*, 9551–9561.

(42) Ervens, B.; Volkamer, R. Glyoxal processing by aerosol multiphase chemistry: towards a kinetic modeling framework of secondary organic aerosol formation in aqueous particles. *Atmos. Chem. Phys.* **2010**, *10*, 8219–8244.

(43) Lim, Y. B.; Tan, Y.; Perri, M. J.; Seitzinger, S. P.; Turpin, B. J. Aqueous chemistry and its role in secondary organic aerosol (SOA) formation. *Atmos. Chem. Phys.* **2010**, *10*, 10521–10539.

(44) Lee, A.; Goldstein, A. H.; Kroll, J. H.; Ng, N. L.; Varutbangkul, V.; Flagan, R. C.; Seinfeld, J. H. Gas-phase products and secondary aerosol yields from the photooxidation of 16 different terpenes. *J. Geophys. Res.* **2006**, *111*.

(45) Nguyen, T. B.; Roach, P. J.; Laskin, J.; Laskin, A.; Nizkorodov, S. A. Effect of humidity on the composition of isoprene photooxidation secondary organic aerosol. *Atmos. Chem. Phys.* **2011**, *11*, 6931–6944.

(46) Niki, H.; Maker, P. D.; Savage, C. M.; Breitenbach, L. P. An FTIR study of mechanisms for the HO radical initiated oxidation of C2H4 in the presence of NO: Detection of glycolaldehyde. *Chemical Physics Letters* **1981**, *80*, 499–503.

(47) Orlando, J.; Tyndall, G.; Bilde, M.; Ferronato, C.; Wallington, T.; Vereecken, L.; Peeters, J. Laboratory study of the mechanism of OH-and Cl-initiated oxidation of ethylene. *J. Phys. Chem. A* **1998**, *102*, 8116–8123.

(48) Spaulding, R. S. Characterization of secondary atmospheric photooxidation products: Evidence for biogenic and anthropogenic sources. *J. Geophys. Res.* **2003**, *108*.

(49) Atkinson, R.; Arey, J. Atmospheric Degradation of Volatile Organic

Compounds. *Chem. Rev.* **2003**, *103*, 4605–4638.

(50) Carrasco, N.; Doussin, J. F.; O'Connor, M.; Wenger, J. C.; Picquet-Varrault, B.; Durand-Jolibois, R.; Carlier, P. Simulation Chamber Studies of the Atmospheric Oxidation of 2-Methyl-3-Buten-2-ol: Reaction with Hydroxyl Radicals and Ozone Under a Variety of Conditions. *J Atmos Chem* **2007**, *56*, 33–55.

(51) Yokelson, R. J.; Susott, R.; Ward, D. E.; Reardon, J.; Griffith, D. W. T. Emissions from smoldering combustion of biomass measured by open-path Fourier transform infrared spectroscopy. *J. Geophys. Res.* **1997**, *102*, 18865–18877.

(52) Akagi, S. K.; Yokelson, R. J.; Wiedinmyer, C.; Alvarado, M. J.; Reid, J. S.; Karl, T.; Crounse, J. D.; Wennberg, P. O. Emission factors for open and domestic biomass burning for use in atmospheric models. *Atmos. Chem. Phys.* **2011**, *11*, 4039–4072.

(53) Burling, I. R.; Yokelson, R. J.; Akagi, S. K.; Urbanski, S. P.; Wold, C. E.; Griffith, D. W. T.; Johnson, T. J.; Reardon, J.; Weise, D. R. Airborne and ground-based measurements of the trace gases and particles emitted by prescribed fires in the United States. *Atmos. Chem. Phys.* **2011**, *11*, 12197–12216.

(54) Betterton, E. A.; Hoffmann, M. R. Henry's law constants of some environmentally important aldehydes. *Environmental Science & Technology* **1988**, *22*, 1415–1418.

(55) Warneck, P. In-cloud chemistry opens pathway to the formation of oxalic acid in the marine atmosphere. *Atmospheric Environment* **2003**, *37*, 2423–2427.

(56) Desboeufs, K.; Losno, R.; Colin, J. Relationship between droplet pH and aerosol dissolution kinetics: Effect of incorporated aerosol particles on droplet pH during cloud processing. *J Atmos Chem* **2003**, *46*, 159–172.

(57) Perri, M. J.; Lim, Y. B.; Seitzinger, S. P.; Turpin, B. J. Organosulfates from glycolaldehyde in aqueous aerosols and clouds: Laboratory studies. *Atmospheric Environment* **2010**, *44*, 2658–2664.

(58) Pruppacher, R. H.; Klett, D. J. *Microphysics of Clouds and Precipitation.* Kluwer Academic Publishers, Dordrecht, The Netherlands, 2nd ed. **1997**, 954.

(59) Warneck, P. Chemistry of the natural atmosphere. International Geophysical Series. *Academic Press, San Diego, California, USA* **2000**, *71*, 469–493.

(60) Berglund, R. N.; Liu, B. Y. H. Generation of monodisperse aerosol standards. *Environmental Science & Technology* **1973**, *7*, 147–153.

(61) Chan, M.; Chan, C. Mass transfer effects in hygroscopic measurements of aerosol particles. *Atmos. Chem. Phys.* **2005**, *5*, 4057–4082.

(62) Turpin, B. J.; Lim, H.-J. Species Contributions to PM2.5 Mass Concentrations: Revisiting Common Assumptions for Estimating Organic Mass. *Aerosol Science and Technology* **2001**, *35*, 602–610.

(63) Pankow, J.; Asher, W. SIMPOL. 1: a simple group contribution method for predicting vapor pressures and enthalpies of vaporization of multifunctional organic compounds. *Atmos. Chem. Phys.* **2008**, *8*, 2773–2796.

(64) Joback, K. G.; Reid, R. C. Estimation of Pure-Component Properties from Group-Contributions. *Chem. Eng. Comm.* **1987**, *57*, 233–243.

(65) Peng, C.; Chan, M. N.; Chan, C. K. The Hygroscopic Properties of Dicarboxylic and Multifunctional Acids: Measurements and UNIFAC Predictions. *Environmental Science & Technology* **2001**, *35*, 4495–4501.

(66) U.S. EPA. *Estimation Programs Interface Suite™* for Microsoft® Windows, v 4.00; United States Environmental Protection Agency (U.S. EPA), Washington, DC, **2010**.

(67) Na, K.; Song, C.; Switzer, C.; Cocker, D. R. Effect of Ammonia on Secondary Organic Aerosol Formation from α-Pinene Ozonolysis in Dry and Humid Conditions. *Environmental Science & Technology* **2007**, *41*, 6096–6102.

(68) Dinar, E.; Anttila, T.; Rudich, Y. CCN Activity and Hygroscopic Growth of Organic Aerosols Following Reactive Uptake of Ammonia. *Environmental Science & Technology* **2008**, *42*, 793–799.

(69) Limbeck, A.; Puxbaum, H.; Otter, L.; Scholes, M. C. Semivolatile behavior of dicarboxylic acids and other polar organic species at a rural background site (Nylsvley, RSA). *Atmospheric Environment* **2001**, *35*, 1853–1862.

(70) Kerminen, V.-M.; Hillamo, R.; Teinilä, K.; Pakkanen, T.; Allegrini, I.; Sparapani, R. Ion balances of size-resolved tropospheric aerosol samples: implications for the acidity and atmospheric processing of aerosols. *Atmospheric Environment* **2001**, *35*, 5255–5265.

(71) Xue, J.; Lau, A. K. H.; Yu, J. Z. A study of acidity on PM2.5 in Hong Kong using online ionic chemical composition measurements. *Atmospheric Environment* **2011**, *45*, 7081–7088.

(72) Whipple, E. B. Structure of glyoxal in water. *Journal of the American Chemical Society* **1970**, *92*, 7183–7186.

(73) Baldwin, J. E. Rules for ring closure. *J. Chem. Soc., Chem. Commun.* **1976**, 734–736.

(74) Lee, A. K. Y.; Zhao, R.; Gao, S. S.; Abbatt, J. P. D. Aqueous-Phase OH Oxidation of Glyoxal: Application of a Novel Analytical Approach Employing Aerosol Mass Spectrometry and Complementary Off-Line Techniques. *J. Phys. Chem. A* **2011**, *115*, 10517–10526.

Table 2-1. Particle geometric diameter (D_p), concentration-weighted densities (ρ), SOA_{aq} mass yields, and their corresponding uncertainty (Δ) as a function of reaction time ($n \geq 3$, 1 mM glycolaldehyde and ~10^{-12} M OH radicals).

Reaction time (min)	$D_p \pm \Delta D_p$ (μm)	$\rho \pm \Delta\rho$ (g/mL)[a]	SOA_{aq} mass yield $\pm \Delta$ SOA_{aq} yield
0[b]	0.64 ± 0.04		
10	0.53 ± 0.03	1.3 ± 0.1	1.2 ± 0.1
20	0.54 ± 0.04	1.3 ± 0.1	0.8 ± 0.1
40	0.54 ± 0.01	1.4 ± 0.4	0.6 ± 0.2
50	0.53 ± 0.04	1.5 ± 0.5	0.6 ± 0.3
70	0.50 ± 0.05	1.6 ± 0.3	0.5 ± 0.2

a – concentration-weighted densities.

b – corresponds to 1 mM glycolaldehyde plus 5 mM hydrogen peroxide (H_2O_2)

Table 2-2. Slopes (m), coefficients of determination (r^2), liquid vapor pressures ($p_L°$), and enthalpies of vaporization (ΔH_{vap}).

	Slope (m) [a]	Standard error (%)	r^2	$p_L°$ (atm) [b]	ΔH_{vap} (kJ/mol) [c]
Organic acids					
Tartaric	1.61	9	0.97	2.63×10^{-12}	103.93
Glutaric	1.20	6	0.99	2.75×10^{-8}	73.574
Succinic	0.844	9	0.96	7.59×10^{-8}	71.348
Oxalic	0.120	2	0.84	5.62×10^{-7}	66.896
Acetic	0.011	1	0.28	2.14×10^{-3}	43.471
				Effective [d] p_L' (atm)	**Effective [e] ΔH_{vap} (kJ/mol)**
Mixed Standards					
Organic acids [f]	0.463	2	0.99	$(1 - 2) \times 10^{-7}$	69.5 - 69.9
Organic acids + Glyoxal [g]	0.667	5	0.96	$(9 \times 10^{-8}) - (1 \times 10^{-7})$	70.6 - 70.9
Experimental Samples					
10 min reaction time	0.480	4	0.85	$(1 - 2) \times 10^{-7}$	69.6 – 70.0
40 min reaction time	0.471	10	0.82	$(1 - 2) \times 10^{-7}$	69.6 - 69.9

a – slopes (in units of g/g) from PM mass versus droplet OM mass plot, Figure 2-5.

b – liquid vapor pressure ($p_L°$) estimated using SIMPOL group contribution method[63]. Vapor pressure of ammonium oxalate was estimated using US EPA: EPI Suite™[66].

c – enthalpy of vaporization (ΔH_{vap}) estimated using the Joback and Reid group contribution method from: www.chemeo.com (Joback and Reid[64]).
d – values estimated from Figure 2-6.
e – values estimated from Appendix A7.
f – mixed standard composed of equal amounts of formic, glycolic, glyoxylic, oxalic succinic, and malonic acids.
g – mixed standard composed of equal amounts of formic, glycolic, glyoxylic, oxalic succinic, and malonic acids, plus glyoxal.

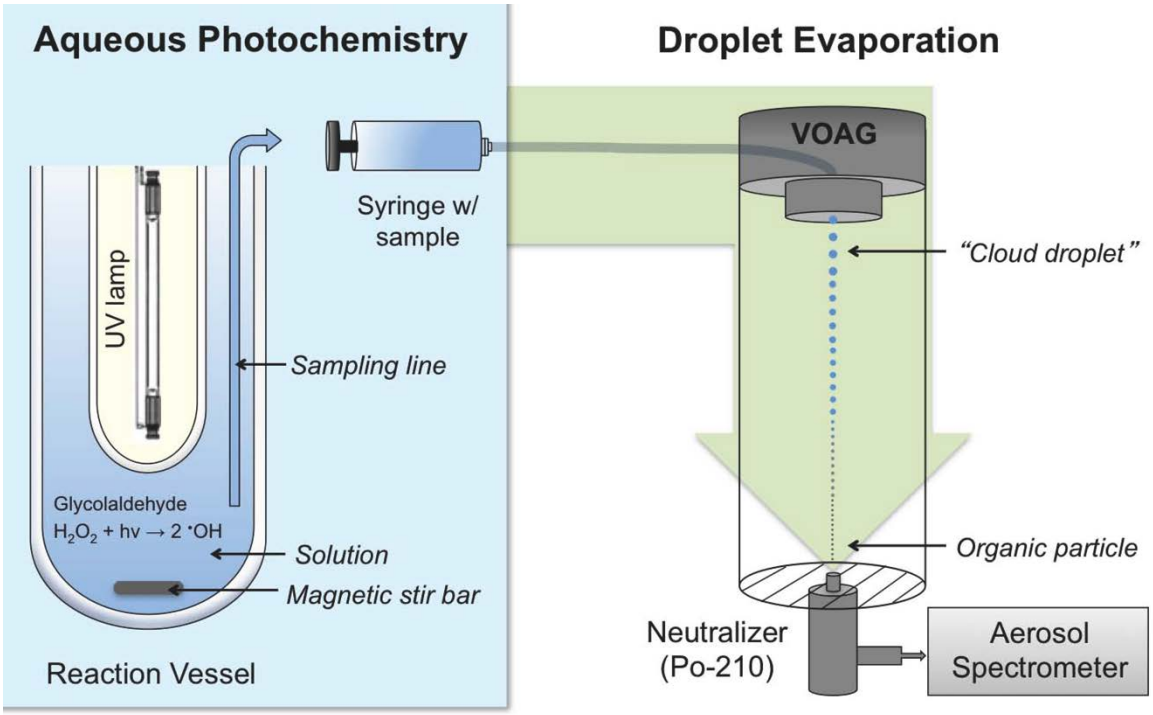

Figure 2-1. Experimental setup for aqueous photooxidation and droplet evaporation. Reaction samples were also analyzed by ion chromatography (IC), electrospray ionization mass spectrometry (ESI-MS), IC ESI-MS, and for total organic carbon (TOC).

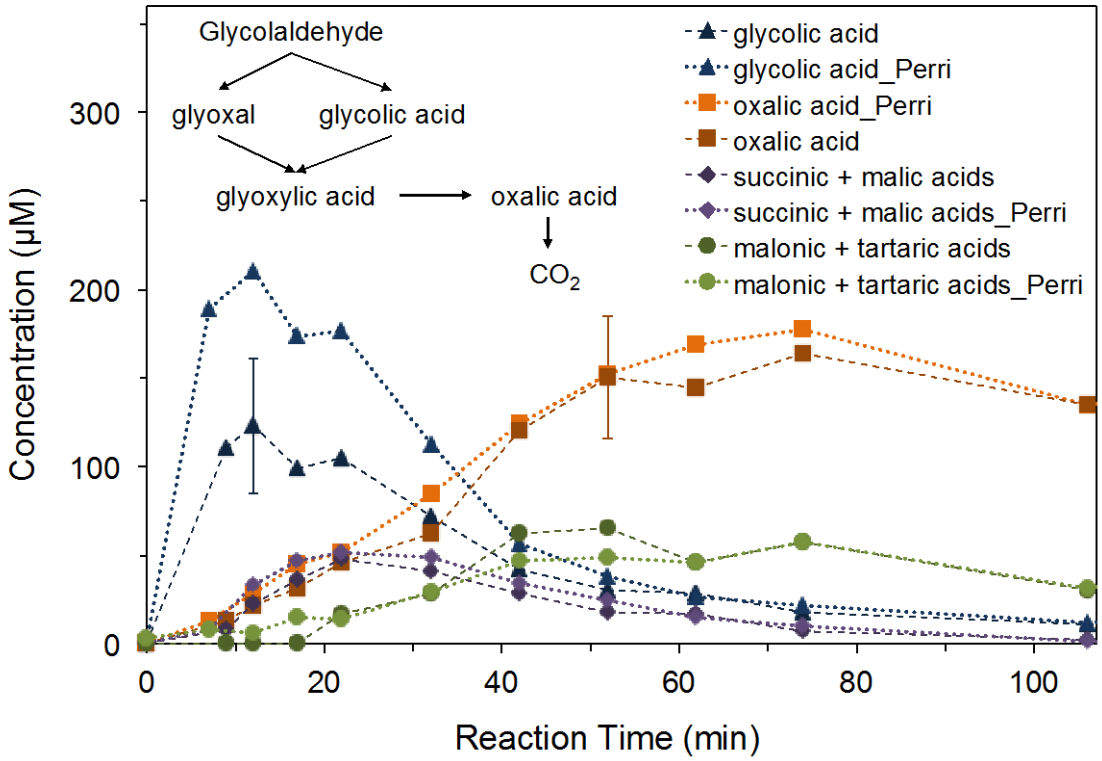

Figure 2-2. Product concentrations from 1 mM glycolaldehyde and OH radicals (~10^{-12} M) by ion chromatography (n = 3). For this work and for concentrations obtained by Perri et al.[36]. Note that succinic plus malic acid as well as malonic plus tartaric acid coelute and were quantified as succinic and malonic acid, respectively (Tan et al.[37]). Glyoxylic acid converts to formic acid in samples awaiting analysis (not shown). (Error bars represent the pooled coefficient of variation between experiments).

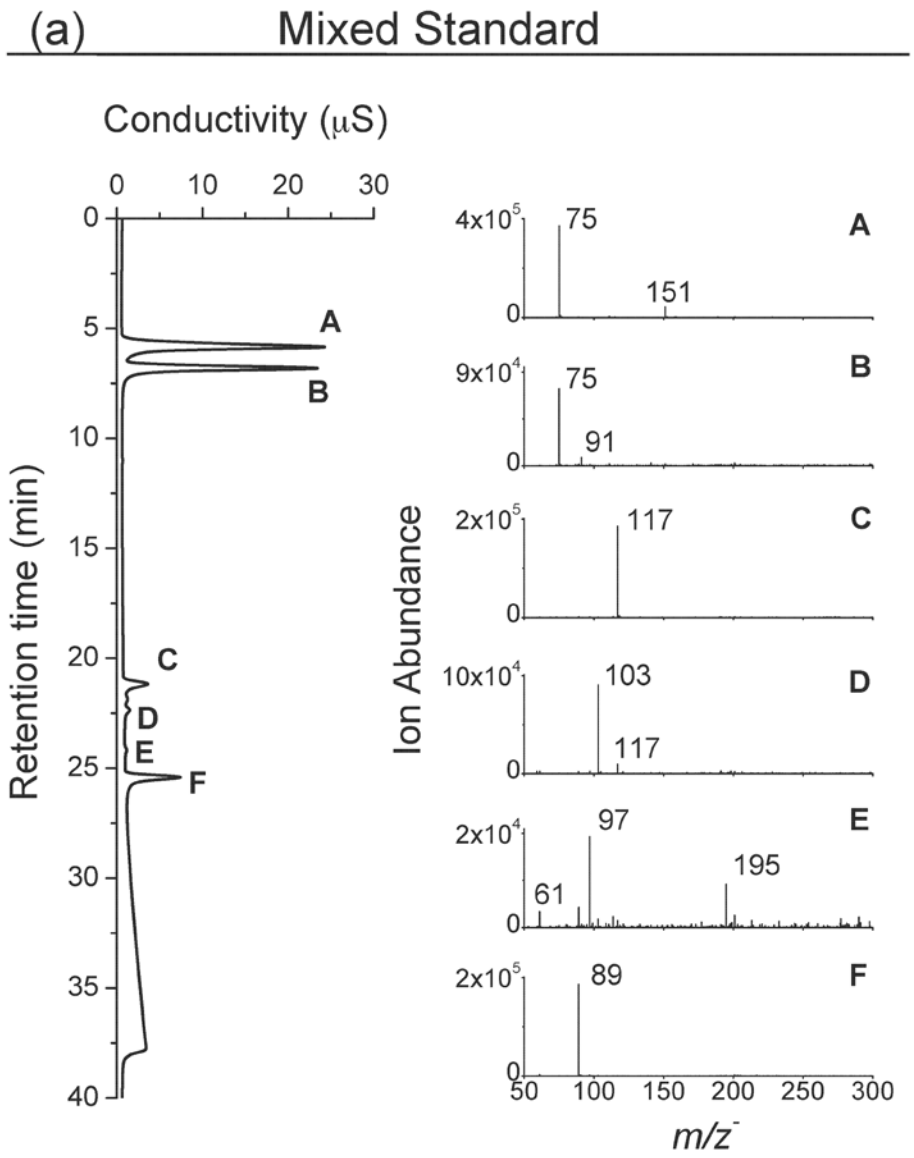

Figure 2-3a. IC-ESI-MS spectra of a mixed standard. (A) glycolic acid (m/z^- 75), (B) formic acid (not detectable by ESI-MS) and residual glycolic acid from peak A, (C) succinic acid (m/z^- 117), (D) malonic acid (m/z^- 103), (E) contaminants, including sulfate (m/z^- 97), and (F) oxalic acid (m/z^- 89).

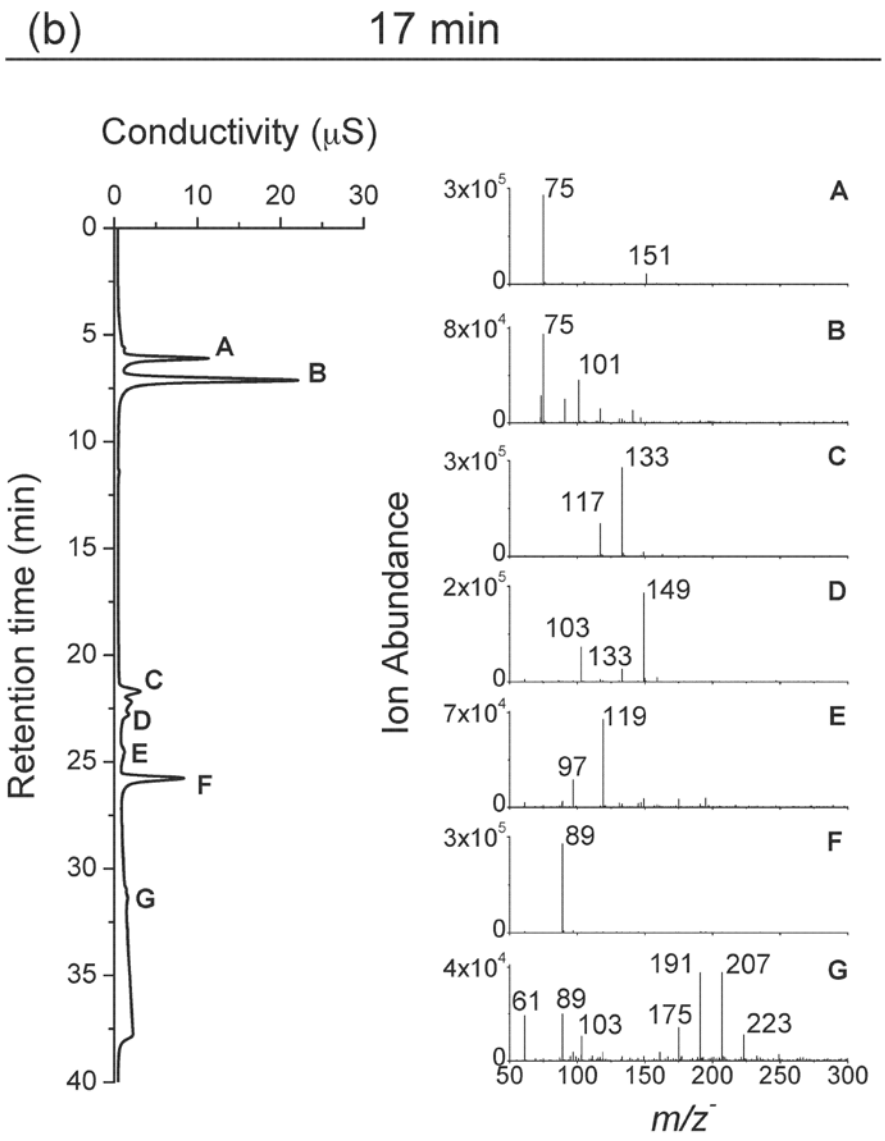

Figure 2-3b. IC-ESI-MS spectra of samples taken from the reaction of 1 mM glycolaldehyde + OH radical at 17 min reaction time. (A) glycolic acid (m/z^- 75), (B) peak with retention time of formic acid, (C) succinic acid (m/z^- 117) and malic acid (m/z^- 133), (D) malonic acid (m/z^- 103) and tartaric acid (m/z^- 149), (E) peak with retention time of sulfate (m/z^- 97), (F) oxalic acid (m/z^- 89), and (G) high-molecular-weight compounds.

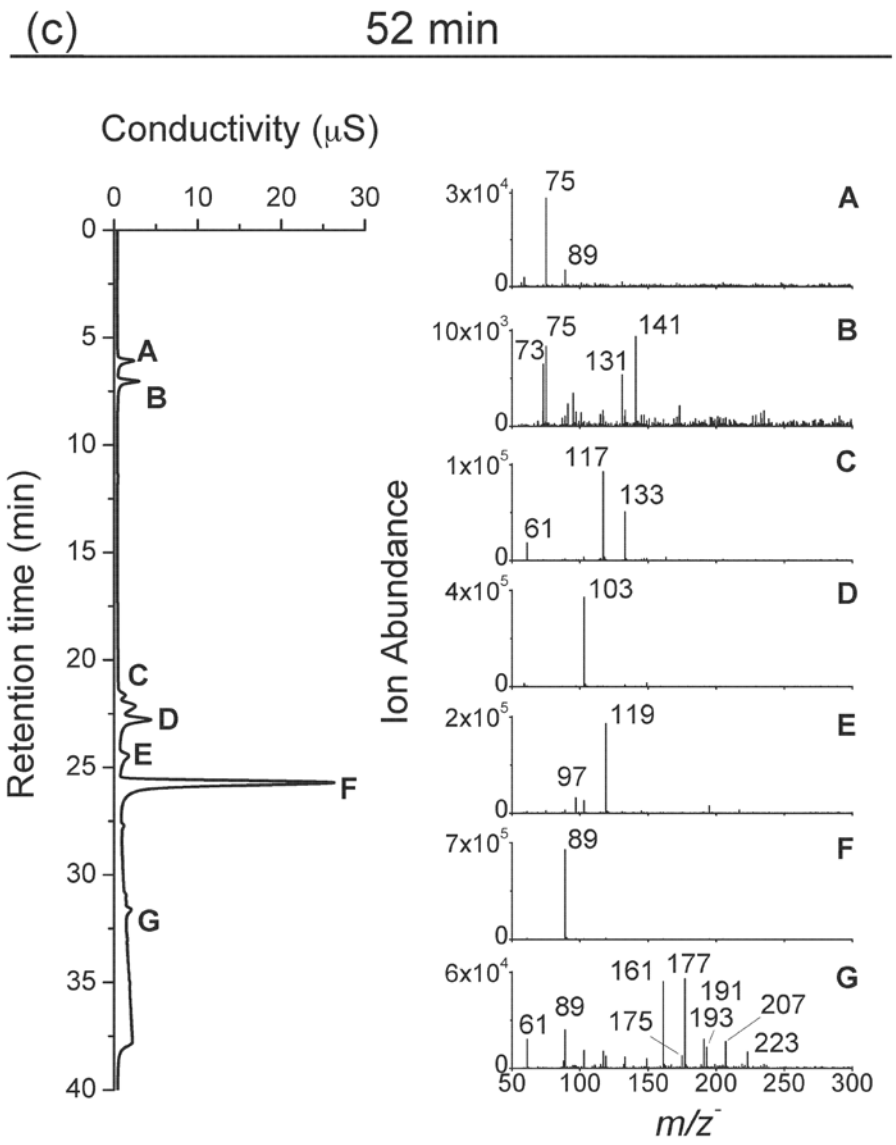

Figure 2-3c. IC-ESI-MS spectra of samples taken from the reaction of 1 mM glycolaldehyde + OH radical at 52 min reaction time. (A) glycolic acid (m/z^- 75), (B) peak with retention time of formic acid, (C) succinic acid (m/z^- 117) and malic acid (m/z^- 133), (D) malonic acid (m/z^- 103) and tartaric acid (m/z^- 149), (E) peak with retention time of sulfate (m/z^- 97), (F) oxalic acid (m/z^- 89), and (G) high-molecular-weight compounds.

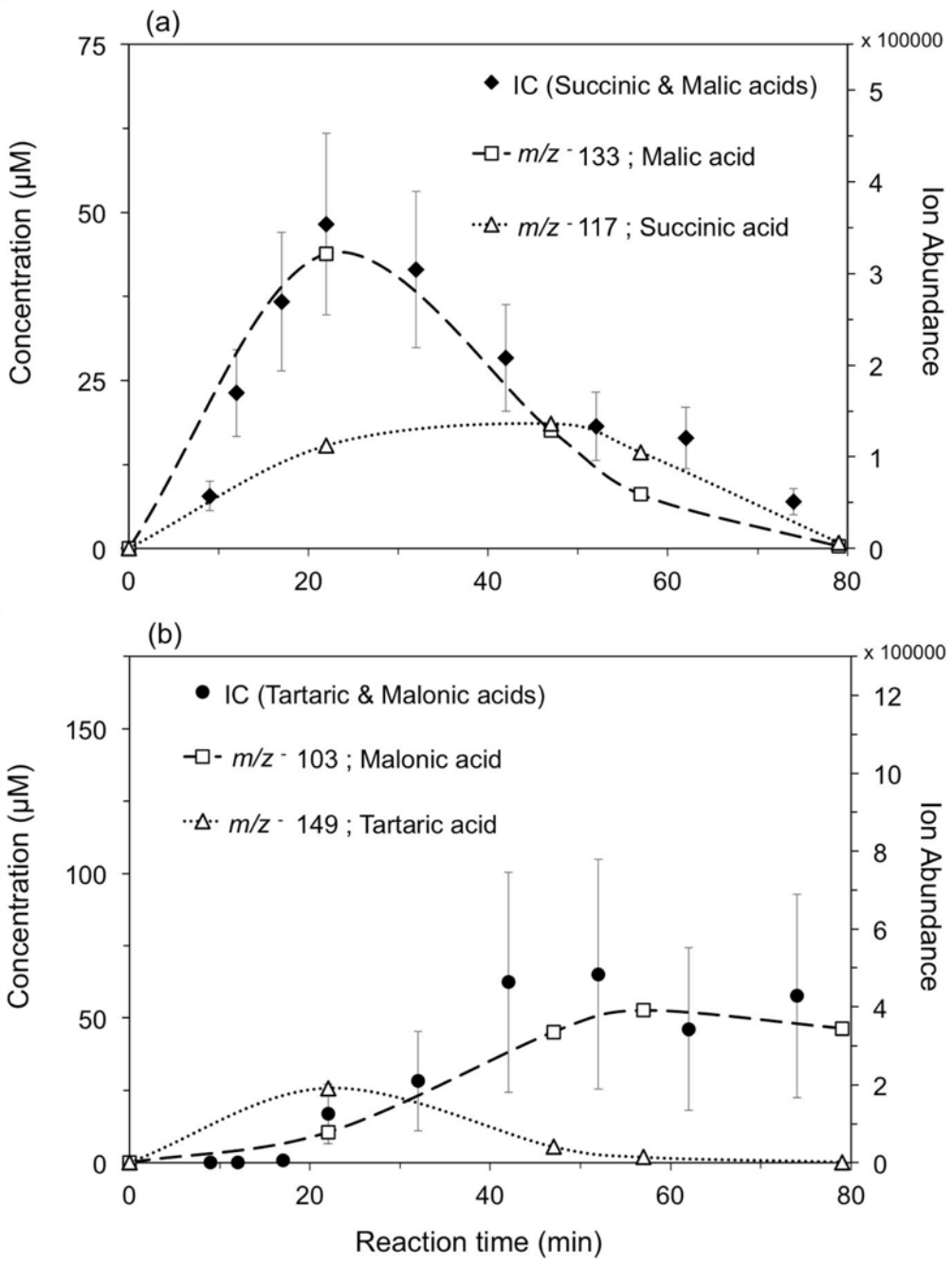

Figure 2-4. IC and IC-ESI-MS ion abundance time profiles. (a) IC time profile of succinic and malic acid concentration from the reaction of 1 mM glycolaldehyde + OH radicals (~10^{-12} M), and overlaid IC-ESI-MS ion abundance time profiles for m/z^- 117 (succinic acid) and m/z^- 133 (malic acid). (b) IC time profile of malonic and tartaric acid concentration, and overlaid IC-ESI-MS ion abundance time profiles for m/z^- 103 (malonic acid) and m/z^- 149 (tartaric acid). (Error bars represent the pooled coefficient of variation between experiments).

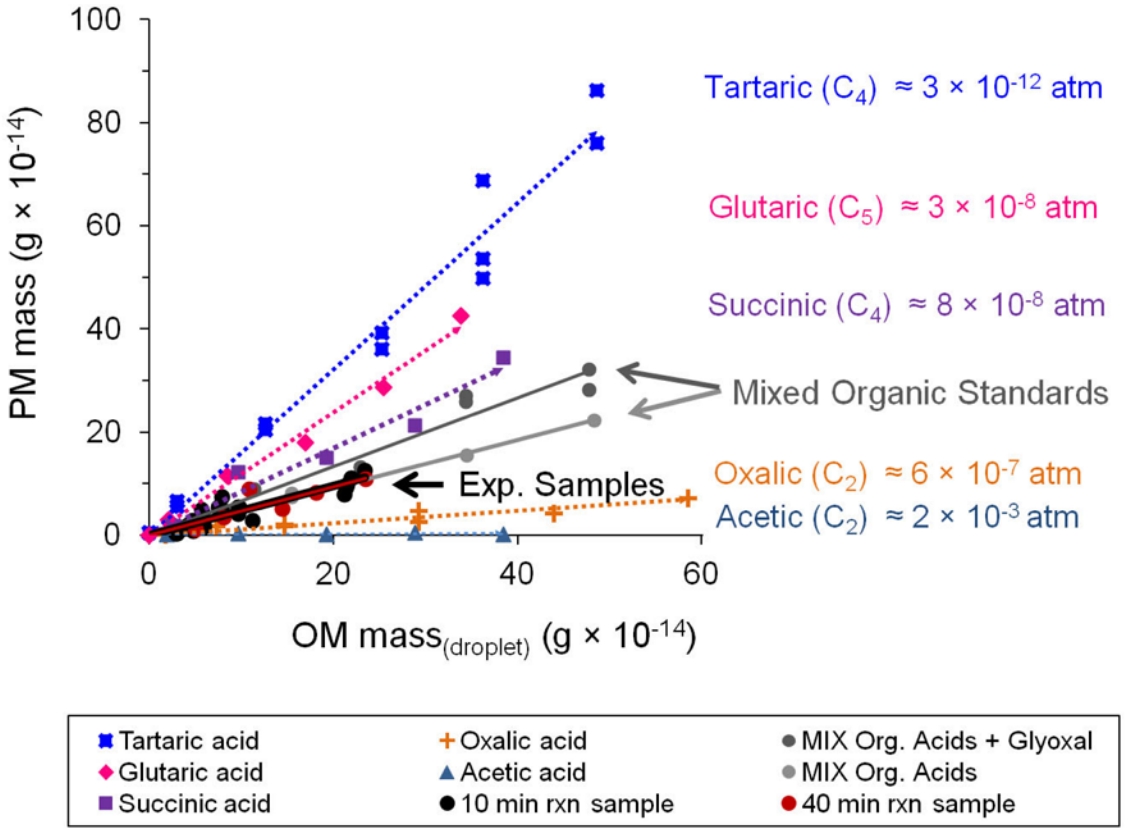

Figure 2-5. Mass of residual particles (PM mass) formed from droplet evaporation of organic acid standard solutions of acetic, oxalic, succinic, glutaric, and tartaric acid. OM mass$_{(droplet)}$ is the mass of organic matter in the droplet. Labels include liquid vapor pressures estimated using the SIMPOL group contribution method[63]. Slopes and r^2 values are reported in Table 2-2 (D_d = 18.3 ± 0.4 μm; RH = 13 ± 2%; t = 24.1 ± 0.3°C).

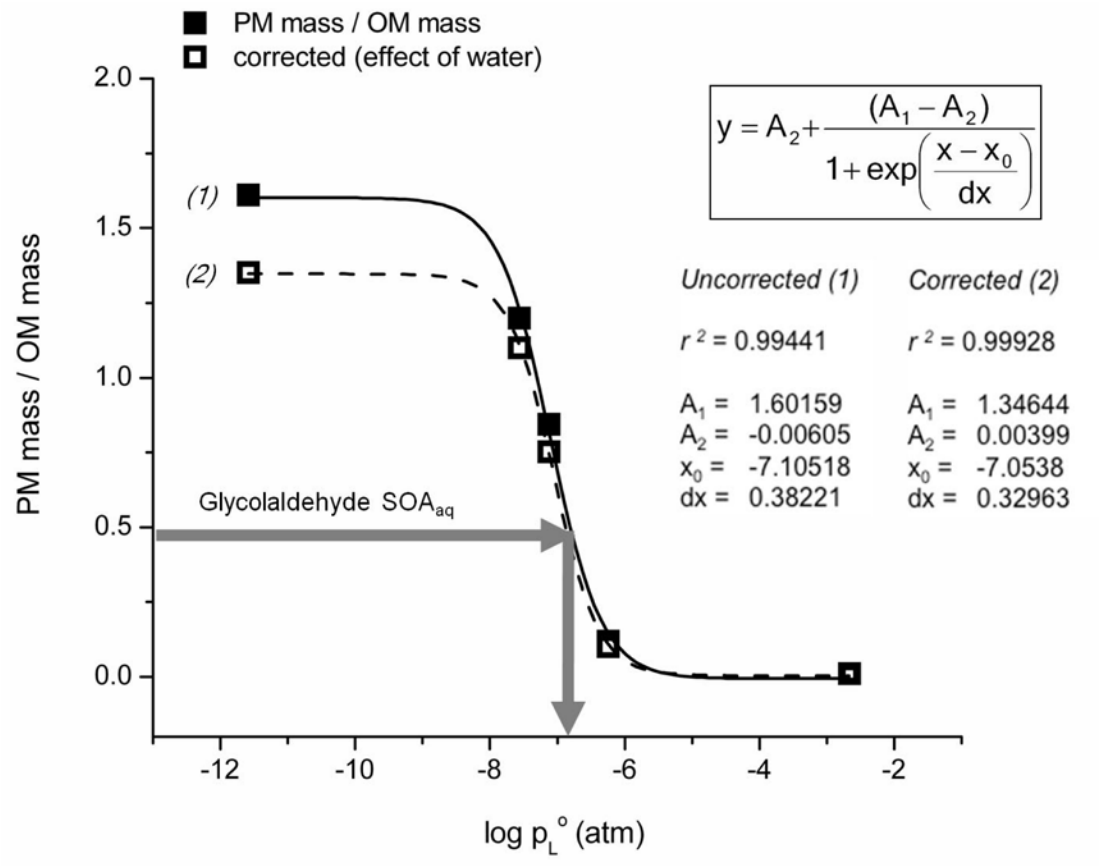

Figure 2-6. Ratio of residual particle mass (PM mass) to droplet organic matter (OM mass) versus log(p_L°). p_L° is the liquid vapor pressure. PM mass/OM mass (in units of g/g) values are the slopes from Figure 2-5 (see also Table 2-2). (1) PM mass/OM mass values from Figure 2-5, where densities were calculated from organic species. (2) PM mass/OM mass values computed using densities calculated with an upper-bound estimate of retained water. Gray arrow indicates the PM mass/OM mass of glycolaldehyde SOA_{aq}.

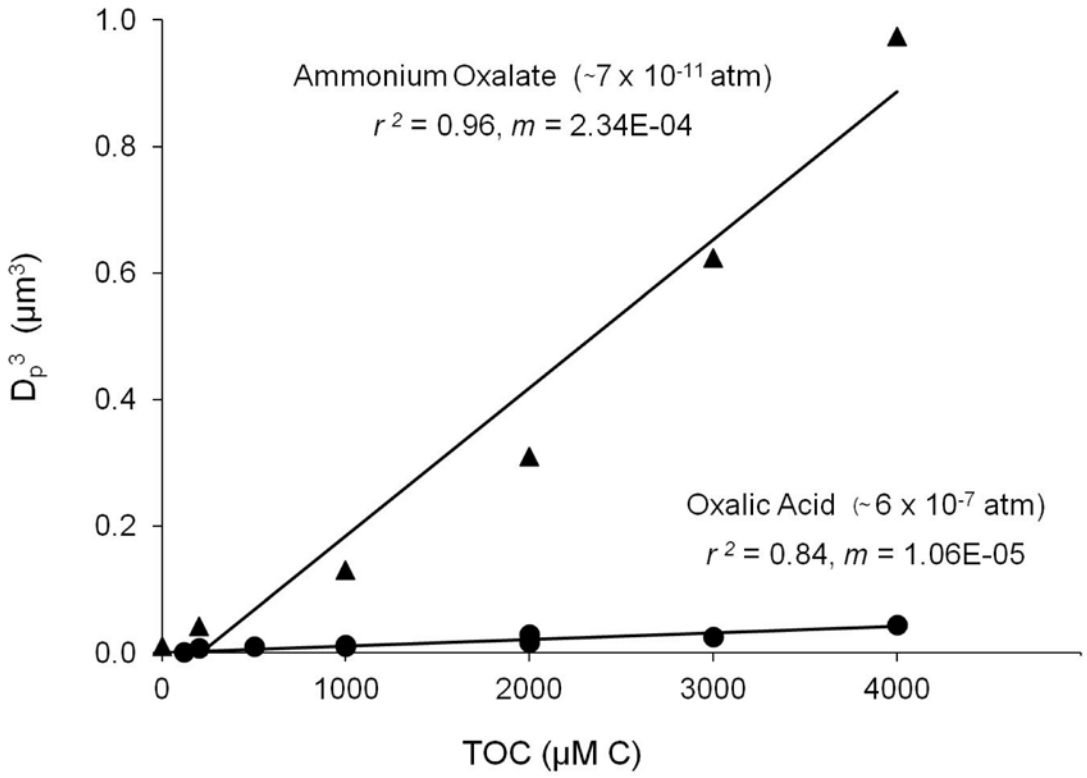

Figure 2-7. Volume (D_p^3) of residual particles and total organic carbon (TOC) in droplets, from droplet evaporation of oxalic acid and ammonium oxalate standard solutions. Liquid vapor pressure of ammonium oxalate $p_L°$ (US EPA: EPI Suite^{TM}[66]) (D_d = 18.3 ± 0.4 µm; RH = 13 ± 2%; t = 23.8 ± 0.3°C). The clear difference between oxalic acid and ammonium oxalate (and day-to-day reproducibility of oxalic and succinic acid results) provide confidence that the VOAG system was free of ammonium contamination.

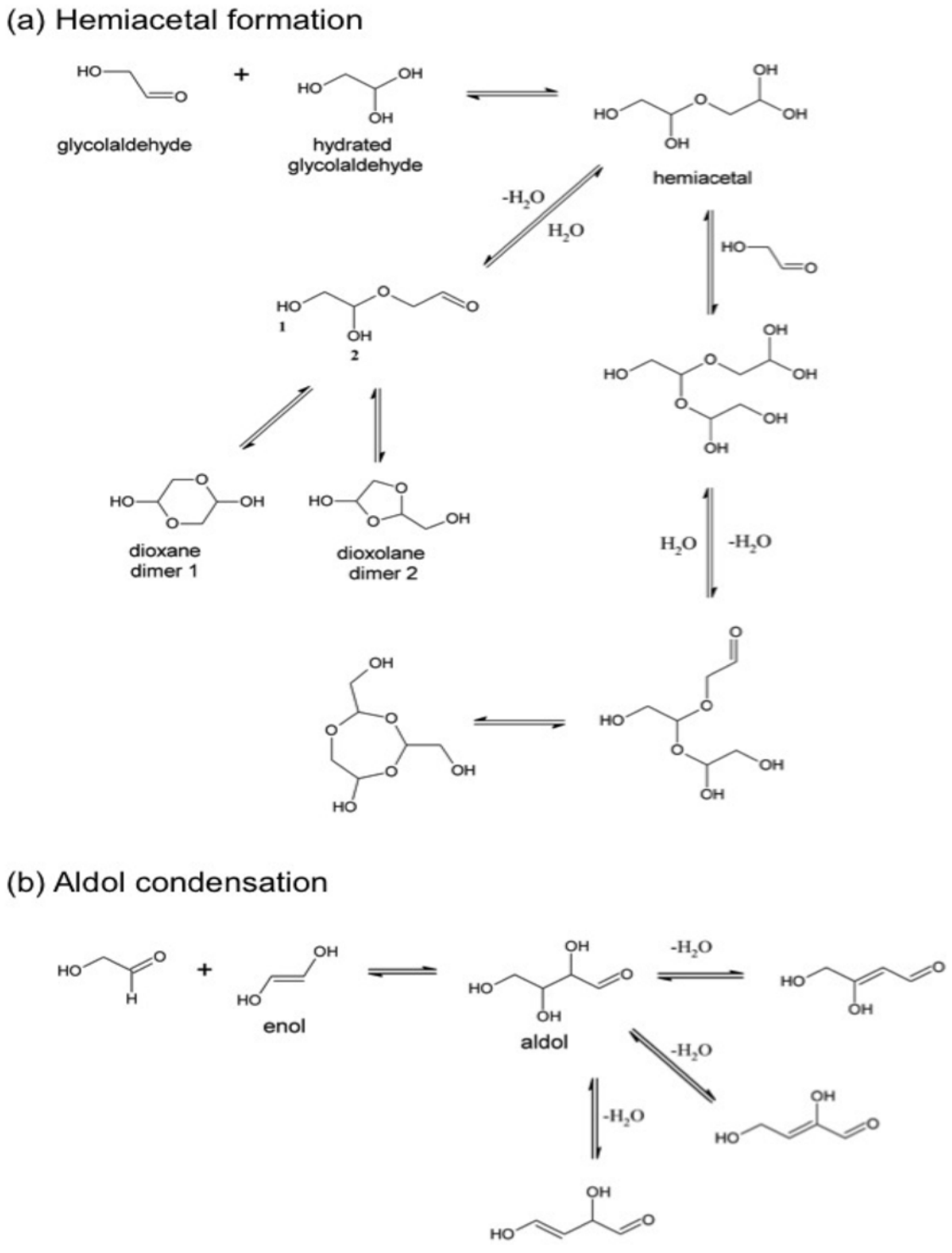

Figure 2-8. Proposed mechanism for the formation of glycolaldehyde oligomers through hemiacetal formation (a) and aldol condensation (b).

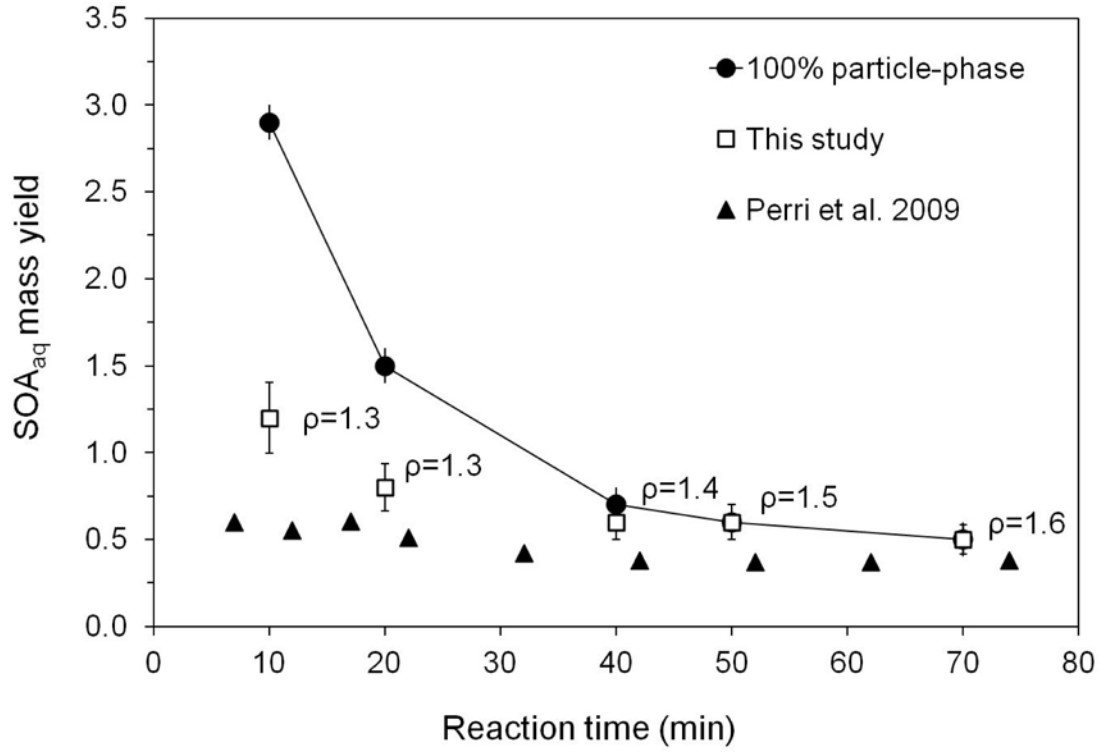

Figure 2-9. SOA_{aq} mass yields from the reaction of 1 mM glycolaldehyde + OH radicals (~10^{-12} M). Squares are mass yields calculated in this study using concentration-weighted densities and assuming spherical particles ($n \geq 3$; D_d = 18.3 ± 0.4 μm; RH = 10 ± 1%; t = 23.7 ± 0.7°C). Triangles are yields estimated by Perri et al.[36] using concentrations of species measured in the reaction vessel and estimating the fraction of each that would remain in the particle-phase from atmospheric measurements. Circles are upper-bound yields obtained if all the organic mass in the droplet remained in the residual particle, calculated using IC quantification of organic acids and model predictions of remaining glycolaldehyde and glyoxal and neglecting unquantified products. (Error bars for open squares represent the pooled coefficient of variation for identical time points across experiments. Error bars for circles are from error propagation).

Chapter 3. Volatility of Glyoxal SOA Formed from Cloud Processing and Droplet Evaporation

Material in this chapter will be submitted for publication as:

Ortiz-Montalvo, D. L.; Lim, Y. B.; Turpin, B. J. Volatility of Glyoxal SOA Formed through Cloud Processing and Droplet Evaporation. *Environmental Science & Technology* **2013**.

3.1 Abstract

Secondary organic aerosol (SOA) is a substantial contributor to atmospheric organic aerosol concentrations. The formation of SOA through reactions in atmospheric waters (clouds, fog and wet aerosol) is now believed to be comparable and occur in parallel with SOA formed through the gas-to-particle partitioning of semi-volatile gas-phase products, although uncertainties remain large. This work characterizes the volatility behavior of the aqueous organic matter (precursor/product mix) formed from in-cloud photooxidation of glyoxal and hydroxyl radicals ($^{\bullet}$OH), thus aiding prediction of SOA via this pathway (Gly SOA_{Cld}). Volatility was assessed through the use of kinetic modeling and droplet evaporation experiments. An effective vapor pressure of ~10^{-7} atm and enthalpy of vaporization of ~70 kJ/mol were estimated for the mixture present after 10 min of cloud chemistry (one cloud cycle). These estimates are similar to those of oxalic acid (~10^{-7} atm and 67 kJ/mol), which is a major product. Neutralization to pH 7 (with ammonium hydroxide) reduced the effective vapor pressure to ~ (10^{-9} – 10^{-12}) atm and increased the enthalpy of vaporization to ~ (80 – 120) kJ/mol, consistent with that of ammonium oxalate (~10^{-11} atm). Salt formation appears to have a large effect on the gas-particle partitioning of the mixture and therefore on the yield of Gly SOA_{Cld}.

3.2 Introduction

Atmospheric particles have adverse effects on the environment, climate and human health[1-3]. Secondary organic aerosol (SOA) is a major fraction of submicron atmospheric particles, ranging from 20% to ~95% of the organic aerosol (OA) mass[4-9], yet its atmospheric formation is still not well understood and hampers the ability of models to characterize the magnitude, dynamics, and distribution of measured OA from particle and precursor emissions[10-12]. There is growing evidence that SOA formation also involves reactions in the aqueous-phase of clouds, fogs and wet aerosols, but these are not commonly included in models (see reviews by Ervens et al.[13] and Gong et al.[14]). Briefly, SOA formation through aqueous chemistry (SOA_{aq}) involves the uptake of gaseous water-soluble organic compounds ($WSOC_{gas}$) into atmospheric waters, followed by oxidation and other reactions that produce highly oxygenated and less volatile compounds that remain in the particle-phase once the cloud droplets evaporate, and thus contribute to the overall SOA burden[15,16]. A few models have incorporated SOA formation through aqueous chemistry and shown better agreement in the magnitude, distribution, and properties of the predicted SOA, although uncertainties remain large[17-20]. Moreover, recent modeling studies[13,21,22] have confirmed that the amount of SOA formed through aqueous chemistry is comparable to traditional SOA formation from gas/particle partitioning (i.e., partitioning of semi-volatile products of gas-phase photochemistry into particulate organic matter[23-26]. Overall, there is still much to learn about the different WSOC precursors of SOA_{aq}, the fate of their products, and how they affect the properties of atmospheric aerosols.

One of the most commonly studied $WSOC_{gas}$ in the field of SOA_{aq} is glyoxal (Gly), a small dicarbonyl ($C_2H_2O_2$) compound found ubiquitously in the atmosphere. Glyoxal is a potentially important SOA_{aq} precursor because of its abundance and high water solubility (Henry's law constant: 3.5×10^5 M atm^{-1})[27,28]. In the gas-phase, Gly forms mainly from the photooxidation of isoprene (21 Tg a^{-1}), and acetylene (8.9 Tg a^{-1}), indirectly from ethylene via glycolaldehyde oxidation (2.5 Tg a^{-1}), and to a minor extent by aromatics like benzene, toluene and xylene, as well as from the ozonolysis of monoterpenes (1.8 Tg a^{-1})[19]. Gly can also be emitted directly into the atmosphere by biomass burning and oil combustion[29,30]. Once dissolved in the aqueous-phase, Gly is rapidly photooxidized by hydroxyl radicals ($^{\bullet}OH$) to form organic acids and higher molecular weight products that are found in the particle-phase in the atmosphere[31-34]. The production of organic acids by Gly photooxidation is favored in the cloud water media, whereas higher molecular weight products (oligomers) are favored in wet aerosols[35]. Furthermore, Gly can also react in the aqueous-phase through non-photochemical (dark) reactions forming: aldol condensation products in wet aerosols[36]; nitrogen containing compounds (e.g., imidazoles) through reactions with amino acids, ammonium ion, and amines in evaporating droplets[37,38], wet aerosol[39], and bulk aqueous solutions that mimic atmospheric aerosol conditions[36,40-42]; as well as oligomers through self-reactions in evaporating droplets[43,44] and aerosol particles[45]. In brief, Gly is an ideal precursor to further our understanding of the physicochemical properties (e.g., volatility) of SOA_{aq} mostly because its SOA_{aq} formation has been studied so extensively.

An appropriate understanding of the volatility of the precursor/product mixture is needed to predict its atmospheric gas-particle partitioning and therefore the SOA

formation potential of Gly (Gly SOA_{Cld}). While properties like vapor pressure and enthalpy of vaporization (ΔH_{vap}) describe the volatility of a pure compound, we require an innovative approach to describe the volatility of the mixture (e.g., Michaud et al.[46] and Ortiz-Montalvo et al.[47]). The incomplete understanding of the ΔH_{vap} of OA is a major source of uncertainty in modeled SOA budgets, as determined by an assessment of SOA modeling uncertainties conducted by Tsigaridis and Kanakidou[12]. While estimates of ΔH_{vap} for SOA products formed through gas-phase oxidation of monoterpenes[48-52] and aromatics[50,51] have been reported, there is only one studies that report ΔH_{vap} for SOA_{aq} assessment[47]. The goal of this paper is to better characterize the volatility of the aqueous Gly + $^{\bullet}$OH precursor/product mix so as to improve prediction of Gly SOA_{Cld}.

In this work, we studied the volatility of the precursor/product mix formed via 10 min of aqueous $^{\bullet}$OH oxidation of glyoxal under cloud relevant conditions. By means of kinetic modeling and droplet evaporation we have provided, for the first time, estimates of fundamental physicochemical properties (vapor pressure and enthalpy of vaporization) of this mixture, which includes Gly, its oxidation products and any additional chemistry that occurs in the evaporating droplets. The estimated vapor pressure and enthalpy of vaporization are ~10^{-7} atm and ~70 kJ/mol, respectively, for two atmospheric scenarios that assumed: (1) depletion of Gly in the cloud droplet (Batch Reactor) or (2) continuous replacement of Gly in the droplet (Continuously Stirred-Tank Reactor). We also evaluated the influence of ammonia (i.e., neutralization, pH 7) on the volatility of the Gly + $^{\bullet}$OH mixture. We found a substantial increase in the fraction remaining in the particle-phase with the addition of ammonium hydroxide (pH 7). The volatility of the neutralized mixture was substantially reduced (~ 10^{-9} – 10^{-12} atm and ~ 80 – 120 kJ/mol), and

although uncertainties were large, the apparent volatility behavior of the neutralized mixture was similar to that of ammonium oxalate. We conclude that the yield of Gly SOA_{Cld} (gas-particle partitioning) from in-cloud oxidation of Gly by OH radicals will depend on the chemical form of the organic acid products.

3.3 Methods

The (precursor + product) composition resulting from 10–30 min reaction of Gly and OH radicals in the aqueous-phase (at cloud relevant conditions) was evaluated via kinetic modeling. Two atmospheric assumptions were evaluated: (1) continuous depletion of Gly in the droplet and (2) continuous replacement of Gly. Solutions were prepared with these compositions to mimic the evaporation of droplets after a single (10 min) cloud processing cycle. Generally, aqueous photooxidation experiments are conducted with relatively high concentrations of H_2O_2 to produce OH radicals in the aqueous-phase; however, excess H_2O_2 in samples waiting analysis react with glyoxylic acid (main product of Gly photooxidation) to form formic acid[53]. Further evidence of glyoxylic acid depletion can be found in Appendix D. This problem is avoided here by using mimic solutions (from model compositions) for droplet evaporation experiments. Cloud droplet evaporation was simulated by means of a Vibrating Orifice Aerosol Generator (VOAG) system[47]. The volatility behavior of the Gly + $^{\bullet}$OH precursor/product mixture was estimated by comparing its behavior in the VOAG system with that of organic standards.

3.3.1 Atmospheric Scenarios using Kinetic Modeling

Kinetic modeling was used to determine the composition of a cloud droplet exposed to Gly and OH radicals after one cloud processing cycle (10 min). Two limiting cases were modeled. The first scenario is represented by a Batch Chemical Reactor and

assumes that the gas-phase production of Gly is slow compared to its aqueous oxidation. Thus Gly in the cloud droplet is depleted with time. In the second, gas-phase production is fast and aqueous Gly is continuously replaced in the droplet (Continuously Stirred-Tank Reactor (CSTR)). The chemical composition of the Gly + $^{\bullet}$OH precursor/product mixture after 10 min of aqueous oxidation obtained from these two models was used to prepare representative mimic solutions that were then analyzed through droplet evaporation experiments.

3.3.1.1 Batch Chemical Reactor Approximation

In the Batch Chemical Reactor, it is assumed that the gas-phase Gly production is slow compared to its degradation pathways; therefore, dissolved Gly reacts completely without further inclusion of Gly from the gas-phase (i.e., Gly depletion). This is the appropriate assumption, for example for SO_2, which is not formed in the interstitial spaces of clouds and is efficiently scavenged when droplets form.

A recently validated aqueous-phase chemical kinetic model was used to study Gly reaction with OH radicals at cloud-relevant concentrations[33,35]. The initial aqueous-phase concentration of Gly in the Batch model was 5 μM, which is within the concentration range found in cloud water (<0.15 – 27 μM)[27]. The concentration of aqueous-phase OH radicals was held constant at 10^{-12} M, which is within estimated atmospheric concentrations (~10^{-12} – 10^{-13} M)[13].

3.3.1.2 Continuously Stirred-Tank Reactor Approximation (CSTR)

For the CSTR modeling, the aqueous Gly chemistry model[35] was run holding the concentration of Gly constant at a cloud relevant concentration of 5 μM. This is the equivalent of a Gly gas-phase concentration of 0.014 ppb at Henry's law equilibrium; i.e.,

using a Henry's law constant equal to 3.5 x 10^5 M atm^{-1}[28]. As in the Batch model runs, the OH radical concentration in the aqueous-phase was kept constant at 10^{-12} M. Unlike the Batch reactor model runs, the CSTR model runs were used to represent cloud processing from precursors that replenish Gly rapidly and in close proximity (e.g., in the interstitial spaces of the clouds).

3.3.2 Mimic Samples

The chemical compositions of the Gly precursor/product mix obtained from the model runs were used to prepare mimic solutions that represented Batch- and CSTR-cloud droplet composition after 10 min reaction. The organic standards used to prepare the mimic solutions were glyoxal (39.7%; Sigma-Aldrich), oxalic acid (0.1008 N; Fluka Analytical), and glyoxylic acid (51.7%; Aldrich). The mimic solutions were prepared by diluting mixtures of organic standards with 18 MΩ milli-Q water. The concentrations of organic standards were scaled up (factor of F =150 for CSTR and F=350 for Batch) to meet the detection limits of the droplet evaporation methods, but still maintaining the same distribution of precursor and products. Additionally, ammonium hydroxide (29.6% as ammonia (NH_3); J.T. Baker) was used to increase the pH of CSTR mimics in order to study the effect of neutralization (pH 7).

3.3.3 Volatility Assessment using Droplet Evaporation Experiments

The methodology used for droplet evaporation and volatility assessment was described in detail by Ortiz-Montalvo et al.[47]. Briefly, six dilutions (0 – 4000 μM C) of each mimic solution and several organic standards (acetic, oxalic, succinic, glutaric, and tartaric acids) were pushed through a Vibrating Orifice Aerosol Generator (VOAG, TSI Model 3450)[54], the resulting droplets were dried to RH of ~10% and their dry diameter

measured with an Optical Particle Counter (OPC, Grimm Aerosol Spectrometer, Model 1.109, 31 channels). Additionally, each mimic solution was analyzed for total organic carbon (TOC, Shimadzu TOC-5000A). Values of OM/OC (i.e., organic mass to organic carbon ratio; Appendix B1) were then used to convert the TOC content in the generated droplets to organic matter ($OM_{droplet}$). The residual optical particle diameters (D_p) measured by the OPC were converted to the mass of residual particles (*PM mass*) by assuming spherical particles and using liquid densities (Appendix B1). The *PM mass* of each organic standard was regressed linearly on *OM mass* and the slopes (*PM mass / OM mass*$_{(droplet)}$) were evaluated against their corresponding liquid vapor pressures (p^o_L) (estimated using the SIMPOL group contribution method)[55]. In order to extend this evaluation to low-volatility compounds, we included ammonium oxalate (99.0%; Fluka Analytical) in this regression, estimating its sub-cooled liquid vapor pressure using EPA-EPI Suite™ Software[56]. The new regression coefficients can be found in Appendix B2. Sigmoidal fits were obtained since *PM mass* divided by droplet *OM mass* (Δ *PM mass* / Δ *OM mass*$_{(droplet)}$ = slope) reflects the fraction of total droplet OM that remains in the particle-phase (i.e., particle fraction). Similarly, the slopes of the organic acid standards were also evaluated against their corresponding enthalpies of vaporization (estimated using a group contribution method that uses the normal boiling point to estimate the enthalpy of vaporization of pure compounds[57]). Note that ammonium oxalate was not included in the sigmoidal regression of enthalpy of vaporization due to a lack of experimental and predictive values. As detailed in Ortiz-Montalvo et al.[47], a correction was made to the original sigmoidal fits to account for the effect that residual water has on particle density, based on the fact that some organic compounds, like tartaric acid, retain

water even at RH as low as 5%[58]. The effective liquid vapor pressure ($p'_{L,eff.}$) and enthalpy of vaporization ($\Delta H_{vap,eff.}$) of the droplet Gly + $^{\bullet}$OH precursor/product mix were estimated from these corrected sigmoidal curves and *PM mass / OM mass*$_{(droplet)}$ of the Gly + $^{\bullet}$OH mimics.

A detail description of how the VOAG operates has been provided previously[47]. Briefly, filtered mimic solutions (or organic standards) were pushed through a 10-μm diameter (nominal ± 25%) orifice generating monodisperse droplets (20-μm nominal diameter). A drying chamber then evaporated the droplets and the diameter of the resulting particles (e.g., SOA) at ~10% RH and ~25°C was measured with the OPC downstream of an ionizer (NRD StaticMaster 2U500, Po-210; to give particles a Boltzmann charge distribution). The diameter of the generated droplets was determined experimentally since the orifice manufacturing tolerance was too large (± 25%). The diameter of the generated droplets was determined by calibrating the system with ammonium sulfate (3.1801 M $(NH_4)_2SO_4$; Fluka Analytical). The droplet diameter (D_d = 17.60 ± 0.03 μm, n=2, r^2=0.99) was obtained from the slope of D_p versus $C^{⅓}$, where D_p = the residual particle diameter, and C = the volumetric concentration of the solute in solution ($cm^3_{solute}/cm^3_{solution}$). The D_p of mimic samples ranged between 0.36 – 1.16 μm, with geometric standard deviations between 1.1 and 1.4. The VOAG system was operated at a frequency of ~160 kHz, liquid flow rate of 0.077 mL/min, dilution air 50 L/min, dispersion air 1 L/min, and particle residence time of 6 s (before entering the OPC) at RH = (12 ± 3)% and t = (24.4 ± 0.7)ºC.

The performance of the VOAG system was tested daily by sampling (in duplicate) standard solutions of 250 μM $(NH_4)_2SO_4$, and using a criterion for acceptance of 10% (or

less) difference between the measured particle diameter of $(NH_4)_2SO_4$ and the theoretical one. Succinic acid standards (99.99%; Sigma-Aldrich) were used as an independent check. Samples of 60 and 750 μM succinic acid (n=10, each) were analyzed in duplicate during each experiment, and a method precision for diameter was obtained (2% and 1%, respectively). The method precision was calculated as the pooled standard deviation of succinic acid particle diameter divided by the mean diameter of succinic acid samples. To test the accuracy of the volatility assessment, samples of malonic acid standard solution (6 dilutions between 0 and 3000 μM C from 0.999 %, Sigma-Aldrich) were sampled just like the mimic solutions. The estimated $p'_{L,eff.}$ for malonic acid (6±7 x 10^{-8} atm) was within an order of magnitude of the calculated theoretical value (2±2 x 10^{-7} atm, SIMPOL group contribution method)[55]. The estimated $\Delta H_{vap,eff.}$ (72 ± 2 kJ/mol) differed by about 4% of the theoretical value (69.12 ± 1.79 kJ/mol, Joback and Reid group contribution method)[57]. We note that an additional uncertainty (~17%) might be introduced by differences in the refractive index between malonic acid (1.479) and polystyrene latex particles (1.59), which were used to make the OPC manufacturer-supplied calibration.

3.4 Results and Discussion

Model results for the aqueous reaction of glyoxal (5 μM) with OH radicals (10^{-12} M) indicated that the major species were oxalic acid, glyoxylic acid, and unreacted glyoxal (Figure 3-1). After 10 min reaction (~lifetime of one cloud droplet) glyoxal is a greater contributor in the Batch scenario (pie charts in Figure 3-1) than in the CSTR scenario. Glyoxal is known to self-oligomerize upon droplet evaporation[43,44], hence, some portion of the glyoxal is expected to contribute to the residual PM (Gly SOA_{Cld}).

Oxalate measurements indicate it is found in the atmosphere mostly in the particle-phase (i.e., ~74%)[59]. It is probably present as a salt (e.g., ammonium oxalate) since the vapor pressure of ammonium oxalate is orders of magnitude lower than oxalic acid (~10^{-7} atm)[47]. Therefore, we expect that the addition of ammonium hydroxide to our 10 min mimic samples will lower the vapor pressure of the mimics by virtue of organic acid salt formation. In this work we confirm that the neutralization of the CSTR Gly + $^{\bullet}$OH precursor/product mix does in fact lower the vapor pressure of the sample, as discussed below.

The neutralization of the Gly + $^{\bullet}$OH mimic (CSTR) significantly increased the retention of PM mass upon droplet evaporation of OM mass (Figure 3-2; pH 7 in solid red versus pH 3 in solid black). In Figure 3-2, the *PM mass* versus *OM mass*$_{(droplet)}$ of the mimics are compared with ammonium oxalate (red colored open squares and dashed line) and organic acid standards (grey symbols and dashed lines). Note compounds with the lowest liquid vapor pressures (see legend) have the largest residual *PM mass* (e.g., tartaric acid and ammonium oxalate) (Figure 3-2). The slope (*PM mass / OM mass*$_{(droplet)}$) of the linear regression is steepest for those compounds, indicating that a larger fraction of the organic mass is retained in the particle-phase. Furthermore, the Gly + $^{\bullet}$OH mimic containing ammonium hydroxide (Figure 3-2 solid red) (pH 7) exhibited the same behavior in the VOAG system as ammonium oxalate (dashed red) and had a much larger slope than the ammonium-free mimic (Figure 3-2 solid black), suggesting that the vapor pressure of the Gly + $^{\bullet}$OH precursor/product mixture decreases by orders of magnitude as a result of neutralization. Even though the slope increased significantly (two-sided *t*-test, $p = 0.05$) when the pH was increased from 3 to 7 (0.43 ± 0.05 and 1.6 ± 0.3, respectively;

Table 3-1), a truly quantitative assessment of the vapor pressure and enthalpy of vaporization for the neutralized sample resulted challenging, as explained below.

The estimated liquid vapor pressures of the pH 3 mimics (Batch and CSTR) are both ~10^{-7} atm according to Figure 3-3. In Figure 3-3, the slopes of Gly + $^{\bullet}$OH mimics (Figure 3-2 and Table 3-1) and sigmoidal regressions of the organic standards were used to determine the effective vapor pressures as illustrated by the corresponding arrows (black - CSTR pH 3; blue - Batch pH 3). Similarly, enthalpies of vaporization (~70 kJ/mol) were determined from a sigmoidal regression shown in Appendix B4. Two sigmoidal regressions are shown (Figure 3-3 and Appendix B4), uncorrected (black solid line) and corrected for retained water (solid grey line). The corrected curves were used to estimate effective vapor pressures and enthalpies of vaporization (Table 3-1). Note that Batch- and CSTR- mimics (pH 3) exhibited very similar behavior in the VOAG system (Figures 3-2 and 3-3; Appendix B4; Table 3-1) even though the composition of these mimics differed (Figure 3-1). Theoretical molar-weighted enthalpies of vaporization are also shown in Table 3-1 for comparison. The difference between theoretical and VOAG-estimated enthalpies can be due to (1) products formed during droplet evaporation because these are not included in the theoretical calculations (e.g., glyoxal oligomers) and/or (2) residual water in the measurements of the VOAG, which would result in larger measured diameters (thus PM volume and mass) and consequently larger *PM mass / OM mass*$_{(droplet)}$ ratios and higher enthalpy estimates. Based on this assessment the values we report in Table 3-1 are likely to be upper-bound estimates.

As shown in Figure 3-3, the neutralized Gly CSTR-SOA$_{Cld}$ sample behaved as if it stayed entirely in the particle-phase at ambient temperature (red dashed lines), much

like ammonium oxalate and tartaric acid (first two points in the upper left of the sigmoidal regressions). We are unable to provide accurate estimates of the volatility of the neutralized (pH 7) Gly + $^{\bullet}$OH mimic because the data for this sample fall within the part of the regression that is insensitive to vapor pressure (Figure 3-3) and enthalpy of vaporization (Appendix B4). This work demonstrates that the CSTR pH 7 mimic has an estimated vapor pressure and enthalpy of vaporization of (10^{-9} – 10^{-12}) atm and ~(80 – 120) kJ/mol, respectively (Table 3-1). In order to provide better estimates of the volatility of the neutralized Gly + $^{\bullet}$OH precursor/product mixture, the experiments conducted here could be redesigned for higher temperatures or lower pressures, which would shift the sigmoidal regression to the left. Regardless of the current uncertainty in estimating the volatility of the neutralized Gly + $^{\bullet}$OH mimic, it is evident that the presence of ammonia in cloud droplets containing Gly and OH radicals will substantially reduce the vapor pressure of the mixture, causing it to behave similar to ammonium oxalate (~10^{-11} atm) and increasing the yield of in-cloud Gly SOA_{aq}. This result is consistent with the work from Na et al.[60] who found that ammonia enhanced SOA formation from α-pinene ozonolysis due to the formation of condensable (organic) salts. These findings indicate that organic salt formation can play an important role in the properties and fate of SOA formed through cloud processing.

3.5 Conclusions

The volatility of Gly + $^{\bullet}$OH precursor/product mixture after 10 min of cloud processing was assessed in this study through the use of droplet evaporation experiments. The effect of neutralization on the volatility of that SOA_{Cld} was also studied here. We found that the volatility was insensitive to the assumption made to model the droplet

composition (i.e., whether or not gas-phase glyoxal production was fast enough to replace reacting glyoxal in the aqueous-phase) (Batch scenario; $p'_{L,eff.}$ = (1±1) x 10^{-7} atm, and $\Delta H_{vap,eff.}$ = 70 ± 2 kJ/mol versus CSTR scenario; $p'_{L,eff.}$ = (2±2) x 10^{-7} atm, and $\Delta H_{vap,eff.}$ = 70 ± 2 kJ/mol). A significant reduction in volatility behavior was observed when the 10 min Gly + $^{\bullet}$OH precursor/product mixture (CSTR) was neutralized from pH 3 ($p'_{L,eff.}$ = 10^{-7} atm, and $\Delta H_{vap,eff.}$ = 70 kJ/mol) to pH 7 ($p'_{L,eff.} \leq 10^{-9} - 10^{-12}$ atm, and $\Delta H_{vap,eff.} \geq 80 -$ 120 kJ/mol) through the addition of ammonium hydroxide. The neutralized Gly + $^{\bullet}$OH mimic appeared to remain entirely in the particle-phase at ambient temperature, as observed for the ammonium oxalate standard. Thus increased ammonia levels can be expected to increase the yield of glyoxal SOA from in-cloud oxidation and droplet evaporation.

3.6 References

(1) U.S. EPA. *Air Quality Criteria for Particulate Matter*; United States Environmental Protection Agency (U.S. EPA), Research Triangle Park, NC, **2004**.

(2) NARSTO. McMurry, P., Shepherd, M., Vickery, J. *Particulate Matter Assessment for Policy Makers: A NARSTO Assessment*; Cambridge University Press, Cambridge, U.K., **2004**.

(3) IPCC *Climate Change 2007: The Physical Science Basis,* Contribution of Working Group I to the Fourth Assessment Report of the Intergovernmental Panel on Climate Change (IPCC), edited by S. Solomon et al., Cambridge University Press, Cambridge, U.K., **2007**.

(4) Lanz, V. A.; Alfarra, M. R.; Baltensperger, U.; Buchmann, B.; Hueglin, C.; Prévôt, A. S. H. Source apportionment of submicron organic aerosols at an urban site by factor analytical modelling of aerosol mass spectra. *Atmos. Chem. Phys.* **2007**, *7*, 1503–1522.

(5) Lanz, V. A.; Alfarra, M. R.; Baltensperger, U.; Buchmann, B.; Hueglin, C.; Szidat, S.; Wehrli, M. N.; Wacker, L.; Weimer, S.; Caseiro, A.; Puxbaum, H.; Prevot, A. S. H. Source Attribution of Submicron Organic Aerosols during Wintertime Inversions by Advanced Factor Analysis of Aerosol Mass Spectra. *Environmental Science & Technology* **2008**, *42*, 214–220.

(6) Lanz, V. A.; Prévôt, A. S. H.; Alfarra, M. R.; Weimer, S.; Mohr, C.; DeCarlo, P. F.; Gianini, M. F. D.; Hueglin, C.; Schneider, J.; favez, O.; D'Anna, B.; George, C.; Baltensperger, U. Characterization of aerosol chemical composition with aerosol mass spectrometry in Central Europe: an overview. *Atmos. Chem. Phys.* **2010**, *10*, 10453–10471.

(7) Yu, S.; Bhave, P. V.; Dennis, R. L.; Mathur, R. Seasonal and Regional Variations of Primary and Secondary Organic Aerosols over the Continental United States: Semi-Empirical Estimates and Model Evaluation. *Environmental Science & Technology* **2007**, *41*, 4690–4697.

(8) Zhang, Q.; Worsnop, D. R.; Canagaratna, M. R.; Jimenez, J. L. Hydrocarbon-like and oxygenated organic aerosols in Pittsburgh: insights into sources and processes of organic aerosols. *Atmos. Chem. Phys.* **2005**, *5*, 3289–3311.

(9) Zhang, Q.; Jimenez, J. L.; Canagaratna, M. R.; Allan, J. D.; Coe, H.; Ulbrich, I.; Alfarra, M. R.; Takami, A.; Middlebrook, A. M.; Sun, Y. L.; Dzepina, K.; Dunlea, E.; Docherty, K.; DeCarlo, P. F.; Salcedo, D.; Onasch, T.; Jayne, J. T.; Miyoshi, T.; Shimono, A.; Hatakeyama, S.; Takegawa, N.; Kondo, Y.; Schneider, J.; Drewnick, F.; Borrmann, S.; Weimer, S.; Demerjian, K.; Williams, P.; Bower, K.; Bahreini, R.; Cottrell, L.; Griffin, R. J.; Rautiainen, J.; Sun, J. Y.; Zhang, Y. M.; Worsnop, D. R. Ubiquity and dominance of oxygenated species in organic aerosols in anthropogenically-influenced Northern Hemisphere midlatitudes. *Geophys. Res. Lett.* **2007**, *34*, L13801.

(10) Hallquist, M.; Wenger, J.; Baltensperger, U.; Rudich, Y.; Simpson, D.; Claeys, M.; Dommen, J.; Donahue, N.; George, C.; Goldstein, A. The formation, properties and impact of secondary organic aerosol: current and emerging issues. *Atmos. Chem. Phys.* **2009**, *9*, 5155–5236.

(11) Heald, C. L.; Jacob, D. J.; Park, R. J.; Russell, L. M.; Huebert, B. J.; Seinfeld, J. H.; Liao, H.; Weber, R. J. A large organic aerosol source in the free troposphere missing from current models. *Geophys. Res. Lett.* **2005**, *32*, L18809.

(12) Tsigaridis, K.; Kanakidou, M. Global modelling of secondary organic aerosol in the troposphere: A sensitivity analysis. *Atmos. Chem. Phys.* **2003**, *3*, 1849–1869.

(13) Ervens, B.; Turpin, B. J.; Weber, R. J. Secondary organic aerosol formation in cloud droplets and aqueous particles (aqSOA): a review of laboratory, field and model studies. *Atmos. Chem. Phys.* **2011**, *11*, 11069–11102.

(14) Gong, W.; Stroud, C.; Zhang, L. Cloud Processing of Gases and Aerosols in Air Quality Modeling. *Atmosphere* **2011**, *2*, 567–616.

(15) Blando, J. D.; Turpin, B. J. Secondary organic aerosol formation in cloud and fog droplets: a literature evaluation of plausibility. *Atmospheric Environment* **2000**, *34*,

1623–1632.

(16) Gelencsér, A.; Varga, Z. Evaluation of the atmospheric significance of multiphase reactions in atmospheric secondary organic aerosol formation. *Atmos. Chem. Phys.* **2005**, *5*, 2823–2831.

(17) Carlton, A. G.; Turpin, B. J.; Altieri, K. E.; Seitzinger, S. P.; Mathur, R.; Roselle, S. J.; Weber, R. J. CMAQ Model Performance Enhanced When In-Cloud Secondary Organic Aerosol is Included: Comparisons of Organic Carbon Predictions with Measurements. *Environmental Science & Technology* **2008**, *42*, 8798–8802.

(18) Chen, J.; Griffin, R. J.; Grini, A.; Tulet, P. Modeling secondary organic aerosol formation through cloud processing of organic compounds. *Atmos. Chem. Phys.* **2007**, *7*, 5343–5355.

(19) Fu, T.-M.; Jacob, D. J.; Wittrock, F.; Burrows, J. P.; Vrekoussis, M.; Henze, D. K. Global budgets of atmospheric glyoxal and methylglyoxal, and implications for formation of secondary organic aerosols. *J. Geophys. Res.* **2008**, *113*, D15303.

(20) Fu, T.-M.; Jacob, D. J.; Heald, C. L. Aqueous-phase reactive uptake of dicarbonyls as a source of organic aerosol over eastern North America. *Atmospheric Environment* **2009**, *43*, 1814–1822.

(21) Gao, S. S.; Abbatt, J. P. D. Kinetics and Mechanism of OH Oxidation of Small Organic Dicarboxylic Acids in Ice: Comparison to Behavior in Aqueous Solution. *J. Phys. Chem. A* **2011**, *115*, 9977–9986.

(22) Liu, J.; Horowitz, L. W.; Fan, S.; Carlton, A. G.; Levy, H., II Global in-cloud production of secondary organic aerosols: Implementation of a detailed chemical mechanism in the GFDL atmospheric model AM3. *J. Geophys. Res.* **2012**, *117*, D15303.

(23) Odum, J. R.; Hoffmann, T.; Bowman, F.; Collins, D.; Flagan, R. C.; Seinfeld, J. H. Gas/particle partitioning and secondary organic aerosol yields. *Environmental Science & Technology* **1996**, *30*, 2580–2585.

(24) Pankow, J. F. An absorption model of gas/particle partitioning of organic compounds in the atmosphere. *Atmospheric Environment* **1994**, *28*, 185–188.

(25) Pankow, J. An absorption model of the gas/aerosol partitioning involved in the formation of secondary organic aerosol. *Atmospheric Environment* **1994**, *28*, 189–193.

(26) Seinfeld, J. H.; Pankow, J. F. Organic Atmospheric Particulate Material. *Annu. Rev. Phys. Chem.* **2003**, *54*, 121–140.

(27) Munger, J. W.; Jacob, D.; Daube, B.; Horowitz, L.; Keene, W.; Heikes, B.

Formaldehyde, glyoxal, and methylglyoxal in air and cloudwater at a rural mountain site in central Virginia. *J. Geophys. Res.* **1995**, *100*, 9325–9325.

(28) Betterton, E. A.; Hoffmann, M. R. Henry's law constants of some environmentally important aldehydes. *Environmental Science & Technology* **1988**, *22*, 1415–1418.

(29) Hays, M. D.; Geron, C. D.; Linna, K. J.; Smith, N. D.; Schauer, J. J. Speciation of Gas-Phase and Fine Particle Emissions from Burning of Foliar Fuels. *Environmental Science & Technology* **2002**, *36*, 2281–2295.

(30) Hays, M. D.; Beck, L.; Barfield, P.; Willis, R. D.; Landis, M. S.; Stevens, R. K.; Preston, W.; Dong, Y. Physical and Chemical Characterization of Residual Oil-Fired Power Plant Emissions. *Energy Fuels* **2009**, *23*, 2544–2551.

(31) Carlton, A. G.; Turpin, B. J.; Altieri, K. E.; Seitzinger, S.; Reff, A.; Lim, H.-J.; Ervens, B. Atmospheric oxalic acid and SOA production from glyoxal: Results of aqueous photooxidation experiments. *Atmospheric Environment* **2007**, *41*, 7588–7602.

(32) Lee, A. K. Y.; Herckes, P.; Leaitch, W. R.; Macdonald, A. M.; Abbatt, J. P. D. Aqueous OH oxidation of ambient organic aerosol and cloud water organics: Formation of highly oxidized products. *Geophys. Res. Lett.* **2011**, *38*, L11805.

(33) Tan, Y.; Perri, M. J.; Seitzinger, S. P.; Turpin, B. J. Effects of Precursor Concentration and Acidic Sulfate in Aqueous Glyoxal−OH Radical Oxidation and Implications for Secondary Organic Aerosol. *Environmental Science & Technology* **2009**, *43*, 8105–8112.

(34) Zhao, R.; Lee, A. K. Y.; Abbatt, J. P. D. Investigation of Aqueous-Phase Photooxidation of Glyoxal and Methylglyoxal by Aerosol Chemical Ionization Mass Spectrometry: Observation of Hydroxyhydroperoxide Formation. *J. Phys. Chem. A* **2012**, *116*, 6253–6263.

(35) Lim, Y. B.; Tan, Y.; Perri, M. J.; Seitzinger, S. P.; Turpin, B. J. Aqueous chemistry and its role in secondary organic aerosol (SOA) formation. *Atmos. Chem. Phys.* **2010**, *10*, 10521–10539.

(36) Shapiro, E. L.; Szprengiel, J.; Sareen, N.; Jen, C. N.; Giordano, M. R.; McNeill, V. Light-absorbing secondary organic material formed by glyoxal in aqueous aerosol mimics. *Atmos. Chem. Phys.* **2009**, *9*, 2289–2300.

(37) De Haan, D. O.; Corrigan, A. L.; Smith, K. W.; Stroik, D. R.; Turley, J. J.; Lee, F. E.; Tolbert, M. A.; Jimenez, J. L.; Cordova, K. E.; Ferrell, G. R. Secondary Organic Aerosol-Forming Reactions of Glyoxal with Amino Acids. *Environmental Science & Technology* **2009**, *43*, 2818–2824.

(38) De Haan, D. O.; Tolbert, M. A.; Jimenez, J. L. Atmospheric condensed-phase reactions of glyoxal with methylamine. *Geophys. Res. Lett.* **2009**, *36*.

(39) Galloway, M.; Chhabra, P.; Chan, A.; Surratt, J.; Flagan, R.; Seinfeld, J.; Keutsch, F. Glyoxal uptake on ammonium sulphate seed aerosol: reaction products and reversibility of uptake under dark and irradiated conditions. *Atmos. Chem. Phys.* **2009**, *9*, 3331–3345.

(40) Kampf, C. J.; Jakob, R.; Hoffmann, T. Identification and characterization of aging products in the glyoxal/ammonium sulfate system – implications for light-absorbing material in atmospheric aerosols. *Atmos. Chem. Phys.* **2012**, *12*, 6323–6333.

(41) Nozière, B.; Dziedzic, P.; Córdova, A. Products and Kinetics of the Liquid-Phase Reaction of Glyoxal Catalyzed by Ammonium Ions (NH 4+). *J. Phys. Chem. A* **2009**, *113*, 231–237.

(42) Yu, G.; Bayer, A. R.; Galloway, M. M.; Korshavn, K. J.; Fry, C. G.; Keutsch, F. N. Glyoxal in Aqueous Ammonium Sulfate Solutions: Products, Kinetics and Hydration Effects. *Environmental Science & Technology* **2011**, *45*, 6336–6342.

(43) De Haan, D. O.; Corrigan, A. L.; Tolbert, M. A.; Jimenez, J. L.; Wood, S. E.; Turley, J. J. Secondary Organic Aerosol Formation by Self-Reactions of Methylglyoxal and Glyoxal in Evaporating Droplets. *Environmental Science & Technology* **2009**, *43*, 8184–8190.

(44) Loeffler, K. W.; Koehler, C. A.; Paul, N. M.; De Haan, D. O. Oligomer Formation in Evaporating Aqueous Glyoxal and Methyl Glyoxal Solutions. *Environmental Science & Technology* **2006**, *40*, 6318–6323.

(45) Liggio, J.; Li, S.-M.; McLaren, R. Reactive uptake of glyoxal by particulate matter. *J. Geophys. Res.* **2005**, *110*, D10304.

(46) Michaud, V.; El Haddad, I.; Liu, Y.; Sellegri, K.; Laj, P.; Villani, P.; Picard, D.; Marchand, N.; Monod, A. In-cloud processes of methacrolein under simulated conditions–Part 3: Hygroscopic and volatility properties of the formed secondary organic aerosol. *Atmos. Chem. Phys.* **2009**, *9*, 5119–5130.

(47) Ortiz-Montalvo, D. L.; Lim, Y. B.; Perri, M. J.; Seitzinger, S. P.; Turpin, B. J. Volatility and Yield of Glycolaldehyde SOA Formed through Aqueous Photochemistry and Droplet Evaporation. *Aerosol Science and Technology* **2012**, *46*, 1002–1014.

(48) Bilde, M.; Pandis, S. N. Evaporation Rates and Vapor Pressures of Individual Aerosol Species Formed in the Atmospheric Oxidation of α- and β-Pinene. *Environmental Science & Technology* **2001**, *35*, 3344–3349.

(49) Hallquist, M.; Wängberg, I.; Ljungström, E. Atmospheric fate of carbonyl oxidation products originating from α-pinene and δ3-carene: Determination of rate of reaction with OH and NO3 radicals, UV absorption cross sections, and vapor pressures. *Environmental Science & Technology* **1997**, *31*, 3166–3172.

(50) Offenberg, J. H.; Kleindienst, T. E.; Jaoui, M.; Lewandowski, M.; Edney, E. O. Thermal properties of secondary organic aerosols. *Geophys. Res. Lett.* **2006**, *33*.

(51) Sheehan, P. E.; Bowman, F. M. Estimated Effects of Temperature on Secondary Organic Aerosol Concentrations. *Environmental Science & Technology* **2001**, *35*, 2129–2135.

(52) Stanier, C. O.; Pathak, R. K.; Pandis, S. N. Measurements of the Volatility of Aerosols from α-Pinene Ozonolysis. *Environmental Science & Technology* **2007**, *41*, 2756–2763.

(53) Tan, Y.; Carlton, A. G.; Seitzinger, S. P.; Turpin, B. J. SOA from methylglyoxal in clouds and wet aerosols: Measurement and prediction of key products. *Atmospheric Environment* **2010**, *44*, 5218–5226.

(54) Berglund, R. N.; Liu, B. Y. H. Generation of monodisperse aerosol standards. *Environmental Science & Technology* **1973**, *7*, 147–153.

(55) Pankow, J.; Asher, W. SIMPOL. 1: a simple group contribution method for predicting vapor pressures and enthalpies of vaporization of multifunctional organic compounds. *Atmos. Chem. Phys.* **2008**, *8*, 2773–2796.

(56) U.S. EPA. *Estimation Programs Interface Suite™* for Microsoft® Windows, v 4.00; United States Environmental Protection Agency (U.S. EPA), Washington, DC, **2010**.

(57) Joback, K. G.; Reid, R. C. Estimation of Pure-Component Properties from Group-Contributions. *Chem. Eng. Comm.* **1987**, *57*, 233–243.

(58) Peng, C.; Chan, M. N.; Chan, C. K. The Hygroscopic Properties of Dicarboxylic and Multifunctional Acids: Measurements and UNIFAC Predictions. *Environmental Science & Technology* **2001**, *35*, 4495–4501.

(59) Limbeck, A.; Puxbaum, H.; Otter, L.; Scholes, M. C. Semivolatile behavior of dicarboxylic acids and other polar organic species at a rural background site (Nylsvley, RSA). *Atmospheric Environment* **2001**, *35*, 1853–1862.

(60) Na, K.; Song, C.; Switzer, C.; Cocker, D. R. Effect of Ammonia on Secondary Organic Aerosol Formation from α-Pinene Ozonolysis in Dry and Humid Conditions. *Environmental Science & Technology* **2007**, *41*, 6096–6102.

(61) Chickos, J. S.; Zhao, H. Measurement of the Vaporization Enthalpy of Complex Mixtures by Correlation-Gas Chromatography. The Vaporization Enthalpy of RP-1, JP-7, and JP-8 Rocket and Jet Fuels at T= 298.15 K. *Energy Fuels* **2005**, *19*, 2064–2073.

(62) Yaws, C. L. Yaws' Handbook of Thermodynamic and Physical Properties of Chemical Compounds. 2003. *Knovel Online version from http://wwwknovelcom*.

(63) Turpin, B. J.; Lim, H.-J. Species Contributions to PM2.5 Mass Concentrations: Revisiting Common Assumptions for Estimating Organic Mass. *Aerosol Science and Technology* **2001**, *35*, 602–610.

(64) Windholdz, M. The Merck Index-An encyclopedia of chemicals and drugs. *Merck & CO., New York, USA* **1976**, 74.

(65) Desboeufs, K.; Losno, R.; Colin, J. Relationship between droplet pH and aerosol dissolution kinetics: Effect of incorporated aerosol particles on droplet pH during cloud processing. *J Atmos Chem* **2003**, *46*, 159–172.

(66) Ervens, B.; Volkamer, R. Glyoxal processing by aerosol multiphase chemistry: towards a kinetic modeling framework of secondary organic aerosol formation in aqueous particles. *Atmos. Chem. Phys.* **2010**, *10*, 8219–8244.

Table 3-1. VOAG results for Gly + $^{\bullet}$OH precursor/product mixtures: slope ($PM\ mass\ /\ OM\ mass_{(droplet)}$) with coefficients of determination (r^2) and standard error, effective liquid vapor pressures ($p'_{L,eff.}$), and effective enthalpies of vaporization ($\Delta H_{vap,eff.}$).

Mimic Sample	pH	Density (g/mL)	Slope [a] $\left[\frac{PM\ mass}{OM\ mass_{(droplet)}}\right]$	Standard Error	r^2	$p'_{L,eff.}$ [b] (atm)	$\Delta H_{vap,eff.}$ [c] (kJ/mol)	Theoretical $\Delta H_{vap,mix}$ [d] (kJ/mol)
Batch 10 min	3	1.3[e]	0.55	0.06	99%	(1±1) x 10^{-7}	70 ± 2	44
CSTR 10 min	3	1.4[e]	0.43	0.05	95%	(2±2) x 10^{-7}	70 ± 2	54
	7	1.4-1.5[f]	1.6[g]	0.3	89%	~(10^{-9} – 10^{-12}) [h]	~80–120 [h]	-

[a] Slopes (in units of g/g) from Figure 3-2 corrected for the effect that retained water (33% upper-bound estimate) could have on the density value used to calculate *PM mass*. Slopes for organic standards are provided in Appendix B2. [b] Effective liquid vapor pressure estimates (at 298.15 K) using the corrected sigmoidal regression shown in Figure 3-3 ± error propagation, which incorporates uncertainty in vapor pressure estimates[55], standard error of slope, and standard error in the coefficients of the sigmoidal regression. The sigmoidal corrected regression equation can be found in Appendix B3. [c] Effective enthalpy of vaporization estimates (at normal boiling point) using corrected sigmoidal regression shown in Appendix B4 ± error propagation, which incorporates uncertainty in enthalpy of vaporization estimates[57], standard error of slope, and standard error in the coefficients of the sigmoidal regression. The sigmoidal corrected regression equation can be found in Appendix B5. [d] Molar weighted theoretical enthalpies of vaporization of product mixtures calculated following Chickos et al.[61] approach, as $\Delta H_{vap,mix} = \sum_i n_i \times \Delta H_{vap,i}$ where n_i is the molar fraction of species *i* (from Figure 3-1) and $\Delta H_{vap,i}$ is the theoretical enthalpy of vaporization of species *i*; (33.486 kJ/mol, 72.57 kJ/mol, and 50.191 kJ/mol for glyoxal, oxalic acid, and glyoxylic acid, respectively[62]). [e] Concentration-weighted density[63] ± 0.1 (error propagation accounting for the uncertainty in the concentrations). [f] Assuming a density between that of CSTR 10 min pH 3 and ammonium oxalate (1.50 g/mL)[64]. [g] The slope without correction for retained water was 1.7 ± 0.3. [h] Estimated range based on the uncorrected sigmoidal regression.

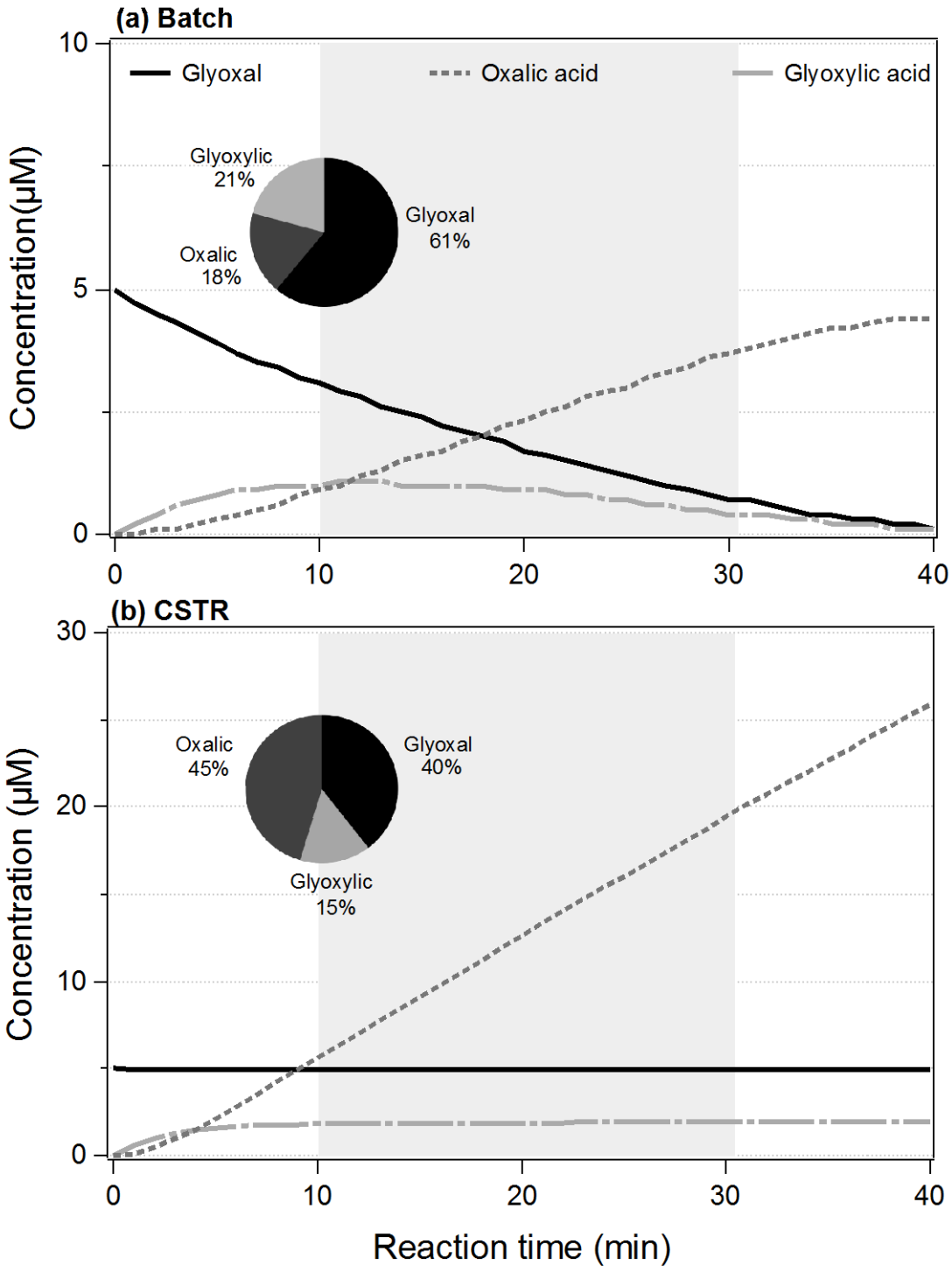

Figure 3-1. Estimated product concentrations of the reaction between 5 μM glyoxal and OH radicals (10^{-12} M). Obtained from the Batch (a) and CSTR (b) assumptions. Pie charts illustrate the (molar) distribution of products (%) at 10 min into the reaction. Shaded areas between 10 and 30 minutes represent cloud droplet lifetimes[65,66].

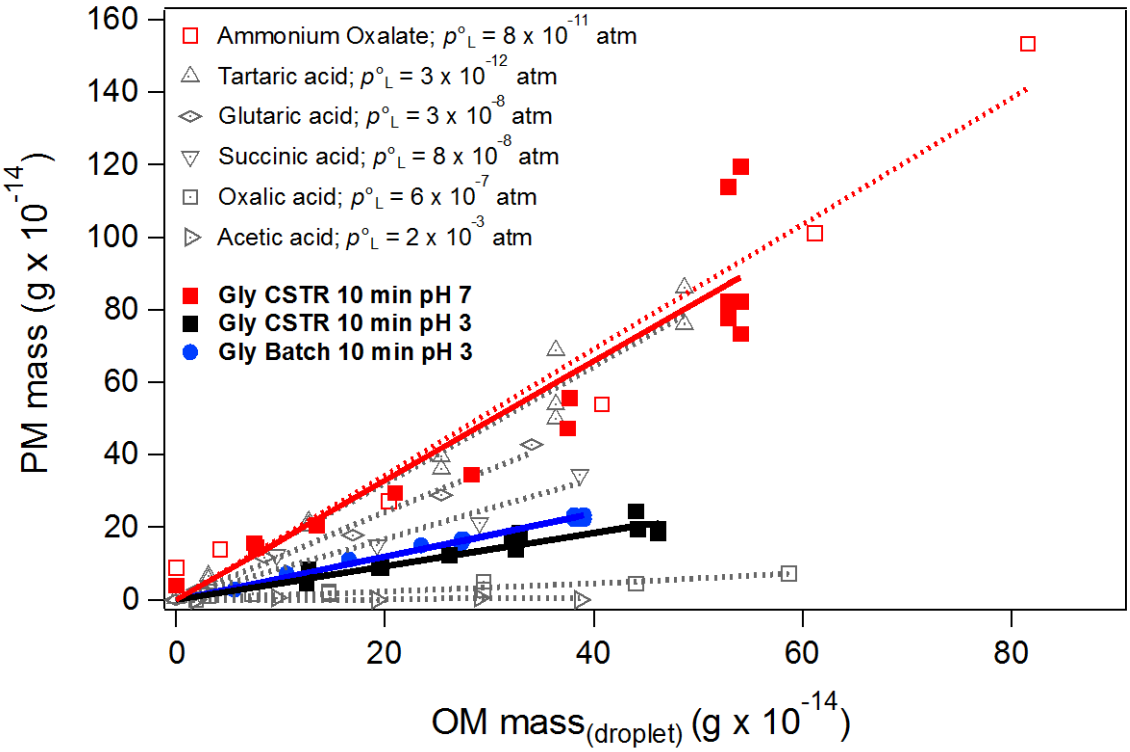

Figure 3-2. Residual PM mass versus initial droplet OM mass obtained from VOAG and TOC analyses, respectively. Solid red squares and solid red line represent the Gly CSTR mimic at pH 7, while solid black squares and solid black line correspond to pH 3**.** Solid blue circles and solid blue line represent the Gly Batch mimic at pH 3. Grey symbols and grey dashed lines are from organic acid standards. The legend includes estimates of liquid vapor pressure (p^{o}_{L}) obtained from Pankow and Asher[55] for the organic acids and from US EPA- EPI Suite™ Software[56] for ammonium oxalate (sub-cooled p^{o}_{L}). Ammonium oxalate (open red squares and red dashed line) also shown. Samples were analyzed at RH = (12 ± 3)% and t = (24.4 ± 0.7)ºC. Slopes and r^2 values are reported in Table 3-1.

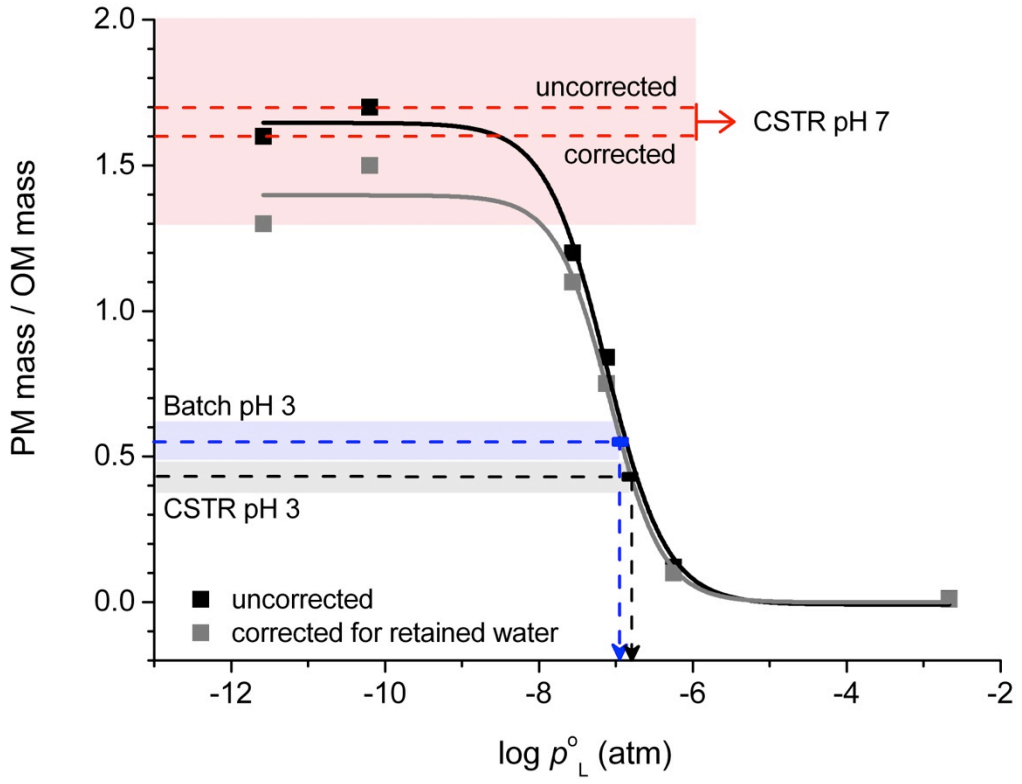

Figure 3-3. Sigmoidal fit of *PM mass / OM mass* versus *log* p^{o}_{L}. *PM mass / OM mass* values (in units of g/g) correspond to slopes from Figure 3-2. Data shown was uncorrected (black solid line) and corrected (solid grey line) for the effect that retained water (33% upper-bound estimate) could have on PM density. Dashed lines show *PM mass / OM mass* of Gly + $^{\bullet}$OH mimics and estimated p^{o}_{L} from the corrected sigmoidal curve: black – CSTR pH 3, blue – Batch pH 3, and red – CSTR pH 7 (both corrected and uncorrected slope values are shown). Shaded areas represent the standard error of the slopes. The liquid vapor pressures of pure compounds (p^{o}_{L}) were obtained using Pankow and Asher[55] for the organic acids and from US EPA- EPI Suite™ Software[56] for ammonium oxalate (sub-cooled p^{o}_{L}). *PM mass / OM mass* values are provided in Table 3-1 for Gly mimics, and in Appendix B2 for the organic standards. The sigmoidal corrected regression equation can be found in Appendix B3.

Chapter 4. Volatility of Methylglyoxal Cloud SOA Formed through OH Radical Oxidation and Droplet Evaporation

Material in this chapter will be submitted for publication as:

Ortiz-Montalvo, D. L.; Schwier, A.; Lim, Y. B.; McNeill, V. F.; Turpin, B. J. Volatility of Methylglyoxal Cloud SOA Formed through OH Radical Oxidation and Droplet Evaporation. *Atmospheric Environment* **2013**.

4.1 Abstract

The volatility of secondary organic aerosol (SOA) formed through cloud processing (aqueous hydroxyl radical oxidation) of methylglyoxal (MGly) was studied. SOA is a substantial contributor to atmospheric organic aerosol; however, its formation via aqueous photochemistry in clouds (SOA_{Cld}) and in aerosols is not well understood. Two atmospheric scenarios of in-cloud aqueous MGly oxidation were evaluated using kinetic models, and results were used to prepare mimic solutions. Droplets made with mimic solutions were then used to assess the volatility of the precursor/product mix using two systems: a Vibrating Orifice Aerosol Generator (VOAG) with an Optical Particle Counter, and an Aerosol Chemical Ionization Mass Spectrometer (Aerosol-CIMS). Droplets of known size were formed, evaporated, and the resulting particles were measured for size in the VOAG system. Additionally, the ion abundance of several individual products (pyruvic acid and oxalic acid + methylglyoxal) was traced as a function of temperature (25–116ºC) in the Aerosol-CIMS to estimate enthalpies of vaporization. Results from VOAG suggest that 10-30 minutes of in-cloud MGly oxidation produces an organic mixture with an effective vapor pressure of (4±7) x 10^{-7} atm at pH 3, which is essentially unaffected by the addition of ammonium hydroxide (pH 7). The fraction remaining in the particle-phase was smaller than previously reported for glycolaldehyde SOA. The enthalpies of

vaporization of pyruvic acid and oxalic acid + methylglyoxal in the mixture (from Aerosol-CIMS) were smaller than the theoretical enthalpies of the pure compounds and smaller than that estimated for the entire precursor/product mix using the VOAG system. The mix of higher volatility (e.g., methylglyoxal) and lower volatility (e.g. methylglyoxal oligomers, pyruvate, oxalate) species at 10-30 min of reaction time creates an intermediate volatility mixture. Lower temperatures, longer contact times (i.e., multiple cloud cycles) to form oxalate, continued chemistry in resulting wet aerosols, and/or formation of lower volatility salts will decrease the vapor pressure and increase methylglyoxal SOA_{Cld}.

4.2 Introduction

There is growing evidence that secondary organic aerosol (SOA) forms through gas-phase oxidation of organics followed by aqueous chemistry in clouds and wet aerosol[1-3]. Organic compounds are predominantly emitted in the gas-phase[4] where they can become fragmented and oxidized by gas-phase photochemistry, and form small water-soluble organic compounds that are ubiquitous and abundant in the atmosphere[5]. The chemistry of several water-soluble organics has been studied because of their potential to form SOA by means of photochemically-initiated radical chemistry (e.g., hydroxyl radical reactions) or non-photochemical reactions (e.g., acid or ammonium catalyzed reactions) in the aqueous-phase (SOA_{aq})[3,6-13]. Most laboratory studies have assessed SOA_{aq} formation using single organic precursors (e.g., methylglyoxal, glyoxal, glycolaldehyde, pyruvic acid, methacrolein, methyl vinyl ketone, and phenols), although glyoxal-methylglyoxal cross-reactions[14] and some more complex mixtures of precursors and SOA products (e.g., Bateman et al.[15]; Lee et al.[16]; Lee et al.[17]; Liu et al.[8] Nguyen et al.[18]) have also been studied. Additionally, SOA_{aq} has been observed to form without oxidation through droplet

evaporation of single organic compounds (e.g., glyoxal and methylglyoxal) that form oligomers through self-reactions[19,20]. The current study focuses on droplet evaporation of products formed by the photooxidation of methylglyoxal (MGly) with hydroxyl radicals ($^{\bullet}OH$) in clouds (MGly SOA_{Cld}).

MGly ($C_3H_4O_2$) is a dicarbonyl compound that is formed in the gas-phase as a secondary oxidation product of biogenic hydrocarbons including isoprene[21,22] and anthropogenic hydrocarbons such as the aromatics toluene, xylenes, and trimethylbenzenes[23-25]. MGly can also be emitted directly into the atmosphere by biomass burning[26] and residual oil burning[27]. The gas-phase lifetime of MGly against OH radical ($^{\bullet}OH$) oxidation is about 0.9 days. It can readily enter the aqueous-phase, due to its high water solubility (effective Henry's law constant, $H_{eff} = 3.71 \times 10^3$ M atm^{-1} at 25°C)[28], and it has been measured in clouds, < 0.3 to 128 μM[29]. In the aqueous-phase, MGly reacts rapidly with OH radicals (~26 min aqueous lifetime with respect to $^{\bullet}OH$) and forms products found predominantly in the particle-phase in the atmosphere (e.g., pyruvate, oxalate, and glyoxylate)[30]. At cloud relevant concentrations, the reaction of MGly with $^{\bullet}OH$ produces small carboxylic acids, mainly pyruvic, acetic, and oxalic acids, and to a minor extent glyoxylic and glycolic acids. At aerosol relevant concentrations (MGly ≥ 2 mM), larger compounds like succinic and malonic acids, higher molecular weight compounds, and oligomers are also formed[11,31-33]. Additionally, MGly can also form SOA_{aq} in the absence of oxidants by self-oligomerization through aldol condensation reactions in evaporating aqueous droplets[19,20].

SOA_{aq} formation is being added to regional and global models[6,34-39]. A better understanding of chemical transformations that can occur during droplet evaporation[10,19,20], vapor pressure and the enthalpy of vaporization of the SOA_{aq}

mixture are needed to aid these efforts[40]. There is very limited information about the volatility of SOA_{aq} and on how the chemical processes during cloud droplet evaporation impact the formation and properties of SOA_{aq}. To our knowledge, Monod and co-workers were the first to investigate the volatility properties of SOA_{aq} formed through aqueous photooxidation and droplet evaporation[41-43]. They found that methacrolein SOA_{aq} became substantially less volatile as the reaction proceeded from 5 hours (80% 100°C-volatile) to 22 hours (20% 100°C-volatile); however, these reaction times are much longer than the lifetimes of cloud droplets which are in the order of several minutes[44]. More recently, Ortiz-Montalvo et al.[10] studied the volatility of the mix of products of aqueous photooxidation and droplet evaporation of (1 mM) glycolaldehyde with (~10^{-12} M) OH radicals after 10-30 min of reaction. They were the first to provide values of effective vapor pressure (~10^{-7} atm) and enthalpy of vaporization (~70 kJ/mol) for glycolaldehyde SOA_{aq}. They hypothesized that the vapor pressure of glycolaldehyde SOA_{aq} would be orders of magnitude lower if the organic acid products (e.g. oxalate) were neutralized to organic salts. Evidence to support this was provided by evaporating droplets of oxalic acid and ammonium oxalate.

The present study provides the first reported estimates of the volatility of MGly cloud SOA_{aq} (SOA_{Cld}) formed through OH radical oxidation and droplet evaporation. Laboratory-validated kinetic models were used to predict the mix of precursors and products present after 10 – 30 min of aqueous MGly oxidation for two atmospheric scenarios. A Vibrating Orifice Aerosol Generator (VOAG) and Aerosol Chemical Ionization Mass Spectrometer (Aerosol-CIMS) were used to measure the effective vapor pressure and enthalpy of vaporization of the mimics and several compounds in the mix. Additionally, the effect of pH (neutralization) on the volatility

of MGly SOA_{Cld} was studied. Some components of these mixtures (i.e., pyruvate, oxalate) are found preferentially in the particle-phase in the atmosphere (i.e., ~60%, ~74% respectively)[30] and methylglyoxal oligomers formed through laboratory droplet evaporation have previously been observed in the particle-phase. This work seeks to better understand these phenomena within the context of in-cloud aqueous methylglyoxal chemistry.

4.3 Methods

The purpose of this work is to characterize the SOA_{Cld} formed from in-cloud photooxidation of MGly and OH radicals ($^{\bullet}OH$) followed by droplet evaporation. VOAG and Aerosol-CIMS systems were used to determine the effective vapor pressure and enthalpy of vaporization of the MGly + $^{\bullet}OH$ precursor/product mix in evaporating droplets for two different atmospheric scenarios. The aqueous chemistry of MGly and $^{\bullet}OH$ has previously been validated by comparing predicted and measured precursor/product concentration dynamics in laboratory batch reactor experiments[32,45]. We used this chemistry to determine the precursor/product composition mix resulting from the $^{\bullet}OH$ oxidation of MGly in cloud droplets (10-30 min) using 1) a batch reactor and 2) a continuously stirred tank reactor (CSTR) approximation. Mimic solutions prepared with these compositions were used in droplet evaporation experiments. Normally, aqueous photooxidation experiments are conducted with relatively high concentrations of H_2O_2 to produce OH radicals in the aqueous-phase; however, excess H_2O_2 in samples waiting analysis reacts with pyruvic acid (main product of MGly photooxidation) to form acetic acid[32]. Further evidence of pyruvic acid depletion can be found in Appendix D. The use of mimic solutions avoids this problem.

Unlike sulfate, MGly is formed in the atmosphere from many precursor gases;

thus it is not immediately apparent whether the batch reactor or CSTR approximation is more appropriate. SO_2 is emitted from the surface and depleted from the gas-phase rapidly in the vicinity of clouds. Thus, aqueous oxidation of SO_2 to sulfate leads to the depletion of SO_2 from the aqueous-phase, and the aqueous SO_2 oxidation system is most appropriately modeled as a batch reactor. If gas-phase production of MGly is slow relative to its aqueous oxidation, the aqueous oxidation of MGly can also be approximated as a batch reactor. If, on the other hand, gas-phase MGly production (and aqueous uptake) is rapid relative to aqueous oxidation, MGly will continue to be replenished in the aqueous-phase as oxidation takes place, and the aqueous oxidation system will be better represented as a CSTR.

The precursor/product compositional mix obtained from the batch and CSTR aqueous MGly model runs were used to prepare mimic solutions. The concentrations of precursor and products were scaled up (factor of F =130 for CSTR and F=250 for Batch) to meet the detection limits of the droplet evaporation methods, but still maintaining the precursor/product distribution expected in cloud droplets. The mimic solutions were then analyzed using two droplet evaporation systems to study the volatility of MGly SOA_{Cld}. The VOAG system provided information about the volatility behavior of the mixture, whereas the Aerosol-CIMS characterized the behavior of individual species within the mixture. This information can be used to improve prediction of MGly SOA_{Cld} in chemical transport models.

4.3.1 Chemical Modeling

The complete chemistry has been published previously[32,45]. In batch reactor modeling[32] the initial MGly concentration was 5 μM, which is within the concentration range found in cloud water (1-10 μM, for droplets ~18 μm in diameter)[29]. MGly decreased as the reaction proceeded. The concentration of $^{\bullet}OH$ was

held constant at 10^{-12} M, which is within the estimated range of atmospheric aqueous-phase concentrations (~10^{-12} to ~10^{-13} M)[3].

For CSTR modeling[45] the aqueous MGly concentration was maintained always at 5 μM[29] and the OH radical concentration at 10^{-12} M. This corresponds to a gas-phase MGly concentration of ~1 ppb, given a Henry's law constant, H, of 3.71 x 10^3 M atm^{-1} [28].

4.3.2 Mimic Samples

Mimic solutions were prepared to match the chemical composition 10 - 30 minutes into batch and CSTR reactions. Mimics were prepared using18 MΩ milli-Q water, methylglyoxal (37.8%; Sigma-Aldrich) and pyruvic (99.1%; Sigma-Aldrich), oxalic (0.1008 N; Fluka Analytical), and acetic (99.99%; Sigma-Aldrich) acids. To study the effects of increasing pH, we used ammonium hydroxide (29.6% as ammonia (NH_3); J.T. Baker) to neutralize CSTR mimics.

4.3.3 VOAG Droplet Evaporation Experiments

Monodisperse droplets of mimic samples were generated and evaporated using the VOAG (TSI Model 3450)[46] followed by a dilution drying chamber (residence time 6 s, RH = (12 ± 3)%, t = (24.1 ± 0.4)ºC). The diameter of the resulting particles (e.g., SOA) was measured with an optical particle counter (OPC, Grimm Aerosol Spectrometer, Model 1.109, 31 channels) downstream of an ionizer (NRD StaticMaster 2U500, Po-210; gives particles a Boltzmann charge distribution), as described in detail by Ortiz-Montalvo et al.[10]. Briefly, the VOAG passes filtered mimic solutions through a 10-μm diameter (nominal ± 25%) orifice producing monodisperse droplets of 20-μm nominal diameter. Because the orifice manufacturing tolerance is large, we determined the diameter of the generated droplets by calibrating the system with ammonium sulfate, $(NH_4)_2SO_4$ (3.1801 M; Fluka Analytical). The

droplet diameter (D_d = 17.9 ± 0.4 μm, n=3, r^2=0.99) was obtained from the slope of D_p versus $C^{1/3}$, where D_p is the residual particle diameter and C is the volumetric concentration of the solute in solution ($cm^3_{solute}/cm^3_{solution}$). The VOAG system operated at a liquid flow rate of 0.077 mL/min, frequency ~160 kHz, dilution air 50 L/min, dispersion air 1 L/min. VOAG's performance was tested daily with a 250 μM $(NH_4)_2SO_4$ standard solution. The criterion for acceptance was ≤ 10% difference between the theoretical and measured diameter of resulting $(NH_4)_2SO_4$ particles.

D_p values of mimic samples ranged between 0.35 – 0.59 μm, with geometric standard deviations between 1.1 and 1.2. Succinic acid standards (99.99%; Sigma-Aldrich) were used as an independent check. The method precision for diameter was 3% and 2%, calculated as the pooled standard deviation divided by the mean of the succinic acid particle diameter (60 μM and 750 μM, respectively). Succinic acid standards were analyzed in duplicate during each experiments (n=8, at each concentration).

Following the methodology described by Ortiz-Montalvo et al.[10] for assessing the volatility of SOA_{aq}, six dilutions (0 – 4000 μM C) of each mimic solution and each organic standard (acetic, oxalic, succinic, glutaric, and tartaric acids) were pushed through the VOAG system. The resulting droplets were dried to ~10% RH and their dry diameter was measured in the OPC. In addition, each mimic solution was analyzed for total organic carbon (TOC, Shimadzu TOC-5000A). The TOC content in the generated droplet was converted to organic matter (OM) mass using organic mass to organic carbon ratios provided in Appendix C1. Method precision (1%) for TOC (four injections/sample) was calculated as the pooled coefficient of variation of duplicate samples (n=40). The residual optical particle diameters (D_p) were converted to the mass of residual particles (*PM mass*) by assuming spherical

particles and using liquid densities (Appendix C1). The *PM mass* of the organic standards was regressed on *OM mass*, and the slopes of each were evaluated against their corresponding liquid vapor pressures ($p°_L$) (estimated using the SIMPOL group contribution method)[47] and enthalpies of vaporization (estimated using group contribution method that uses the normal boiling point to estimate the enthalpy of vaporization of pure compounds)[48]. Sigmoidal fits were obtained since the *PM mass* divided by droplet *OM mass* (*PM mass / OM mass*$_{(droplet)}$) reflects the fraction of total droplet organic matter that remains in the particle-phase (i.e., particle fraction). Because some organic compounds, like tartaric acid, retain water even at RH = 5% [49], a correction was made to the original sigmoidal curve to account for the effect of residual water on particle density, as detailed in Ortiz-Montalvo et al.[10]. The effective liquid vapor pressure ($p'_{L,eff.}$) and enthalpy of vaporization ($\Delta H_{vap,eff.}$) of the mimics (mix of MGly precursors and products) were estimated from the corrected sigmoidal curves. Malonic acid standard solutions (6 dilutions between 0 and 3000 µM C from 0.999 %, Sigma-Aldrich) were treated as mimic solutions to provide an accuracy check. The estimated $p'_{L,eff.}$ for malonic acid (1±1 x 10^{-7} atm) is of the same order of magnitude as the calculated theoretical value (2±2 x 10^{-7} atm, SIMPOL group contribution method)[47]. The estimated $\Delta H_{vap,eff.}$ (72 ± 2 kJ/mol) differed from the theoretical value by 4% (69.12 ± 1.79 kJ/mol, Joback and Reid group contribution method)[48]. An uncertainty of ~17% is introduced because of differences between the refractive index of malonic acid (1.479) and polystyrene latex particles (1.59; used for OPC manufacturer-supplied calibration).

Droplet evaporation experiments were also run with the following 1 mM standards: oxalic acid, oxalic acid + ammonium hydroxide, ammonium oxalate (99.0%; Fluka Analytical), pyruvic acid, pyruvic acid + ammonium hydroxide, and

sodium pyruvate (100 mM; Thermo Scientific) (Figure 4-1). Note that ammonium pyruvate is not sold commercially. Ammonium hydroxide, when added, was added to reach pH 7. The ratio of the residual PM volume to *OM mass*$_{(droplet)}$ (*PM vol. / OM mass*$_{(droplet)}$) for oxalic acid + ammonium hydroxide was identical to that of ammonium oxalate, verifying that the addition of ammonium hydroxide effectively neutralized organic acids (Figure 4-1). Note that *PM vol. / OM mass*$_{(droplet)}$ is proportional to the fraction remaining in the particle-phase and increases with decreasing vapor pressure. In addition, it was observed that the neutralization of oxalic acid (ammonium oxalate production) had a higher *PM vol. / OM mass*$_{(droplet)}$ than pyruvic acid neutralization.

4.3.4 Aerosol-CIMS Analysis

Bulk mimic solutions were also analyzed by Chemical Ionization Mass Spectrometry (Aerosol-CIMS)[50,51]. Bulk mimic solutions were aerosolized with N_2 using a constant output atomizer (TSI 3076; operated at 2.5 L/min). Generated droplets passed through a diffusion dryer and were combined with a dry N_2 dilution flow (3.5 – 9.5 L/min) to keep the RH below ~12%. The flow then entered a volatilization region (23 cm long, 1.08 cm ID stainless steel tube wrapped in heating tape) where the aerosols were introduced to temperatures ranging between room temperature (25ºC) and 116ºC in order to volatilize the organics for gas-phase detection. The residence time from atomization to volatilization was about 6 seconds. Directly after the volatilization region, a portion of the flow (1.8 L/min, maintained by a critical orifice) entered the chemical ionization region of the mass spectrometer. Another portion (0.3 L/min) was characterized using a scanning mobility particle sizer (TSI). Remaining flow was exhausted. The generated aerosol had a lognormal number size distribution with a geometric mean particle diameter of 29±3 nm and

geometric standard deviation of 1.3. CIMS measurements were made in negative detection mode using I^- reagent ions, generated by flowing 2.5 L/min N_2 over a permeation tube of CH_3I held at 52°C and sending it through a ^{210}Po ionizer (NRD) into the chemical ionization region of the Aerosol-CIMS.

Volatilization studies were conducted by tracing the mass-to-charge ratios (*m/z*) of the detectable organics and evaluating how the signal responded to changes in temperature (i.e., 25 – 116ºC). A full mass spectrum was first performed on each mimic sample in order to determine which species were detectable in the gas-phase in negative detection mode. Oxalic acid and MGly both appear at *m/z* 217 as $I^-\cdot C_2H_2O_4$ and $I^-\cdot C_3H_4O_2\cdot H_2O$, respectively. Pyruvic acid appears at *m/z* 215 as $I^-\cdot C_3H_4O_3$. Acetic acid was detected at *m/z* 187 as $I^-\cdot C_2H_4O_2$; however, no analysis of acetic acid was performed because initial evaluations showed a constant signal over the range of temperature tested, suggesting it was present entirely in the gas-phase at 25ºC. The Clausius-Clapeyron relation was used to calculate the effective enthalpy of vaporization, $\Delta H_{vap,eff.}$ (kJ/mol) for each individual species present in the mixture. This was done by plotting $ln(S/S_i)$ versus $1/T$, where S/S_i is the ratio of the Aerosol-CIMS signal at a given temperature (T, in Kelvin) to the initial (i) signal at room temperature. The background signal present before atomizing the sample solution was subtracted from S and from S_i. Since S/S_i is equivalent to the ratio of partial pressures p/p_i of the organic compound being traced, the slope of the linear regression of $ln(S/S_i)$ on $1/T$ is equal to $-\Delta H/R$, where R is the ideal gas law constant.

Each mimic solution was analyzed at least twice. A solution of 1 mM oxalic acid standard (from 0.05 M; Fluka Analytical) was also analyzed (only once); its measured $\Delta H_{vap,eff.}$ (69 ± 33 kJ/mol) was within ~5% of the theoretical value (72.57

kJ/mol)[52]. An example of how $\Delta H_{vap,eff.}$ was obtained from the Aerosol-CIMS data is presented in the supplemental information (Appendix E).

4.4 Results

4.4.1 Modeled Droplet Composition

Precursor and product concentration dynamics as well as the composition of mimics at 10 and 30 minutes are shown in Figure 4-2. Note that typical times for one cloud cycle range between 10 – 30 minutes[44,53]. Among the four mimics, the 30 min Batch and 10 min CSTR mimic samples were the most different. Therefore, we selected these for droplet evaporation experiments, in order to bound the range of vapor pressures and enthalpies of vaporization of the precursor/product mixtures formed after one cloud processing cycle of MGly in the presence of $^{\bullet}$OH. (Note, an air mass encountering cloudy conditions typically undergoes multiple (~10) cloud cycles of 10-30 min duration over the course of a day.) The continuous accumulation of pyruvic acid (pink line) observed in the CSTR model is due to the continuous dissolution of gas-phase MGly in the CSTR model. Formaldehyde mainly forms from the reaction of $^{\bullet}$OH and acetic acid (a major product of MGly + $^{\bullet}$OH)[11,45].

4.4.2 VOAG – Vapor Pressure and Enthalpy of Vaporization

The $p'_{L,eff.}$ and $\Delta H_{vap,eff.}$ of CSTR and Batch mimics were comparable: 3-6 x 10^{-7} atm and 67-69 kJ/mol, respectively (Table 4-1, Figure 4-3, Appendix C2). The 30 min Batch mimic, which had a higher percentage of organic acids and less MGly, had a slightly lower but not significantly different $p'_{L,eff}$ than the 10 min CSTR mimic. Similarly, the reduction in $p'_{L,eff}$ accomplished by neutralization (pH 7) of the CSTR mimic was small (factor of two) and the difference was not significant.

Figure 4-3 shows the mass of residual particles (*PM mass*) and mass of organic matter in the droplet ($OM\ mass_{(droplet)}$) from droplet evaporation experiments

conducted with organic acid standards and mimics. The *PM mass* of organic acid standards (oxalic, succinic, glutaric, and tartaric acids) is well correlated with *OM mass*$_{(droplet)}$ (r^2 = 0.84–0.99) with the exception of acetic acid, which was quite volatile. Coefficients of determination (r^2) of *PM mass* on *OM mass*$_{(droplet)}$ for Batch 30 min (solid blue circles) and CSTR 10 min (at pH 3 and pH 7; solid black triangles and red squares, respectively) mimics were 69-93% (Table 4-1). The slopes (*PM mass / OM mass*$_{(droplet)}$) reflect the fraction of total droplet organic matter remaining in the particle-phase (e.g., particle fraction) and are reported in Table 4-1. The sample with the highest particle fraction was the neutralized (pH 7) 10 min CSTR mimic, which had a slope of 0.27. In contrast, the sample with the lowest particle fraction (slope = 0.10) was the 10 min pH 3 CSTR mimic. The 30 min Batch mimic fell in between with a slope of 0.17.

The sigmoidal curve in the inset of in Figure 4-3 is a fit to the *PM mass / OM mass*$_{(droplet)}$ versus log p°_{L} for the organic acid standards, uncorrected (dashed) and corrected (solid) for the upper bound influence of retained water on density. Also shown in the inset are the corresponding *PM mass / OM mass*$_{(droplet)}$ values for the Batch (inset middle blue dashed arrow) and CSTR samples (inset upper red arrow for pH 7; lower green dashed arrow for pH 3), pointing to their estimated effective liquid vapor pressures ($p'_{L,eff}$). The $p'_{L,eff}$ values, taken from the sigmoidal regression, are reported in Table 4-1. Overall, the volatilities of the three mimics were within a factor of two, with the largest difference found between the 10 min CSTR mimic at pH 7 (3E-7) and pH 3 (6E-7). A decrease in volatility is consistent with lower reported vapor pressures of organic acid salts compared to their corresponding acids.

Values of $\Delta H_{vap,eff.}$ for Batch and CSTR mimics (Table 4-1) were estimated using a similar approach (Appendix C2). $\Delta H_{vap,eff}$ estimates (~68 kJ/mol) for the mix

of MGly + $^{\bullet}$OH precursors and products (mimics) fall within the range of the ΔH_{vap} values of the pure individual components that comprised the CSTR and Batch samples (23–73 kJ/mol)[52]. No significant difference was observed between ΔH_{vap} estimates for the different mimics. The factor of two decrease in $p'_{L,eff}$ between the pH 3 and pH 7 CSTR mimics was accompanied by a (non-significant) increase of only 2 kJ/mol in the $\Delta H_{vap,eff}$. Also shown in Table 4-1 are theoretical molar-weighted enthalpies of vaporization for comparison. A difference of ~40-50% is observed between theoretical and effective ΔH_{vap}. Possible reasons are discussed in section 4.5.

This work suggests that the MGly + $^{\bullet}$OH precursor/product mix created after processing through one cloud cycle (10-30 min) has a $p'_{L,eff}$ and $\Delta H_{vap,eff.}$ of (4±7) x 10^{-7} atm and 68±3 kJ/mol, respectively. Note that longer in-cloud reaction times (i.e., multiple cloud cycles) will push the product mix toward oxalate, which if present as a salt would lower the volatility of the mixture (see ammonium oxalate slopes, Figure 4-1). To our knowledge, this is the first study to provide estimates of vapor pressure and enthalpy of vaporization of cloud SOA formed from MGly + $^{\bullet}$OH and droplet evaporation.

4.4.3 Aerosol-CIMS – Enthalpy of Vaporization of Methylglyoxal Mimics

The estimated $\Delta H_{vap,eff.}$ of selected individual organic species contained in aerosol created by atomizing and drying the CSTR and Batch mimic mixtures were provided by Aerosol-CIMS (Table 4-2). While oligomers might have formed during the drying process, their evolution with temperature was not observed. Thus, the enthalpies provided here might not include all components of the aerosol mixture. ΔH_{vap} values for pyruvic acid (*m/z* 215) and oxalic acid + methylglyoxal (*m/z* 217) were both lower than the theoretical ΔH_{vap} values of the pure compounds. For example, the $\Delta H_{vap,eff}$ of pyruvic acid in the mixture was ~5–19 kJ/mol compared to

45.74 kJ/mol for pure pyruvic acid. The reduction in $\Delta H_{vap,eff}$ for a compound in a mixture compare to the ΔH_{vap} of the pure compound is consistent with previous findings (McNeill et al.[50] and Donahue et al.[54]; ozonolysis products of oleate and α-pinene, respectively). Changes in $\Delta H_{vap,eff}$ with pH are within the measurement uncertainty (Table 4-2). Aerosol-CIMS supporting data can be found in Appendix E; these results are discussed in further detail below.

4.5 Discussions and Conclusions

In this study, effective enthalpies of vaporization were measured for mimics of the MGly + $^{\bullet}$OH precursor/product mixtures present after one cycle (10-30 min) of cloud processing (68±3 kJ/mol; VOAG system) and for selected individual compounds in aerosols generated from the mixture (5-19 pyruvic acid, 31-34 MGly + oxalic acid; Aerosol-CIMS). The VOAG system also measured the effective sub-cooled liquid vapor pressures of the MGly + $^{\bullet}$OH precursor/product mixture (4±7 E-7 atm), which decreased by only a factor of two with neutralization from pH 3 to 7 (i.e., through addition of ammonium hydroxide).

The $\Delta H_{vap,eff.}$ of the MGly + $^{\bullet}$OH precursor/product mixture (VOAG system) was similar to that measured for glycolaldehyde + $^{\bullet}$OH precursor/product mix (~70 kJ/mol) using the same approach[10]. Both MGly and glycolaldehyde VOAG $\Delta H_{vap,eff.}$ results fell within the range of ΔH_{vap} values for the pure individual components in the mixtures. The observed difference (~40-50%) between theoretical (molar-weighted) and VOAG-estimated enthalpies could be due to (1) compounds formed during droplet evaporation (e.g., methylglyoxal oligomers) because they were not included in the theoretical calculation, and/or (2) retention of residual water in the measurements of the VOAG, which would result in larger measured diameters (thus PM volume and mass) and consequently larger $PM\ mass\ /\ OM\ mass_{(droplet)}$ ratios and higher VOAG

enthalpy estimates. Based on this assessment the values we report in Table 4-1 are likely to be upper-bound estimates. In contrast to the VOAG results for $\Delta H_{vap,eff.}$ of precursor/product mixtures, the (Aerosol-CIMS) $\Delta H_{vap,eff.}$ of individual compounds within the mimic aerosols were smaller than the $\Delta H_{vap,eff.}$ values of the pure compounds, in agreement with other Aerosol-CIMS measurements of the ΔH_{vap} of individual species within internally mixed aerosol particles.

The $\Delta H_{vap,eff.}$ values obtained by the VOAG method for the MGly + $^{\bullet}$OH mimic mixtures are much larger than those obtained for pyruvic acid and oxalic acid + MGly from the Aerosol-CIMS method. There are several possible reasons that $\Delta H_{vap,eff}$ values measured by Aerosol-CIMS and VOAG might differ. For one, VOAG experiments are conducted with the entire mimic solution (including volatile components), whereas the Aerosol-CIMS experiments are performed only on the portion of the mimic that remains in the aerosol phase. In the VOAG experiments *PM mass/OM mass*$_{(droplet)}$ values reflect the fraction of the *total* mimic organic matter that remains in the particle-phase. This quantity is compared to *PM mass / OM mass*$_{(droplet)}$ values for single standards of known $\Delta H_{vap,eff}$. So the results reflect the $\Delta H_{vap,eff}$ of the entire mimic mixture and any products formed during the evaporation process. For example, among the components of this mixture is MGly. A portion of MGly will evaporate and a portion is likely to oligomerize during droplet evaporation. In either case it will influence the $\Delta H_{vap,eff}$ of the mixture as measured in the VOAG. However, the $\Delta H_{vap,eff}$ values of MGly and MGly oligomers will only be measured in the Aerosol-CIMS if these species are in the aerosol phase at 25°C and volatilize below 116°C.

Effective vapor pressures of the CSTR and Batch methylglyoxal + OH precursor/product mimic mixtures are very similar to the $p'_{L,eff}$ (1-2 x 10^{-7} atm)

measured for the mixture produced from the photooxidation of (1 mM) glycolaldehyde with (~10^{-12} M) OH radicals in a batch reactor using the same VOAG system[10]. In the glycolaldehyde study, we argued that the $p'_{L,eff}$ would be orders of magnitude lower if the organic acids were neutralized (pH 7) since organic salts have much lower vapor pressures than the organic acids. We still believe that this is true for glycolaldehyde because oxalate is a major product, at least at 40 min, and the volatility of ammonium oxalate is 4 orders of magnitude lower than that of oxalic acid (Figure 4-1). Additionally, the fact that oxalate is found in the atmosphere predominantly in the particle-phase, despite the high vapor pressure of oxalic acid, suggests that a lower volatility form of oxalate is atmospherically dominant. Furthermore, in our glyoxal study we found that neutralization did affect the volatility of aqueous glyoxal + $^{\bullet}$OH mixture (Chapter 3). However, in the current MGly study, the addition of ammonia (from pH 3 to 7) to the CSTR 10 min sample (i.e. to form ammonium pyruvate) lowered the $p'_{L,eff.}$ by only a factor of 2 and not orders of magnitude as we expected. The degree of vapor pressure reduction is likely to depend on the properties of the organic salts being formed as seen in Figure 4-1. In Figure 4-1 values of PM volume/OM mass (from the VOAG System) and sub-cooled liquid vapor pressures are provided for pyruvic and oxalic acids and their ammonium and/or sodium salts. Clearly, salt formation reduces the vapor pressure of pyruvate, but not to the degree observed for oxalate. Nevertheless, atmospheric measurements have found that most pyruvate is in the particle-phase (e.g., 61%)[30]. These results and our previous findings[10] indicate that organic salt formation can play an important role in the properties and fate of SOA formed through cloud processing, but that it will depend on the gas-particle partitioning of the formed salts. There is a need to better

understand the predominant forms that these organic acids take in the atmosphere because of their effect on gas-particle partitioning of SOA.

Overall, our volatility assessment indicates that one cloud cycle of MGly + $^{\bullet}$OH produces a mix of lower and higher volatility products and that the overall mixture is of intermediate volatility (3 x 10^{-7} atm in the presence of ammonia). There are several ways in which the volatility of this material might decrease further. 1) Because of its high oxygen-to-carbon ratio (O:C ~ 0.8 – 1.1), we expect this material to re-dissolve and undergo additional cloud processing cycles. Based on our model results we expect oxalate to be the major product from MGly + $^{\bullet}$OH after 10 – 20 cloud cycles (Appendix C3). Note that ammonium oxalate has a vapor pressure of ~10^{-11} atm (Figure 4-1). Thus we expect a full day of cloud processing to lead to a substantial reduction in the volatility of the MGly + $^{\bullet}$OH precursor/product mix. 2) Aqueous chemistry can also continue in the wet aerosol that is present in the cloud outflow. At the much higher organic concentrations in wet aerosols, radical-radical reactions become more important and we expect to find the formation of low volatility oligomers[45]. 3) The predominant chemical form of the organic acid products of MGly + $^{\bullet}$OH (pyruvate, oxalate, acetate) in the atmosphere is not known. Binding with other cations (e.g. to form other salts) or transition metals could potentially reduce the volatility of this mix.

In conclusion, effective vapor pressure ($p'_{L,eff.}$) and enthalpy of vaporization ($\Delta H_{vap,eff.}$) values were estimated for the aqueous photooxidation products of methylglyoxal with OH radicals (as modeled at cloud relevant conditions using two atmospheric scenarios) followed by droplet evaporation (MGly SOA_{Cld}). It is worth noting that the terms effective enthalpy of vaporization and effective vapor pressure used here are not exact thermodynamic properties like those of pure compounds as

they are meant to include potential uncertainties (e.g., measurements over a curved surface opposed to a flat surface) that result from the unconventional methods used in this study. The volatility assessment indicated that neutralization of MGly + $^{\bullet}$OH organic acid products with ammonia resulted in only a modest (not statistically significant) decrease in the effective vapor pressure, 3–6 x 10^{-7} atm and increase in the enthalpy of vaporization 67–69 kJ/mol. The volatility of MGly SOA_{Cld} was also comparable between the Batch (MGly depletion) and CSTR (MGly at steady-state) models, which is in agreement with our previous work where we found that the volatility estimates of glyoxal + $^{\bullet}$OH mimics were comparable in both assumptions (e.g.,CSTR and Batch) (Chapter 3). Our study shows that for one cloud cycle the MGly + $^{\bullet}$OH precursor/product mix (even neutralized) has an intermediate vapor pressure, meaning that a majority of this organic mixture will not remain in a dry particle after droplet evaporation. There are several ways that the fraction found in the particle-phase might be greater (volatility lower): (1) pyruvate (main product) could be present in a different chemical form, (2) chemical processing could take place for multiple cloud cycles to reach a maximum yield of oxalate, (3) chemical processing could continue in the wet aerosol formed after droplet evaporation forming low volatility oligomers, (4) water bound to the hygroscopic particle could enhance retention of the soluble, intermediate volatility products. An understanding of the gas-particle partitioning of atmospheric pyruvate is critical for addressing the apparent discrepancy between laboratory and ambient measurements, and for better understanding the importance of methylglyoxal as a SOA_{Cld} precursor.

4.6 References

(1) Blando, J. D.; Turpin, B. J. Secondary organic aerosol formation in cloud and fog droplets: a literature evaluation of plausibility. *Atmospheric Environment* **2000**, *34*, 1623–1632.

(2) Gelencsér, A.; Varga, Z. Evaluation of the atmospheric significance of multiphase reactions in atmospheric secondary organic aerosol formation. *Atmos. Chem. Phys.* **2005**, *5*, 2823–2831.

(3) Ervens, B.; Turpin, B. J.; Weber, R. J. Secondary organic aerosol formation in cloud droplets and aqueous particles (aqSOA): a review of laboratory, field and model studies. *Atmos. Chem. Phys.* **2011**, *11*, 11069–11102.

(4) Fraser, M. P.; Grosjean, D.; Grosjean, E.; Rasmussen, R. A.; Cass, G. R. Air quality model evaluation data for organics. 1. Bulk chemical composition and gas/particle distribution factors. *Environmental Science & Technology* **1996**, *30*, 1731–1743.

(5) Millet, D. B. Atmospheric volatile organic compound measurements during the Pittsburgh Air Quality Study: Results, interpretation, and quantification of primary and secondary contributions. *J. Geophys. Res.* **2005**, *110*, D07S07.

(6) Gong, W.; Stroud, C.; Zhang, L. Cloud Processing of Gases and Aerosols in Air Quality Modeling. *Atmosphere* **2011**, *2*, 567–616.

(7) Lee, A. K. Y.; Zhao, R.; Gao, S. S.; Abbatt, J. P. D. Aqueous-Phase OH Oxidation of Glyoxal: Application of a Novel Analytical Approach Employing Aerosol Mass Spectrometry and Complementary Off-Line Techniques. *J. Phys. Chem. A* **2011**, *115*, 10517–10526.

(8) Liu, Y.; Monod, A.; Tritscher, T.; Praplan, A. P.; DeCarlo, P. F.; Temime-Roussel, B.; Quivet, E.; Marchand, N.; Dommen, J.; Baltensperger, U. Aqueous phase processing of secondary organic aerosol from isoprene photooxidation. *Atmos. Chem. Phys.* **2012**, *12*, 5879–5895.

(9) Liu, Y.; Siekmann, F.; Renard, P.; Zein, El, A.; Salque, G.; El Haddad, I.; Temime-Roussel, B.; Voisin, D.; Thissen, R.; Monod, A. Oligomer and SOA formation through aqueous phase photooxidation of methacrolein and methyl vinyl ketone. *Atmospheric Environment* **2012**, *49*, 123–129.

(10) Ortiz-Montalvo, D. L.; Lim, Y. B.; Perri, M. J.; Seitzinger, S. P.; Turpin, B. J. Volatility and Yield of Glycolaldehyde SOA Formed through Aqueous Photochemistry and Droplet Evaporation. *Aerosol Science and Technology* **2012**, *46*, 1002–1014.

(11) Tan, Y.; Lim, Y. B.; Altieri, K. E.; Seitzinger, S. P.; Turpin, B. J. Mechanisms leading to oligomers and SOA through aqueous photooxidation: insights from OH radical oxidation of acetic acid and methylglyoxal. *Atmos. Chem. Phys.* **2012**, *12*, 801–813.

(12) Zhao, R.; Lee, A. K. Y.; Abbatt, J. P. D. Investigation of Aqueous-Phase Photooxidation of Glyoxal and Methylglyoxal by Aerosol Chemical Ionization Mass Spectrometry: Observation of Hydroxyhydroperoxide Formation. *J. Phys. Chem. A*

2012, *116*, 6253–6263.

(13) De Haan, D. O.; Hawkins, L. N.; Kononenko, J. A.; Turley, J. J.; Corrigan, A. L.; Tolbert, M. A.; Jimenez, J. L. Formation of Nitrogen-Containing Oligomers by Methylglyoxal and Amines in Simulated Evaporating Cloud Droplets. *Environmental Science & Technology* **2011**, *45*, 984–991.

(14) Schwier, A. N.; Sareen, N.; Mitroo, D.; Shapiro, E. L.; McNeill, V. F. Glyoxal-Methylglyoxal Cross-Reactions in Secondary Organic Aerosol Formation. *Environmental Science & Technology* **2010**, *44*, 6174–6182.

(15) Bateman, A. P.; Nizkorodov, S. A.; Laskin, J.; Laskin, A. Photolytic processing of secondary organic aerosols dissolved in cloud droplets. *Phys. Chem. Chem. Phys.* **2011**, *13*, 12199–12212.

(16) Lee, A. K. Y.; Herckes, P.; Leaitch, W. R.; Macdonald, A. M.; Abbatt, J. P. D. Aqueous OH oxidation of ambient organic aerosol and cloud water organics: Formation of highly oxidized products. *Geophys. Res. Lett.* **2011**, *38*, L11805.

(17) Lee, A. K. Y.; Hayden, K. L.; Herckes, P.; Leaitch, W. R.; Liggio, J.; Macdonald, A. M.; Abbatt, J. P. D. Characterization of aerosol and cloud water at a mountain site during WACS 2010: secondary organic aerosol formation through oxidative cloud processing. *Atmos. Chem. Phys.* **2012**, *12*, 7103–7116.

(18) Nguyen, T. B.; Lee, P. B.; Updyke, K. M.; Bones, D. L.; Laskin, J.; Laskin, A.; Nizkorodov, S. A. Formation of nitrogen- and sulfur-containing light-absorbing compounds accelerated by evaporation of water from secondary organic aerosols. *J. Geophys. Res.* **2012**, *117*, D01207.

(19) Loeffler, K. W.; Koehler, C. A.; Paul, N. M.; De Haan, D. O. Oligomer Formation in Evaporating Aqueous Glyoxal and Methyl Glyoxal Solutions. *Environmental Science & Technology* **2006**, *40*, 6318–6323.

(20) De Haan, D. O.; Corrigan, A. L.; Tolbert, M. A.; Jimenez, J. L.; Wood, S. E.; Turley, J. J. Secondary Organic Aerosol Formation by Self-Reactions of Methylglyoxal and Glyoxal in Evaporating Droplets. *Environmental Science & Technology* **2009**, *43*, 8184–8190.

(21) Grosjean, D.; Williams, E. L.; Grosjean, E. Atmospheric chemistry of isoprene and of its carbonyl products - Environmental Science & Technology (ACS Publications). *Environmental Science & Technology* **1993**, *27*, 830–840.

(22) Atkinson, R.; Arey, J. Atmospheric Degradation of Volatile Organic Compounds. *Chem. Rev.* **2003**, *103*, 4605–4638.

(23) Tuazon, E. C.; Atkinson, R.; Mac Leod, H.; Biermann, H. W.; Winer, A. M.; Carter, W. P. L.; Pitts, J. N., Jr Yields of glyoxal and methylglyoxal from the nitrogen oxide (NOx)-air photooxidations of toluene and m-and p-xylene. *Environmental*

Science & Technology **1984**, *18*, 981–984.

(24) Smith, D. F.; Kleindienst, T. E.; McIver, C. D. Journal of Atmospheric Chemistry, Volume 34, Number 3 - SpringerLink. *J Atmos Chem* **1999**, *34*, 339–364.

(25) Nishino, N.; Arey, J.; Atkinson, R. Formation Yields of Glyoxal and Methylglyoxal from the Gas-Phase OH Radical-Initiated Reactions of Toluene, Xylenes, and Trimethylbenzenes as a Function of NO 2Concentration. *J. Phys. Chem. A* **2010**, *114*, 10140–10147.

(26) Hays, M. D.; Geron, C. D.; Linna, K. J.; Smith, N. D.; Schauer, J. J. Speciation of Gas-Phase and Fine Particle Emissions from Burning of Foliar Fuels. *Environmental Science & Technology* **2002**, *36*, 2281–2295.

(27) Hays, M. D.; Beck, L.; Barfield, P.; Willis, R. D.; Landis, M. S.; Stevens, R. K.; Preston, W.; Dong, Y. Physical and Chemical Characterization of Residual Oil-Fired Power Plant Emissions. *Energy Fuels* **2009**, *23*, 2544–2551.

(28) Betterton, E. A.; Hoffmann, M. R. Henry's law constants of some environmentally important aldehydes. *Environmental Science & Technology* **1988**, *22*, 1415–1418.

(29) Munger, J. W.; Jacob, D.; Daube, B.; Horowitz, L.; Keene, W.; Heikes, B. Formaldehyde, glyoxal, and methylglyoxal in air and cloudwater at a rural mountain site in central Virginia. *J. Geophys. Res.* **1995**, *100*, 9325–9325.

(30) Limbeck, A.; Puxbaum, H.; Otter, L.; Scholes, M. C. Semivolatile behavior of dicarboxylic acids and other polar organic species at a rural background site (Nylsvley, RSA). *Atmospheric Environment* **2001**, *35*, 1853–1862.

(31) Altieri, K. E.; Seitzinger, S. P.; Carlton, A. G.; Turpin, B. J.; Klein, G. C.; Marshall, A. G. Oligomers formed through in-cloud methylglyoxal reactions: Chemical composition, properties, and mechanisms investigated by ultra-high resolution FT-ICR mass spectrometry. *Atmospheric Environment* **2008**, *42*, 1476–1490.

(32) Tan, Y.; Carlton, A. G.; Seitzinger, S. P.; Turpin, B. J. SOA from methylglyoxal in clouds and wet aerosols: Measurement and prediction of key products. *Atmospheric Environment* **2010**, *44*, 5218–5226.

(33) Zhao, R.; Lee, A. K. Y.; Abbatt, J. P. D. Investigation of Aqueous-Phase Photooxidation of Glyoxal and Methylglyoxal by Aerosol Chemical Ionization Mass Spectrometry: Observation of Hydroxyhydroperoxide Formation. *J. Phys. Chem. A* **2012**, 120302141348000.

(34) Chen, J.; Griffin, R. J.; Grini, A.; Tulet, P. Modeling secondary organic aerosol formation through cloud processing of organic compounds. *Atmos. Chem. Phys.* **2007**, *7*, 5343–5355.

(35) Carlton, A. G.; Turpin, B. J.; Altieri, K. E.; Seitzinger, S. P.; Mathur, R.; Roselle, S. J.; Weber, R. J. CMAQ Model Performance Enhanced When In-Cloud Secondary Organic Aerosol is Included: Comparisons of Organic Carbon Predictions with Measurements. *Environmental Science & Technology* **2008**, *42*, 8798–8802.

(36) Fu, T.-M.; Jacob, D. J.; Wittrock, F.; Burrows, J. P.; Vrekoussis, M.; Henze, D. K. Global budgets of atmospheric glyoxal and methylglyoxal, and implications for formation of secondary organic aerosols. *J. Geophys. Res.* **2008**, *113*, D15303.

(37) Fu, T.-M.; Jacob, D. J.; Heald, C. L. Aqueous-phase reactive uptake of dicarbonyls as a source of organic aerosol over eastern North America. *Atmospheric Environment* **2009**, *43*, 1814–1822.

(38) Lin, G.; Penner, J. E.; Sillman, S.; Taraborrelli, D.; Lelieveld, J. Global modeling of SOA formation from dicarbonyls, epoxides, organic nitrates and peroxides. *Atmos. Chem. Phys.* **2012**, *12*, 4743–4774.

(39) Liu, J.; Horowitz, L. W.; Fan, S.; Carlton, A. G.; Levy, H., II Global in-cloud production of secondary organic aerosols: Implementation of a detailed chemical mechanism in the GFDL atmospheric model AM3. *J. Geophys. Res.* **2012**, *117*, D15303.

(40) Tsigaridis, K.; Kanakidou, M. Global modelling of secondary organic aerosol in the troposphere: A sensitivity analysis. *Atmos. Chem. Phys.* **2003**, *3*, 1849–1869.

(41) El Haddad, I.; Liu, Y.; Nieto-Gligorovski, L.; Michaud, V.; Temime-Roussel, B.; Quivet, E.; Marchand, N.; Sellegri, K.; Monod, A. In-cloud processes of methacrolein under simulated conditions – Part 2: Formation of secondary organic aerosol. *Atmos. Chem. Phys.* **2009**, *9*, 5107–5117.

(42) Liu, Y.; El Haddad, I.; Scarfogliero, M.; Nieto-Gligorovski, L.; Temime-Roussel, B.; Quivet, E.; Marchand, N.; Picquet-Varrault, B.; Monod, A. In-cloud processes of methacrolein under simulated conditions–Part 1: Aqueous phase photooxidation. *Atmos. Chem. Phys.* **2009**, *9*, 5093–5105.

(43) Michaud, V.; El Haddad, I.; Liu, Y.; Sellegri, K.; Laj, P.; Villani, P.; Picard, D.; Marchand, N.; Monod, A. In-cloud processes of methacrolein under simulated conditions–Part 3: Hygroscopic and volatility properties of the formed secondary organic aerosol. *Atmos. Chem. Phys.* **2009**, *9*, 5119–5130.

(44) Ervens, B.; Volkamer, R. Glyoxal processing by aerosol multiphase chemistry: towards a kinetic modeling framework of secondary organic aerosol formation in aqueous particles. *Atmos. Chem. Phys.* **2010**, *10*, 8219–8244.

(45) Lim, Y. B.; Tan, Y.; Turpin, B. J. Chemical insights, explicit chemistry and yields of secondary organic aerosol from methylglyoxal and glyoxal. *Atmos. Chem. Phys. Discuss.* **2013**, *13*, 4687–4725.

(46) Berglund, R. N.; Liu, B. Y. H. Generation of monodisperse aerosol standards. *Environmental Science & Technology* **1973**, *7*, 147–153.

(47) Pankow, J.; Asher, W. SIMPOL. 1: a simple group contribution method for predicting vapor pressures and enthalpies of vaporization of multifunctional organic compounds. *Atmos. Chem. Phys.* **2008**, *8*, 2773–2796.

(48) Joback, K. G.; Reid, R. C. Estimation of Pure-Component Properties from Group-Contributions. *Chem. Eng. Comm.* **1987**, *57*, 233–243.

(49) Peng, C.; Chan, M. N.; Chan, C. K. The Hygroscopic Properties of Dicarboxylic and Multifunctional Acids: Measurements and UNIFAC Predictions. *Environmental Science & Technology* **2001**, *35*, 4495–4501.

(50) McNeill, V. F.; Wolfe, G. M.; Thornton, J. A. The Oxidation of Oleate in Submicron Aqueous Salt Aerosols: Evidence of a Surface Process. *J. Phys. Chem. A* **2007**, *111*, 1073–1083.

(51) Sareen, N.; Schwier, A.; Shapiro, E.; Mitroo, D.; McNeill, V. Secondary organic material formed by methylglyoxal in aqueous aerosol mimics. *Atmos. Chem. Phys.* **2010**, *10*, 997–1016.

(52) Yaws, C. L. Yaws' Handbook of Thermodynamic and Physical Properties of Chemical Compounds. 2003. *Knovel Online version from http://wwwknovelcom*.

(53) Desboeufs, K.; Losno, R.; Colin, J. Relationship between droplet pH and aerosol dissolution kinetics: Effect of incorporated aerosol particles on droplet pH during cloud processing. *J Atmos Chem* **2003**, *46*, 159–172.

(54) Donahue, N. M.; Huff Hartz, K. E.; Chuong, B.; Presto, A. A.; Stanier, C. O.; Rosenhørn, T.; Robinson, A. L.; Pandis, S. N. Critical factors determining the variation in SOA yields from terpene ozonolysis: A combined experimental and computational study. *Faraday Discuss.* **2005**, *130*, 295–309.

(55) Chickos, J. S.; Zhao, H. Measurement of the Vaporization Enthalpy of Complex Mixtures by Correlation-Gas Chromatography. The Vaporization Enthalpy of RP-1, JP-7, and JP-8 Rocket and Jet Fuels at T= 298.15 K. *Energy Fuels* **2005**, *19*, 2064–2073.

(56) Turpin, B. J.; Lim, H.-J. Species Contributions to PM2.5 Mass Concentrations: Revisiting Common Assumptions for Estimating Organic Mass. *Aerosol Science and Technology* **2001**, *35*, 602–610.

(57) Hilal, S. H.; Karickhoff, S. W.; Carreira, L. A. Prediction of the Vapor Pressure Boiling Point, Heat of Vaporization and Diffusion Coefficient of Organic Compounds. *QSAR Comb. Sci.* **2003**, *22*, 565–574.

(58) U.S. EPA. *Estimation Programs Interface Suite™* for Microsoft® Windows,

v 4.00; United States Environmental Protection Agency (U.S. EPA), Washington, DC, **2010**.

Table 4-1. VOAG results for MGly + $^{\bullet}$OH precursor/product mixtures: slope ($PM\ mass\ /\ OM\ mass_{(droplet)}$) with coefficients of determination (r^2) and standard error, effective liquid vapor pressures ($p'_{L,eff.}$), and effective enthalpies of vaporization ($\Delta H_{vap,eff.}$).

Mimic Sample	pH	Density (g/mL)	Slope [a] $\left[\frac{PM\ mass}{OM\ mass_{(droplet)}}\right]$	Standard Error	r^2	$p'_{L,eff.}$ [b] (atm)	$\Delta H_{vap,eff.}$ [c] (kJ/mol)	Theoretical $\Delta H_{vap,mix}$ [d] (kJ/mol)
Batch 30 min	3	1.2[e]	0.17	0.04	69%	(4±4) x 10^{-7}	68 ± 2	44
CSTR 10 min	3	1.1[e]	0.10	0.02	74%	(6±6) x 10^{-7}	67 ± 2	42
	7	1.1[f]	0.27	0.05	93%	(3±2) x 10^{-7}	69 ± 2	42

[a] Slopes (in units of g/g) from Figure 4-3 corrected by the effect of retained water (33% upper-bound estimate) on the density used to calculate *PM mass*. Slopes for organic acid standards are provided in Ortiz-Montalvo et al.[10]. [b] Effective liquid vapor pressure estimates (at 298.15 K) using a sigmoidal regression provided in Ortiz-Montalvo et al.[10], which was confined by estimates of vapor pressure of pure compounds using SIMPOL group contribution method[47] ± error propagation (incorporates uncertainty in Pankow and Asher[47] estimates, standard error of slope, and standard error in the coefficients of the sigmoidal regression). [c] Effective enthalpy of vaporization estimates (at normal boiling point) using a sigmoidal regression provided in Ortiz-Montalvo et al.[10], which was defined by estimates of enthalpy of vaporization of pure compounds at normal boiling point[48] ± error propagation (incorporates uncertainty in Joback and Reid[48], standard error of slope, and standard error in the coefficients of the sigmoidal regression). [d] Molar weighted theoretical enthalpies of vaporization of product mixtures calculated following Chickos et al.[55] approach, as $\Delta H_{vap,mix} = \sum_i n_i \times \Delta H_{vap,i}$ where n_i is the molar fraction of species *i* (from Figure 4-2) and $\Delta H_{vap,i}$ is the theoretical enthalpy of vaporization of species *i* (reported in Table 4-2). [e] Concentration-weighted density[56] ± 0.1 (error propagation accounting for the uncertainty in the concentrations). [f] Assumed the same density as for CSTR 10 min pH 3. Sensitivity analysis showed that with varying density (from 0.8 to 1.5 g/mL), the enthalpy of vaporization and vapor pressure were essentially unchanged (68–69 kJ/mol and (3–2) x 10^{-7} atm, respectively).

Table 4-2. Effective enthalpies of vaporization ($\Delta H_{vap,\ eff.}$) for individual products of MGly + $^{\bullet}$OH, calculated from the Clausius-Clapeyron analysis of Aerosol-CIMS data.

		$\Delta H_{vap,\ eff.}$ [a] (kJ/mol)		
Organic Species	**Theoretical ΔH_{vap} (kJ/mol)**	**Batch 30 min**	**CSTR 10 min**	
		pH 3.8	**pH 3.7**	**pH 4.6**
Pyruvic acid (*m/z 215*)	45.74[b]	$6^{\pm 2}$	$19^{\pm 9}$	$5^{\pm 3}$
Oxalic acid / Methylglyoxal (*m/z 217*)	72.57[b] / 38[c]	$34^{\pm 2}$	$31^{\pm 5}$	$32^{\pm 3}$

a – effective enthalpy of vaporization at 25-116ºC; average values weighted by the standard deviations (n=2) ± one standard deviation (in superscript).

b – theoretical enthalpy of vaporization taken from Yaws' Handbook of Thermodynamic and Physical Properties[52].

c – theoretical enthalpy of vaporization taken from SPARC online calculator[57].

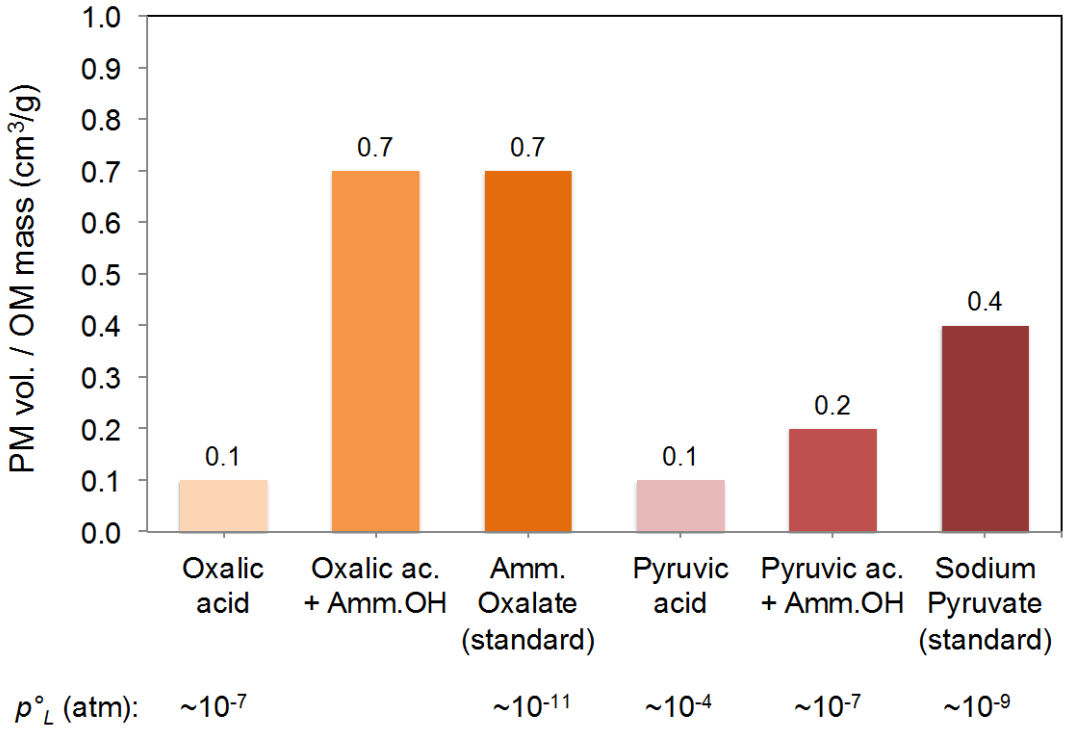

Figure 4-1. Ratios of residual PM volume to *OM mass*$_{(droplet)}$ (*PM vol. / OM mass*$_{(droplet)}$) obtained in the VOAG system. Acquired from 1 mM standard solutions of oxalic acid, ammonium oxalate, pyruvic acid, and sodium pyruvate, as well as solutions prepared by mixing 1 mM oxalic acid + ammonium hydroxide (Amm. OH) and 1 mM pyruvic acid + ammonium hydroxide (pH ≈ 7) to form ammonium oxalate (Amm. Oxalate) and ammonium pyruvate, respectively. Liquid vapor pressure ($p°_L$) estimates for the acids were obtained from SIMPOL group contribution method[47] and for the organic salts (sub-cooled $p°_L$) using EPA-EPI Suite™ Software[58].

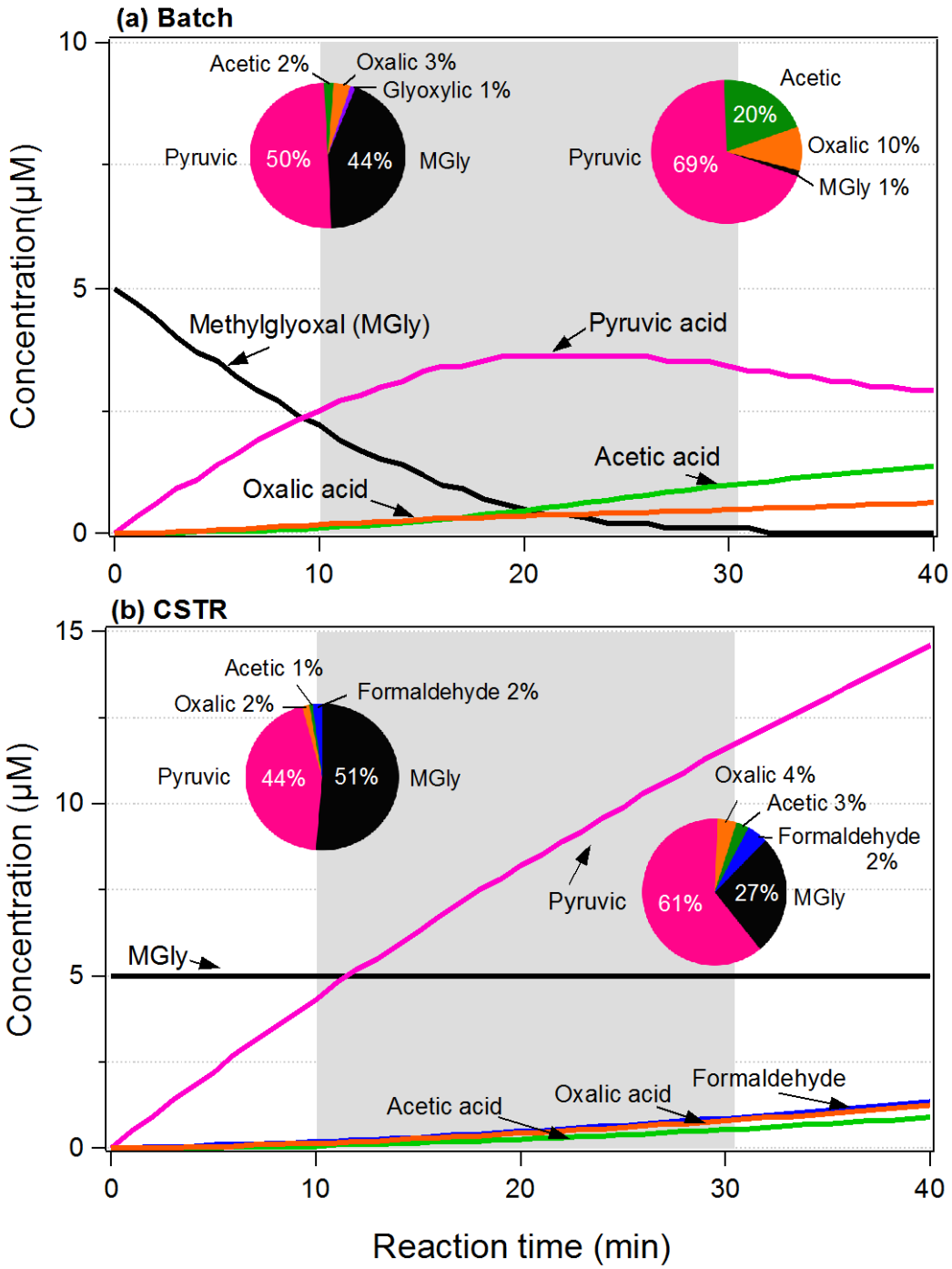

Figure 4-2. (a) Batch and (b) Continuously Stirred-Tank Reactor (CSTR) model results for the aqueous photooxidation of 5 μM methylglyoxal (MGly) with 10^{-12} M OH radicals. Methylglyoxal (black), pyruvic acid (pink), acetic acid (green), oxalic acid (orange), and formaldehyde (blue). Pie charts provide the droplet composition (molar fraction %) for specific reaction times (10 and 30 min). Background shading highlights the cloud droplet lifetimes of 10–30 min[44,53].

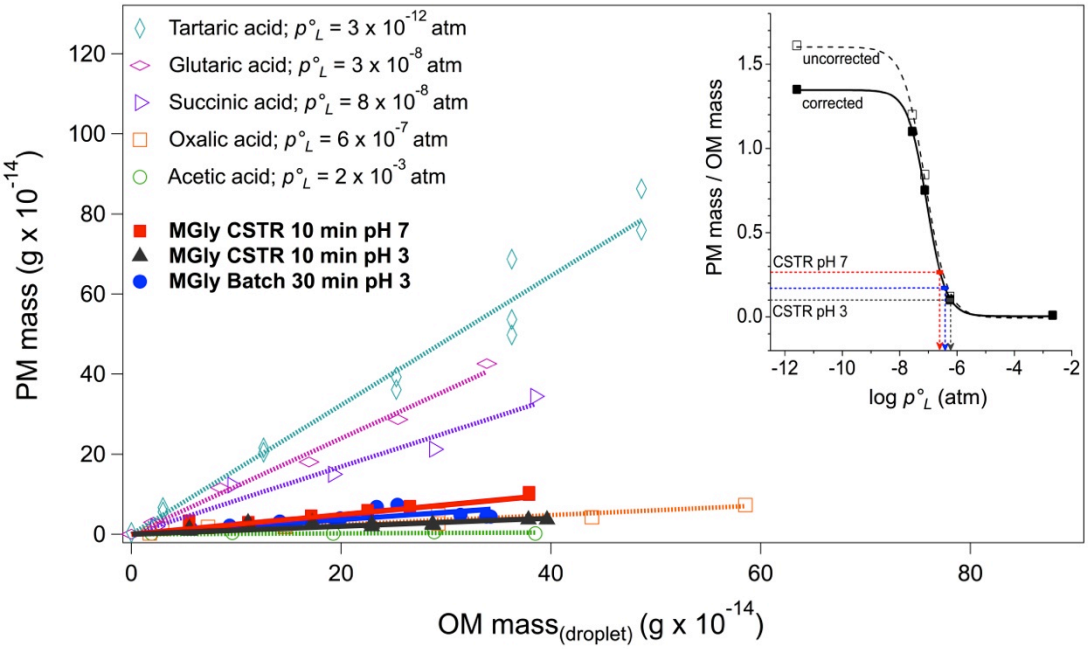

Figure 4-3. Residual particle mass (*PM mass*) and *OM mass*$_{(droplet)}$ formed from VOAG droplet evaporation experiments. *OM mass*$_{(droplet)}$ is the mass of organic matter in the initial droplet before evaporation. Shown are organic acid standard solutions (dashed light-colored lines): acetic, oxalic, succinic, glutaric, and tartaric acid, as well as mimic sample solutions (solid dark-colored lines): Batch 30 min pH 3, CSTR 10 min pH 3, and CSTR 10 min pH 7. Mimic samples and standards were analyzed at RH = (12 ± 3)% and t = (24.1 ± 0.4)ºC. Inset illustrates the sigmoidal regression of *PM mass / OM mass* vs. *log* p^{o}_{L} of standards (black squares with solid line) and illustrates how the $p'_{L,eff.}$ of mimic samples is determined from the measured *PM mass / OM mass*$_{(droplet)}$: CSTR 10 min mimic pH 7 (inset red dashed line), Batch 30 min pH 3 (inset blue dashed line), and CSTR 10 min pH 3 (inset dark grey dashed line). (Table 4-1 provides estimated effective vapor pressures and enthalpies of vaporization).

Chapter 5. Summary, Implications and Future Directions

5.1 Summary and Recent Advancements

Aerosol particles contribute to air pollution and climate change[1]. SOA represents a substantial fraction of the tropospheric aerosol[2-6]. Still, its formation mechanisms and properties are not well understood[7,8]. There is growing evidence suggesting that SOA can form through reactions in atmospheric waters (i.e., clouds, fogs, and aerosol water)[9]. Although some aqueous chemistry involved in SOA formation through cloud processing (SOA_{Cld}) has now been incorporated into a few air quality models[10], it is yet unknown to what extent the newly formed organic material remains in the particle-phase after droplet evaporation. Measurements of SOA_{Cld} mass yields and volatility (e.g., vapor pressure, enthalpy of vaporization) are needed for accurate prediction of SOA in global and regional air quality models. Discoveries in this dissertation lead to an improved understanding of SOA formation through cloud water chemistry and droplet evaporation (i.e., SOA_{Cld}). Although the formation of carboxylic acids and oligomers formed from aqueous OH radical oxidation of glycolaldehyde, methylglyoxal, and glyoxal was previously demonstrated at cloud relevant conditions, this dissertation describes the first studies to simulate cloud droplet evaporation and estimate the volatility of these mixtures. This dissertation confirms that carboxylic acids (i.e., glycolic, pyruvic, oxalic acids) are the major oxidation products at cloud relevant glyoxal, glycolaldehyde and methylglyoxal concentrations; in the presence of dissolved ammonia these acids are neutralized to form organic salts and their retention in the particle-phase increases, in the case of oxalate the increase is substantial. The effective vapor pressure, enthalpy of vaporization, and mass yields of the aqueous precursor/product mixtures were determined

for glyoxal, glycolaldehyde and methylglyoxal plus OH radicals. These measurements can be used to validate and refine the treatment of SOA_{Cld} formation in climate models and regional air quality models.

Aqueous-phase photooxidation followed by droplet evaporation leads to formation of particles. This, and a small number of other concurrent studies, have now demonstrated that particulate matter forms through aqueous-phase reactions followed by droplet evaporation[11-14]. This dissertation (Chapter 2 and 4; Ortiz-Montalvo et al.[14]) is the first to demonstrate SOA_{Cld} formation from the aqueous photooxidation of glycolaldehyde or methylglyoxal with OH radicals followed by droplet evaporation. Lee et al.[12] and the work herein (Chapters 3) demonstrate that glyoxal forms particulate matter via aqueous OH radical oxidation and droplet evaporation. El Haddad et al.[11] were the first to show that methacrolein forms particulate matter through aqueous photooxidation and droplet evaporation. Recent work by Liu et al.[13] used the approach by El Haddad et al.[11] to show that methyl vinyl ketone (and methacrolein) also forms particulate matter through these processes.

To my knowledge, El Haddad et al.[11] were the first to combine aqueous photooxidation reactions with droplet evaporation. They reacted (2 – 5 mM) methacrolein with OH radicals (from photolysis of 0.4 M H_2O_2), then nebulized the sample solutions and dried the droplets in a mixing chamber. [Experiments were performed at 25°C and normal pH (unbuffured solutions), the averaged residence time of the aerosol in the whole setup was 20 min, and the RH in the mixing chamber was 20-30%]. Their SOA_{aq} mass yields from methacrolein ranged from 2 to 12% for reaction times of 5 to 22 hours, respectively (i.e., yields were calculated as the ratio between SOA_{aq} formed, in milligram

per liter of evaporated water, and the consumed methacrolein, in milligram per liter of evaporated water). A recent study[13] from the same group evaluated the aqueous-phase (~10^{-13} M) OH radical oxidation of methyl vinyl ketone (4 – 20 mM) followed by droplet evaporation under the same conditions as El Haddad et al[11]. The SOA_{aq} mass yields from methyl vinyl ketone (for 4 mM initial concentration) ranged from 4 to 10% for reaction times between 5 and 20 hours, respectively (i.e. yields calculated the same way as in El Haddad et al[11]). A limitation of both studies[11,13] was that droplet evaporation was conducted on samples that had undergone ≥5 hours of OH radical oxidation. In contrast, cloud droplet lifetimes are on the order of several minutes[15,16]. Normally, an air mass might undergo several (~10) cloud cycles in a day. Another limitation was the need for a substantial correction due to losses in the nebulizer system. In contrast, the experimental approach used in this dissertation does not require correction for particle losses since measurements where based on one single-size droplet generating one single-size particle, and thus facilitating the calculation of SOA_{Cld} mass yields by dividing the mass of one particle by the mass of precursor that reacted from one droplet.

Another, novel experimental design has been developed by Lee et al.[12] to conduct aqueous photooxidation reactions of (3 mM) glyoxal with $^{\bullet}OH$ radicals (~10^{-13} M from photolysis of 13.3 mM H_2O_2) while simultaneously atomizing and evaporating droplets of bulk solution. After evaporation of water and volatile organics, the formed SOA_{aq} was analyzed continuously by aerosol mass spectrometry (AMS). Online AMS and offline ion chromatography (IC) were used to quantify some major organic products like formic, glyoxylic, and oxalic acids as well as unreacted glyoxal. [Experiments were performed at room temperature, unknown pH, and no information about the residence time of the

drying droplet or relative humidity was provided]. The total (cumulative) SOA mass yield determined for glyoxal photooxidation was about 20% at 20 min reaction time and was calculated as the total mass of individual products (formic, glyoxylic, and oxalic acids) divided by the mass of glyoxal reacted[12]. In contrast, SOA_{Cld} mass yields (i.e., mass of formed particulate matter divided by the mass of precursor reacted in one cloud droplet) obtained from this dissertation are summarized in Table 5-1 and discussed below.

Our assessment of glyoxal $^{\bullet}OH$ oxidation and droplet evaporation resulted in far greater (~207%) SOA_{Cld} mass yields than previously reported by Lee et al.[12], for somewhat similar conditions: 10 min reaction time in Batch scenario (i.e., depletion of glyoxal with time), ~10^{-12} M $^{\bullet}OH$. Note while the chemistry was modeled at low (cloud relevant) concentrations, the droplet evaporation took place from more concentrated (350x) mimics to meet the detection limits of the VOAG; see Appendix F for details. [Droplet evaporation was performed on unbuffered mimic solution droplets using filtered dry air, at RH = (12 ± 3)%, t = (24.4 ± 0.7)ºC, and 6 second residence time]. In comparison, SOA_{Cld} mass yields for the CSTR scenario (i.e., glyoxal at steady-state) were lower (~100%), in agreement with the higher PM to $OM_{(droplet)}$ mass ratios observed for Batch mimic samples (Figure 3-2 and Table 3-1; Chapter 3). Also, a substantial increase in SOA mass yields (~438%, which includes the mass of ammonium) was observed upon neutralization (pH 7 with ammonium hydroxide) of the CSTR mimic samples, as a result of ammonium oxalate formation and possibly other products from the reaction of glyoxal and ammonium ion[17,18]. Overall, the SOA_{Cld} mass yields reported in this work (~100-207%, at normal pH; Table 5-1) account for glyoxal oligomers formed

through droplet evaporation[19,20], which are not included in the yields of Lee et al.[12]. Likewise, a recent chemical modeling study[21] studying the aqueous photooxidation of glyoxal (0.1–10 μM) with OH radicals (~10^{-12} M) has reported SOA mass yields of ~120% for Batch and CSTR models (<60 min reaction times). The yields reported by Lim et al.[21] were defined as the mass of oxalic acid that remained in the particle-phase (as oxalate) divided by the amount of glyoxal reacted, and assumed that 90% of oxalate remains in the particle-phase, based on atmospheric measurements. Lim et al.[21] neglected the formation of glyoxal oligomers through droplet evaporation. In addition to the unaccounted glyoxal oligomers, their yields could be even greater if the mass of ammonium oxalate was considered instead of oxalic acid, as was the case in the VOAG estimates herein. As discussed in Chapter 2 and 3, atmospheric oxalate is mostly measured in the particle-phase and our work suggests that it is found as an oxalate salt (e.g., ammonium oxalate) rather than an acid, based on the high volatility observed for oxalic acid in our droplet evaporation experiments[14].

We report SOA mass yields of 5 to 20% for methylglyoxal $^{\bullet}$OH oxidation and droplet evaporation experiments (including Batch, CSTR, and neutralized CSTR mimic; at similar conditions as for glyoxal experiments); detailed information about yield calculations can be found in Appendix F. These yields are lower than predicted by Lim et al.[21] (~80%), who assumed that 70% of pyruvate remained in the particle-phase, as suggested by atmospheric measurements[22]. As discussed in Chapter 4, methylglyoxal + $^{\bullet}$OH precursor/product mixtures (pyruvic acid as major product) were relatively volatile, even when the mimics were neutralized with ammonium hydroxide to form ammonium pyruvate, suggesting that the observed pyruvate in the atmosphere (in the particle-phase)

is probably in the form of some other pyruvate species other than pyruvic acid or ammonium pyruvate. This could explain why our SOA_{Cld} mass yields for methylglyoxal were much lower than estimated by Lim et al.[21], which assumes gas-particle partitioning of pyruvate as reported for atmospheric measurements.

The large variation in SOA_{Cld} mass yields depicted from these studies suggests the importance of further research into the gas-particle partitioning of aqueous OM. It also suggests the importance of reporting key experimental conditions, like a well-defined yield, initial concentrations of reacting species, reaction times, pH, temperature, relative humidity, and particle residence time. Also, with future technological advancements and creative methods, studies might come closer to simulating cloud processing under real atmospheric conditions. For example, a few studies are now using more complex mixtures (e.g., cloud water samples, water-extracted fraction of ambient- and lab- SOA_{OM}, and glyoxal + water-soluble lab SOA_{OM}) to study the formation of particles through aqueous-phase photooxidation[23-25], direct photolysis[26], and acid-catalyzed[27] reactions followed by droplet evaporation. Still, more research is needed to unravel the complexities of both aqueous-phase chemistry and droplet evaporation chemistry.

Droplet evaporation chemistry enhances SOA_{Cld} formation. The evaporation of glyoxal and methylglyoxal containing droplets has been previously shown to form particles via aldehyde oligomerization[19,20]. In Chapter 2 of this Dissertation, I propose that glycolaldehyde can also oligomerize in evaporating droplets via hemiacetal formation and aldol condensation[14]. Evidence consistent with this hypothesis is shown by a substantial retention of OM mass in the particle-phase upon evaporation of

glycolaldehyde droplets (Appendix A8). Additional evidence is shown by our measured glycolaldehyde SOA_{Cld} mass yields (i.e., mass of SOA_{Cld} formed per mass of glycolaldehyde reacted), which were greater (60-120% for 10-40 min reaction time; Table 5-1)[14] than previously predicted (40-60%, same reaction times)[28] when quantified glycolaldehyde SOA_{aq} products were assigned particle-fractions as measured in the atmosphere. Possible explanations for this difference include: (1) formation of oligomers (e.g. from unreacted glycolaldehyde and glyoxal) during droplet evaporation, (2) inclusion of unquantified products formed by glycolaldehyde photooxidation, (3) differences in gas-partitioning (e.g., experimental versus atmospheric conditions), and (4) water retention in dried particles. These possibilities are discussed in more detail in Chapter 2. Oligomers formed via droplet evaporation will contribute to atmospheric SOA, since droplet evaporation is a common process in the atmosphere. Note that the understanding of the chemistry that occurs during droplet evaporation is still incomplete and adds to the uncertainty in SOA formation via cloud processing[10].

Since the drying process increases the concentration of dissolved organics in the droplets it can also accelerate reactions that are typically slow under atmospheric conditions. For example, Nguyen et al.[27] found that the evaporation of droplets containing dissolved SOA products and ammonium sulfate accelerated the production of nitrogen-containing light absorbing compounds by at least three orders of magnitude, compared to similar reactions in aqueous solution. Similarly, De Haan et al.[29] found that reactions between methylglyoxal and amino acids, methylamine, and ammonium sulfate in drying droplets formed light-absorbing nitrogen-containing oligomers, melanoidins, and methylimidazole salts that remain in the aerosol phase. These studies have shown

that droplet evaporation can have substantial effects on the composition and optical properties of the dissolved organics. The effects of droplet evaporation on SOA_{Cld} optical properties is an important area for future research, as discussed below in Section 5.2.

Summarized results: Particle mass retention from droplet evaporation experiments. Figure 5-1 synthesizes the results obtained in Chapters 2, 3, and 4 for droplet evaporation experiments conducted on organic standards, SOA_{Cld} precursors, and mixtures of SOA_{Cld} precursor (i.e., glycolaldehyde, glyoxal, and methylglyoxal) + products of aqueous OH radical oxidation. Shown in Figure 5-1 are ratios of residual particulate matter mass (PM mass) to the mass of organic matter in the droplet (OM mass) (aka *PM mass / OM mass*). These ratios reflect the fraction of total droplet OM that remains in the particle-phase after droplet evaporation. *PM mass / OM mass* ratios were determined by the slope of *PM mass* versus *OM mass* from each sample, as explained in more detail in Chapters 2, 3, and 4. Note that slopes greater than one necessarily mean that some non-organic material was retained in the particle-phase (i.e., water or ammonium). Droplet evaporation experiments were conducted at RH = 10-13%, t = 24-25ºC, 6 s residence time, and sample reaction times between 10 and 40 minutes (for SOA_{Cld} samples). Retention of material in the particle-phase after droplet evaporation was observed for all samples but with varying magnitudes. Results suggest that the amount of organic mass that is retained in the particle-phase after droplet evaporation is highly dependent on the volatility (shown in the labels for the organic standards) and chemical form of the organic products, favoring neutralized organics (e.g., organic salts) and aldehyde products (e.g., oligomer formation from glyoxal and glycolaldehyde). These are discussed in more detail below.

The volatility of SOA_{Cld} is similar to the volatility of the organic mixture contained in it. This dissertation improves our quantitative understanding of SOA_{Cld} formation by characterizing the volatility of the droplet organic matter present after 10-30 min of aqueous OH radical oxidation of glyoxal, methylglyoxal or glycolaldehyde. To my knowledge, this dissertation is the first (and only) to estimate the effective vapor pressure ($p'_{L,eff.}$) and enthalpy of vaporization ($\Delta H_{vap,eff.}$) of droplet organic matter. The incomplete understanding of the enthalpy of vaporization of organic aerosol has been found to be a major source of uncertainty in modeled SOA budgets, as determined by an assessment of SOA modeling uncertainties[30]. The estimated properties are summarized in Table 5-1. In general, the $p'_{L,eff.}$ values are within the same order of magnitude (~10^{-7} atm) as the mixed standard of organic acids also described in Table 5-1. The $\Delta H_{vap,eff}$ for the precursor/product mixtures and the organic acid mixed standard are also comparable at ~70 kJ/mol. Currently, no other similar studies exist for comparison. One study assessed the volatility of the aerosol (SOA_{Cld}) formed from the aqueous photooxidation of methacrolein followed by evaporation of nebulized droplets[31]. They monitored the relative size change of the resulting particles with changing temperature and fixed relative humidity (10%), and measured the residual volume fraction (RVF), which is inversely proportional to volatility. They found that methacrolein SOA_{Cld} became substantially less volatile as the reaction proceeded from 5 hours (RVF = 34% at 100°C) to 22 hours (RVF = 81% at 100°C), suggesting that the SOA formed by cloud processing is mostly volatile at 100°C at the beginning of the reaction, but becomes less volatile with increasing time possibly due to oligomer formation.

Addition of ammonium enhances particle retention and decreases volatility. This dissertation presents, for the first time, evidence that the neutralization of SOA_{Cld} products (carboxylic acid salt formation) can substantially reduce the volatility of the droplet OM. Specifically, droplet evaporation experiments were conducted for glyoxal photooxidation products at pH 3 and pH 7 (neutralized by ammonia), and a comparison between their volatility was assessed (Chapter 3). The addition of ammonia led to a substantial increase in particle-phase retention (Figure 5-1) and reduction in vapor pressure (Table 5-1). Although the uncertainties in the estimated vapor pressure are large, the volatility behavior and particle-phase retention are very similar to that of ammonium oxalate, which has a sub-cooled liquid vapor pressure of $\sim 10^{-11}$ atm (Figure 5-1). This finding is consistent with the work by Na et al.[32], which showed that ammonia enhanced the formation of SOA from α-pinene ozonolysis due to the formation of condensable (organic) salts. Additionally, work by Dinar et al.[33] verified that the reactive uptake of ammonia by organic acids (e.g, adipic and citric acid) formed ammonium salts that can substantially influence the chemical and physical properties of the aerosol. These results suggest that the glyoxal+$^{\bullet}$OH cloud droplet precursor/product OM mixture could behave like a semi-volatile compound that partitions between the gas- and condensed- phases or could behave like a low-volatility compound that remains mainly in the aerosol phase, depending on the availability of a neutralizing agent (e.g, ammonia). In contrast, the addition of ammonium hydroxide to the methylglyoxal+$^{\bullet}$OH precursor/product mix resulted in only small (factor of 2) reductions in aerosol volatility (Chapter 4). Organic salts are known to have volatilities that are orders of magnitude lower compared to their corresponding organic acids. For example, oxalic acid has a vapor pressure in the order of

~10^{-7} atm whereas the vapor pressure of ammonium oxalate is about 4 orders of magnitude lower (Figure 5-1). These findings suggest that the gas-particle partitioning behavior of SOA_{Cld} depends strongly on whether products are present in the atmosphere as acids or salts (neutralized).

In the atmosphere, compounds like pyruvate, glyoxylate, and oxalate are mostly found in the particle-phase (i.e., 61%, 70%, and 74%, respectively)[22] despite the fact that these *acids* have relatively high vapor pressures. Acid displacement reactions and reactions with polyvalent metal ions could both reduce the volatility of organic acids formed through cloud chemistry. For example, a recent study provided field observation and laboratory evidence that organic salts can form from drying droplets containing sea salt (mainly NaCl) and weak carboxylic acids, like malonic, malic, citric, and tartaric acid[34]. The driving force in the formation of these organic salts is an acid-displacement reaction that releases hydrogen chloride (HCl) as a gas, leaving behind an organic salt precipitate. Since drying enhances this process and droplet evaporation is very common in atmospheric waters, acid-displacement reactions are expected to be potentially important is areas where marine aerosol can mix with SOA_{Cld} (typically composed of organic acids). Another process that could enhance the retention of dissolved organics in the aerosol phase is the reaction between dicarboxylic acids (like oxalic acid, a major component of SOA_{Cld}) and polyvalent metal ions (i.e., Ca^{2+}, Zn^{2+}, and Hg^{2+})[35,36] found in clouds and aerosols of natural and anthropogenic sources. The study by Furukawa and Takahashi[36] found that metal oxalate complexes formed from dissolved oxalate in the presence of metal ions; 10-60% with Ca^{2+} and 20-100% with Zn^{2+}. The ability of these metal oxalate complexes to form a solid precipitate is controlled by the solubility of each

complex. As the water in droplets starts to evaporate, the complexes with the lowest solubility precipitate more favorably. All of the above mentioned processes, whether formation of organometallic complexes or organic salt formation through neutralization or acid-displacement, can increase the yield of SOA_{Cld} by increasing the fraction of droplet OM that remains in the particle-phase after droplet evaporation. Currently, none of these processes are being taken into consideration in modeling efforts.

The following are expected to also increase the retention of dissolved organics in the particle-phase after cloud droplet evaporation: (1) lower temperatures, because they reduce vapor pressures; (2) larger liquid water contents in aerosols in the cloud outflow because some organics that would otherwise evaporate will be retained in that water and because oxidation chemistry can continue in the wet aerosol, forming oligomers[21,37]; (3) in the case of methylglyoxal, more cloud processing cycles so as to form oxalate (found predominantly in the particle-phase in the atmosphere, probably as a salt or complex); (4) neutralization of organic acids by other atmospheric nitrogenous bases (e.g., amines) or base cations from soil particles like K^+, Ca^{2+}, or Mg^{+2}; (5) acid-displacement, e.g., between sea salt and carboxylic acids; and (6) formation of organometallic complexes between dicarboxylic acids and metal ions (e.g., Cu^{2+}, Zn^{2+}, Hg^{2+}, Pb^{2+}, Mg^{2+}, Fe^{2+}).

SOA_{Cld} might have a greater impact on atmospheric chemistry and climate than originally understood, as demonstrated by the findings discussed above, including the potential for precursor aldehydes to oligomerize and for organic acid products to form salts and organometallic complexes in evaporating cloud droplets. These processes could induce significant changes in the chemical, physical and optical properties of SOA_{Cld} and warrant further research.

Effective air pollution management and climate change mitigation strategies require models that include key processes linking emissions to concentrations and properties of atmospheric particulate matter. The research herein contributes by providing SOA mass yields along with key physicochemical properties (i.e., vapor pressure and enthalpy of vaporization) that are needed to refine the treatment of SOA formation via aqueous chemistry in regional and global chemical transport models. Chemical transport models can directly use our SOA mass yields (i.e., by multiplying the mass yield by the amount of aqueous-phase precursor that reacted) after simulating the production of gas-phase precursor, the uptake of precursor into the aqueous-phase, and the amount (mass) of precursor reacted by OH radical oxidation in the aqueous-phase. The corresponding vapor pressure and enthalpy of vaporization can then be used in the model to describe how the SOA mass yield changes with temperature (e.g., temperature sensitivity of gas-particle partitioning) and the evolution of SOA_{Cld} in the atmosphere[38].

5.2 Implications and Future Directions

Atmospheric implications of enhanced chemistry in evaporating droplets. The process of evaporation enhances the reactivity of dissolved organics by (1) increasing the concentration of all the components, (2) increasing the acidity in the droplet and allowing acid catalyzed reactions, (3) enabling precipitation of low solubility products in solution, (4) facilitating dehydration of aldehydes and allowing oligomerization reactions, and (5) accelerating reactions that are normally too slow in bulk solution. Droplet evaporation is a common process in the atmosphere, yet our understanding of its contribution to SOA_{Cld} formation is still very limited. ***Future SOA_{Cld} studies should incorporate more droplet evaporation experiments*** and fully investigate the role that processes like neutralization,

acid-displacement, and oligomerization play in SOA_{Cld} formation. For example, future neutralization studies should investigate the efficiency that different atmospheric bases have in generating SOA_{Cld} in the presence of dissolved organic acids in evaporating droplets. Similarly, future droplet evaporation studies should investigate the potential and efficiency of other atmospherically relevant aldehydes (e.g., methacrolein, acetaldehyde, and formaldehyde) to undergo self-reactions and form oligomers. Also, future investigations need to quantify the potential contribution that acid-displacement reactions have in the process of evaporating droplets that contain sea salt and photooxidation products (organic acids) of cloud processing. The latter studies should evaluate the enhancement of SOA formation in geographical areas where biogenic and anthropogenic SOA_{Cld} photooxidation products are likely to meet with marine aerosol (sea salt). Moreover, laboratory studies should investigate if dicarboxylic acids found in SOA_{Cld}, other than oxalic acid, form organometallic complexes with different polyvalent metal ions upon droplet evaporation. Finally, the induced changes in SOA_{Cld} chemical, physical (e.g., volatility), and optical (e.g., scattering coefficient) properties from these processes could have significant impacts on the chemistry and fate of atmospheric particles, as well as on climate change. Therefore, future atmospheric modeling studies must include these processes into their assessments.

SOA_{Cld} optical properties and implications to climate change. Understanding the optical properties of aerosols is crucial for quantifying the effect that aerosols have on climate. Aerosols can scatter and absorb radiation having a cooling or warming effect on the Earth, respectively, also known as the direct radiative effect. Given that SOA is a substantial contributor to atmospheric aerosols, it is important to understand the optical

properties of SOA and what processes cause variations in those properties. Processes not mentioned above that could substantially change the optical properties of the studied SOA_{Cld} include aqueous-phase reactions of organics with nitrogen-containing reactants like amino acids[39], ammonium sulfate[17,27,40-44], and amines[29,45,46] that produce light-absorbing compounds. Inclusion of droplet evaporation to some of the latter processes also enhances reactivity[27,39] and suggests that cloud processing is a potential source of light-absorbing material in the atmosphere. ***Future studies should measure the changes in SOA_{Cld} optical properties due to enhanced organic reactivity by droplet evaporation.*** I propose that the methodology presented in my dissertation be expanded to measure the optical properties of laboratory-generated SOA_{Cld} from glycolaldehyde, methylglyoxal, glyoxal, other precursors, and/or mixtures of reactive organic species. Techniques like the multi-angle aerosol spectrometer probe (MASP) and the multi-angle absorption photometer (MAAP) can be placed at the outlet of the VOAG system (Vibrating Orifice Aerosol Generator) to continuously measure aerosol light scattering and absorption of the generated SOA_{Cld}, respectively. Furthermore, the inclusion of an aerodynamic particle sizer spectrometer (in parallel to the optical particle counter used in the VOAG system) would enable the measurement of residual particle density, and thus provide more accurate PM mass values. [Note that the presence of light-absorbing products could affect the refractive index of our measured particles and introduce some uncertainty to the diameters measured by the optical particle counter in the VOAG system].

SOA_{Cld} high oxidation state, hygroscopicity, and implications to climate change. Oxidation state (O:C) can be used to gage how readily aerosols retain water (e.g., hygroscopicity). Aerosols with high O:C ratios are highly oxygenated and will have

higher affinity towards water molecules. Because of their affinity towards water, hygroscopic aerosols can serve as cloud condensation nuclei (CCN) influencing cloud formation and lifetime also known as the indirect radiative effect. The precursors of SOA_{Cld} formation are water-soluble and generally have high O:C ratios (~1). Therefore, SOA_{Cld} is expected to have high O:C ratios and be hygroscopic. Since the SOA_{Cld} generated by the VOAG system in my research was not characterized chemically after droplet evaporation, a quantitative measure of its O:C ratio was not provided. Nonetheless, it is clear that the O:C ratios will be high. To support this, recent work by Lee et al.[23] reveals that the aqueous photooxidation (and droplet evaporation) of glyoxal together with water-extracted compounds from biogenic SOA produces highly oxidized SOA. Their work has provided strong evidence that the properties of organic aerosol formed through aqueous-phase oxidation are similar to the properties of organic aerosol observed globally. Similarly, Wong et al.[47] observed an increase in O:C ratios from the aqueous photooxidation (followed by droplet evaporation) of water-extracted ambient organic aerosols. They also confirmed that the O:C ratio is directly proportional to aerosol hygroscopicity (measured from the CCN activity of size-selected particles). In order to have a better understanding of the impacts that SOA_{Cld} has on climate change via the indirect radiative effect, ***future studies must measure the hygroscopicity of SOA_{Cld}.*** The CCN activity of laboratory-generated SOA_{Cld} could be measured by modifying the VOAG system to incorporate measurements from a CCN Counter and Condensation Particle Counter (CPC). The CCN activity would be determined from the ratio of CCN-active particle number to the total particle number concentration (from the CPC). Moreover, the hygroscopic growth factor (HGF) is calculated as the ratio between the

diameter of a humidified particle to the diameter of the dry particle. The HGF of laboratory-generated SOA_{Cld} could also be measured from considerable modifications to the VOAG system. For example, after droplet evaporation in the VOAG system the monodisperse SOA_{Cld} particles could be exposed to different relative humidities, and the particle diameter of dry (RH ≈ 10%) and humid (RH = 50 – 90%) SOA_{Cld} particles could be then measured using two particle sizers (e.g., Optical Particle Sizer, or Scanning Mobility Particle Sizer Spectrometer) located before and after the humidifying process, respectively. This process is analogous the commonly used Volatility-Hygroscopicity Tandem Differential Mobility Analyzer (VHTDMA), but does not require the use of differential mobility analyzers since the aerosol generated by the VOAG system is already monodisperse.

Atmospheric implications of microbial activity and SOA_{Cld}. Microorganisms like bacteria, fungi, and yeast, are ubiquitous in the atmosphere and have been measured extensively in cloud water[48-52]. However, their role in atmospheric aqueous chemistry has only recently begun to be assessed[51,53-58]. These recent studies have found that microorganisms can efficiently transform and use atmospheric dicarboxylic acids as nutrients for their metabolic processes. Since dicarboxylic acids are major products of SOA_{Cld}, it is possible that SOA_{Cld} formation potentially contributes to microbial growth in clouds. Moreover, biodegradation rates were found to be comparable to aqueous photodegradation (e.g., OH radicals) of carboxylic acids present in cloud water[57,58]. These studies also found that microbial activity is competitive even at low cloud water temperatures (e.g., 5ºC). This suggests that microbial activity and photochemical processes could take place simultaneously in cloud water chemistry. Our current

understanding of the effects that microbial activity has on SOA_{Cld} formation and properties is very limited, and thus, future laboratory and modeling studies will be needed to fill this knowledge gap.

SOA_{Cld} implications to health. The direct health effects of SOA_{Cld} are currently unknown; nonetheless, SOA is a major component of the widely studied $PM_{2.5}$ (i.e., particulate matter with diameter ≤ 2.5 μm). $PM_{2.5}$ exposure is associated with adverse health effects including respiratory and cardiovascular morbidity and mortality, as well as reduced life expectancy[59-62]. There is still much to learn about what specific particle component or combination of components are most responsible for the observed health effects. Collaborative studies involving epidemiologists, toxicologists, and exposure assessment researchers must continue in order to determine whether the products of SOA_{Cld} formation contribute to aerosol-related health effects. Advancements in technology and data processing will likely aid the development of an improved understanding of the toxic effects of chemicals. For example, the Environmental Protection Agency has joined forces with the National Institute of Environmental Health Sciences, the National Institute of Health, and the Food and Drug Administration to launch a high-tech robot with a high speed screening system (Tox21 Robot)[63] that can test the toxicity of thousands of chemicals and assess their effects on human health.

Implications of global warming on biomass burning and SOA_{Cld} formation. Biomass burning can emit substantial amounts of compounds including glycolaldehyde and acetic acid (4–20 and 40 Tg a^{-1}, respectively)[64-66], which are known precursors of SOA_{Cld}[14,28,67]. Emissions of these SOA_{Cld} precursors are expected to increase as the frequency and duration of biomass burning increase as a consequence of the high

temperatures, extreme weather, and drought of global warming[68,69]. This suggests that global warming is likely to enhance SOA_{Cld} formation from selected precursors and should be the subject of further research.

5.3 References

(1) Seinfeld, J. H.; Pandis, S. N. Atmospheric Chemistry and Physics: From Air Pollution to Climate Change. *John Wiley & Sons, New York* **1998**.

(2) Turpin, B. J.; Huntzicker, J. J. Identification of secondary organic aerosol episodes and quantitation of primary and secondary organic aerosol concentrations during SCAQS. *Atmospheric Environment* **1995**, *29*, 3527–3544.

(3) Turpin, B. J.; Saxena, P.; Andrews, E. Measuring and simulating particulate organics in the atmosphere: problems and prospects. *Atmospheric Environment* **2000**, *34*, 2983–3013.

(4) Kanakidou, M.; Seinfeld, J. H.; Pandis, S. N.; Barnes, I.; Dentener, F. J.; Facchini, M. C.; Van Dingenen, R.; Ervens, B.; Nenes, A.; Nielsen, C. J.; Swietlicki, E.; Putaud, J. P.; Balkanski, Y.; Fuzzi, S.; Horth, J.; Moortgat, G. K.; Winterhalter, R.; Myhre, C. E. L.; Tsigaridis, K.; Vignati, E.; Stephanou, E. G.; Wilson, J. Organic aerosol and global climate modelling: a review. *Atmos. Chem. Phys.* **2005**, *5*, 1053–1123.

(5) Polidori, A.; Turpin, B. J.; Lim, H.-J.; Cabada, J. C.; Subramanian, R.; Pandis, S. N.; Robinson, A. L. Local and Regional Secondary Organic Aerosol: Insights from a Year of Semi-Continuous Carbon Measurements at Pittsburgh. *Aerosol Science and Technology* **2006**, *40*, 861–872.

(6) Zhang, Q.; Jimenez, J. L.; Canagaratna, M. R.; Allan, J. D.; Coe, H.; Ulbrich, I.; Alfarra, M. R.; Takami, A.; Middlebrook, A. M.; Sun, Y. L.; Dzepina, K.; Dunlea, E.; Docherty, K.; DeCarlo, P. F.; Salcedo, D.; Onasch, T.; Jayne, J. T.; Miyoshi, T.; Shimono, A.; Hatakeyama, S.; Takegawa, N.; Kondo, Y.; Schneider, J.; Drewnick, F.; Borrmann, S.; Weimer, S.; Demerjian, K.; Williams, P.; Bower, K.; Bahreini, R.; Cottrell, L.; Griffin, R. J.; Rautiainen, J.; Sun, J. Y.; Zhang, Y. M.; Worsnop, D. R. Ubiquity and dominance of oxygenated species in organic aerosols in anthropogenically-influenced Northern Hemisphere midlatitudes. *Geophys. Res. Lett.* **2007**, *34*, L13801.

(7) Hallquist, M.; Wenger, J.; Baltensperger, U.; Rudich, Y.; Simpson, D.; Claeys, M.; Dommen, J.; Donahue, N.; George, C.; Goldstein, A. The formation, properties and impact of secondary organic aerosol: current and emerging issues. *Atmos. Chem. Phys.* **2009**, *9*, 5155–5236.

(8) EPA U.S. EPA. *Air Quality Criteria for Particulate Matter*; United States

Environmental Protection Agency (U.S. EPA), Research Triangle Park, NC, **2004**.

(9) Ervens, B.; Turpin, B. J.; Weber, R. J. Secondary organic aerosol formation in cloud droplets and aqueous particles (aqSOA): a review of laboratory, field and model studies. *Atmos. Chem. Phys.* **2011**, *11*, 11069–11102.

(10) Gong, W.; Stroud, C.; Zhang, L. Cloud Processing of Gases and Aerosols in Air Quality Modeling. *Atmosphere* **2011**, *2*, 567–616.

(11) El Haddad, I.; Liu, Y.; Nieto-Gligorovski, L.; Michaud, V.; Temime-Roussel, B.; Quivet, E.; Marchand, N.; Sellegri, K.; Monod, A. In-cloud processes of methacrolein under simulated conditions – Part 2: Formation of secondary organic aerosol. *Atmos. Chem. Phys.* **2009**, *9*, 5107–5117.

(12) Lee, A. K. Y.; Zhao, R.; Gao, S. S.; Abbatt, J. P. D. Aqueous-Phase OH Oxidation of Glyoxal: Application of a Novel Analytical Approach Employing Aerosol Mass Spectrometry and Complementary Off-Line Techniques. *J. Phys. Chem. A* **2011**, *115*, 10517–10526.

(13) Liu, Y.; Siekmann, F.; Renard, P.; Zein, El, A.; Salque, G.; El Haddad, I.; Temime-Roussel, B.; Voisin, D.; Thissen, R.; Monod, A. Oligomer and SOA formation through aqueous phase photooxidation of methacrolein and methyl vinyl ketone. *Atmospheric Environment* **2012**, *49*, 123–129.

(14) Ortiz-Montalvo, D. L.; Lim, Y. B.; Perri, M. J.; Seitzinger, S. P.; Turpin, B. J. Volatility and Yield of Glycolaldehyde SOA Formed through Aqueous Photochemistry and Droplet Evaporation. *Aerosol Science and Technology* **2012**, *46*, 1002–1014.

(15) Desboeufs, K.; Losno, R.; Colin, J. Relationship between droplet pH and aerosol dissolution kinetics: Effect of incorporated aerosol particles on droplet pH during cloud processing. *J Atmos Chem* **2003**, *46*, 159–172.

(16) Ervens, B.; Volkamer, R. Glyoxal processing by aerosol multiphase chemistry: towards a kinetic modeling framework of secondary organic aerosol formation in aqueous particles. *Atmos. Chem. Phys.* **2010**, *10*, 8219–8244.

(17) Nozière, B.; Dziedzic, P.; Córdova, A. Products and Kinetics of the Liquid-Phase Reaction of Glyoxal Catalyzed by Ammonium Ions (NH_4^+). *J. Phys. Chem. A* **2009**, *113*, 231–237.

(18) Nozière, B.; Dziedzic, P.; Córdova, A. Inorganic ammonium salts and carbonate salts are efficient catalysts for aldol condensation in atmospheric aerosols. *Phys. Chem. Chem. Phys.* **2010**, *12*, 3864–3872.

(19) Loeffler, K. W.; Koehler, C. A.; Paul, N. M.; De Haan, D. O. Oligomer

Formation in Evaporating Aqueous Glyoxal and Methyl Glyoxal Solutions. *Environmental Science & Technology* **2006**, *40*, 6318–6323.

(20) De Haan, D. O.; Corrigan, A. L.; Tolbert, M. A.; Jimenez, J. L.; Wood, S. E.; Turley, J. J. Secondary Organic Aerosol Formation by Self-Reactions of Methylglyoxal and Glyoxal in Evaporating Droplets. *Environmental Science & Technology* **2009**, *43*, 8184–8190.

(21) Lim, Y. B.; Tan, Y.; Turpin, B. J. Chemical insights, explicit chemistry and yields of secondary organic aerosol from methylglyoxal and glyoxal. *Atmos. Chem. Phys. Discuss.* **2013**, *13*, 4687–4725.

(22) Limbeck, A.; Puxbaum, H.; Otter, L.; Scholes, M. C. Semivolatile behavior of dicarboxylic acids and other polar organic species at a rural background site (Nylsvley, RSA). *Atmospheric Environment* **2001**, *35*, 1853–1862.

(23) Lee, A. K. Y.; Herckes, P.; Leaitch, W. R.; Macdonald, A. M.; Abbatt, J. P. D. Aqueous OH oxidation of ambient organic aerosol and cloud water organics: Formation of highly oxidized products. *Geophys. Res. Lett.* **2011**, *38*, L11805.

(24) Lee, A. K. Y.; Hayden, K. L.; Herckes, P.; Leaitch, W. R.; Liggio, J.; Macdonald, A. M.; Abbatt, J. P. D. Characterization of aerosol and cloud water at a mountain site during WACS 2010: secondary organic aerosol formation through oxidative cloud processing. *Atmos. Chem. Phys.* **2012**, *12*, 7103–7116.

(25) Liu, Y.; Monod, A.; Tritscher, T.; Praplan, A. P.; DeCarlo, P. F.; Temime-Roussel, B.; Quivet, E.; Marchand, N.; Dommen, J.; Baltensperger, U. Aqueous phase processing of secondary organic aerosol from isoprene photooxidation. *Atmos. Chem. Phys.* **2012**, *12*, 5879–5895.

(26) Bateman, A. P.; Nizkorodov, S. A.; Laskin, J.; Laskin, A. Photolytic processing of secondary organic aerosols dissolved in cloud droplets. *Phys. Chem. Chem. Phys.* **2011**, *13*, 12199–12212.

(27) Nguyen, T. B.; Lee, P. B.; Updyke, K. M.; Bones, D. L.; Laskin, J.; Laskin, A.; Nizkorodov, S. A. Formation of nitrogen- and sulfur-containing light-absorbing compounds accelerated by evaporation of water from secondary organic aerosols. *J. Geophys. Res.* **2012**, *117*, D01207.

(28) Perri, M. J.; Seitzinger, S.; Turpin, B. J. Secondary organic aerosol production from aqueous photooxidation of glycolaldehyde: Laboratory experiments. *Atmospheric Environment* **2009**, *43*, 1487–1497.

(29) De Haan, D. O.; Hawkins, L. N.; Kononenko, J. A.; Turley, J. J.; Corrigan, A. L.; Tolbert, M. A.; Jimenez, J. L. Formation of Nitrogen-Containing Oligomers by

Methylglyoxal and Amines in Simulated Evaporating Cloud Droplets. *Environmental Science & Technology* **2011**, *45*, 984–991.

(30) Tsigaridis, K.; Kanakidou, M. Global modelling of secondary organic aerosol in the troposphere: A sensitivity analysis. *Atmos. Chem. Phys.* **2003**, *3*, 1849–1869.

(31) Michaud, V.; El Haddad, I.; Liu, Y.; Sellegri, K.; Laj, P.; Villani, P.; Picard, D.; Marchand, N.; Monod, A. In-cloud processes of methacrolein under simulated conditions–Part 3: Hygroscopic and volatility properties of the formed secondary organic aerosol. *Atmos. Chem. Phys.* **2009**, *9*, 5119–5130.

(32) Na, K.; Song, C.; Switzer, C.; Cocker, D. R. Effect of Ammonia on Secondary Organic Aerosol Formation from α-Pinene Ozonolysis in Dry and Humid Conditions. *Environmental Science & Technology* **2007**, *41*, 6096–6102.

(33) Dinar, E.; Anttila, T.; Rudich, Y. CCN Activity and Hygroscopic Growth of Organic Aerosols Following Reactive Uptake of Ammonia. *Environmental Science & Technology* **2008**, *42*, 793–799.

(34) Laskin, A.; Moffet, R. C.; Gilles, M. K.; Fast, J. D.; Zaveri, R. A.; Wang, B.; Nigge, P.; Shutthanandan, J. Tropospheric chemistry of internally mixed sea salt and organic particles: Surprising reactivity of NaCl with weak organic acids. *J. Geophys. Res.* **2012**, *117*, D15302.

(35) Si, L.; Ariya, P. A. Reduction of Oxidized Mercury Species by Dicarboxylic Acids (C 2−C 4): Kinetic and Product Studies. *Environmental Science & Technology* **2008**, *42*, 5150–5155.

(36) Furukawa, T.; Takahashi, Y. Oxalate metal complexes in aerosol particles: implications for the hygroscopicity of oxalate-containing particles. *Atmos. Chem. Phys.* **2011**, *11*, 4289–4301.

(37) Lim, Y. B.; Tan, Y.; Perri, M. J.; Seitzinger, S. P.; Turpin, B. J. Aqueous chemistry and its role in secondary organic aerosol (SOA) formation. *Atmos. Chem. Phys.* **2010**, *10*, 10521–10539.

(38) Jimenez, J. L.; Canagaratna, M. R.; Donahue, N. M.; Prévôt, A. S. H.; Zhang, Q.; Kroll, J. H.; DeCarlo, P. F.; Allan, J. D.; Coe, H.; Ng, N. L.; Aiken, A. C.; Docherty, K. S.; Ulbrich, I. M.; Grieshop, A. P.; Robinson, A. L.; Duplissy, J.; Smith, J. D.; Wilson, K. R.; Lanz, V. A.; Hueglin, C.; Sun, Y. L.; Tian, J.; Laaksonen, A.; Raatikainen, T.; Rautiainen, J.; Vaattovaara, P.; Ehn, M.; Kulmala, M.; Tomlinson, J. M.; Collins, D. R.; Cubison, M. J.; E.; Dunlea, J.; Huffman, J. A.; Onasch, T. B.; Alfarra, M. R.; Williams, P. I.; Bower, K.; Kondo, Y.; Schneider, J.; Drewnick, F.; Borrmann, S.; Weimer, S.; Demerjian, K.; Salcedo, D.; Cottrell, L.; Griffin, R.; Takami, A.; Miyoshi, T.; Hatakeyama, S.; Shimono, A.; Sun, J. Y.; Zhang, Y. M.; Dzepina, K.; Kimmel, J. R.;

Sueper, D.; Jayne, J. T.; Herndon, S. C.; Trimborn, A. M.; Williams, L. R.; Wood, E. C.; Middlebrook, A. M.; Kolb, C. E.; Baltensperger, U.; Worsnop, D. R. Evolution of Organic Aerosols in the Atmosphere. *Science* **2009**, *326*, 1525–1529.

(39) De Haan, D. O.; Corrigan, A. L.; Smith, K. W.; Stroik, D. R.; Turley, J. J.; Lee, F. E.; Tolbert, M. A.; Jimenez, J. L.; Cordova, K. E.; Ferrell, G. R. Secondary Organic Aerosol-Forming Reactions of Glyoxal with Amino Acids. *Environmental Science & Technology* **2009**, *43*, 2818–2824.

(40) Shapiro, E. L.; Szprengiel, J.; Sareen, N.; Jen, C. N.; Giordano, M. R.; McNeill, V. Light-absorbing secondary organic material formed by glyoxal in aqueous aerosol mimics. *Atmos. Chem. Phys.* **2009**, *9*, 2289–2300.

(41) Sareen, N.; Schwier, A.; Shapiro, E.; Mitroo, D.; McNeill, V. Secondary organic material formed by methylglyoxal in aqueous aerosol mimics. *Atmos. Chem. Phys.* **2010**, *10*, 997–1016.

(42) Schwier, A. N.; Sareen, N.; Mitroo, D.; Shapiro, E. L.; McNeill, V. F. Glyoxal-Methylglyoxal Cross-Reactions in Secondary Organic Aerosol Formation. *Environmental Science & Technology* **2010**, *44*, 6174–6182.

(43) Yu, G.; Bayer, A. R.; Galloway, M. M.; Korshavn, K. J.; Fry, C. G.; Keutsch, F. N. Glyoxal in Aqueous Ammonium Sulfate Solutions: Products, Kinetics and Hydration Effects. *Environmental Science & Technology* **2011**, *45*, 6336–6342.

(44) Kampf, C. J.; Jakob, R.; Hoffmann, T. Identification and characterization of aging products in the glyoxal/ammonium sulfate system – implications for light-absorbing material in atmospheric aerosols. *Atmos. Chem. Phys.* **2012**, *12*, 6323–6333.

(45) De Haan, D. O.; Tolbert, M. A.; Jimenez, J. L. Atmospheric condensed-phase reactions of glyoxal with methylamine. *Geophys. Res. Lett.* **2009**, *36*.

(46) Kua, J.; Krizner, H. E.; De Haan, D. O. Thermodynamics and Kinetics of Imidazole Formation from Glyoxal, Methylamine, and Formaldehyde: A Computational Study. *J. Phys. Chem. A* **2011**, *115*, 1667–1675.

(47) Wong, J. P. S.; Lee, A. K. Y.; Slowik, J. G.; Cziczo, D. J.; Leaitch, W. R.; Macdonald, A.; Abbatt, J. P. D. Oxidation of ambient biogenic secondary organic aerosol by hydroxyl radicals: Effects on cloud condensation nuclei activity. *Geophys. Res. Lett.* **2011**, *38*, L22805.

(48) Bauer, H.; Kasper-Giebl, A.; Löflund, M.; Giebl, H.; Hitzenberger, R.; Zibuschka, F.; Puxbaum, H. The contribution of bacteria and fungal spores to the organic carbon content of cloud water, precipitation and aerosols. *Atmospheric Research* **2002**, *64*, 109–119.

(49) Amato, P.; Parazols, M.; Sancelme, M.; Laj, P.; Mailhot, G.; Delort, A.-M. Microorganisms isolated from the water phase of tropospheric clouds at the Puy de DÃ´me: major groups and growth abilities at low temperatures. *FEMS Microbiology Ecology* **2007**, *59*, 242–254.

(50) Amato, P.; Parazols, M.; Sancelme, M.; Mailhot, G.; Laj, P.; Delort, A.-M. An important oceanic source of micro-organisms for cloud water at the Puy de Dôme (France). *Atmospheric Environment* **2007**, *41*, 8253–8263.

(51) Vaïtilingom, M.; Attard, E.; Gaiani, N.; Sancelme, M.; Deguillaume, L.; Flossmann, A. I.; Amato, P.; Delort, A.-M. Long-term features of cloud microbiology at the puy de DOme (France). *Atmospheric Environment* **2012**, *56*, 88–100.

(52) DeLeon-Rodriguez, N.; Lathem, T. L.; M, R.-R. L.; Barazesh, J. M.; Anderson, B. E.; Beyersdorf, A. J.; Ziemba, L. D.; Bergin, M.; Nenes, A.; Konstantinidis, K. T. Microbiome of the upper troposphere: Species composition and prevalence, effects of tropical storms, and atmospheric implications. *Proceedings of the National Academy of Sciences* **2013**, 1–6.

(53) Ariya, P. A. Microbiological degradation of atmospheric organic compounds. *Geophys. Res. Lett.* **2002**, *29*, 2077.

(54) Amato, P.; Ménager, M.; Sancelme, M.; Laj, P.; Mailhot, G.; Delort, A.-M. Microbial population in cloud water at the Puy de Dôme: Implications for the chemistry of clouds. *Atmospheric Environment* **2005**, *39*, 4143–4153.

(55) Amato, P.; Demeer, F.; Melaouhi, A.; Fontanella, S.; Martin-Biesse, A. S.; Sancelme, M.; Laj, P.; Delort, A. M. A fate for organic acids, formaldehyde and methanol in cloud water: their biotransformation by micro-organisms. *Atmos. Chem. Phys.* **2007**, *7*, 4159–4169.

(56) Deguillaume, L.; Leriche, M.; Amato, P.; Ariya, P. A.; Delort, A. M.; Pöschl, U.; Chaumerliac, N.; Bauer, H.; Flossmann, A. I.; Morris, C. E. Microbiology and atmospheric processes: chemical interactions of Primary Biological Aerosols. *Biogeosciences Discuss.* **2008**, *5*, 841–870.

(57) Delort, A.-M.; Vaïtilingom, M.; Amato, P.; Sancelme, M.; Parazols, M.; Mailhot, G.; Laj, P.; Deguillaume, L. A short overview of the microbial population in clouds: Potential roles in atmospheric chemistry and nucleation processes. *Atmospheric Research* **2010**, *98*, 249–260.

(58) Vaïtilingom, M.; Charbouillot, T.; Deguillaume, L.; Maisonobe, R.; Parazols, M.; Amato, P.; Sancelme, M.; Delort, A. M. Atmospheric chemistry of carboxylic acids: microbial implication versus photochemistry. *Atmos. Chem. Phys.* **2011**, *11*, 8721–8733.

(59) Davidson, C. I.; Phalen, R. F.; Solomon, P. A. Airborne Particulate Matter and Human Health: A Review. *Aerosol Science and Technology* **2005**, *39*, 737–749.

(60) Nel, A. Air Pollution-Related Illness: Effects of Particles. *Science* **2005**, *308*, 804–806.

(61) Pope, C. A., III; Dockery, D. W. Health effects of fine particulate air pollution: lines that connect. *Journal of Air & Waste Management* **2006**, *56*, 709–742.

(62) Pope, C. A., III; Ezzati, M.; Dockery, D. W. Fine-particulate air pollution and life expectancy in the United States. *New England Journal of Medicine* **2009**, *360*, 376–386.

(63) Jacobs, J. P. Agencies Hope Robot Can Speed Toxics Evaluations, End Animal Testing. *The New York Times* **2011**, 1–4.

(64) Yokelson, R. J.; Susott, R.; Ward, D. E.; Reardon, J.; Griffith, D. W. T. Emissions from smoldering combustion of biomass measured by open-path Fourier transform infrared spectroscopy. *J. Geophys. Res.* **1997**, *102*, 18865–18877.

(65) Akagi, S. K.; Yokelson, R. J.; Wiedinmyer, C.; Alvarado, M. J.; Reid, J. S.; Karl, T.; Crounse, J. D.; Wennberg, P. O. Emission factors for open and domestic biomass burning for use in atmospheric models. *Atmos. Chem. Phys.* **2011**, *11*, 4039–4072.

(66) Burling, I. R.; Yokelson, R. J.; Akagi, S. K.; Urbanski, S. P.; Wold, C. E.; Griffith, D. W. T.; Johnson, T. J.; Reardon, J.; Weise, D. R. Airborne and ground-based measurements of the trace gases and particles emitted by prescribed fires in the United States. *Atmos. Chem. Phys.* **2011**, *11*, 12197–12216.

(67) Tan, Y.; Lim, Y. B.; Altieri, K. E.; Seitzinger, S. P.; Turpin, B. J. Mechanisms leading to oligomers and SOA through aqueous photooxidation: insights from OH radical oxidation of acetic acid and methylglyoxal. *Atmos. Chem. Phys.* **2012**, *12*, 801–813.

(68) Kasischke, E. S.; Christensen, N. L., Jr; Stocks, B. J. Fire, global warming, and the carbon balance of boreal forests. *Ecological Applications* **1995**, *5*, 437–451.

(69) Flannigan, M.; Stocks, B.; Turetsky, M.; Wotton, M. Impacts of climate change on fire activity and fire management in the circumboreal forest. *Global Change Biology* **2009**, *15*, 549–560.

(70) Pankow, J.; Asher, W. SIMPOL. 1: a simple group contribution method for predicting vapor pressures and enthalpies of vaporization of multifunctional organic compounds. *Atmos. Chem. Phys.* **2008**, *8*, 2773–2796.

(71) EPA U.S. EPA. *Estimation Programs Interface Suite™* for Microsoft® Windows, v 4.00; United States Environmental Protection Agency (U.S. EPA), Washington, DC, **2010**.

Table 5-1. Summary of estimated effective vapor pressure ($p'_{L,eff.}$) and enthalpy of vaporization ($\Delta H_{vap,eff.}$) for glycolaldehyde (GLYDE), methylglyoxal (MGly), and glyoxal (Gly) SOA_{Cld}, and mixtures of organic standards.

Sample	SOA mass Yields [a]	$p'_{L,eff.}$ (atm)	$\Delta H_{vap,eff.}$ (kJ/mol)	Comments RH = 10 – 13% t = 24 – 25°C
GLYDE SOA_{Cld} (10, 40 min)	60–120%	(1–2) × 10^{-7}	~ 70	Aqueous photooxidation of 1mM GLYDE + 10^{-12} M OH radicals. Droplet evaporation. Chapter 2.
MGly SOA_{Cld} (10, 30 min) pH 3–7	5–20% [b]	(3–6) × 10^{-7}	~ 68	MGly + OH cloud mimics and droplet evaporation. Batch and CSTR model assumptions; see Chapter 3.
Gly SOA_{Cld} (10 min) pH 3	100–207% [b]	(1–2) × 10^{-7}	~ 70	Gly + OH cloud mimics and droplet evaporation. Batch and CSTR model assumptions. Chapter 4.
Gly SOA_{Cld} (10 min) pH 7	438% [b]	~ (10^{-8} – 10^{-16})	~ (80 – 120)	Gly + OH cloud mimics, ammonia neutralization and droplet evaporation. CSTR model assumptions Chapter 4.
Organic Acid Mixed Standard	–	(1–2) × 10^{-7}	~ 70	Equal amounts of formic, glycolic, glyoxylic, oxalic succinic, and malonic acid standards. Chapter 2.
Org. Ac. + Glyoxal Mixed Standard	–	~ 1 × 10^{-7}	~ 71	Equal amounts of formic, glycolic, glyoxylic, oxalic succinic, and malonic acid plus glyoxal. Chapter 2.

[a] Defined as PM mass divided by consumed precursor mass. [b] See Appendix F for assumptions and detailed calculations.

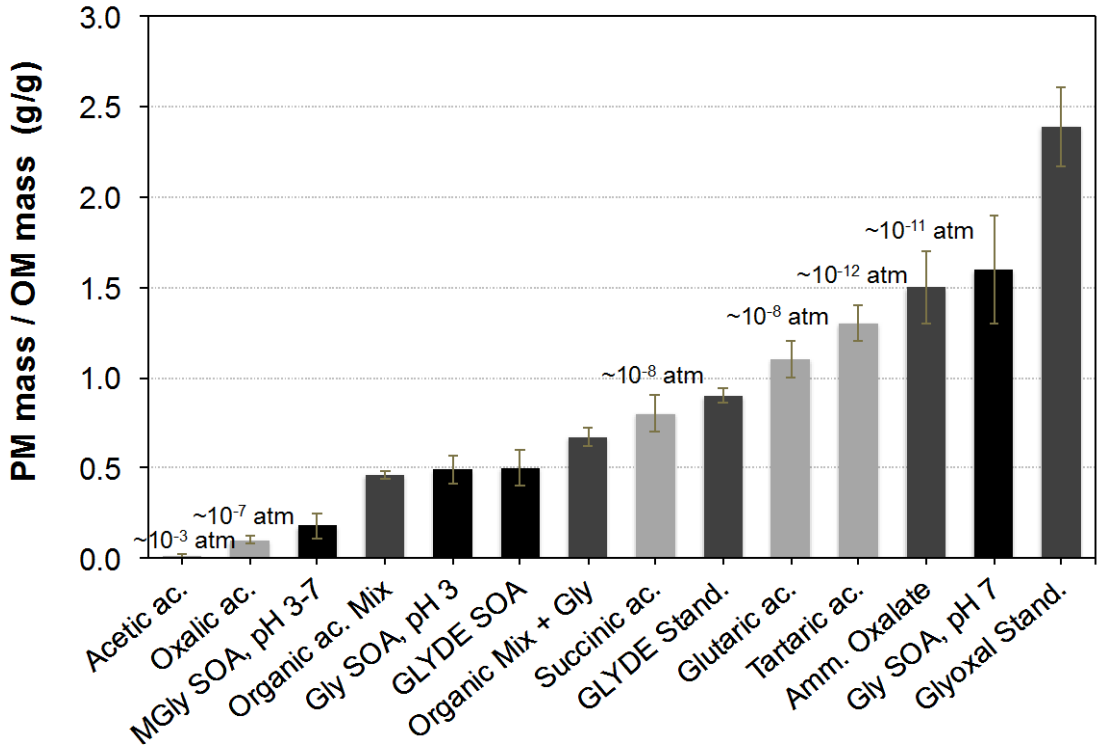

Figure 5-1. Ratios of residual particulate matter mass (PM mass) to the mass of organic matter in the droplet (OM mass). *PM mass / OM mass* reflects the fraction of total droplet OM that remains in the particle-phase after droplet evaporation. Color legend: SOA_{Cld} samples are shown in **black**; organic acid standards in **light grey**; and in **dark grey** samples used for comparison, like glyoxal, glycolaldehyde, and ammonium oxalate standards, as well as mixtures of organic acid standards (w/ and w/o glyoxal; see Table 5-1). Labels indicate liquid vapor pressure estimates of organic acids obtained from SIMPOL group contribution method[70], and the estimated sub-cooled liquid vapor pressure of ammonium oxalate obtained from EPA-EPI Suite™ software[71]. Droplet evaporation experiments were conducted at RH = 10 – 13%, t = 24 – 25ºC, 6 s residence time, and sample reaction times between 10 and 40 minutes (for SOA_{Cld} samples). *PM mass / OM mass* ratios were determined by the slope of PM mass versus OM mass from each sample, as explained in more detail in Chapters 2, 3, and 4. Error bars illustrate the standard error of the slopes.

Appendix A: Supplemental Information for Chapter 2

Appendix A1

Standard Operating Procedure (SOP): Droplet Evaporation System

VOAG & OPC instruments

Table of Contents

1. OVERVIEW

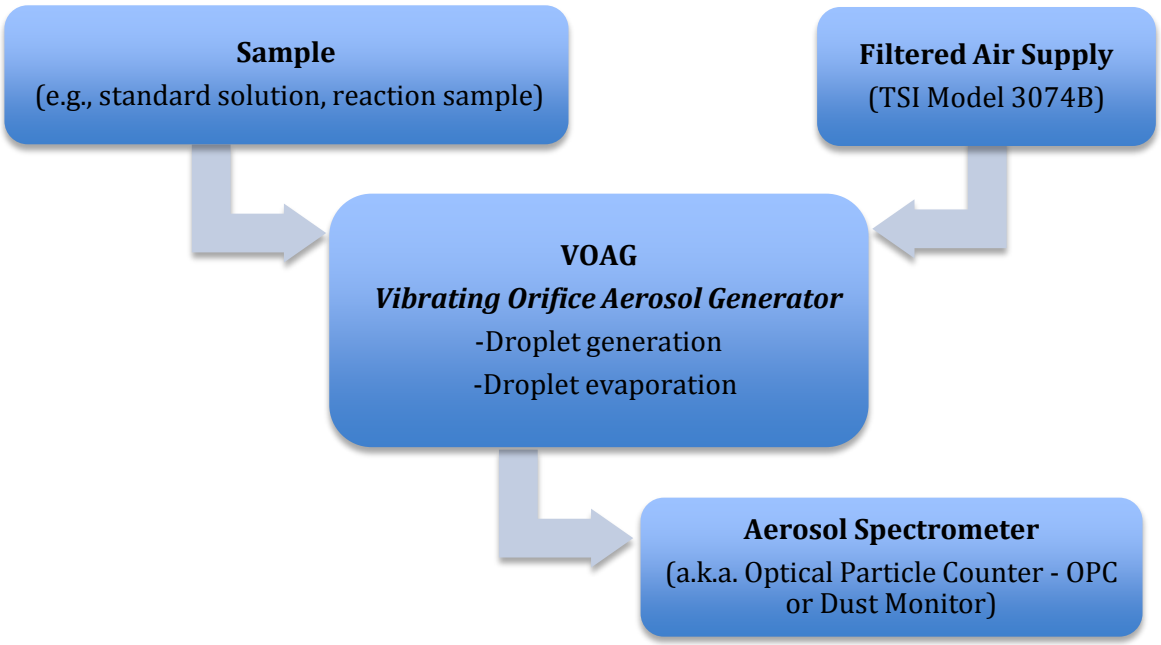

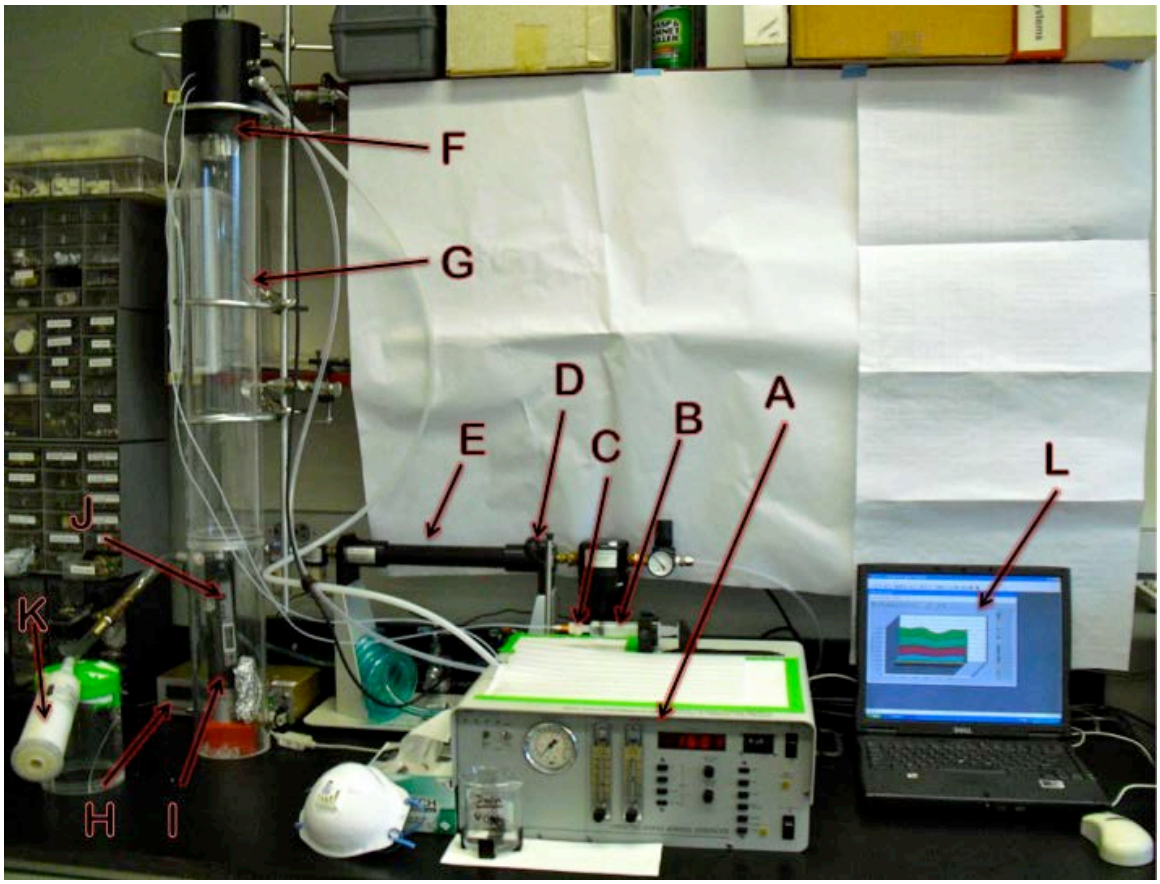

Figure 1. Droplet evaporation system which consists of a Filtered Air Supply (TSI Model 3074B), a vibrating orifice aerosol generator (VOAG TSI Model 3450), and an Aerosol Spectrometer (Grimm Model 1.109) also known as Optical Particle Counter (OPC).

A) VOAG's front panel controls, see Figure 2;
B) syringe with sample (placed in syringe holder and pushed by syringe pump);
C) liquid filter holder (with 0.4 μm Isopore membrane filter from Millipore);
D) halogen lamp
E) filtered air supply, see Figure 3;
F) droplet generator assembly, see Figure 4;
G) drying chamber, see Figure 5;
H) OPC, see Figure 6;
I) ionizer (NRD StaticMaster 2U500, Po-210) to give the particles a Boltzmann charge distribution, see Figure 6;
J) Humidity/Temperature pen (Traceable Model 4093), see Figure 6;
K) HEPA filter (exhaust air);
L) laptop with OPC software (on-screen: real-time histogram of indoor air).

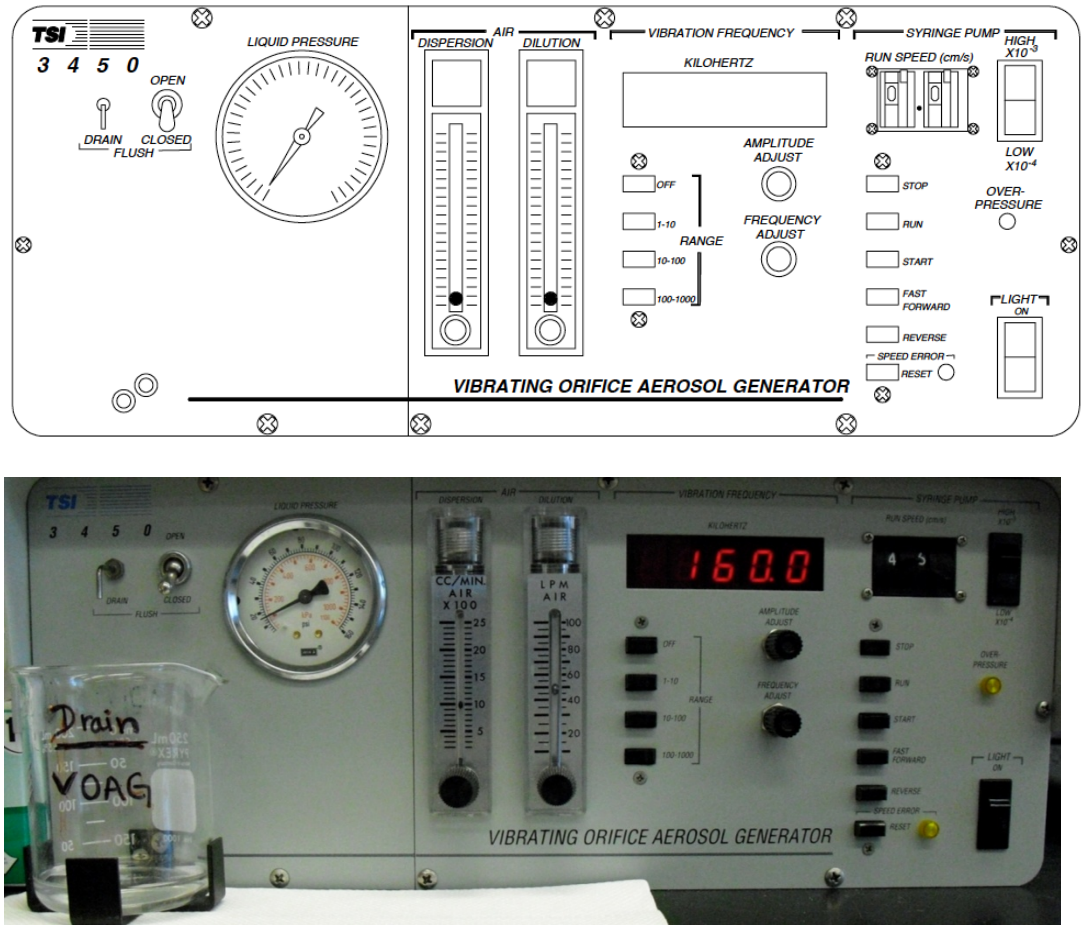

Figure 2. VOAG's Front Panel Controls and Indicators. (Power button on the back)

Figure 3. Filtered Air Supply. From left to right: two coalescing filters (DX and BX grade to remove water/oil and particles), membrane dryer to remove moisture, a final carbon-vapor filter to absorb any remaining oil vapors, and gas regulator for pressure

adjustment.

a)

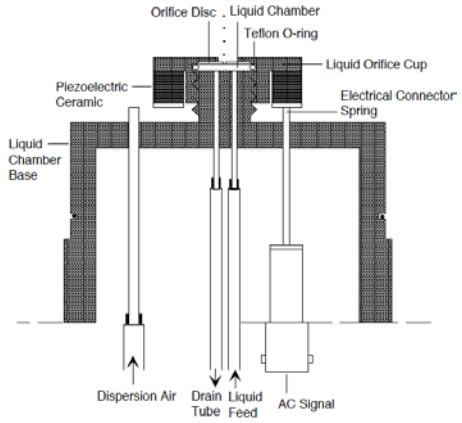

b)

c)

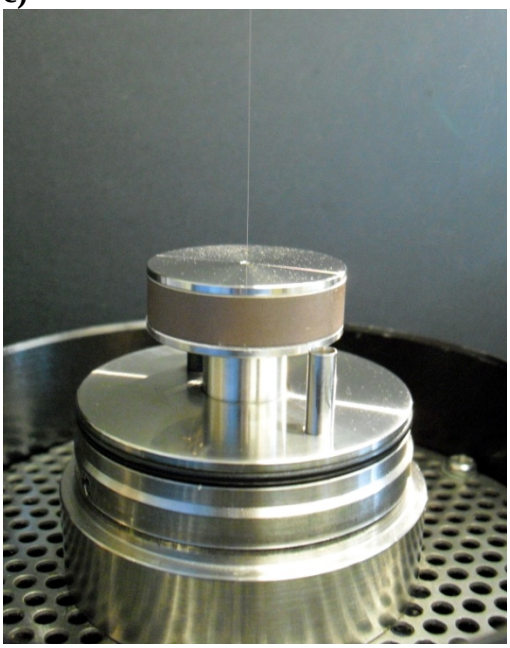

d)

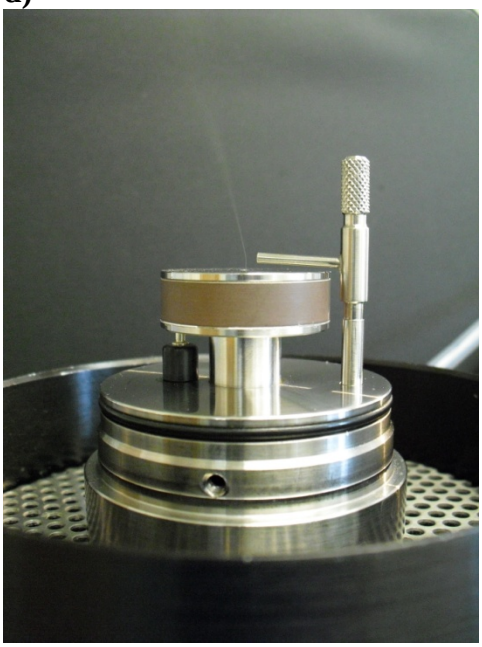

Figure 4. Vibrating orifice assembly; **a**) schematic diagram of the droplet generator; **b**) droplet generator assembly with dispersion cover tighten with two thumbscrews; **c**) liquid jet stream; **d**) assembly with dispersion nozzle; to determine the operating frequency range (section 2.B.b) and for deflection test (section 2.B.c).

Note: This assembly produces uniform droplets by passing filtered solutions through the vibrating orifice, which imparts a periodic disturbance of a set frequency to the liquid jet, producing a controlled and uniform liquid jet breakup [*Berglund & Liu, 1973*]. Also refer to Model 3450 Vibrating Orifice Aerosol Generator, Instruction Manual, October 2002.

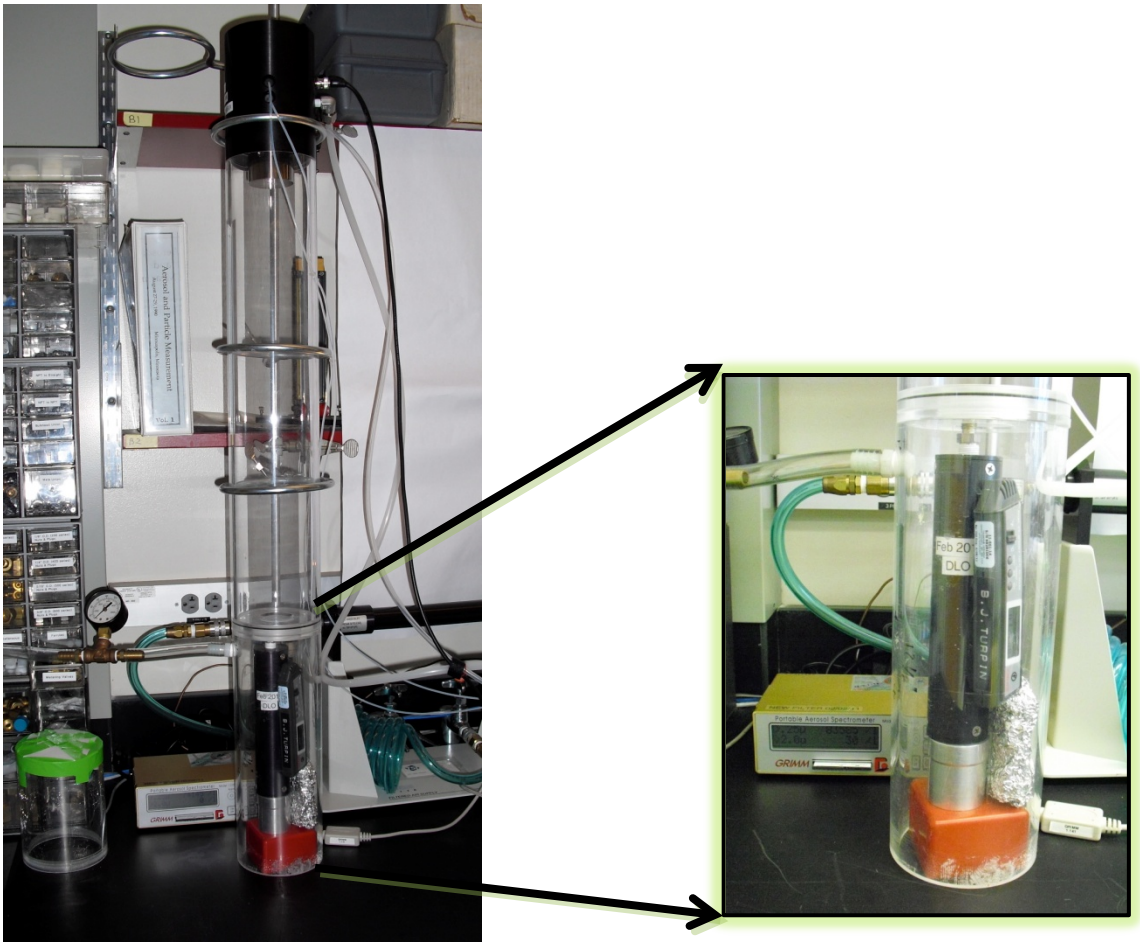

Figure 5. Drying chamber.

Figure 6. Close-up: OPC on the back; Ionizer (inside the black cylinder); Humidity/Temperature pen (to the right of the black cylinder).

Note: The uniform droplet stream (Figure 4) goes through the center of the drying chamber, with a turbulent air jet dispersing the droplets and preventing coagulation. The dispersed droplets merge with a larger volume of filtered dry air, which evaporates water and other volatile components of the droplets, leaving low volatility particles. The diameter of the resulting monodispersed particles will be measured by the OPC placed at the outlet of the VOAG. The OPC measures size and number of particles simultaneously. It uses a laser diode as light source to illuminate particles in a sample volume of air. The scattering light pulse of every single particle is counted and the intensity of its scattering light signal classified to a certain particle size. It estimates the particle size from a manufacturer-calibration curve obtained with monodispersed spherical particles of known size and refractive index (i.e., Poly-Styrene Latex, PSL).

Table 4-2
Nominal Operating Conditions for Aerosol Generator

Orifice Diameter* (µm)	Syringe Capacity (cm^3)	Syringe Pump Run Speed (cm/s)	Liquid Feed Rate (cm^3/min)	Frequency Range* (kHz)	Droplet Diameter Range (µm)
A. Standard operating conditions: continuous and uninterrupted for 0.3 to 2.5 hours					
100	60	6.6×10^{-3}	2.2	1–10	191–412
50	60	1.8×10^{-3}	0.59	8–20	98–132
35	60	9.1×10^{-4}	0.30	15–50	58–86
20	20	8.2×10^{-4}	0.139	40–80	38–48
10	10	8.2×10^{-4}	0.080	150–300	21–26
B. Optional operating conditions: continuous and uninterrupted for 4 to 6 hours					
20	60	4.2×10^{-4}	0.139	40–80	38–48
10	20	4.6×10^{-4}	0.080	150–300	21–26

*These values are nominal. Due to normal manufacturing tolerances, the orifice and droplet diameters may differ from the nominal values by ±25% and the frequency by a factor of two. The actual operating frequency range for each orifice should be determined by the jet-deflection method described in "Tuning the Generator to Proper Operating Frequency" in this chapter. The droplet diameter is then calculated by using equation 6 in Appendix A.

Table 4-3
Syringe Pump Operating Modes

Mode	Explanation
Stop	Stops the syringe pump motor. Note that the syringe pump automatically stops when the ram has traversed the entire length of the lead screw, whether moving forward or backward.
Start	Starts the syringe running at a higher speed and torque to get a quick buildup of pressure in the system by forcing the liquid through the tiny orifice.
Run	Runs the pump at slow, steady pressure for stable aerosol generation. Note that if the torque on the ram gets too high, the pump may stall even if the system pressure is too low. This can be due to the plunger becoming sticky (particularly with larger syringes), or to the lead screw becoming coated with contaminants.
Fast-Forward	Moves the ram rod quickly forward to close the gap between the ram and the syringe plunger.
Reverse	Quickly moves the ram back from the syringe to allow installation of a new, full syringe. Note that the reverse mode may not work if the system pressure is too high. To relieve the pressure, open the drain valve an try the Reverse mode again.

2. PRE-SAMPLING

A. Cleaning procedure

a. Syringes

All samples are injected into the system using 25 mL syringes. These need to be previously ultrasonicated (for 15 minutes) and thoroughly rinsed with 18 MOhm milli-Q water. Fill clean syringes with 18 MOhm milli-Q water until ready to use.

b. VOAG

Before any experiment the system must be flushed with enough reagent grade isopropyl alcohol followed by milli-Q water. If the system is not used on a regularly basis flush the system with about 50 mL of isopropyl alcohol (reagent).

To flush the liquid feed system, follow these steps.

1. Make sure the 250 mL beaker is in the mounting bracket on the front panel. (Figure 2)

2. Open the drain valve. (See Figure 2; “OPEN” on “FLUSH”). Press the POWER button on the back of the VOAG.

3. Fill a 25 mL syringe with reagent grade isopropyl alcohol.

4. Slide the syringe into the syringe holder found next to the pump or already attached to a stationary syringe. (black metallic ring)

5. Attach the filled syringe to the filter holder and place the syringe on the pump (Figure 1). [It is good practice to visually check the 0.4 μm Isopore membrane filter (inside the filter holder) for any slits, before attaching the syringe to the filter holder. *See instructions bellow to change the filter.]

6. Tighten the thumbscrew into the syringe holder.

7. Make sure the syringe pump run speed is set to 4.6×10^{-4} cm/s. (Figure 2; “SYRINGE PUMP”). [Use Table 4.2 of VOAG’s Instruction Manual, also included in this SOP, to use the correct settings suitable for the orifice and syringe being used. Standard operation of VOAG in our laboratory is a 10 μm nominal orifice with a 20 - 25 mL syringe.]

8. Press FAST FORWARD to start the pump in the Fast-Forward mode. (To be familiarized with the operating modes of the syringe pump see Table 4.3 of VOAG’s Instruction Manual, also included in this SOP). When the pump ram

makes contact with the syringe, switch the pump to the START mode (Figure 2). Check that the liquid is flowing through the tubing and coming out from the drain. Also check that bubbles in the tubing have been carried out of the system by the liquid flow.

9. When the syringe is empty (or has stopped), press REVERSE and detach the empty syringe from the filter holder. [Note: when the syringe ram is in the full-forward position, meaning the syringe is empty, the pump will indicate a SPEED ERROR and a light comes on in the right bottom corner of VOAG's Front Panel (Figure 2). Once you press REVERSE the light should go off.]

Perform the following steps to change the filter:

1. Place the 0.4 μm Isopore membrane filter between the screen and the round gasket with the screen on the downstream side to support the filter.

2. Screw the filter holder together tightly by hand.

3. Saturate the filter with isopropanol.

4. Flush the liquid system with at least 50 cm^3 of isopropanol each time you change the liquid filter.

5. Check the filter holder for leaks by wiping the filter case with an absorbent tissue and rechecking it a few minutes later. If the filter holder is wet, it is leaking. Tighten the filter holder or replace it with a new one.

B. Liquid jet stream

a. How to start the liquid jet stream

The liquid jet must be first started with reagent grade isopropyl alcohol in a syringe to verify that the orifice is clean, then replace the syringe of alcohol with a syringe of milli-Q water or sample solution.

To start the liquid jet, refer to Table 4-3 and follow these steps:

1. Loosen the two thumbscrews that attach the dispersion cover to the droplet generator assembly (Figure 4b).

2. Remove the dispersion cover by covering the hole in the cover with your thumb and turning on the dispersion air. This forces the cover off and exposes the piezoelectric ceramic.

3. Place the alcohol-filled syringe on the syringe pump. Make sure the drain valve is open. Start the pump in the FAST FORWARD mode. When the pump ram makes contact with the syringe, switch the pump to the START mode. When the syringe has been half-emptied and there are no air bubbles in the liquid feed line, CLOSE the drain valve. Pressure builds up quickly and the liquid jet starts.

> Note: If the liquid jet does not start, use an absorbent tissue (or lens cleaning paper) to wipe off any accumulated liquid above the orifice while the pump is in the START mode. If the jet still fails to start, OPEN the drain valve.

4. Switch the pump to the RUN mode. Use the halogen light to look at the jet stream (switch is at the bottom right corner of control panel; “LIGHT” Figure 2). Verify that the jet is consistent and perpendicular to the face of the orifice plate (Figure 4c). If you cannot start the jet, refer to the orifice cleaning procedure in the Section 2.B.d. or refer to Chapter 5 of VOAG’s Instruction Manual.

5. REVERSE the pump and release pressure in the system by opening the drain valve. Remove the alcohol-filled syringe.

6. Install the water solution-filled syringe on the syringe pump. Start the pump in the FAST FORWARD mode. Hold the syringe in place for proper contact. When the pump ram makes contact with the syringe, switch the pump to the START mode. Make sure any air bubbles from the syringe or filter holder at the tip of the syringe pass through the system and out the drain, and close the drain valve. Pressure builds up quickly and the liquid jet starts. Cover with the pretend-mini-drying-chamber shown in the bottom left corner of Figure 5 (with bright green tape on the top to hold filter).

> Note: If the liquid jet does not start, use an absorbent tissue (or lens cleaning paper) to wipe off any accumulated liquid above the orifice while the pump is in the START mode. If the jet still fails to start, OPEN the drain valve.

7. Repeat step 4.

8. Allow the pressure in the system to decrease and stabilize. Depending on how high the pressure was before you switched to the RUN mode, and on the size of the orifice, the pressure usually takes five minutes or more to stabilize. Place a

> Note: Most orifices stabilize at pressures between 5 and 30 pounds per square inch. The larger orifices stabilize at pressures below 5 pounds per square inch and may not be detectable on the pressure gauge.

9. When the pressure is stable, tune the signal generator to the proper operating frequency using the following procedure.

b. Setting Proper Operating Frequency

Observe the jet stream while you change the frequency and amplitude settings.

1. Start the jet stream and allow at least 5 minutes for the liquid feed rate to stabilize. [While waiting cover the jet stream with the pretend-mini-drying-chamber shown in the bottom left corner of Figure 5 (with bright green tape on the top to hold filter).]

2. Attach the small stainless-steel elbow (the deflection nozzle) to the dispersion air outlet (Figure 4d).

3. Set the dispersion air to 700 cm^3/min (between 5 and 10 on the DISPERTION rotameter; Figure 2).

4. Start the signal generator by pushing the "10–100" range button and set the FREQUENCY ADJUST to the bottom of the range given in Table 4-2 above for the orifice installed (i.e., for a 10 μm orifice begin at 150 kHz).

5. Set the AMPLITUDE ADJUST to nearly full-scale.

6. Gradually increase the frequency and watch the jet carefully.

7. When the droplets are uniform, the jet is deflected as a single stream (see figure below; Figure 4-3 of VOAG's Instruction Manual). When the frequency has reached the upper limit of the frequency range (f_{max}) for the specific orifice, the droplets become nonuniform and the jet appears as a nonuniform spray (upper left corner of the figure bellow). Uniform droplets can generally be produced over a range of frequencies from f_{max} to 0.5 f_{max} and lower. However, within this frequency range are isolated bands of frequencies in which satellite droplets are produced. Since the satellite droplets are smaller and likewise very uniform, they are deflected as a separate stream (upper right drawing of the figure bellow). The satellites can sometimes be eliminated by reducing or increasing the amplitude on the signal generator.

8. Make a note of the frequency range for future reference.

Note: The f_{max} is independent of the constituents of the solution, so the solution can be changed without doing the operating range test each time.

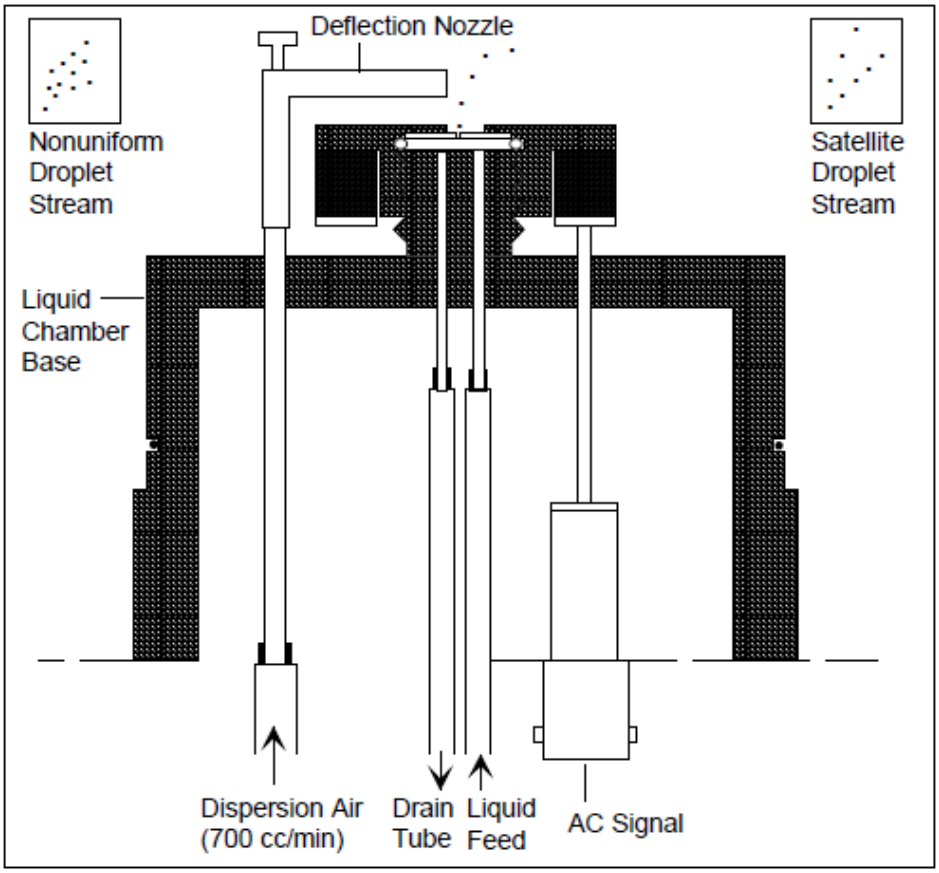

Figure 4-3
Checking Droplet Uniformity

c. Deflection test

You should perform the following test each time you restart the liquid jet. This is to check that a particular frequency setting is producing monodisperse droplets (no satellites).

1. Repeat steps 1-3 of section 2.B.b *"Setting Proper Operating Frequency"*.

2. Start the signal generator by pushing the "10–100" range button and set the FREQUENCY ADJUST at a frequency equal to 0.6 f_{max} (determined by the operating range test above).

4. Set the amplitude to nearly full-scale.

5. Remove the deflection nozzle, put the dispersion cover back on the droplet generator assembly, and tighten the two thumbscrews (Figure 4b).

d. Orifice cleaning procedures – for clogging issues

i. Back-flushing the orifice

This consists of back-flushing the orifice with air. You won't need to disassemble the droplet generator and hence it should be performed before the two procedures discussed next.

1. Turn off the syringe pump.

2. OPEN the drain valve.

3. Install a dispersion cap over the generator head. (Do not lock in place with thumbscrews.)

4. Turn on the dispersion air.

5. Press your thumb on the outlet to the dispersion cap, building up pressure that can only escape by back-flushing through the orifice and out the drain valve. [You can bear down on the outlet with a great deal of pressure. When enough pressure builds up, the dispersion cap pops off the O-ring. You must force enough air through the orifice to ensure the particles that were plugging it are pushed far enough toward the drain valve to prevent re-plugging of the orifice. A small amount of bubbling or spurting at the drain valve indicates that back-flushing has occurred.]

6. CLOSE the drain valve.

7. Restart the droplet generator with clean isopropanol and allow it to run for at least 10 minutes.

ii. Soaking in detergent solution

If back-flushing does not work soak the orifice in a filtered detergent solution. This requires disassembling the droplet generator first; refer to ***"Removing the Orifice Disk"***, page 5-2 of VOAG's Instruction Manual. To learn how to make the filtered detergent solution and how to clean the orifice please go to ***"Cleaning the Orifices"***, page 5-5 of VOAG's Instruction Manual. To place the orifice back in the droplet generator follow the instructions for ***"Replacing the Orifice Disk"*** in page 5-3 of VOAG's Instruction Manual. For more information refer to ***"Troubleshooting"*** in page 5-8 of VOAG's Instruction Manual.

iii. Gently brushing with HCl

If nothing seems to work, do the following procedure as a last resource. [Note: do NOT sonicate the orifice!]

1. Take the orifice out of the droplet generator following the instructions on page 5-2 of VOAG's Instruction Manual (***"Removing the Orifice Disk"***).

2. Place the orifice on a clean glass surface.

3. Put two or three droplets of 0.1M HCl on the orifice for less than 3 minutes.

4. Gently brush the orifice with a soft fine brush, keeping track of time (no more than three minutes).

5. Quickly rinse the orifice in filtered water.

6. Rinse the orifice in filtered isopropanol.

7. Place the orifice back in the droplet generator, following the instructions for ***"Replacing the Orifice Disk"*** in page 5-3 of VOAG's Instruction Manual.

C. Preconditioning the Drying Chamber

The drying chamber must be set at a relative humidity of 10% before sampling can be performed. This is done by flowing air through the drying chamber until it reaches RH = 10%. You can do this while preparing samples or right after starting the liquid jet with isopropanol.

1. Turn on the Humidity/Temperature pen (Traceable Model 4093) and place it inside the drying chamber as shown in Figures 1, 5, and 6.

2. Make sure the droplet generator has the dispersion cap and is tighten with the thumbscrews (Figure 4b).

3. Place the droplet generator on top of the drying chamber as shown in Figure 1.

4. Set the dispersion air to 1000 cm^3/min or more (between 10 and 15 on the DISPERTION rotameter; Figure 2).

5. Set the dilution air to 50 lpm (DILUTION rotameter; Figure 2).

6. Wait until the hygrometer reads RH = 10%.

D. Calibration

Due to manufacturing tolerances the orifice and droplet diameters may differ from the nominal values by ±25%; hence, the droplet diameter is determined by calibrating the system with ammonium sulfate, $(NH_4)_2SO_4$ (3.1801 M, Fluka Analytical). The slope of D_p vs. $C^{1/3}$, from the relation $D_p = D_d\, C^{1/3}$, indicates the diameter of the generated droplets – where: D_d is droplet diameter (µm), D_p is particle diameter (µm), and C is the volumetric concentration of the solute in the solution ($cm^3_{solute}/cm^3_{solution}$). The calibration should be performed before and after a project (involving different experiments) is concluded, a mid-project calibration is also suggested.

1. Prepare different dilutions of ammonium sulfate and store them for multiple calibrations. Note: always store the WATER used to prepare the solutions as it ALSO need to be sampled.

2. Fill syringes with the ammonium sulfate solutions and sample them through the VOAG-OPC system as discussed in the following sections.

3. After gathering the data, plot D_p vs. $C^{1/3}$ and report the slope of the linear regression as D_d (be aware of unit conversion).

3. SAMPLING

A. Sample Preparation

If you will analyze standard solutions, make sure to store and keep the WATER you used to prepare the solutions since it needs to be sampled as well. If you will analyze samples from the reaction vessel, store and keep enough dynamic water blank for analysis. Refer to the corresponding SOP's for best practices on how to prepare samples.

You will need to prepare a succinic acid standard solution as well as a standard solution of ammonium sulfate (with their corresponding water). These will be used to evaluate the reproducibility and accuracy of the VOAG, respectively. Therefore make sure the concentrations used are always the same (currently using 60 µM and 750 µM for succinic acid and 250 µM for ammonium sulfate). These solutions should be sampled at the BEGINNING and END of each day of experiments to check that the VOAG is working properly before and after sampling the solutions of interest.

1. Fill syringe with sample solution.

2. Repeat steps 6-8 of section 2.B.a ***"How to start the liquid jet stream"***, but with sample solution instead of water. Note: keep in mind that the corresponding water used to prepare the sample needs to be sampled as well on the same day.

3. Follow instructions described in section 2.B.c ***"Deflection test"*** to check that the droplets are monodispered. [Note: FREQUENCY has to be the same for all samples]

4. Place the dispersion cap and tighten with the thumbscrews (Figure 4b).

5. Make sure the Humidity/Temperature pen (i.e., hygrometer) is turned on and inside the drying chamber.

6. Place the droplet generator on top of the drying chamber as shown in Figure 1.

7. Set the dispersion air to 1000 cm^3/min or more (between 10 and 15 on the DISPERTION rotameter; Figure 2). [Note: you should be consistent with this setting]

8. Set the dilution air to 50 lpm (DILUTION rotameter; Figure 2).

9. The hygrometer should read RH = 10%, if it is higher then wait until the humidity is 10%.

10. Record the parameters and settings as presented below.

11. Start the OPC system (see section 3.C ***"OPC Measurements"***).

B. Record Entry: Template and Example

VOAG settings:

Orifice = _____
Run Speed = _____ Droplet diameter = _____
Liquid feet rate, Q = _____ Operating Frequency = _____

__ check here if VOAG was cleaned with isopropanol (reagent grade) and water

Location (GRIMM Folder) :_____

Sample name = _____
Date = _____
OPC File name = _____

Frequency = _____ Dispersion air = _____
Stable pressure = _____ Dilution air = _____

Start time = _____ RH = _____ @ _____°C
End time = _____ RH = _____ @ _____°C

Example of a 10 µm orifice that was installed in the droplet generator on May 24th 2010; hence ID # 100524 (e.g., year-month-day):

VOAG settings:

Orifice = 10 µm ID # 100524
Run Speed = 4.6 x 10^{-4} cm/s
Liquid feet rate, Q = 0.077 cm^3/min (measured in our system)
Droplet diameter = ~18.3 µm (based on calibrations)
Operating Frequency = ~ 160 kHz

✓ check here if VOAG was cleaned with isopropanol (reagent grade) and water

Location (GRIMM Folder): (write name of folder where data will be stored)

Sample name = (name your sample; e.g., concentration, compound, date prepared, #)
Date = (write the date of experiment)
OPC File name = (write date followed by short sample name – This is the file name you will save in the OPC software for this sample)

(read the following from VOAG's control panel at start of OPC sampling)
Frequency = 160.0 kHz Dispersion air = 10 cc/min x 100
Stable pressure = ~23 psi Dilution air = 50 Lpm

(read the following from OPC software and from Humidity/Temperature pen at the beginning and end of each sample run)
Start time = (hour:minutes:seconds) RH = 10 % @ 24.4 °C
End time = (hour:minutes:seconds) RH = 10 % @ 24.3 °C

C. OPC measurements

1. Make sure the OPC is connected to the laptop via USB-to-serial port cable.
2. Connect the OPC to the outlet and press the POWER button.
3. You will shortly hear a beep sound and a filter test question will show up on the digital screen of the OPC. It will ask whether or not the filter has been changed.
4. Press the "–" key to indicate that the filter has not been replaced. [This is done when the interest is on particle SIZE measurements; if the interest is on MASS then must refer to the OPC manual for instructions on how to change filter for mass measurements].
5. After responding to this question the OPC will conduct a self-test. The OPC will do a self-test prior to every instrument start in order to verify the proper functioning of the instrument. The self-test takes about half a minute. After successful completion of the self-test, the instrument will display the message SELF TEST OK.
6. The OPC will automatically start measuring the particles but the data will not be stored until you create a file in the software.

7. On the desktop, click on the “Dust Monitor” icon. This will open GRIMM Software # 1.177 – Version 3.30.
8. Click on the first icon on the upper left corner (below the “File” tab). The icon symbol looks like a page and should read “New Measurement” when you place the cursor on the icon.
9. Once you click “New Measurement” a window pops out titled “Online Measurement”; see figure below:

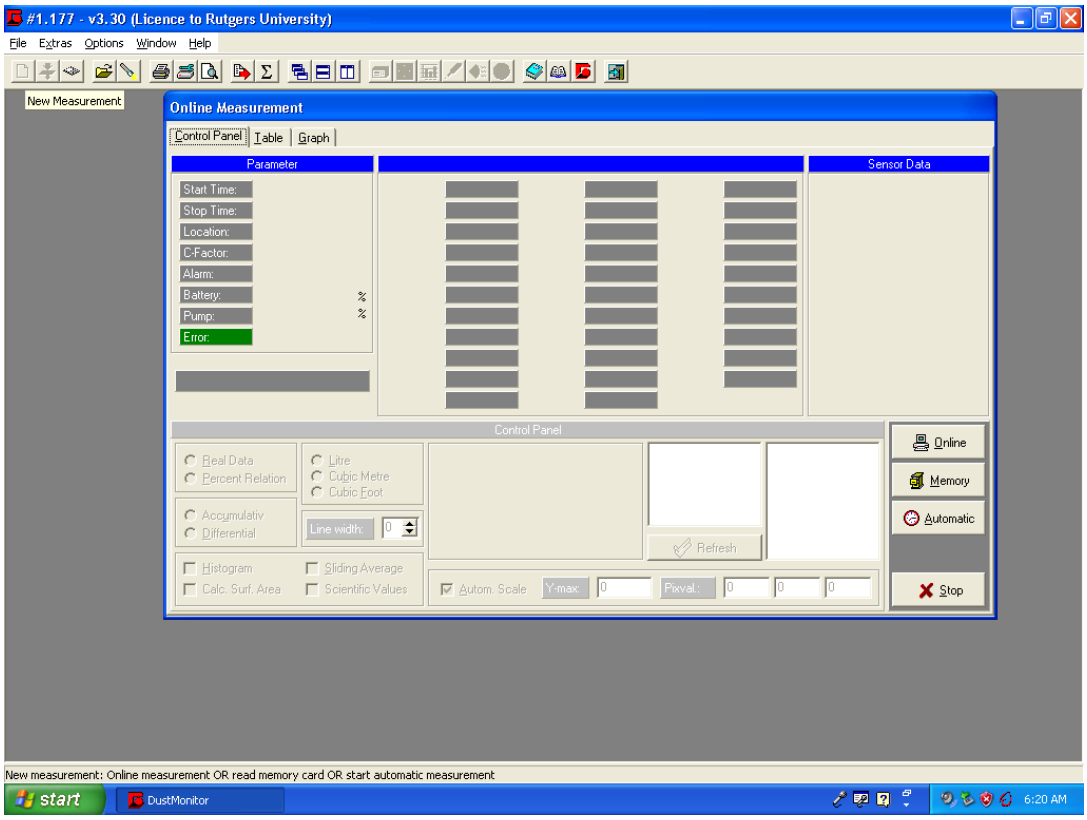

10. Always wait for at least 3 minutes after the droplet generator has been placed on top of the drying chamber. This will help flush ambient particles. Make sure three or more minutes have passed before continuing with the next steps.
11. Click “Online” on the bottom right corner of the “Online Measurement” window.
12. On the “Save As” window that opens up, use the “Save in” drop-down list to select a folder or create a new folder where you want to save your data [Note: record the name of this folder and location/path in the “Location (GRIMM Folder)”, see section 3.B of ***Record Entry***]. Name the file on the “File name” box and write this file name on your records (see “OPC File name” on the record entry section 3.B). See figure below:

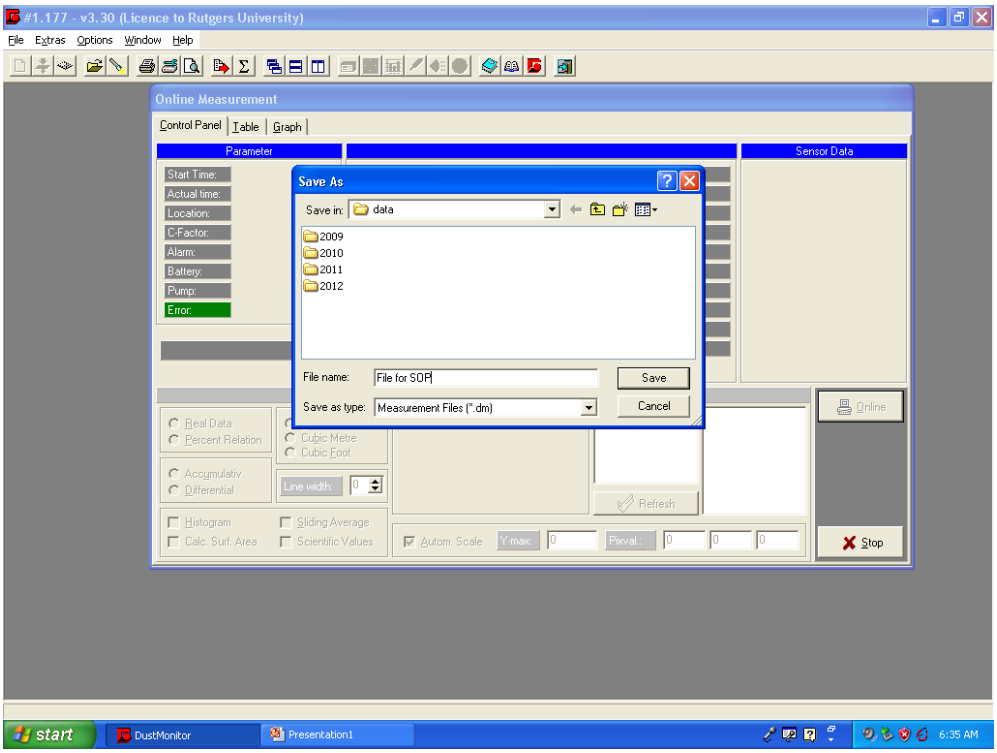

13. Click “Save”.
14. Wait until the OPC finish the self-tests and the “Control Panel” of the “Online Measurement” windows starts to populate; see figure below:

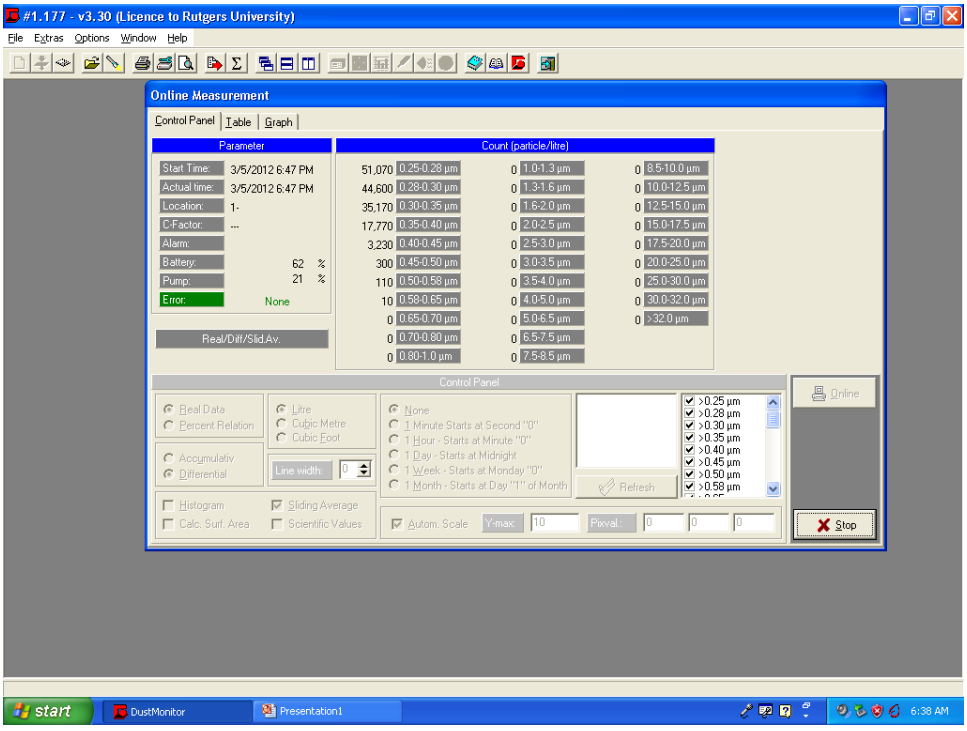

15. Once you see that the measurements appear in the “Control Panel” click on the “Table” tab. See figure below:

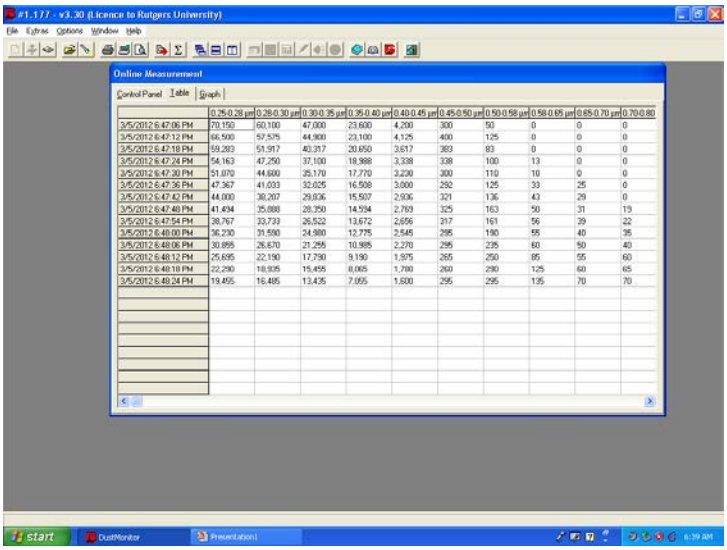

16. The first column will indicate the start time of the sample. Record the time on the “Start time” section of the record entry (see section 3.B).
17. Check the humidity and temperature reading in the hygrometer (underneath the drying chamber) and write them next to the “Start time” (see section 3.B).
18. Read from VOAG’s control panel and write the “Frequency”, “Stable pressure”, “Dispersion air”, and “Dilution air”. Make sure these values are in agreement with the specifications discussed in section 3.A. At this point you could only adjust the Frequency, Dispersion air, or Dilution air if needed.
19. After the appropriate information has been documented click on the “Graph” tab in the “Online Measurement” window. This will show you the real-time measurements in form of a histogram. See the figure below for an example of the histogram of ambient indoor particles in our laboratory:

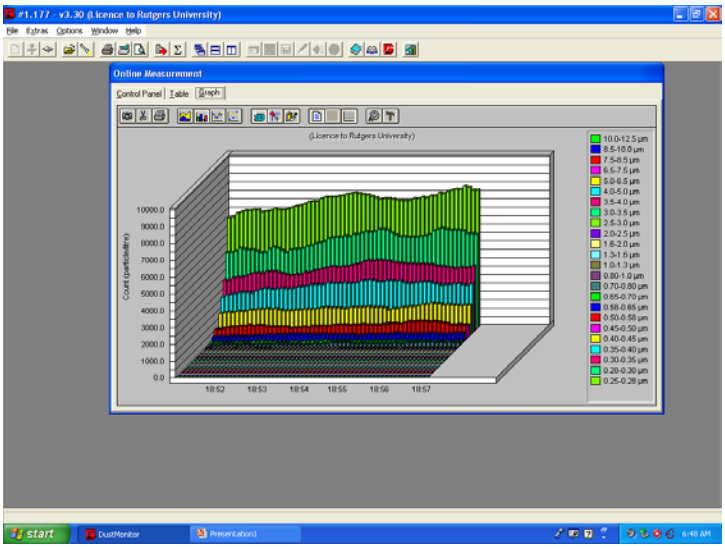

20. Make sure the signal is strong and stable. You will need about 10 minutes of clear and stable signal for data analysis. Make sure to make a note of the specific time this takes place. [Note: sometimes the signal will take longer to stabilize and so the "Star time" reported earlier should not be used for data analysis, instead use the time you make a note of in your records].
21. You can click on the icon with the camera symbol (upper left corner) in the "Graph" window to take a snapshot of the histogram and paste into powerpoint or word document. (Optional but recommended for a quick visual track of your samples).
22. When 10 minutes of stable signal have passed, click on the "Control Panel" tab on the "Online Measurement" window and then click "Stop".
23. Click on the "Table" tab and record the "End time" in your documents (see section 3.B).
24. Read the humidity and temperature displayed in the hygrometer (underneath the drying chamber) and write them next to the "End time"
25. Go back to the "Control Panel" tab on the "Online Measurement" window and click "End".
26. When all the samples for the day have been analyzed you must export all the files in order to process the data in excel at a later time. To export the files, click on the 9th icon from left to right on the Dust Monitor home window. This icon symbol has a red arrow pointing to the right and reads "Export data" when you put the cursor on the icon.
27. A window opens with the name "Export data to an ASCII file". On 'Separator' select 'comma'. On 'Data' select 'Measurement data'. On 'Unit Parameter' select 'headline'. Click on "Export Data". See figure below:

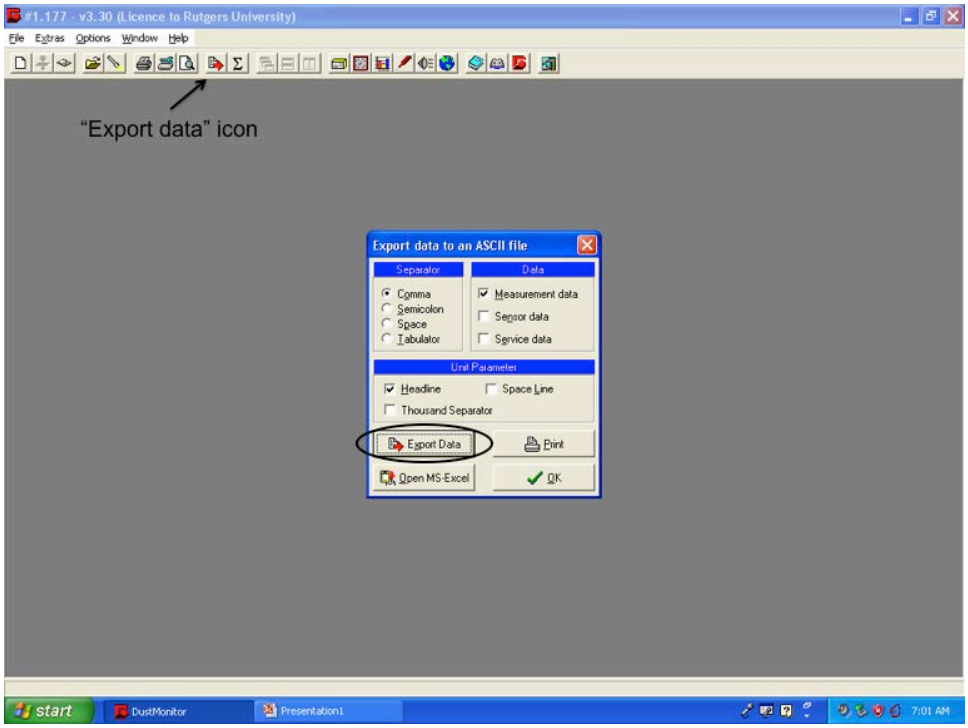

28. A new window opens titled “Open”, browse for the folder you selected or created on step 12. Open the folder and highlight/select ALL the files (you can press Control + A in your keyboard to select all), then click ‘Open’.
29. Click “Ok” on the “Information” window that pops up.
30. Finally, click “Ok” in the “Export data to an ASCII file” window.

4. SHUTDOWN

A. OPC shutdown

Close the GRIMM software and press the OPC’s POWER button. Make sure to turn off the Humidity/Temperature pen (i.e., hygrometer).

B. Post-cleaning

Please follow the Cleaning Procedure for the VOAG system (Section 2.A.b) and the syringes (Section 2.A.a).

C. VOAG shutdown

After cleaning the VOAG system, press the POWER button on the back of the VOAG and make sure that the droplet generator assemply has the dispersion cover on with thumbscrews (see Figure 4.b). Is good practice to conceal the hole in the dispersion cover with parafilm to avoid contamination and clogging from indoor particles.

5. OPC DATA PROCESSING

The OPC’s GRIMM Software generates data files (.txt format) with the following key information:

File name, Date/time of sample, Count (particle/liter) every 6 seconds for each size bin:

(0.25-0.28 µm), (0.28-0.30 µm), (0.30-0.35 µm), (0.35-0.40 µm), (0.40-0.45 µm), (0.45-0.50 µm), (0.50-0.58 µm), (0.58-0.65 µm), (0.65-0.70 µm), (0.70-0.80 µm), (0.80-1.0 µm), (1.0-1.3 µm), (1.3-1.6 µm), (1.6-2.0 µm), (2.0-2.5 µm), (2.5-3.0 µm), (3.0-3.5 µm), (3.5-4.0 µm), (4.0-5.0 µm), (5.0-6.5 µm), (6.5-7.5 µm), (7.5-8.5 µm), (8.5-10.0 µm), (10.0-12.5 µm), (12.5-15.0 µm), (15.0-17.5 µm), (17.5-20.0 µm), (20.0-25.0 µm), (25.0-30.0 µm), (30.0-32.0 µm), (>32.0 µm).

1. Open a New Excel Workbook and IMPORT OPC's .txt file. Excel will ask you to choose which file to open, you must browse to find the desired file, which will have the "OPC File name" as recorded in the data entry, see Section 3.B.

   Select the following in the Text Import Wizard:

   Original data type (file type): "Delimited"

   Click "Next >"

   Delimiters: "Tab" and "Comma"

   Click "Finished" and then OK.

2. The excel spreadsheet will be populated with the data from the .txt file and it will automatically generate labels for each column. See figure below:

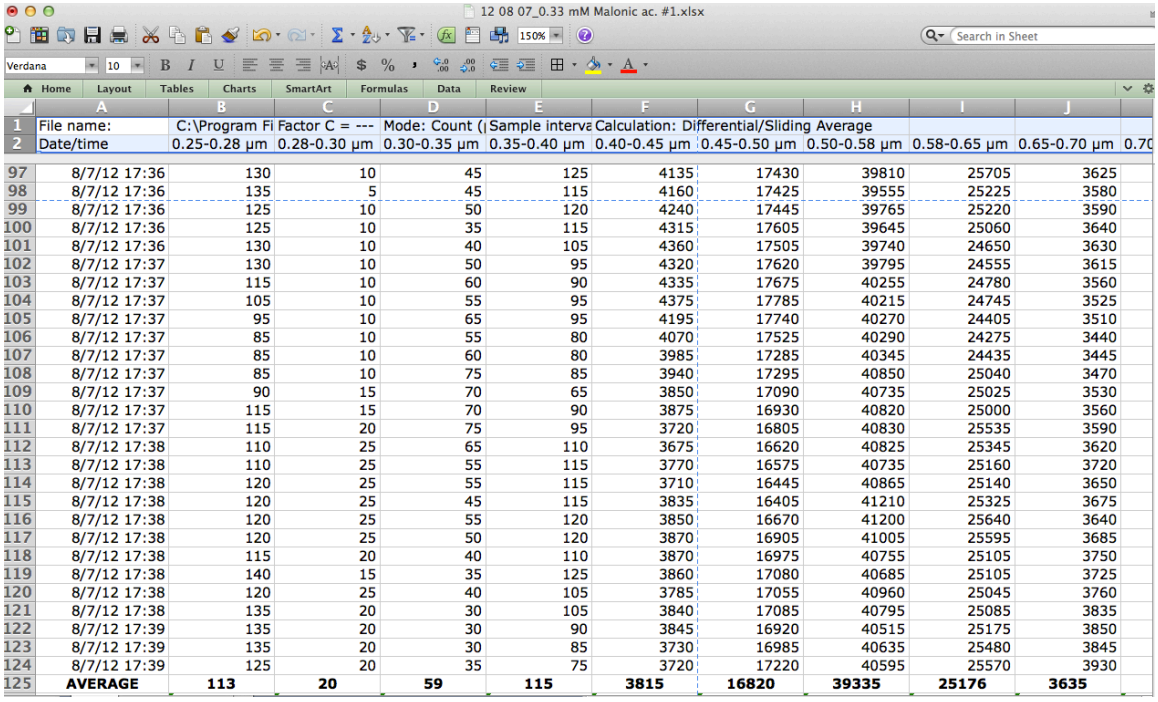

12 08 07_0.33 mM Malonic ac. #1.xlsx

	A	B	C	D	E	F	G	H	I	J
1	File name:	C:\Program Fi	Factor C = ---	Mode: Count ((	Sample interva	Calculation: Differential/Sliding Average				
2	Date/time	0.25-0.28 µm	0.28-0.30 µm	0.30-0.35 µm	0.35-0.40 µm	0.40-0.45 µm	0.45-0.50 µm	0.50-0.58 µm	0.58-0.65 µm	0.65-0.70 µm	0.7(
97	8/7/12 17:36	130	10	45	125	4135	17430	39810	25705	3625	
98	8/7/12 17:36	135	5	45	115	4160	17425	39555	25225	3580	
99	8/7/12 17:36	125	10	50	120	4240	17445	39765	25220	3590	
100	8/7/12 17:36	125	10	35	115	4315	17605	39645	25060	3640	
101	8/7/12 17:36	130	10	40	105	4360	17505	39740	24650	3630	
102	8/7/12 17:37	130	10	50	95	4320	17620	39795	24555	3615	
103	8/7/12 17:37	115	10	60	90	4335	17675	40255	24780	3560	
104	8/7/12 17:37	105	10	55	95	4375	17785	40215	24745	3525	
105	8/7/12 17:37	95	10	65	95	4195	17740	40270	24405	3510	
106	8/7/12 17:37	85	10	55	80	4070	17525	40290	24275	3440	
107	8/7/12 17:37	85	10	60	80	3985	17285	40345	24435	3445	
108	8/7/12 17:37	85	10	75	85	3940	17295	40850	25040	3470	
109	8/7/12 17:37	90	15	70	65	3850	17090	40735	25025	3530	
110	8/7/12 17:37	115	15	70	90	3875	16930	40820	25000	3560	
111	8/7/12 17:37	115	20	75	95	3720	16805	40830	25535	3590	
112	8/7/12 17:38	110	25	65	110	3675	16620	40825	25345	3620	
113	8/7/12 17:38	110	25	55	115	3770	16575	40735	25160	3720	
114	8/7/12 17:38	120	25	55	115	3710	16445	40865	25140	3650	
115	8/7/12 17:38	120	25	45	115	3835	16405	41210	25325	3675	
116	8/7/12 17:38	120	25	55	120	3850	16670	41200	25640	3640	
117	8/7/12 17:38	120	25	50	120	3870	16905	41005	25595	3685	
118	8/7/12 17:38	115	20	40	110	3870	16975	40755	25105	3750	
119	8/7/12 17:38	140	15	35	125	3860	17080	40685	25105	3725	
120	8/7/12 17:38	120	25	40	105	3785	17055	40960	25045	3760	
121	8/7/12 17:38	135	20	30	105	3840	17085	40795	25085	3835	
122	8/7/12 17:39	135	20	30	90	3845	16920	40515	25175	3850	
123	8/7/12 17:39	135	20	30	85	3730	16985	40635	25480	3845	
124	8/7/12 17:39	125	20	35	75	3720	17220	40595	25570	3930	
125	**AVERAGE**	**113**	**20**	**59**	**115**	**3815**	**16820**	**39335**	**25176**	**3635**	

3. Calculate the average count for each size bin, as shown in the figure above. Make sure to ONLY use the data for the time recorded in your notes. This should correspond to at least 10 minutes of clear and stable signal as discussed in step #20 of Section 3.C. (Note: Always discard the first minute of sampling, generally rows 3 to 11).

4. Use the calculated average counts per size bin to calculate the geometric mean diameter (D_g) and geometric standard deviation (σ_g) for each sample and dynamic blank, using the following equations:

$$\log\left(D_g\right)=\frac{\sum_{i=1}^{N} n_i \log\left(D_i\right)}{\sum_{i=1}^{N} n_i} \quad \Rightarrow \quad D_g = 10^{\left(\frac{\sum_{i=1}^{N} n_i \log(D_i)}{\sum_{i=1}^{N} n_i}\right)}$$

and

$$\log\left(\sigma_g\right)=\sqrt{\frac{\sum_{i=1}^{N} n_i \left(\log\left(D_i / D_g\right)\right)^2}{\sum_{i=1}^{N} n_i - 1}} \quad \Rightarrow \quad \sigma_g = 10^{\sqrt{\frac{\sum_{i=1}^{N} n_i \left(\log\left(D_i / D_g\right)\right)^2}{\sum_{i=1}^{N} n_i - 1}}}$$

Where: n_i = particle count in size bin *i* (average calculated in the previous step #3)

D_i = average diameter of bin *i* (µm)

5. In order to account for contaminants in the water/dynamic blank you need to convert D_g of the sample to volume (assuming spherical shape: $V = \frac{\pi}{6}(D_g)^3$) and subtract it to the volume of contaminant from the corresponding water/dynamic sample (calculated the same way). The 'contaminant-free' volume is then converted back to particle diameter, and reported as the residual particle diameter, $\mathbf{D_p}$.
6. $\mathbf{D_p}$ (in µm) can then be converted to **mass of particulate matter** (*PM* in grams) by calculating its volume (assuming spherical volume) and multiplying by an appropriate density (ρ in g/cm^3) suitable to the sample, in the following way:

$$PM\ mass\ [g] = \tfrac{\pi}{6} \times \left(D_p[\mu m]\right)^3 \times \left(\rho\left[\frac{g}{cm^3}\right]\right) \times \left(\frac{1 cm^3}{10^{12}\mu m^3}\right)$$

Appendix A2

OM/OC Ratios and Densities for various Organic Compounds and Mixtures

	OM/OC	density [a] (g/mL)	corrected density [b] (g/mL)
Organic compounds			
Acetic acid	2.5	1.0492	1.0
Formic acid	3.8	1.22	-
Glycolaldehyde	2.5	1.366	-
Glycolic acid	3.2	1.30 [c]	-
Glyoxal	2.4	1.14	-
Glyoxylic acid	3.1	1.32 [c]	-
Glutaric acid	2.2	1.4188	1.3
Malonic acid	2.9	1.619	-
Oxalic acid	3.8	1.650 [d]	1.4
Succinic	2.5	1.572	1.4
Tartaric	3.1	1.788	1.5
Mixed Standards			
Organic acids [e]	3.2 [g]	1.4 [h]	1.3
Organic acids + Glyoxal [f]	3.1 [g]	1.4 [h]	1.3
Experimental Samples			
10 min reaction time	2.8 ± 0.1 [g]	1.3 [h]	1.2
40 min reaction time	3.5 ± 1.3 [g]	1.4 [h]	1.3

a – (Lide 1990) unless otherwise noted.
b – lower-bound densities; calculated assuming 33% water.
c – from SPARC online calculator (Hilal et al. 2003).
d – density of oxalic acid dihydrate (Weast 1979).
e – mixed standard, equal amounts of formic, glycolic, glyoxylic, oxalic succinic, and malonic acids.
f – mixed standard, equal amounts of formic, glycolic, glyoxylic, oxalic succinic, and malonic acids, plus glyoxal.
g – concentration-weighted organic matter (OM) divided by concentration-weighted organic carbon (OC).
h - concentration-weighted density.

Appendix A3

Example Calculations of $OM_{(droplet)}$ Mass for Succinic Acid Standard

$$\boldsymbol{OM_{(droplet)}\ mass_i = (TOC)_i \times \frac{12g\ C}{1\ mole\ C} \times \left(\frac{OM}{OC}\right)_i \times \left(\frac{\pi}{6} D_d^3\right)}$$

Where:

$OM_{(droplet)}$ mass = mass (g) of organic matter in a droplet of sample *i*

TOC_i = total organic carbon $\left(\frac{moles\ C}{L}\right)$ of sample *i.* (This values were calculated for individual organic standards and measured with a TOC analyzer for reaction samples).

D_d = droplet diameter (m). (Assumed spherical volume).

Conversion factor: 1000 L = 1 m^3

$\left(\frac{OM}{OC}\right)_i$ = organic mass to organic carbon mass ratio of sample *i*

For i = organic standard:

$$\left(\frac{OM}{OC}\right)_i = MW_i \left(in\ \frac{g}{mole}\right) \times \left(\frac{1\ mole\ i}{\#\ mole\ C}\right) \times \frac{1\ mole\ C}{12\ g\ C}$$

For mixed sample of species i: (concentration-weighted OM and OC)

$$\frac{(OM)_{mix}}{(OC)_{mix}} = \frac{\sum_i \frac{C_i (OM)_i}{C_i}}{\sum_i \frac{C_i (OC)_i}{C_i}} = \frac{\frac{C_1(OM)_1 + C_2(OM)_2 + \cdots}{C_1 + C_2 + \cdots}}{\frac{C_1(OC)_1 + C_2(OC)_2 + \cdots}{C_1 + C_2 + \cdots}}$$

Example calculation for 750µM succinic acid (SA) sample ($C_4H_6O_4$, MW=118.09g/mol):

1) $TOC_{(SA)}$ = (750 x 10^{-6} *moles/L*)×(4 moles C / 1 mole SA) = 0.003 *moles C / L*

2) $\left(\frac{OM}{OC}\right)_{SA} = \left(\frac{118.09\ g}{mole}\right)_{SA} \times \left(\frac{1\ mole\ SA}{4\ mole\ C}\right) \times \frac{1\ mole\ C}{12\ g\ C} = 2.5\ \frac{g\ OM}{g\ C}$

3) D_d = 18.3 µm = 18.3 x 10^{-6} m

$OM_{(droplet)}\ mass_{SA} =$

$$\left(0.003\frac{moles\ C}{L}\right) \times \frac{12g\ C}{1\ mole\ C} \times \left(2.5\frac{g\ OM}{g\ C}\right)_i \times \left(\frac{\pi}{6}(18.3 \times 10^{-6} m)^3\right) \times \frac{1000\ L}{1\ m^3}$$

$\therefore\ OM_{(droplet)}\ mass_{SA} = \boldsymbol{3\ \times\ 10^{-13}\ g\ OM_{SA}}$

Appendix A4

Total Organic Carbon (TOC) Analysis of Glycolaldehyde (1 mM) + OH Radical ($\sim 10^{-12}$ M) Experiment

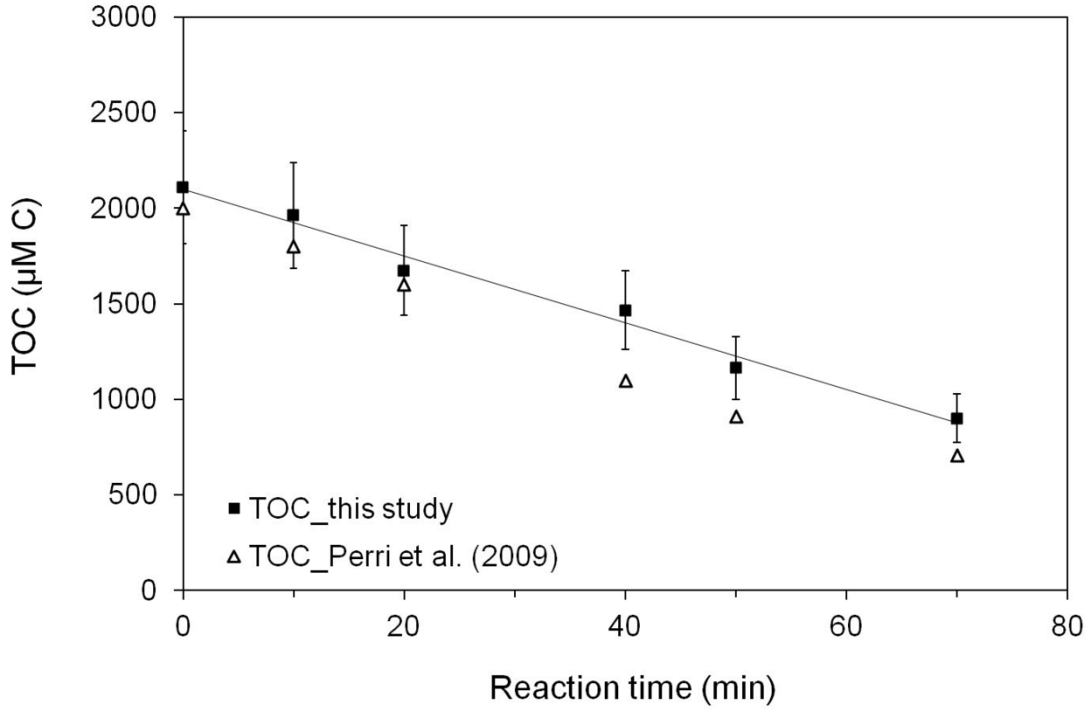

TOC as a function of glycolaldehyde + OH radical reaction time. TOC values from this study are shown in squares, and Perri et al. (2009) in triangles. Error bars represent the pooled coefficient of variation between experiments.

Appendix A5

ESI-MS Mass Spectra of Glycolaldehyde (1 mM) + OH Radical (~10^{-12} M) Reaction

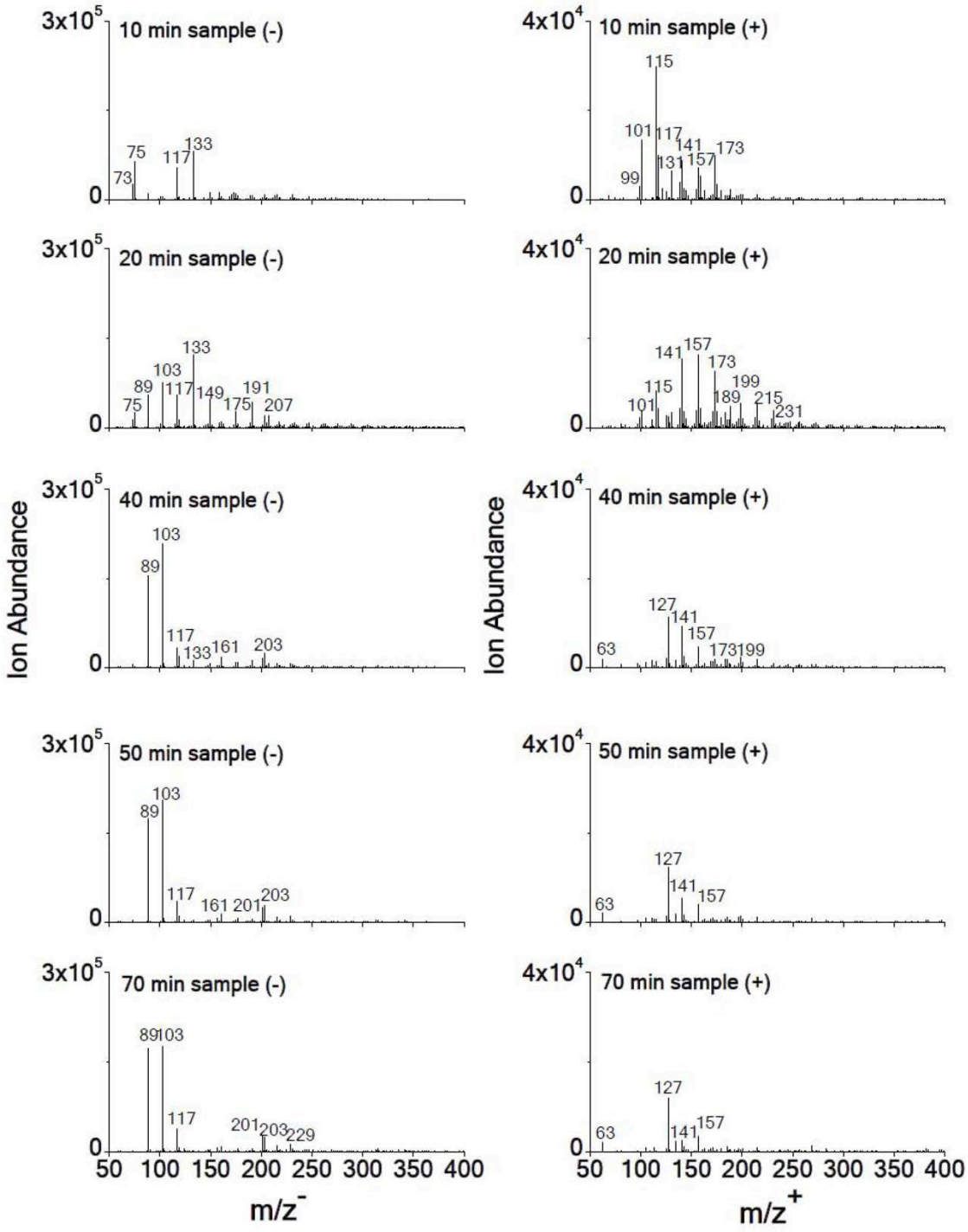

Samples taken at different reaction times in the negative and positive ESI-MS modes.

Appendix A6

Ion Abundance Time Profiles from IC-ESI-MS Analysis of Glycolaldehyde (1 mM) + OH Radical (~10^{-12} M) Reaction

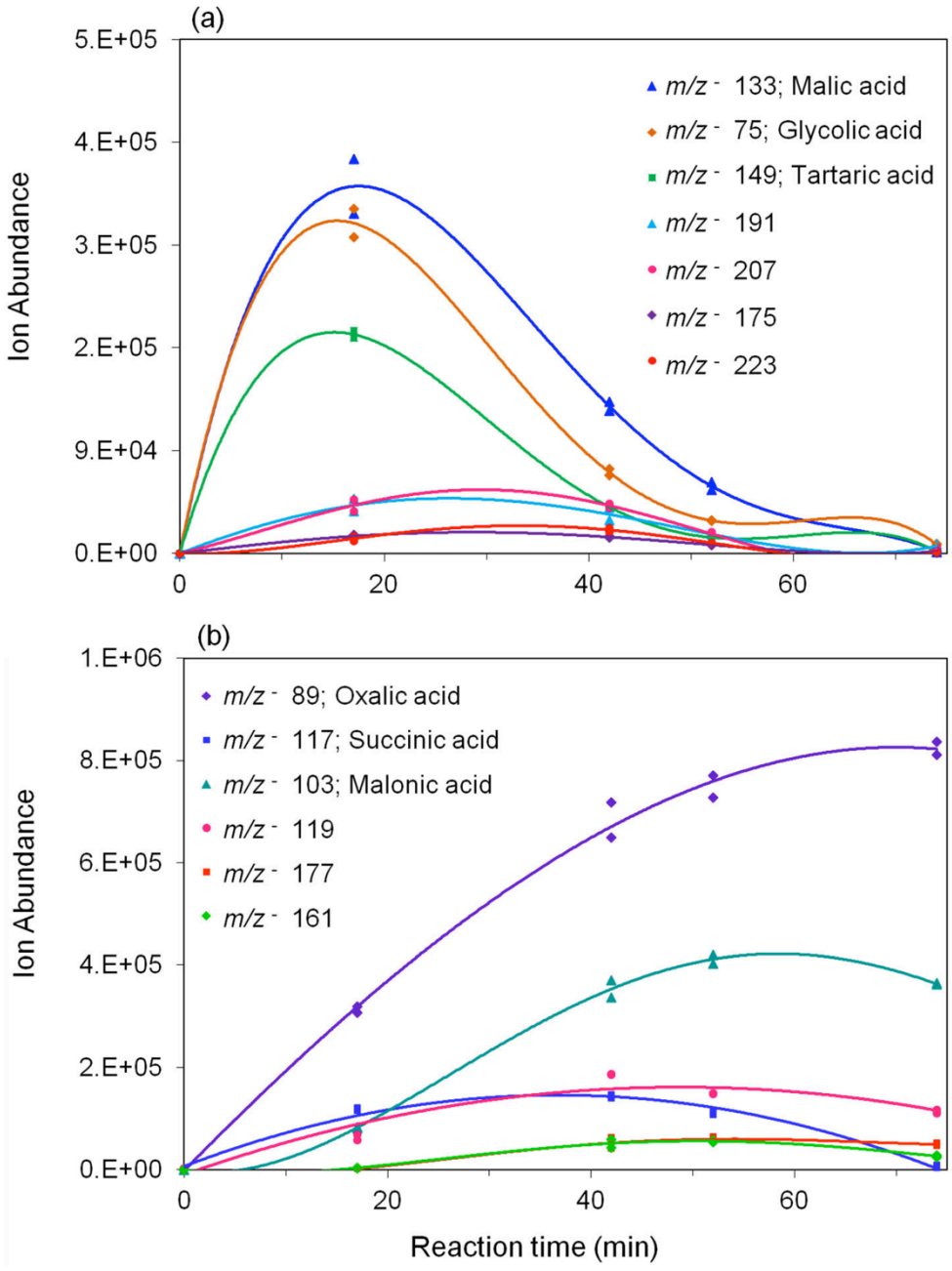

(a) Products peaking before 40 minutes; (b) Products peaking after 40 minutes. Sulfate m/z^- 97 was constant, not shown.

Appendix A7

PM mass / OM mass Ratio versus log (ΔH_{vap})

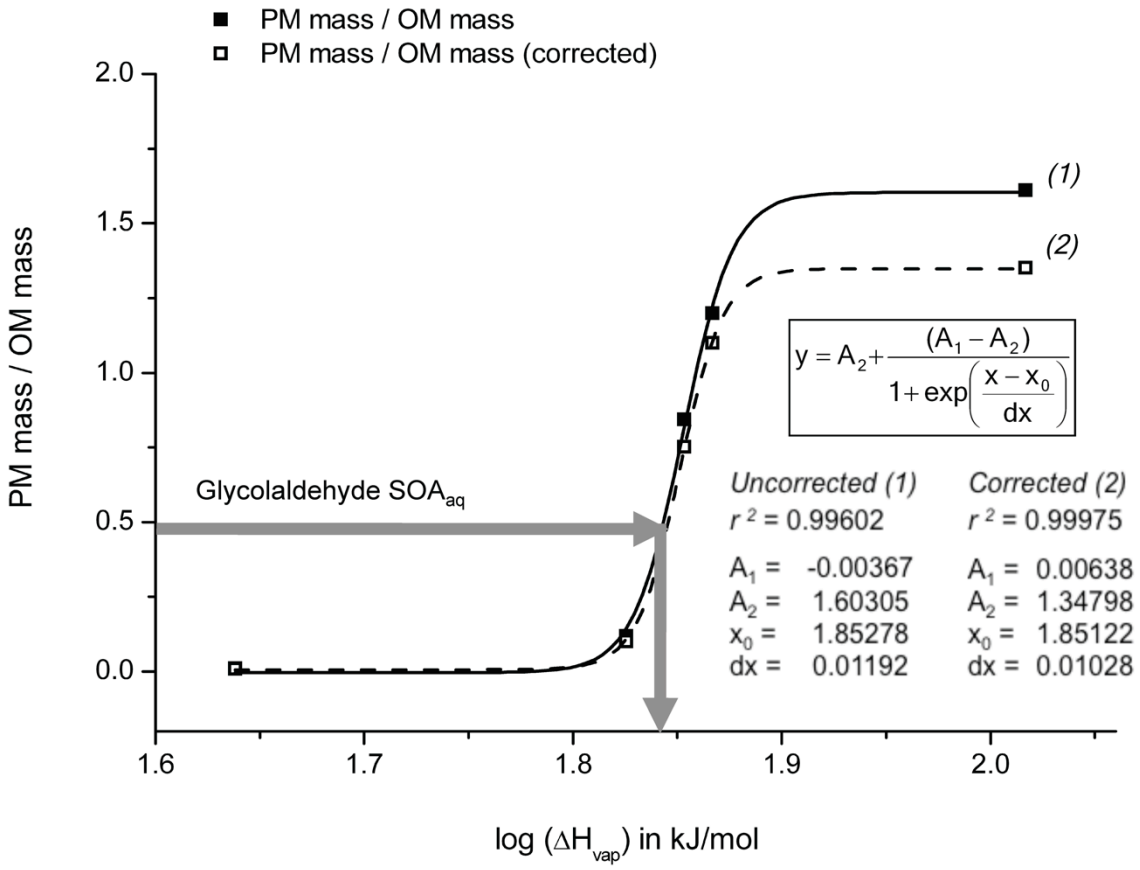

Ratio of residual particle mass to droplet organic mass (PM mass / OM mass in units of g/g) versus log(ΔH_{vap}), where ΔH_{vap} is the enthalpy of vaporization. (PM mass / OM mass) from Figure 2-5 (see also Table 2-2). (1) PM mass / OM mass values from Figure 2-5, where densities were calculated from organic species. (2) PM mass / OM mass values computed using densities calculated with an upper-bound estimate of retained water (Appendix A2). Grey arrow indicates the PM mass / OM mass of glycolaldehyde SOA_{aq}.

Appendix A8

Aerosol Formation from Droplet Evaporation of Glycolaldehyde and Glyoxal

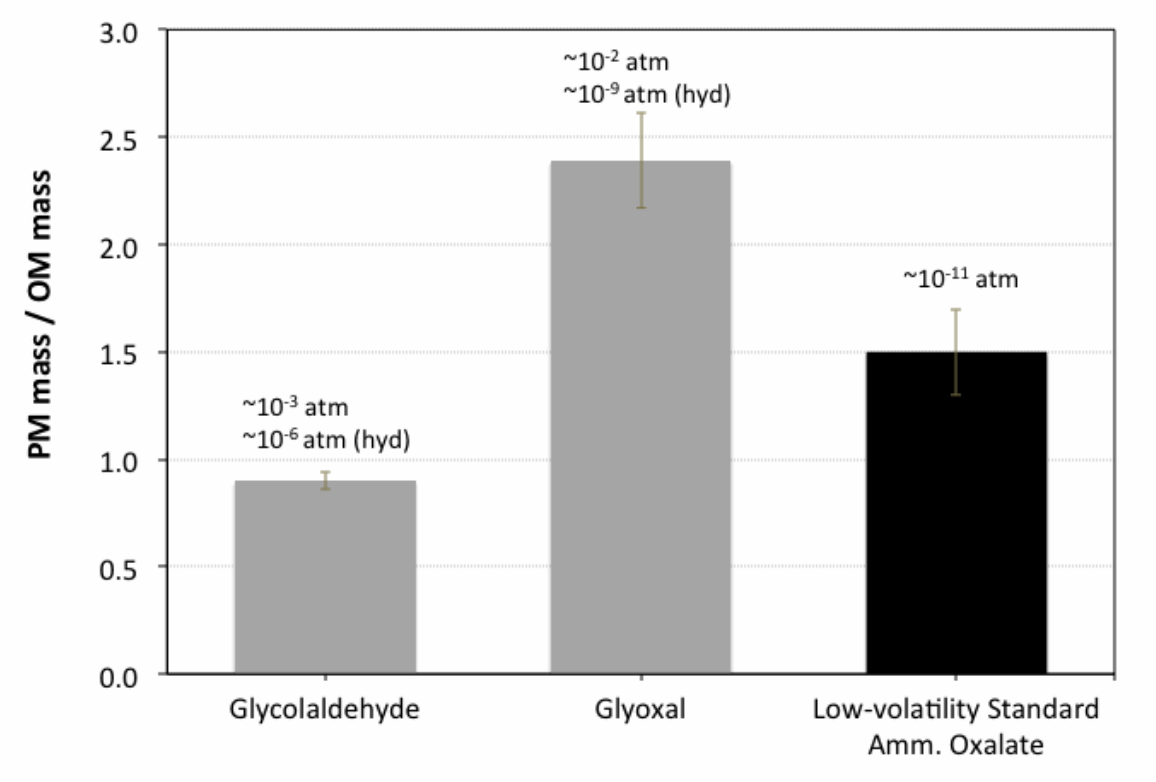

Evidence supporting the hypothesis that, like glyoxal (Loeffler et al. 2006; De Haan et al. 2009), glycolaldehyde can also oligomerize in evaporating droplets as shown by the retention of OM mass in the particle-phase upon evaporation of glycolaldehyde droplets. *PM mass / OM mass* (in units of g/g) reflects the fraction of total droplet OM that remains in the particle-phase after droplet evaporation. Labels report liquid vapor pressures (atm) estimated for unhydrated and hydrated (hyd) glycolaldehyde and glyoxal using the SIMPOL group contribution method (Pankow and Asher 2008), and for ammonium oxalate (sub-cooled liquid vapor pressure) using EPA's EPI Suite™ Software (U.S. EPA 2010). Results from ammonium oxalate droplets evaporation experiments are shown to illustrate the behavior of a low-volatility compound in our VOAG system.

Appendix A References

De Haan, D. O.; Corrigan, A. L.; Tolbert, M. A.; Jimenez, J. L.; Wood, S. E.; Turley, J. J. Secondary Organic Aerosol Formation by Self-Reactions of Methylglyoxal and Glyoxal in Evaporating Droplets. *Environmental Science & Technology* **2009**, *43*, 8184–8190.

Hilal, S. H.; Karickhoff, S. W.; Carreira, L. A. Prediction of the Vapor Pressure Boiling Point, Heat of Vaporization and Diffusion Coefficient of Organic Compounds. *QSAR Comb. Sci.*, **2003**, *22*, 565–574.

Lide, D. R. *Handbook of Chemistry and Physics*. CRC Press, Boca Raton, 71st ed., **1990**, pp. 3-17–3-474.

Loeffler, K. W.; Koehler, C. A.; Paul, N. M.; De Haan, D. O. Oligomer Formation in Evaporating Aqueous Glyoxal and Methyl Glyoxal Solutions. *Environmental Science & Technology* **2006**, *40*, 6318–6323.

Pankow, J.; Asher, W. SIMPOL. 1: a simple group contribution method for predicting vapor pressures and enthalpies of vaporization of multifunctional organic compounds. *Atmos. Chem. Phys.* **2008**, *8*, 2773–2796.

Perri, M. J.; Seitzinger, S.; Turpin, B. J. Secondary organic aerosol production from aqueous photooxidation of glycolaldehyde: Laboratory experiments. *Atmospheric Environment* **2009**, *43*, 1487–1497.

U.S. EPA. *Estimation Programs Interface Suite™* for Microsoft® Windows, v 4.00; United States Environmental Protection Agency (U.S. EPA), Washington, DC, **2010**.

Weast, R. C. *Handbook of Chemistry and Physics*. CRC Press, Boca Raton, 60th ed., **1979**, p. C-409.

Appendix B: Supplemental Information for Chapter 3

Appendix B1

Organic Mass to Organic Carbon Ratios (OM/OC) and Density used to Calculate PM mass and OM mass

	OM/OC	density (g/mL) [a]	corrected density (g/mL) [b]
Organic compounds			
Acetic acid	2.5	1.0492	1.0
Ammonium oxalate	5.2	1.5 [c]	1.3
Glutaric acid	2.2	1.4188	1.3
Glyoxal	2.4	1.14	-
Glyoxylic acid	3.1	1.32 [d]	
Malonic acid	2.9	1.619	1.4
Oxalic acid	3.8	1.650 [e]	1.4
Succinic	2.5	1.572	1.4
Tartaric	3.1	1.788	1.5
Experimental Samples			
Batch 10 min	2.8 ± 0.3 [f]	1.3 ± 0.1 [g]	1.2
CSTR 10 min	3.1 ± 0.2 [f]	1.4 ± 0.1 [g]	1.3

a – from the Handbook of Chemistry and Physics (Lide 1990) unless otherwise noted.
b – lower-bound densities; calculated assuming that 33% of water was retained in the particles.
c – obtained from The Merck Index (Windholz 1976).
d – from SPARC online calculator (Hilal et al. 2003).
e – density of oxalic acid dihydrate (Weast 1979).
f – concentration-weighted organic matter (OM) divided by concentration-weighted organic carbon (OC) ± error propagation accounting for the uncertainty in the concentrations.
g – concentration-weighted density ± error propagation accounting for the uncertainty in the concentrations.

Appendix B2

Uncorrected and Corrected* Slopes (*PM mass / OM mass*$_{(droplet)}$ ratios) obtained from linear regressions shown in Figure 3-2

*Correction for the effect that retained water (33% upper-bound estimate) could have on the densities (Appendix B1) used to calculate PM mass.

Organic Standard	Uncorrected Slope	Standard Error	r^2	Corrected Slope	Standard Error
Ammonium oxalate	1.7	0.2	0.960	1.5	0.2
Tartaric acid	1.6	0.1	0.967	1.3	0.1
Glutaric acid	1.2	0.1	0.989	1.1	0.1
Succinic acid	0.84	0.09	0.959	0.8	0.1
Oxalic acid	0.12	0.02	0.836	0.10	0.02
Acetic acid	0.011	0.009	0.283	0.010	0.009

Appendix B3

Sigmoidal regression between corrected *PM mass / OM mass*$_{(droplet)}$ and *log* p^o_L

(illustrated in Figure 3-3)

Model	Boltzmann	
Equation	$y = A_2 + (A_1-A_2)/(1 + \exp((x-x_0)/dx))$	
Reduced Chi-Squared	0.01042	
Adjusted R-Square	0.97323	
	Value	**Standard Error**
A_1	1.39722	0.07157
A_2	-4.83768E-4	0.0946
x_0	-7.08308	0.11965
dx	0.34688	0.11124

Appendix B4

Sigmoidal Regression of *PM mass / OM mass* versus *log* ΔH_{vap}

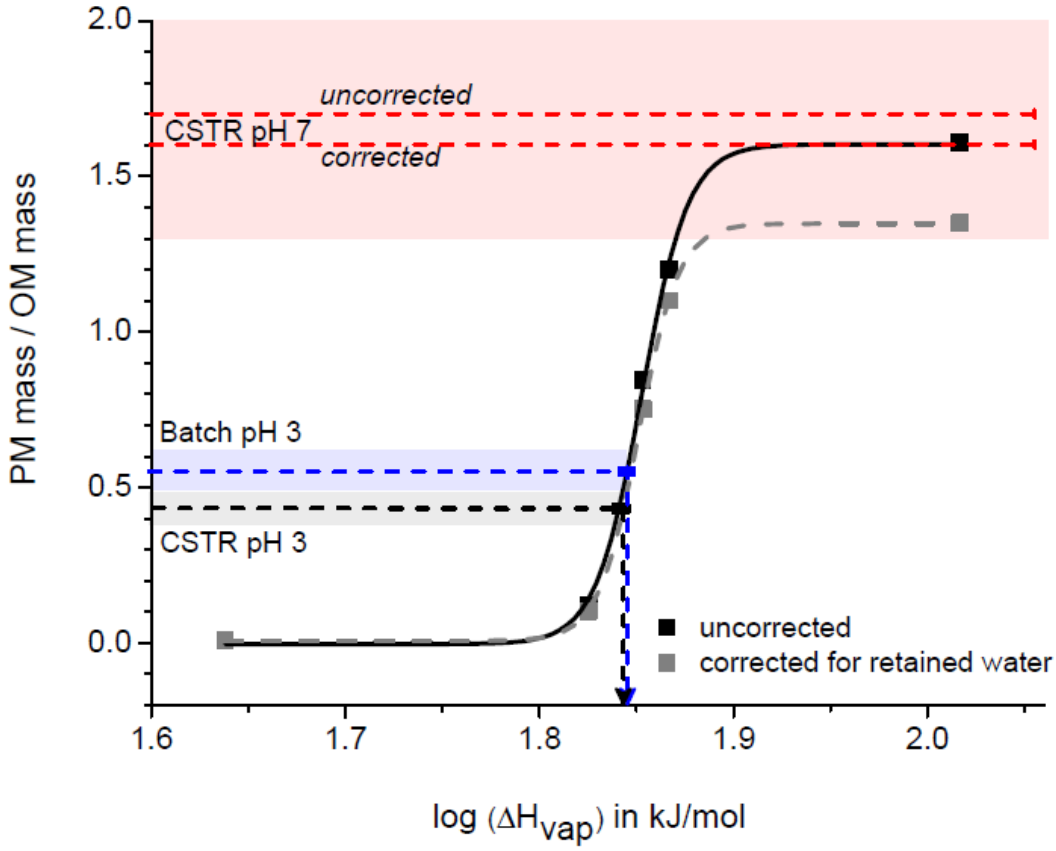

PM mass / OM mass (in units of g/g) values correspond to slopes from Figure 3-2. Data shown was uncorrected (black solid line) and corrected (dashed grey line) for the effect that retained water (33% upper-bound estimate) could have on PM density. Dashed lines show *PM mass / OM mass* of Gly + $^{\bullet}$OH mimics and estimated ΔH_{vap} from the corrected sigmoidal curve: black – CSTR pH 3, blue – Batch pH 3, and red – CSTR pH 7 (both corrected and uncorrected slope values are shown). Shaded areas represent the standard error of the slopes. Estimates of enthalpy of vaporization (ΔH_{vap}) of pure compounds at normal boiling point were obtained from Joback and Reid (1987). *PM mass / OM mass* values are provided in Table 3-1 for Gly + $^{\bullet}$OH mimics, and in Appendix B2 for the organic standards. The sigmoidal corrected regression equation can be found in Appendix B5.

Appendix B5

Sigmoidal regression between corrected *PM mass / OM mass*$_{(droplet)}$ and *log* ΔH_{vap}

(illustrated in Appendix B4)

Model	Boltzmann	
Equation	$y = A_2 + (A_1-A_2)/(1 + \exp((x-x_0)/dx))$	
Reduced Chi-Squared	8.72092E-5	
Adjusted R-Square	0.99975	
	Value	**Standard Error**
A_1	0.00638	0.00861
A_2	1.34798	0.00912
x_0	1.85122	3.71373E-4
dx	0.01028	3.35683E-4

Appendix B References

Hilal, S. H.; Karickhoff, S. W.; Carreira, L. A. Prediction of the Vapor Pressure Boiling Point, Heat of Vaporization and Diffusion Coefficient of Organic Compounds. *QSAR Comb. Sci.,* **2003**, *22*, 565–574.

Joback, K. G.; Reid, R. C. Estimation of Pure-Component Properties from Group-Contributions. *Chem. Eng. Comm.*, **1987**, *57*, 233–243.

Lide, D. R. *Handbook of Chemistry and Physics*. CRC Press, Boca Raton, 71st ed., **1990**, pp. 3-17–3-474.

Weast, R. C. *Handbook of Chemistry and Physics*. CRC Press, Boca Raton, 60th ed., **1979**, p. C-409.

Windholz, M. *The Merck Index: An Encyclopedia of Chemicals and Drugs*, edited by S. Budavari et al., 9th ed. Merck & Co., Inc., Rahway, NJ, **1976**, p. 74.

Appendix C: Supplemental Information for Chapter 4

Appendix C1

Organic Mass to Organic Carbon Ratios (OM/OC) and Density used to Calculate PM mass and OM mass

	OM/OC	density [a] (g/mL)	corrected density [b] (g/mL)
Organic compounds			
Acetic acid	2.5	1.0492	1.0
Glutaric acid	2.2	1.4188	1.3
Malonic acid	2.9	1.619	1.4
Methylglyoxal	2.0	1.0455	-
Oxalic acid	3.8	1.650 [c]	1.4
Pyruvic acid	2.4	1.2272	-
Succinic	2.5	1.572	1.4
Tartaric	3.1	1.788	1.5
Experimental Samples			
Batch 30 min	2.5 ± 0.1 [d]	1.2 ± 0.1 [e]	1.1
CSTR 10 min	2.2 ± 0.1 [d]	1.1 ± 0.1 [e]	1.1

a – from the Handbook of Chemistry and Physics (Lide 1990) unless otherwise noted.
b – lower-bound densities; calculated assuming 33% water.
c – density of oxalic acid dihydrate (Weast 1979).
d – concentration-weighted organic matter (OM) divided by concentration-weighted organic carbon (OC) ± error propagation accounting for the uncertainty in the concentrations.
e – concentration-weighted density ± error propagation accounting for the uncertainty in the concentrations.

Appendix C2

Sigmoidal Regression of *PM mass / OM mass* versus *log* ΔH_{vap}

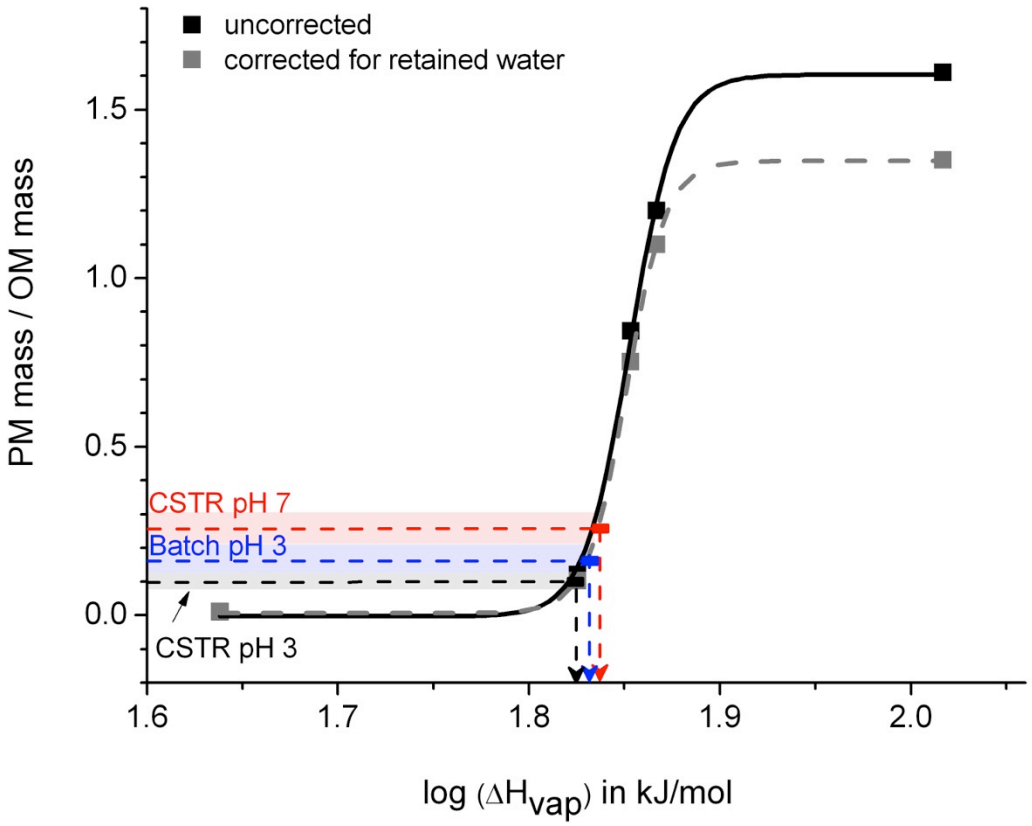

PM mass / OM mass (in units of g/g) values correspond to slopes from Figure 4-3. Data shown was uncorrected (black solid line) and corrected (dashed grey line) for the effect that retained water (33% upper-bound estimate) could have on PM density. Dashed lines show *PM mass / OM mass* of MGly + $^{\bullet}$OH mimics and estimated ΔH_{vap} from the corrected sigmoidal curve: black – CSTR pH 3, blue – Batch pH 3, and red – CSTR pH 7. Shaded areas represent the standard error of the slopes. Estimates of enthalpy of vaporization (ΔH_{vap}) of pure compounds at normal boiling point were obtained from Joback and Reid (1987). *PM mass / OM mass* values are provided in Table 4-1 for MGly + $^{\bullet}$OH mimics. The sigmoidal regression equation is provided in Ortiz-Montalvo et al. (2012).

Appendix C3

Chemical Modeling Results of 5 µM Methylglyoxal + OH Radicals

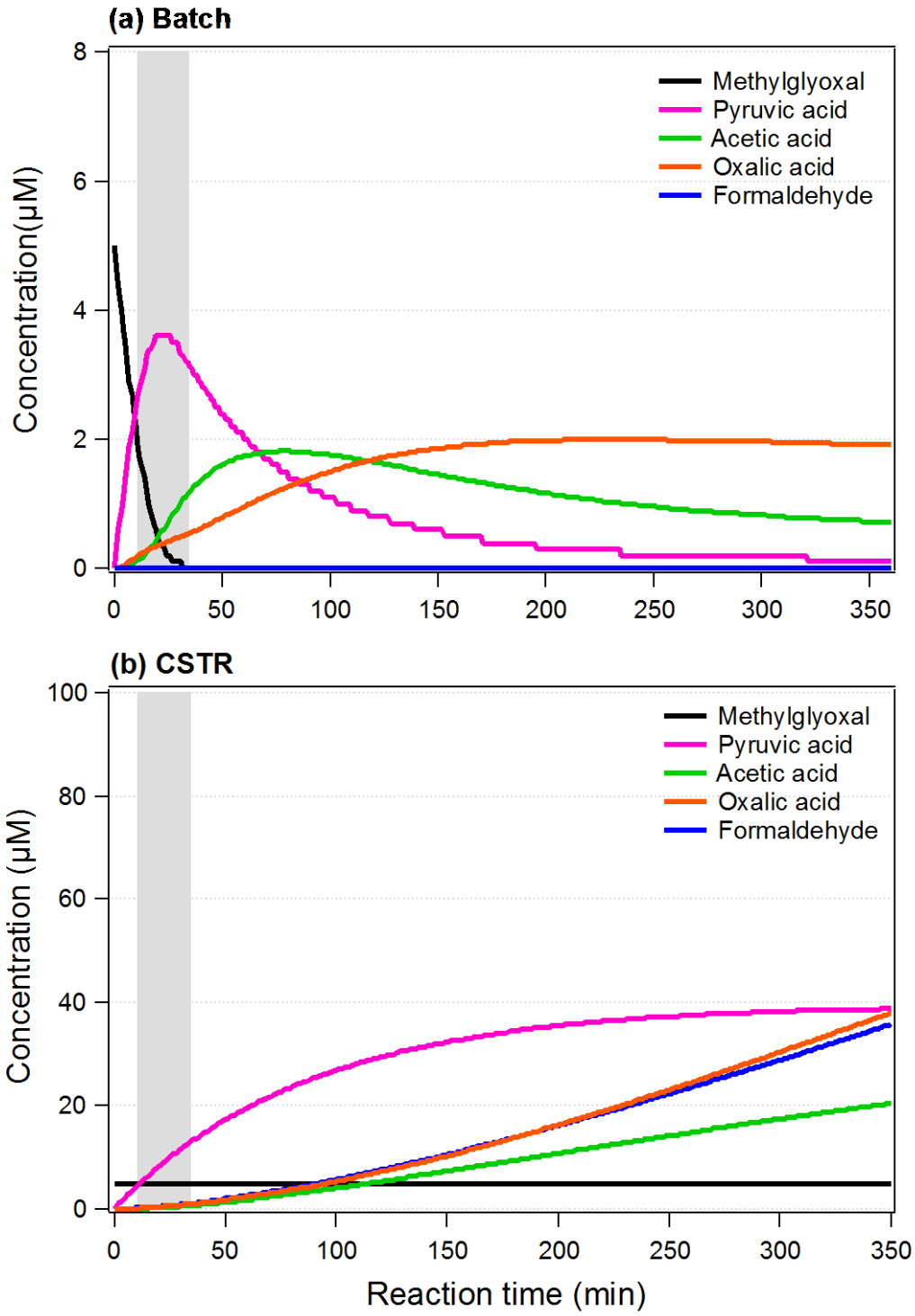

(a) Batch and (b) Continuously Stirred-Tank Reactor (CSTR) model results for the aqueous photooxidation of 5 µM methylglyoxal (MGLY) with 10^{-12} M OH radicals. Shaded areas illustrate typical times for 1 cloud cycle, 10–30 min (Desboeufs et al., 2003; Ervens and Volkamer, 2010).

Appendix C References

Desboeufs, K.; Losno, R.; Colin, J. Relationship between droplet pH and aerosol dissolution kinetics: Effect of incorporated aerosol particles on droplet pH during cloud processing. *J Atmos Chem* **2003**, *46*, 159–172.

Ervens, B.; Volkamer, R. Glyoxal processing by aerosol multiphase chemistry: towards a kinetic modeling framework of secondary organic aerosol formation in aqueous particles. *Atmos. Chem. Phys.* **2010**, *10*, 8219–8244.

Joback, K. G.; Reid, R. C. Estimation of Pure-Component Properties from Group-Contributions. *Chem. Eng. Comm.* **1987**, *57*, 233–243.

Lide, D. R. *Handbook of Chemistry and Physics*. CRC Press, Boca Raton, 71st ed., **1990**, pp. 3-17–3-474.

Ortiz-Montalvo, D. L.; Lim, Y. B.; Perri, M. J.; Seitzinger, S. P.; Turpin, B. J. Volatility and Yield of Glycolaldehyde SOA Formed through Aqueous Photochemistry and Droplet Evaporation. *Aerosol Science and Technology* **2012**, *46*, 1002–1014.

Weast, R. C. *Handbook of Chemistry and Physics*. CRC Press, Boca Raton, 60th ed., **1979**, p. C-409.

Appendix D

Catalase Experiments: Depletion of Pyruvic and Glyoxylic Acids with H_2O_2

Results obtained from Ion Chromatography (IC)

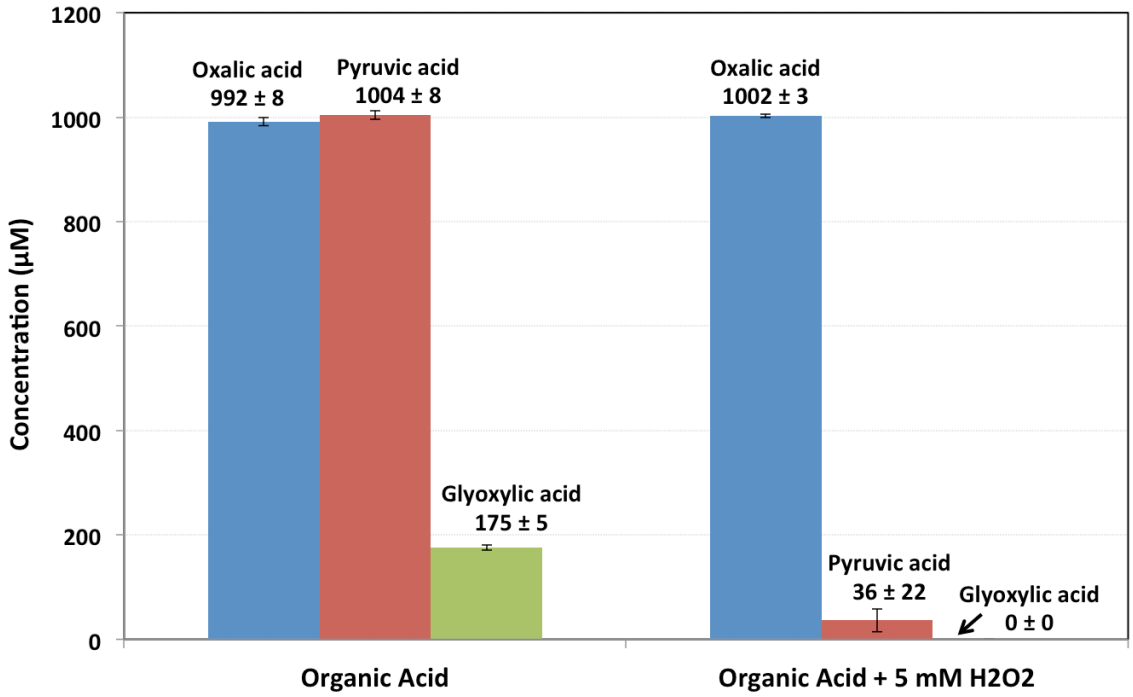

Product of Pyruvic acid + H_2O_2 –> **Acetic acid** (1002 ± 25 µM)

Product of Glyoxylic acid + H_2O_2 –> **Formic acid** (223 ± 2 µM)

According to Stefan et al. (1996), 1 unit of catalase from bovine liver decomposes 1 µmol H_2O_2 / min @ pH = 7.0, 25°C. For example, to calculate the volume of catalase needed to be added to a 10 mL sample in order to decompose 5000 µM H_2O_2, we first need to determine how many µmol of H_2O_2 are present in the sample:

$$\left(\frac{5000\ \mu mol\ H_2O_2}{L}\right) \times \left(\frac{1\ L}{1000\ mL}\right) \times (10\ mL)_{sample\ vol.} = 50\ \mu mol\ H_2O_2$$

Therefore, we need 50 units of catalase to destroy 50 µmol H_2O_2.

Using a 1% solution of catalase containing 5,346 units/mL (from a stock solution of 534,660 units/mL) we determine that (50 units ÷ 5,346 units/mL) **9.35 µL of 1% catalase** is needed to destroy 50 µmol H_2O_2.

Since our typical experiments conditions are not the specified conditions reported by Stefan et al. (1996) (e.g., pH 7), we need to test this theoretical value. Shown below are recoveries (calculated from IC data) of acids like pyruvic, glyoxylic, and oxalic acids as a function of H_2O_2 concentrations, sample volumes, and catalase volumes.

Mixed Standard ([Oxalic acid] = [Pyruvic acid] = 1000 µM, [Glyoxylic acid] = 200µM) in **10 mL sample**. 1% catalase stock solution contained ~5,346 units/mL.

H_2O_2 (µM)	**Catalase (µL) added in 10 mL sample**	**Recovery (%)**		
		Pyruvic Ac.	**Glyoxylic Ac.**	**Oxalic Ac.**
5000	**9.35 (theor.)**	20	0	101
	(after 16 hrs)	5	0	100
	10	21	0	99
	(after 17 hrs)	5	0	99
	20	21	0	100
	(after 17 hrs)	6	0	100
	30	22	0	100
	(after 17 hrs)	7	0	99
	40	25	0	100
	(after 17 hrs)	9	0	100
	50	28	0	100
	(after 17 hrs)	13	0	99
	100	74	2	98
	(after 17 hrs)	64	4	98
	500	95	100	93
	(after 19 hrs)	95	99	94

The performance of the catalase is measure by the recoveries of pyruvic and glyoxylic acids, which are rapidly depleted by H_2O_2 in samples awaiting analysis.

Mixed Standard ([Oxalic acid] = [Pyruvic acid] = 1000 μM, [Glyoxylic acid] = 200μM) in **1 mL sample**. 1% catalase stock solution contained ~5,346 units/mL.

H_2O_2 (μM)	Catalase (μL) added in 1 mL sample	Recovery (%)		
		Pyruvic Acid	Glyoxylic Acid	Oxalic Acid
5000	**10**	32	0	100
	20	45	0	101
	50	92	25	100
	100	99	102	98
	500	98	107	97

Mixed Standard ([Glyoxylic acid] = [Pyruvic acid] = 50 μM, [Oxalic acid] = 25 μM) in **3 mL sample**. 0.1% catalase stock solution contained ~534 units/mL.

H_2O_2 (μM)	Catalase (μL) added in 3mL sample	Recovery (%)		
		Pyruvic Acid	Glyoxylic Acid	Oxalic Acid
50	**6**	88.9	61.3	96.8
	12	95.8	92.2	105
	16	105	101	101
150	**36**	100	111	101
	(after 10 hrs)	103	96	101
	50	99	108	102
	(after 10 hrs)	98	101	100

Mixed Standard ([Oxalic acid] = [Pyruvic acid] = 1000 μM, [Glyoxylic acid] = 200μM) in **25 mL sample**. 1% catalase stock solution contained ~5,346 units/mL.

H_2O_2 (μM)	Catalase (μL) added in 25 mL sample	Recovery (%)		
		Pyruvic Acid	Glyoxylic Acid	Oxalic Acid
5000	**500**	75	0	96
	(after 19 hrs)	68	15	98
	750	95	90	96
	(after 19 hrs)	94	96	96
	1000	97	101	95
	(after 19 hrs)	95	100	94

Recommendations for catalase use based on the results shown above:

Sample volume (mL)	H_2O_2 (µM)	H_2O_2 (µmol)	Catalase [a] vol. (µL)	Catalase [a] (units)	Recovery Pyruvic ac. (%)	Recovery Glyoxylic ac. (%)	Recovery Oxalic ac. (%)
1	5000	5	100	534	99	102	98
3	50	0.15	16 [b]	8 [b]	105	101	101
3	150	0.45	50 [b]	26 [b]	98 - 99	101 - 108	100 - 102
10	5000	50	500	2,673	95	99 - 100	93 - 94
25	5000	125	1000	5,346	95 - 97	100 - 101	94 - 95

a – 1% catalase stock solution containing ~5,346 units/mL, unless otherwise specified.
b – 0.1% catalase stock solution containing ~534 units/mL.

It is highly recommended that newer experiments conducted under different conditions (e.g., sample volume, H_2O_2 concentration, catalase units) test the appropriate volumes of catalase needed to decompose the excess H_2O_2 in their samples and obtain the highest recoveries for pyruvic and glyoxylic acids.

Appendix D References

Stefan, M.I.; Hoy, A.R.; Bolton, J.R. Kinetics and mechanism of the degradation and mineralization of acetone in dilute aqueous solution sensitized by the UV photolysis of hydrogen peroxide. *Environmental Science & Technology*, **1996**, *30*, 2382–2390.

Appendix E

Aerosol-CIMS Data and $\Delta H_{vap,eff.}$ estimates

E1. Example Procedure: Calculating $\Delta H_{vap,eff.}$ from Aerosol-CIMS data

Oxalic acid standard (1 mM)

Oxalic acid's mass-to-charge ratio (*m/z* 217) was traced and evaluated against increasing temperatures (RT= room temperature (25), 40, 59, 77, 95, 116, and 137ºC), as illustrated bellow (purple trace). The gray colored trace in the background corresponds to the signal of the I^- reagent ions. (Before passing the sample through the Aerosol-CIMS a background measurement of *m/z* 217 was obtained.)

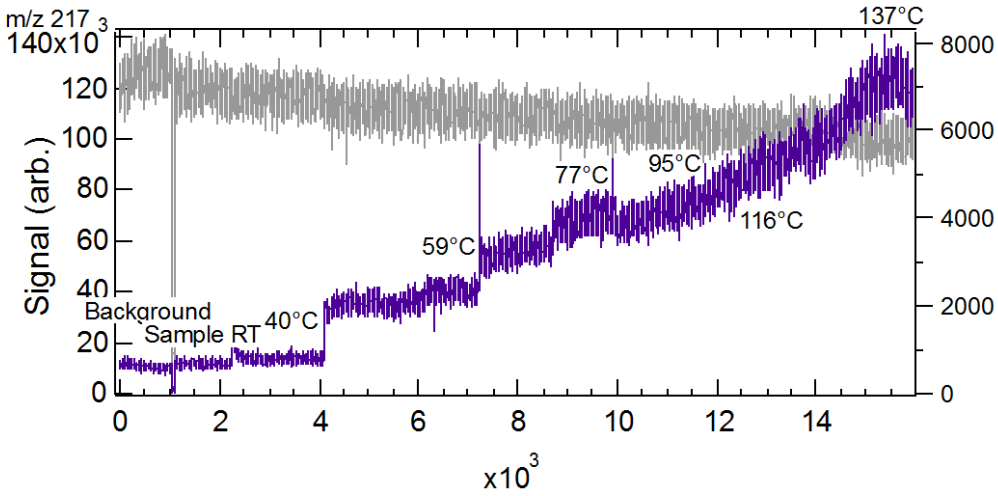

The averaged signal was taken for each temperature (25-137ºC). The averaged background signal of *m/z* 217 was then subtracted to the each averaged signal. All signals were then divided by the averaged initial signal at room temperature (S/S_i). The natural log was taken to each value ($ln(S/S_i)$) and plotted against their corresponding temperatures ($1/T$, in K), as shown below (solid circles):

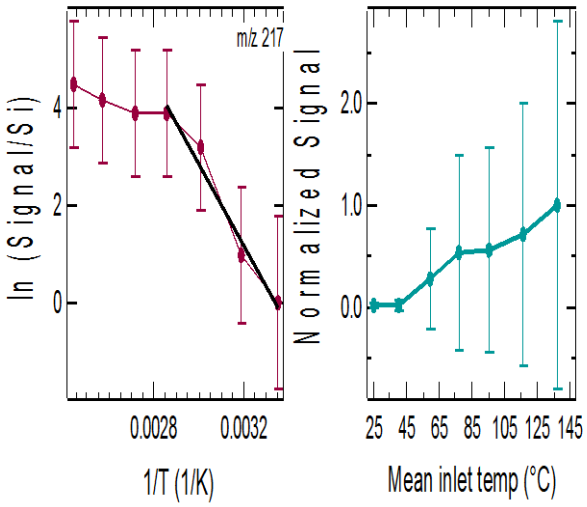

A linear regression was obtained for the steepest points (black line, above figure) and the slope was used to calculate the $\Delta H_{vap,eff.}$ from the Clausius-Clapeyron relation:

$$\ln\left(\frac{P_1}{P_2}\right) = \frac{\Delta H_{vap}}{R}\left(\frac{1}{T_2} - \frac{1}{T_1}\right) \cong \ln\left(\frac{S}{S_i}\right)$$

Where S/S_i is equivalent to the ratio of partial pressures P_1/P_2 of the organic compound being traced, the slope of the linear regression of $ln(S/S_i)$ on $1/T$ is equal to $-\Delta H/R$, and R is the ideal gas law constant.

Oxalic Acid	**Exp. $\Delta H_{vap,eff.}$ (kJ/mol)**		**Theoretical[a] ΔH_{vap} (kJ/mol)**	**% Error**
(*m/z* 217)	69	± 33	72.57	5%

a – taken from Yaws' Handbook of Thermodynamic and Physical Properties (Yaws, 2003).

E2. Aerosol-CIMS Supporting Data for Chapter 4 (Methylglyoxal SOA_{aq})

Pyruvic acid (in Batch pH 3.8 sample) - m/z 215

Trial #1

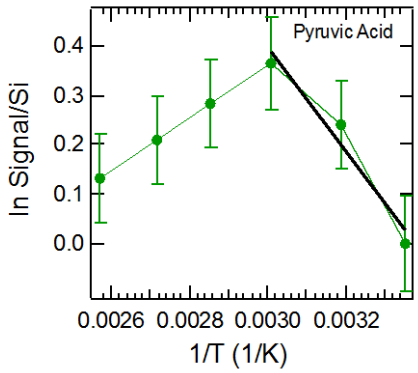

Trial #2

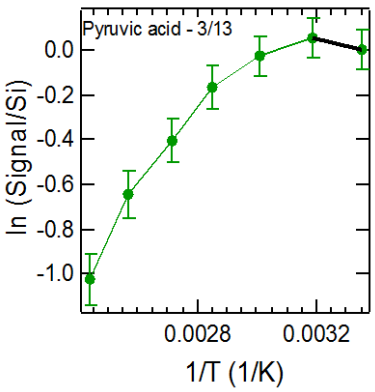

Pyruvic acid	**Exp. $\Delta H_{vap,eff.}$ (kJ/mol)**				**Average[a] $\Delta H_{vap,eff.}$**	**Theoretical[b] ΔH_{vap} (kJ/mol)**
	Trial #1		**Trial #2**			
m/z 215	6	± 2	3	± 6	6 ± 2	45.74

[a] Average weighted by the standard deviations in each trial ± one standard deviation.
[b] From Yaws' Handbook of Thermodynamic and Physical Properties (Yaws, 2003).

Pyruvic acid (in CSTR pH 3.7 sample) - m/z 215

Trial #1

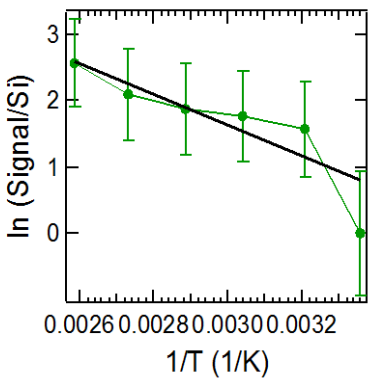

Trial #2

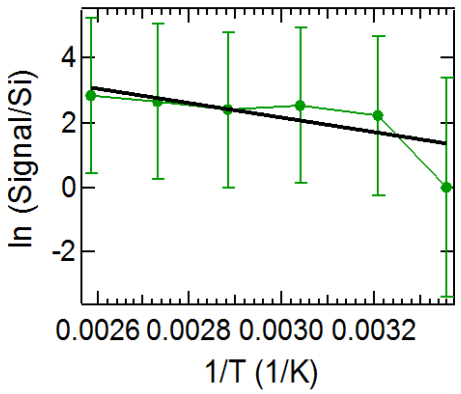

Pyruvic acid	**Exp. $\Delta H_{vap,eff.}$ (kJ/mol)**				**Average[a] $\Delta H_{vap,eff.}$**	**Theoretical[b] ΔH_{vap} (kJ/mol)**
	Trial #1		**Trial #2**			
m/z 215	19	± 10	18	± 35	19 ± 9	45.74

[a] Average weighted by the standard deviations in each trial ± one standard deviation.
[b] From Yaws' Handbook of Thermodynamic and Physical Properties (Yaws, 2003).

Pyruvic acid (in CSTR pH 4.6 sample) - m/z 215

Trial #1

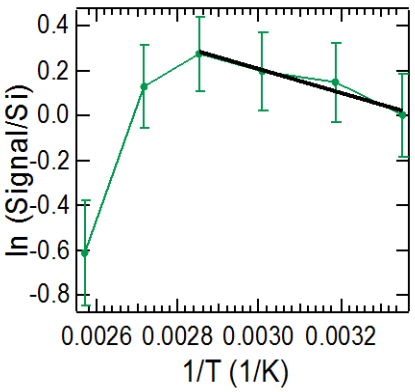

Trial #2

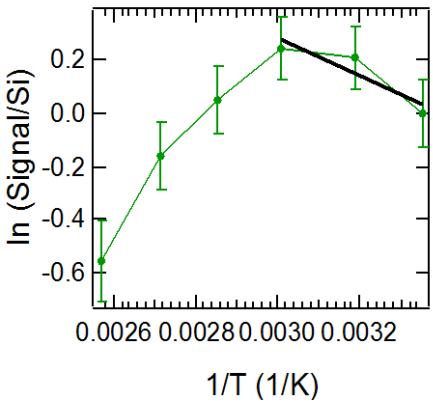

Pyruvic acid	**Exp. $\Delta H_{vap,eff.}$ (kJ/mol)**				**Average[a] $\Delta H_{vap,eff.}$**	**Theoretical[b] ΔH_{vap} (kJ/mol)**
	Trial #1		**Trial #2**			
m/z 215	4	± 4	6	± 4	5 ± 3	45.74

[a] Average weighted by the standard deviations in each trial ± one standard deviation.
[b] From Yaws' Handbook of Thermodynamic and Physical Properties (Yaws, 2003).

Oxalic acid + Methylglyoxal signal (in Batch pH 3.8 sample) - m/z 217

Trial #1

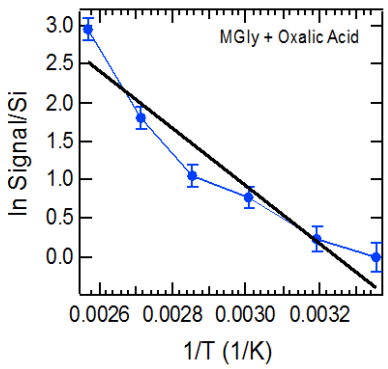

Trial #2

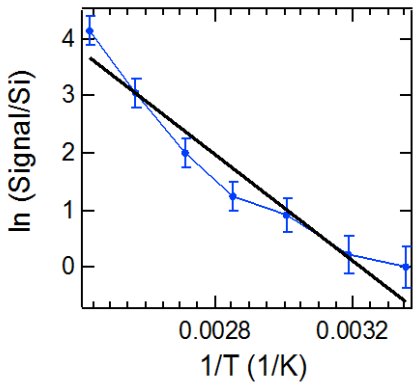

Oxalic Acid + Methylglyoxal	**Exp. $\Delta H_{vap,eff.}$ (kJ/mol)**				**Average[a] $\Delta H_{vap,eff.}$**	**Theoretical[b] ΔH_{vap} (kJ/mol)**
	Trial #1		**Trial #2**			
m/z 217	31	± 2	39	± 3	34 ± 2	Oxalic - 72.57 MG - 38

[a] Average weighted by the standard deviations in each trial ± one standard deviation.
[b] From Yaws' Handbook of Thermodynamic & Physical Properties (Yaws, 2003) (oxalic acid) and the SPARC online calculator (Hilal et al., 2003) (methylglyoxal).

Oxalic acid + Methylglyoxal signal (in CSTR pH 3.7 sample) - m/z 217

Trial #1

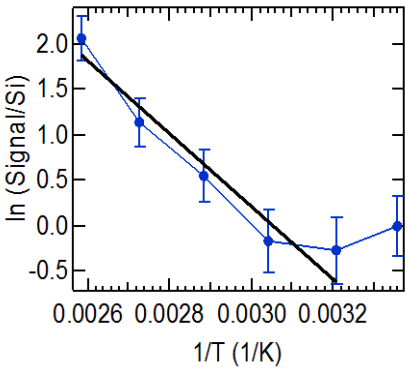

Trial #2

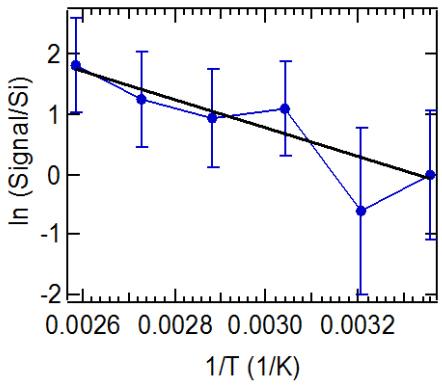

Oxalic Acid + Methylglyoxal	**Exp. $\Delta H_{vap,eff.}$ (kJ/mol)**				**Average[a] $\Delta H_{vap,eff.}$**	**Theoretical[b] ΔH_{vap} (kJ/mol)**
	Trial #1		**Trial #2**			
m/z 217	34	± 5	20	± 12	31 ± 5	Oxalic - 72.57 MG - 38

[a] Average weighted by the standard deviations in each trial ± one standard deviation.
[b] From Yaws' Handbook of Thermodynamic & Physical Properties (Yaws, 2003) (oxalic acid) and the SPARC online calculator (Hilal et al., 2003) (methylglyoxal).

Oxalic acid + Methylglyoxal signal (in CSTR pH 4.6 sample) - m/z 217

Trial #1

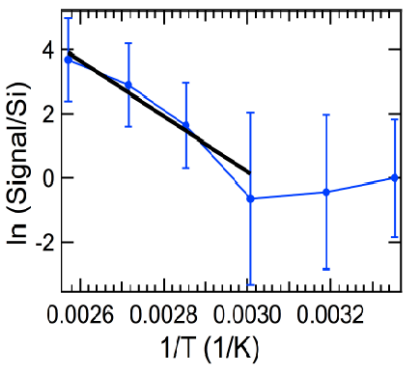

Trial #2

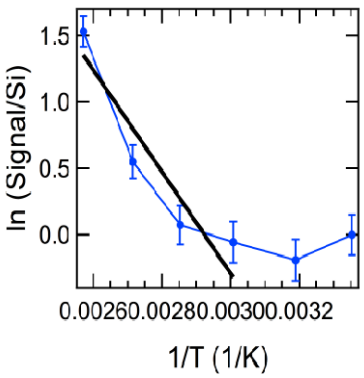

Oxalic Acid + Methylglyoxal	**Exp. $\Delta H_{vap,eff.}$ (kJ/mol)**				**Average[a] $\Delta H_{vap,eff.}$**	**Theoretical[b] ΔH_{vap} (kJ/mol)**
	Trial #1		**Trial #2**			
m/z 217	72	± 45	32	± 3	32 ± 3	Oxalic - 72.57 MG - 38

[a] Average weighted by the standard deviations in each trial ± one standard deviation.
[b] From Yaws' Handbook of Thermodynamic & Physical Properties (Yaws, 2003) (oxalic acid) and the SPARC online calculator (Hilal et al., 2003) (methylglyoxal, MG).

Appendix E References

Hilal, S. H.; Karickhoff, S. W.; Carreira, L. A. Prediction of the Vapor Pressure Boiling Point, Heat of Vaporization and Diffusion Coefficient of Organic Compounds. *QSAR Comb. Sci.*, **2003**, *22*, 565–574.

Yaws, C.L. Yaws' Handbook of Thermodynamic and Physical Properties of Chemical Compounds, **2003**. Knovel. Online version from http://www.knovel.com

Appendix F

SOA Mass Yields from Droplet Evaporation of CSTR and Batch Mimics

	Glyoxal			Methylglyoxal		
Scenario	**Batch**	**CSTR**	**CSTR (pH 7)**	**Batch**	**CSTR**	**CSTR (pH 7)**
Rxn Time	**10 min**	**10 min**	**10 min**	**30 min**	**10 min**	**10 min**
Yield	**207%**	**100%**	**438%**	**20%**	**5%**	**14%**
ΔYield	17%	11%	84%	2%	1%	1%
Avg. D_p (μm)	0.70	0.65	1.05	0.45	0.43	0.59
ΔD_p (μm)	0.01	0.03	0.08	0.01	0.01	0.01
ρ (g/cm^3)	1.3	1.4	1.45	1.2	1.1	1.1
$\Delta\rho$ (g/cm^3)	0.1	0.1	0.2	0.1	0.1	0.1
ΔC_i (moles/L)	2E-06	8E-06	8E-06	5E-06	3E-05	3E-05
F	350	150	150	275	130	130
D_d (μm)	17.60	17.60	17.60	17.9	17.9	17.9
ΔD_d (μm)	0.03	0.03	0.03	0.4	0.4	0.4
MW_i (g/mole)	58.04	58.04	58.04	72.021	72.021	72.021
ΔMW_i (g/mole)	0.01	0.01	0.01	0.001	0.001	0.001

Calculated as:

$$Mass\ Yield_i = \frac{\text{PM mass formed}}{(\Delta \text{ mass of precursor}, i)_{droplet}} = \frac{\left(\frac{\pi}{6} D_p^3\right) \times \rho}{\Delta C_i \times F \times MW_i \times \left(\frac{\pi}{6} D_d^3\right)}$$

Where:

i = unhydrated precursor; D_p = averaged particle diameter size (μm) measured by the optical particle counter (OPC) used in the droplet evaporation experiments (values corrected for the volume of contaminants in water blanks); ρ = concentration-

weighted density of organic matter mixture (g/cm^3) as discussed in Chapters 3 and 4; ΔC_i = initial moles/L of *i* – final moles/L of *i*, obtained from model predictions (*see details below); *F* = factor used to scale up the concentrations of organic standards in order to meet the detection limits of the droplet evaporation methods, but still maintaining the same distribution of precursor and products (Chapter 3 and 4); MW_i = molecular weight of *i* (g/moles); D_d = initial droplet diameter (µm). This calculation assumes particles and droplets are spherical. Conversion factor used: 1L = 1000 cm^3.

The error in mass yield of *i* ($\Delta Yield_i$) was calculated using the following error propagation:

$$\Delta Yield_i = Yield_i \sqrt{\left[3 \times \left(\frac{\Delta D_p}{D_p}\right)^2\right] + \left(\frac{\Delta \rho}{\rho}\right)^2 + \left[3 \times \left(\frac{\Delta D_d}{D_d}\right)^2\right] + \left(\frac{\Delta MW_i}{MW_i}\right)^2}$$

*The reacted precursor concentrations (ΔC_i) in the Batch scenario were calculated directly from the model; however, since this is not possible in the CSTR model (steady-sate concentration of precursor) they were calculated from the (molar) sum of the major products (i.e., Glyoxal: oxalic acid, glyoxylic acid, formic acid and CO_2; Methylglyoxal: pyruvic acid, acetic acid, glyoxylic acid, formic acid, formaldehyde, and CO_2), using stoichiometric coefficients of 1 for all except CO_2 which was assumed to be 2 since two molecules of CO_2 are produced from one molecule of oxalic acid.